

Synthesis of 19,20- epoxydocosapentaenoic acid mimics and their ethanalamides

Cecilia Marianne Lennartsson Bekkhus



Thesis for the degree Master of Pharmacy

45 credits

Section for pharmaceutical chemistry
Department of Pharmacy
Faculty of Mathematics and Natural Sciences

UNIVERSITY OF OSLO

May 2023

Cecilia Marianne Lennartsson Bekkhus ©

2023

Synthesis of 19,20-epoxydocosapentaenoic acid mimics and their ethanolamides

Cecilia Marianne Lennartsson Bekkhus

<http://www.duo.uio.no/>

Print production: Reprosentralen, University of Oslo

Acknowledgments

First and foremost, I would like to express my deepest gratitude to Associate Professor Anders Vik and Ph.D. student Marcus de Bourg for allowing me to participate in such an exciting project in medicinal chemistry.

As expected, my primary supervisor Anders has been an outstanding mentor throughout this project. I am incredibly grateful for your ongoing knowledge of chemistry, constructive feedback, and motivation over this past year. You have always had the door open to answer my questions and provided valuable advice. I could not have asked for a better supervisor.

Marcus also deserves extra thank you. I am truly grateful for all the time you have put into teaching me in the lab and for patiently answering all my questions, especially in the beginning. Thank you for your patience, as I know I can be a bit scattered at times.

Further, I would like to thank Professor Trond Vidar Hansen and Dr. Åsmund Kaupang for their inspiring teaching and support. Of course, I would also like to thank the rest of the LIPCHEM group; Karina, Åshild, Mina, and Mathias for an amazing year. We have made many unforgettable memories from lunch breaks, hallway meetings, and post-study/work hangouts. You have taught me a lot professionally, in addition to all the shenanigans we've been up to. I dare to claim that I ended up in the best research group.

And not least, a big thank you goes to my favorite classmates; Julie, Marte, Hilde, Lene, and Ole Martin. Thank you for all the laughter, tears, and lessons learned these past five years.

Lastly, I would like to extend my greatest appreciation to my family for their unwavering support throughout my entire education.

Oslo, Mai 2023

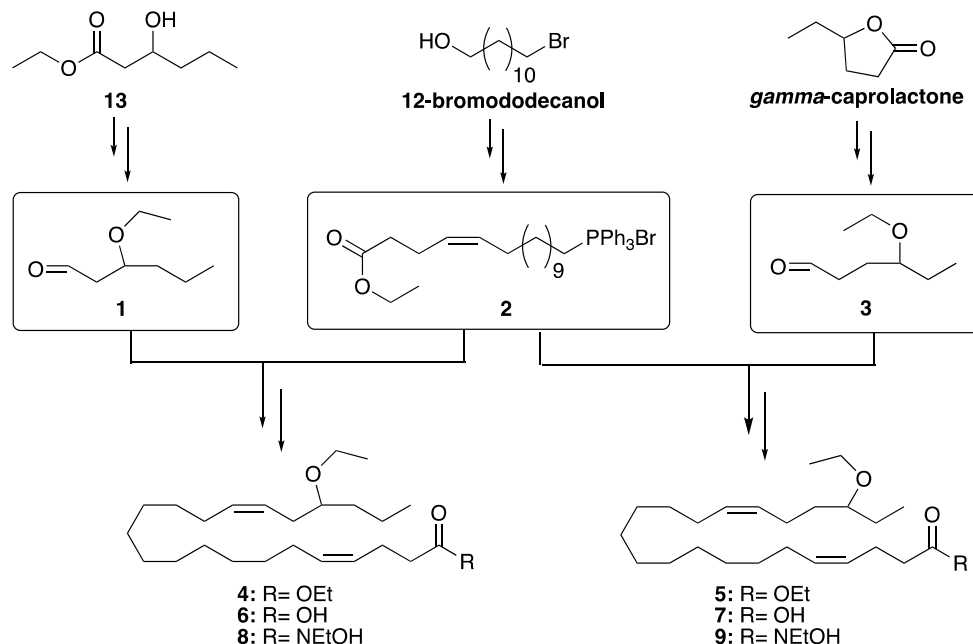
Cecilia Bekkhus

Cecilia Marianne Lennartsson Bekkhus

Abstract

Epoxy fatty acids, generated from polyunsaturated fatty acids via cytochrome P 450-enzymes, are a class of lipid mediators associated with a range of bioactions, including anti-inflammatory effects. Soluble epoxide hydrolase enzyme regulates the levels of epoxy fatty acids. The biological properties of epoxy fatty acids can be studied via stable synthetic mimics.

This master thesis presents the successful preparation of four potential epoxy fatty acids mimics of 19,20-epoxydocosapentaenoic acid and their ethanolamides, outlined in the graphical abstract below. For these mimics, ethoxy ethers were chosen as bioisosteres for the epoxide. Additional alterations have been in terms of increasing the carbon backbone's saturation, to lessen auto-oxidation. These alterations could make the mimic less prone to metabolic degradation, especially hydrolysis by the soluble epoxide hydrolase. A total of 18 molecules were synthesized and characterized, of which 16 were previously not reported in the literature. Key steps include the *Z*-selective Wittig coupling of the key fragments; Wittig salt **2** and aldehyde **1** or **3**.

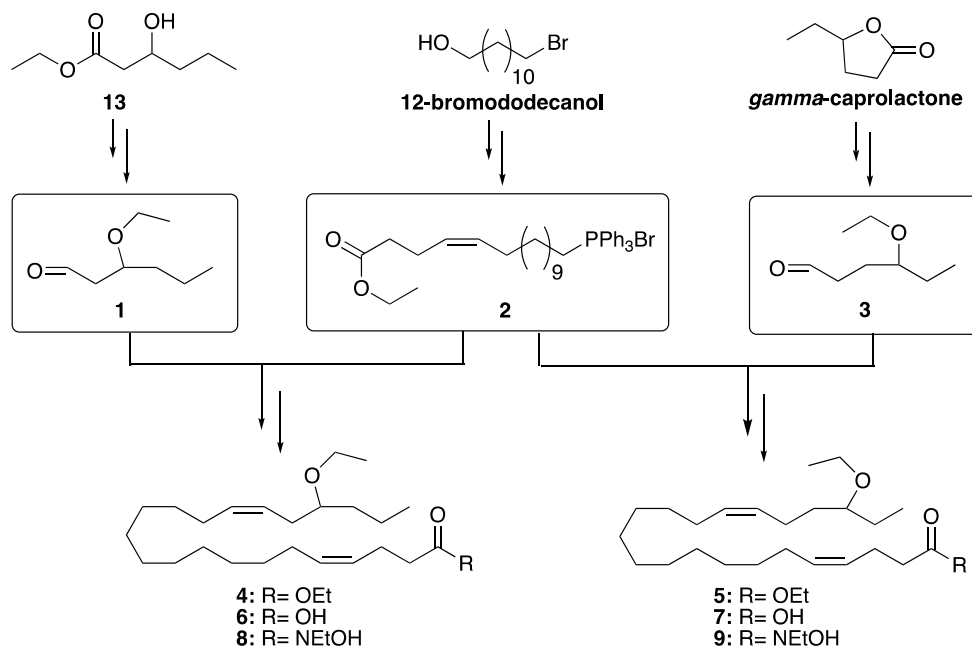


Graphical abstract of the synthesis of the four epoxy fatty acid mimics **6-9**.

Sammendrag

Fettsyreepoksider, generert fra flerumettede fettsyrer via cytokrom P 450-enzym, er forbundet med en rekke biologiske funksjoner, inkludert anti-inflammatorisk effekt. Løselig epoksid hydrolase enzym regulerer nivåene av fettsyreepoksidene. De biologiske effektene av fettsyreepoksidene kan undersøkes via stabile syntetiske analoger.

Denne masteroppgaven presenterer vellykket fremstilling av fire potensielle fettsyreepoksid analoger av 19,20-epoksydokokosapentaensyre og dens etanolamider, avbildet i det grafiske sammendraget nedenfor. Disse molekylene har etoksytere som bioisoster for epoksidet. Ytterligere endringer har blitt gjort i form av økt mettetthet av karbonskjelettet, for å minke forekomsten av auto-oksidasjon. Disse grepene kan potensielt gjøre molekylene mindre utsatt for metabolsk degradering i kroppen, spesielt hydrolyse av løselig epoksid hydrolase enzymet. Totalt 18 molekyler har blitt syntetisert og karakterisert, hvorav 16 ikke har vært rapportert tidligere i litteraturen. Hovedreaksjoner inkluderer *Z*-sektiv Wittig reaksjon av nøkkelfragmentene Wittig salt **2** og aldehyd **1** eller **3**.



Grafisk sammendrag av de fire fettsyreepoksid-analogene **6-9**.

List of abbreviations

2-AG	2- Aracidonylglycerol
AA	Arachidonic acid
AEA	Arachidonoyl ethanolamide
ALA	Alpha-linolenic acid
α SMA	Alpha smooth muscle actin
CAM	Cerium Ammonium Molybdate stain
CB1	Cannabinoid receptor 1
CB2	Cannabinoid receptor 2
EDCI	1-(3-Dimethylaminopropyl)-3-ethyl carbodiimide hydrochloride
CDI	<i>N, N'</i> -Carbonyldiimidazole
COSY	Correlated spectroscopy
COX	Cyclooxygenase
CYP450	Cytochrome P 450
DCC	<i>N, N'</i> -dicyclohexylcarbodiimide
DCM	Dichloromethane
DHA	Docosahexaneic acid
DHEA	Docosahexanoyl ethanolamide
DMAP	4-methylamino pyridine
DMF	Dimethylformamide
DMP	Dess-Martin periodinane
DMSO	Dimethylsulfoxide
DPA	Docosapentaenoic acid
EA	Ethanolamide
eCB	Endocannabinoid
EEQ	Epoxyeicosatetraenoic acid
EET	Epoxyeicosatrienoic acid
EpDPA	Epoxydocosapentaenoic acid

EpDPA-EA	Epoxydocosapentaenoic acid ethanolamide
FFA	Free fatty acid
FGF-2	Fibroblast growth factor 2
GPCR	G-protein coupled receptor
HMBC	Heteronuclear multiple bond correlation
HMPA	Hexamethylphosphoramide
HSQC	Heteronuclear single quantum coherence
Hz	Hertz
<i>I</i>	Spin
IL-10	Interleukin-10
IL-6	Interleukin-6
<i>J</i>	Coupling constant
JH1	Juvenile hormone 1
LA	Linolenic acid
LOX	Lipoxygenase
NaHMDS	Sodium bis(trimethylsilyl)amide
NMR	Nuclear magnetic resonance
PLA	Phospholipase
ppm	Parts per million
PUFA	Polyunsaturated fatty acid
R _f	Retention factor
SAR	Structure-activity-relationship
sEH	Soluble epoxide hydrolase
sEHi	Soluble epoxide hydrolase inhibitor
SPM	Specialized pro-resolving mediators
TBAF	Tetrabutylammonium fluoride
TBS	<i>tert</i> -Butyldimethylsilyl
TEA	Triethylamine

TGF β	growth factor <i>beta</i>
THF	Tetrahydrofurane
TLC	Thin-layer chromatography
TLR	Toll-like receptors
VEGF	Vascular endothelial growth factor

Table of content

1	Aim of study	11
2	Introduction	12
2.1	<i>Polyunsaturated fatty acids</i>	13
2.1.1	Biosynthesis of PUFAs	13
2.2	<i>Inflammation</i>	15
2.2.1	Acute inflammation	15
2.2.2	Chronic inflammation	16
2.2.3	Fibrosis	17
2.3	<i>Metabolism of PUFAs</i>	18
2.3.1	Cyclooxygenases	18
2.3.2	Lipoxygenases	18
2.3.3	CYP450	19
2.3.4	Endocannabinoids	20
2.3.5	Soluble epoxide enzyme	21
2.3.6	Soluble epoxide enzyme inhibitors	22
2.3.7	Biological actions of EpDPAs and EpDPA-EAs	24
2.3.8	Previous work on EpFA-mimics	25
2.3.9	Mimics synthesized by the LIPCHEM group	28
3	Synthetic methods	30
3.1	<i>Parikh-Doering oxidation</i>	30
3.2	<i>Wittig reaction</i>	31
3.3	<i>O-alkylation in the presence of an ester</i>	33
3.4	<i>Protection of alcohols with silyl groups</i>	34
3.5	<i>Amide coupling with CDI</i>	35
4	Results and discussion	37
4.1	<i>Overview</i>	37
4.2	<i>Synthesis of Wittig salt 2</i>	38
4.2.1	Synthesis of 12-bromododecanal 10	38
4.2.2	Characterization of 12-bromododecanal 10	39
4.2.3	Synthesis of Z-alkene 12	39
4.2.4	Characterization of Z-alkene 12	40
4.2.5	Synthesis of Wittig salt 2	41
4.2.6	Characterization of Wittig salt 2	41
4.3	<i>Synthesis of aldehyde 1</i>	43
4.3.1	Alkylation of alcohol 13	43
4.3.2	Characterization of ether 14	44
4.3.3	Reduction of ester 14	45
4.3.4	Characterization of alcohol 15	45
4.3.5	Oxidation of alcohol 15	46
4.3.6	Characterization of aldehyde 1	47
4.5	<i>Synthesis of aldehyde 3</i>	48
4.5.1	Hydrolysis of <i>gamma</i> -caprolactone	49
4.5.2	Characterization of ester 17	50
4.5.3	Alkylation of alcohol 17	50
4.5.4	Reduction of <i>gamma</i> -caprolactone	51

4.5.5	Characterization of diol 19	53
4.5.6	Selective TBS-protection of diol 20	53
4.5.7	Characterization of TBS-protected alcohol 20	54
4.5.8	Synthesis of ether 21b.....	54
4.5.9	Characterization of ether 21a.....	55
4.5.10	Characterization of deprotected alcohol 21b	56
4.5.11	Oxidation of alcohol 21b	57
4.5.12	Characterization of aldehyde 3	58
4.6	Synthesis of target molecules.....	59
4.6.1	Synthesis of Z-alkene 4	59
4.6.2	Characterization of Z-alkene 4	60
4.6.3	Synthesis of 19,20-EpDPA mimic 6.....	60
4.6.4	Characterization of 19,20-EpDPA mimic 6	61
4.6.5	Synthesis of Z-alkene 5.....	63
4.6.6	Characterization of Z-alkene 5	64
4.6.7	Synthesis of 19,20-EpDPA mimic 7.....	65
4.6.8	Characterization of 19,20-EpDPA mimic 7	65
4.6.9	Synthesis of 19,20-EpDPA-EA 9	68
4.6.10	Characterization of 19,20-EpDPA-EA mimic 9	69
4.6.11	Synthesis of 19,20-EpDPA-EA 8	71
4.6.12	Characterization of 19,20-EpDPA-EA mimic 8	71
5	Conclusion.....	75
5.1	Future works.....	76
6	Experimental.....	77
6.1	Material and apparatus.....	77
6.2	Experimental procedures.....	78
6.2.1	Synthesis of 12-bromododecanal 10.....	78
6.2.2	Synthesis of Z-alkene 12	78
6.2.3	Synthesis of Wittig salt 2.....	79
6.2.4	Synthesis of ether 14.....	80
6.2.5	Reduction of ester 14.....	80
6.2.6	Synthesis of aldehyde 1	81
6.2.7	Synthesis of Z-alkene 4.....	82
6.2.8	Synthesis of target molecule 6.....	82
6.2.9	Hydrolysis of <i>gamma</i> -caprolactone.....	83
6.2.10	Reduction of <i>gamma</i> -caprolactone	84
6.2.11	Selective TBS-protection of compound 19.....	85
6.2.12	Alkylation and deprotection of compound 20	85
6.2.13	DMP oxidation of alcohol 21b.....	86
6.2.14	Synthesis of Z-alkene 5.....	87
6.2.15	Synthesis of target molecule 7	88
6.2.16	Synthesis of 19,20-EpDPA-EA mimic 9.....	88
6.2.17	Synthesis of 19,20-EpDPA-EA mimic 8.....	89
7	References	91

1 Aim of study

The aim of this project in medicinal chemistry was to synthesize stable mimics of 19,20-epoxydocosapentaenoic acid (EpDPA) and its ethanolamide. These compounds could contribute toward the understanding of their biological activities in biochemistry, disease, and health. Recent studies have revealed that the compounds exert anti-inflammatory¹, anti-fibrotic², antihyperalgesic³, and cardioprotective⁴ effects. In addition to exerting biological activity, the mimics should be stable to enzymatic degradation, especially the soluble epoxide hydrolase enzyme (sEH) and other enzymatic degradation pathways.

In September 2021, the LIPCHEM group initiated their effort toward synthesizing these new stable 19,20-EpDPA analogs. Initially, either amide, urea, or oxamide was applied as a bioisosteric group for the epoxide in the 19,20-position. Overall, alkoxy groups are to a lesser extent investigated. For this study, ethyl ethers of both the 19,20-EpDPA acids and ethanolamides (EA) will be prepared as the bioisosteric group.

The mimics **6-9**, displayed in Figure 1 below, will be sent in for biological evaluation. The biological screening will be performed in collaboration with research groups in the network of Professor Bruce D. Hammock at the University of California, Davis. The biological testing will involve their ability to reduce lipopolysaccharide-induced neuroinflammation and oxidative stress in BV2 microglia cell lines. Additionally, the compounds will be evaluated for their ability to reduce alkali-induced fibrosis in both mice and cell-line models.

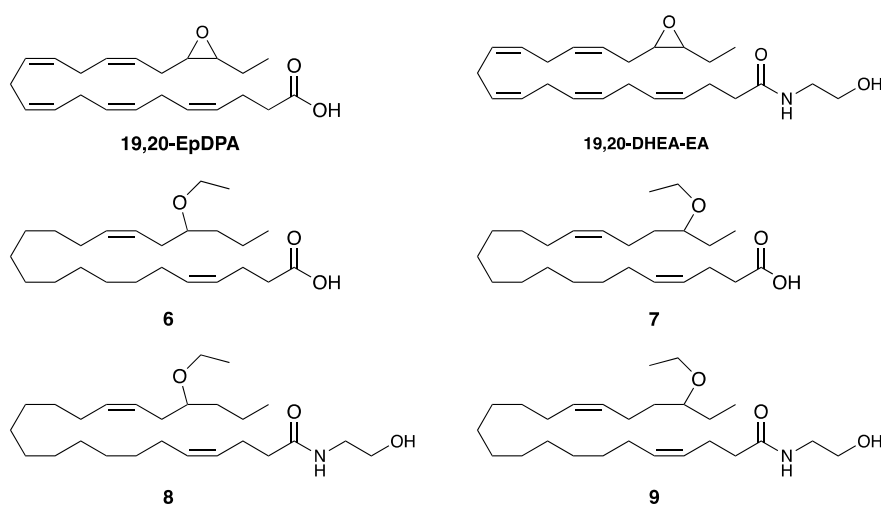
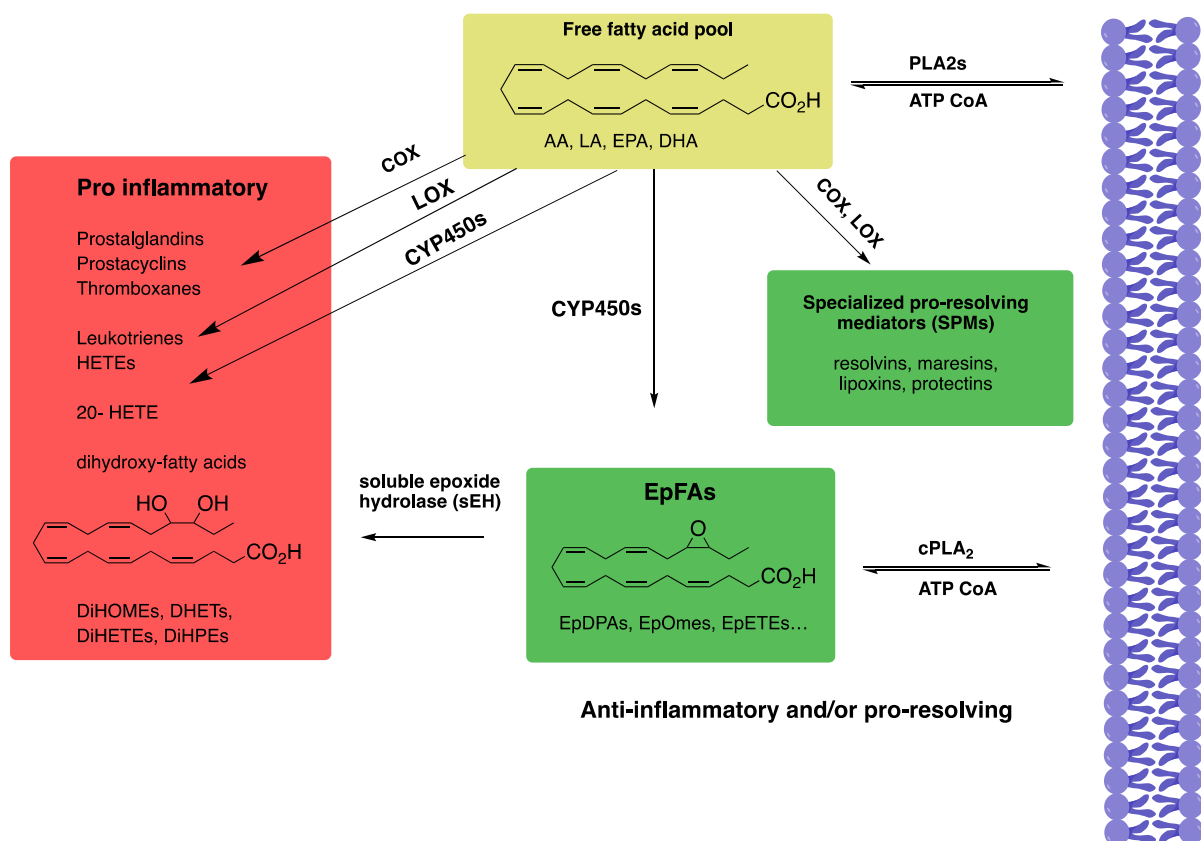


Figure 1 Endogenous 19,20-EpDPA and -EpDPA-EA, and the mimics of 19,20-EpDPA (**6** and **7**) and 19,20-EpDPA-EA (**8** and **9**).

2 Introduction

Endogenous lipid mediators derived from ω -3 and ω -6 polyunsaturated fatty acids play a key role in regulating the initiation and resolution of inflammation⁵. Recently, attention has been drawn to a specific type of lipid mediator- epoxy fatty acids and their role in inflammation resolution. Most of the studies have focused on epoxygenated fatty acids (EpFAs) derived from Arachidonic acid and their pro-inflammatory properties⁶. In contrast, fewer studies have examined the anti-inflammatory properties of EpDPA (epoxydocosapentaenoic acid), derived from docosahexaenoic acid⁷. Recent studies have shown that EpDPAs are central in angiogenesis, vascular dilation, inflammation, and cell differentiation^{1, 8, 9}. DHA and its epoxy metabolites will be the focus of this introduction. The metabolic pathways of polyunsaturated fatty acids (PUFAs) are displayed in Scheme 1.



Scheme 1 Metabolism of the PUFAs LA, AA, EPA, and DHA. Modified Figure from Morisseau and Hammock¹⁰.

2.1 Polyunsaturated fatty acids

Fatty acids consist of a chain of carbon atoms, containing a carboxylic acid at one end and often a methyl group at the other. The carbon atom next to the carbonyl is referred to as *alpha* (α) and the subsequent one is referred to as *beta* (β). Moreover, the carbon atom in the methyl group is designated *omega* (ω). Fatty acids can be categorized by their level of saturation. Those containing a double bond are classified as unsaturated and termed polyunsaturated if containing several double bonds. Likewise, if containing only one double bond they are termed monounsaturated fatty acid (MUFA). If the fatty acid only contains single bonds it is called a saturated fatty acid. Further characterization is based on the location of the last double bond of the omega end. A fatty acid with a double-bond between the third and fourth carbon is called ω -3 fatty acid, this applies to other positions such as double bonds between carbon 5 and 6 would be a ω -6 fatty acid. The alkene can either have *Z*- or *E*-configuration, which means that the hydrogens are on the same side of the double bond or each side respectively¹¹. Three of the most important PUFAs in humans are arachidonic acid (ω -6), docosahexaenoic acid (ω -3) and eicosapentaenoic acid (EPA, ω -3), displayed in Figure 2.

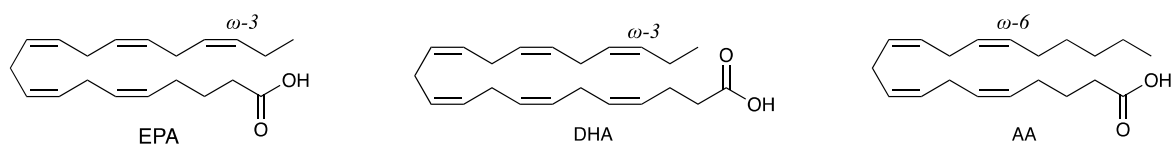
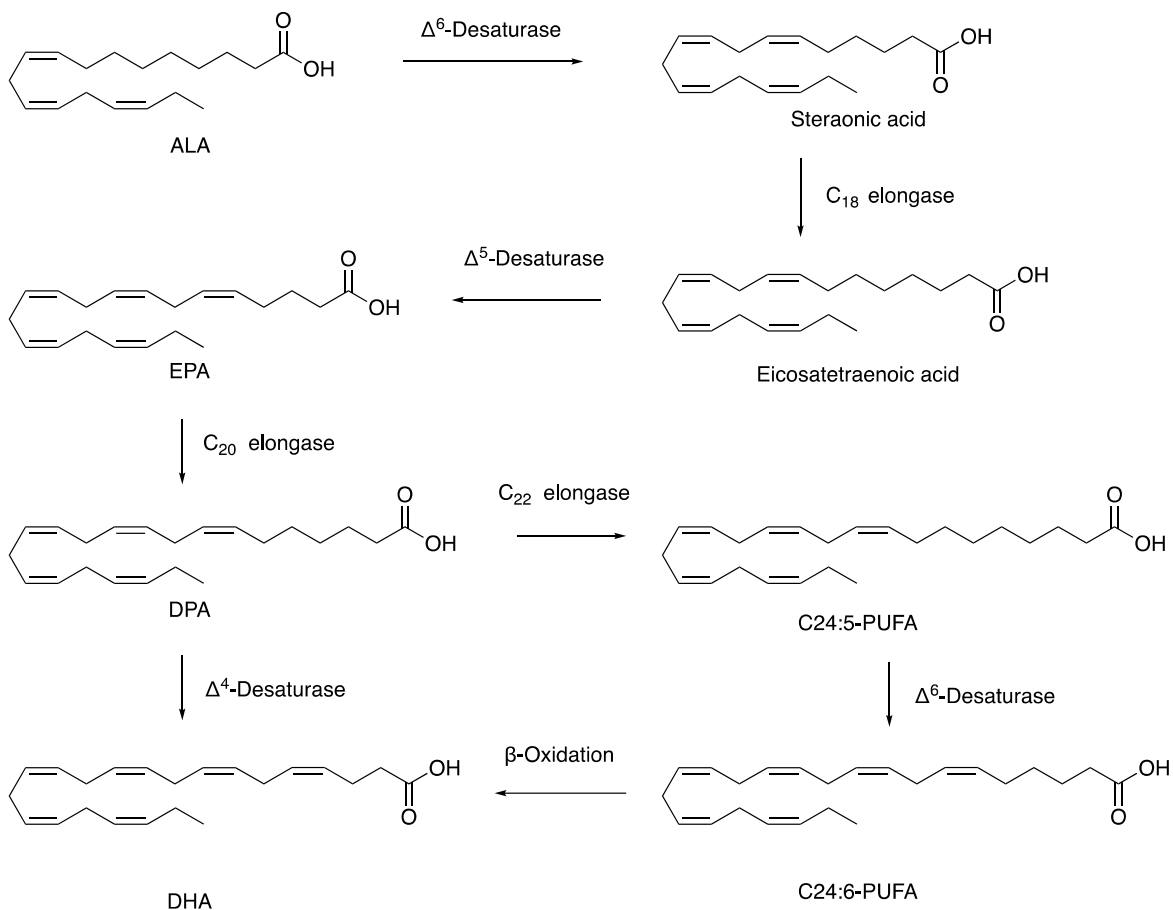


Figure 2 Chemical structures of the PUFAs EPA, DHA, and AA.

2.1.1 Biosynthesis of PUFAs

Humans need PUFAs to synthesize a variety of different important physiological molecules. However, humans cannot synthesize ω -3 and ω -6 PUFAs. Therefore, they must be provided through the diet *or* be biosynthesized from other essential fatty acids. Linolenic acid (LA) and *alpha*-linolenic acid (ALA) can be found in several vegetable oils, such as rapeseed oil. These can be converted to longer-chain PUFAs. LA is the precursor to AA, and ALA to DHA and EPA. Desaturases and elongases located in the liver will convert the essential fatty acids to ω -3 and ω -6 PUFAs^{5 12}. The biosynthesis of the mentioned fatty acids is displayed in Scheme 2.



Scheme 2 Outline of the biosynthesis for EPA, DHA, and AA. For simplicity, free acids are drawn. Modified scheme from A. Vik and T. V. Hansen¹³.

DHA is one of the most abundant ω -3 PUFAs in the brain. Up to 20 % of the gray matters total lipids consist of DHA¹⁴. It is also a key component in neural tissue and an important modulator of the central and enteric nervous system¹⁵. In addition, DHA is involved in anti-inflammatory processes and affects cellular characteristics, such as membrane fluidity and neuronal cell growth and differentiation¹⁵.

The biosynthesis of DHA is not fully understood. It is thought to occur from the diet by converting EPA via docosapentaenoic acid (DPA) as an intermediate. However, a rather new hypothesis, “The Sprecher shunt” suggests that DHA is synthesized by a retro-conversion route by *beta*-oxidation in peroxisomes, called the aerobic Δ^4 desaturation-independent pathway¹⁶. Thus, EPA is twice elongated yielding a 24-carbon intermediate, thereafter desaturated and then

shortened to DHA by beta-oxidation. This hypothesis is bolstered by the identification of a *Thraustochytrium* $\Delta 4$ desaturase involved in the synthesis of DHA¹⁷.

2.2 Inflammation

Inflammation is divided into acute and chronic inflammation, depending on the extent and duration of the process. Acute inflammation can result in chronic inflammation when left uncontrolled. This can lead to a variety of diseases such as cardiovascular disease, diabetes, chronic kidney disease, and cancer¹⁸. Untreated inflammation can result in fibrosis, defined as overgrowth and the formation of scarring tissue. Fibrosis can lead to unnormal organ function and thereby fibrotic diseases¹⁹.

2.2.1 Acute inflammation

Acute inflammation is, if controlled, generally beneficial. The inflammation response protects the body against noxious stimuli such as infectious organisms and restores homeostasis. It is an innate adaptive response with limited specificity. The reaction will recruit soluble mediators like cytokines, acute phase proteins, and chemokines to promote the migration of neutrophils and macrophages to the area of inflammation²⁰.

Macrophages at site recognize harmful substances via receptors of the innate immune system, such as Toll-like receptors (TLRs). Microbial toxins such as lipopolysaccharides are recognized by these receptors. The initial recognition leads to the production of a variety of inflammatory mediators, including chemokines, cytokines, vasoactive amines, eicosanoids, and products of proteolytic cascades¹⁵. Blood vessel dilatation allows selective extravasation of neutrophils and prevents the exit of erythrocytes. Granulocytes, mainly neutrophils, will arrive at site first. These can both absorb microbes and injured tissue, in addition to secrete substances that dissolve dead tissue¹⁵. A microscopic view of inflamed lungs is displayed in Figure 3.

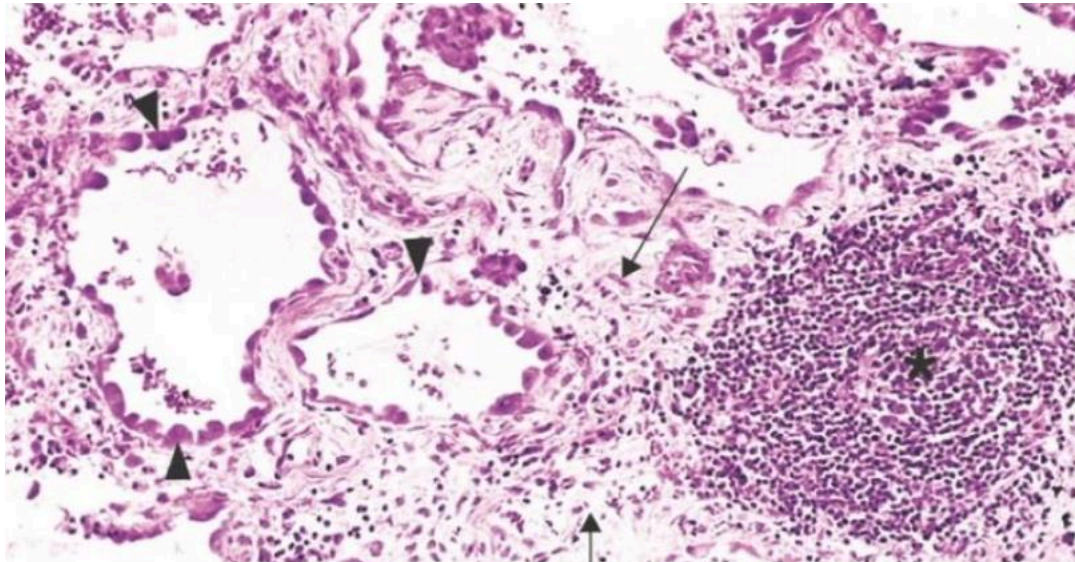


Figure 3 Microscopic view of inflamed lungs, showing both recruitment of chronic inflammatory cells (asterisk) and fibrosis (arrows). Figure adapted from K. Primdahl²¹.

A successful acute inflammatory response should result in the elimination of the infectious agent, and result in a resolving and repairing phase. This process is mediated by the tissue-resident macrophages. First, prostaglandins act as the pro-inflammatory lipid mediator dominating the initial phase of inflammation. The activation of macrophages results in a switch of the metabolic pathways of PUFAs. The metabolic pathway changes result in increased levels of lipoxins, resolvins, maresins, and protectins which have been shown to have anti-inflammatory and resolving properties²²⁻²⁶. These mediators are collectively termed specialized pro-resolving mediators (SPMs). The SPMs promote the resolution of inflammation by regulating leukocyte trafficking, polymorphonuclear neutrophil-, and monocyte recruitment. Restoration of homeostasis is obtained by the activation of macrophage-assisted phagocytosis which clears the inflammatory exudate and tissue damage²⁷.

2.2.2 Chronic inflammation

If acute inflammation is not resolved, it may result in chronic inflammation. Chronic inflammation is a slow, long-termed inflammation lasting for several months, even up to years. The extent and effects may vary from disease to disease⁵. Many of the features of acute inflammation such as vasodilatation, capillary permeability, and diapedesis will continue through the chronic state. Eventually, there will be a predominance of macrophages, lymphocytes, and plasma cells, replacing the short-lived neutrophils at the inflammation site.

These cells start producing inflammatory cytokines, and growth factor enzymes- contributing to the development of tissue damage and secondary repair including fibrosis⁵.

The hallmark of acute inflammation is the accumulation of white blood cells, including eosinophils. These cells are designed to neutralize and eliminate hazardous agents. Upon fulfilling their role, the white blood cells must be removed. If not removed they could do untold damage by releasing hydrolytic and proteolytic enzymes as well as generating reactive oxygen species²⁸. Therefore, the white blood cells undergo apoptosis when finished. The apoptotic cells express surface molecules that allow their recognition and phagocytosis by macrophages²⁸. Recognition by the macrophages may lead to the release of anti-inflammatory cytokines such as interleukin-10 (IL-10) and tumor growth factor beta (TGF β). If the apoptotic cells are not recognized and disposed of, they may undergo secondary necrosis releasing damaging intracellular contents and amplifying the inflammatory response²⁸. It has been suggested that delayed apoptosis is a central element in various inflammatory diseases such as Crohn's disease, asthma, and chronic obstructive pulmonary disease^{28, 29}.

2.2.3 Fibrosis

Untreated chronic inflammation can result in fibrosis. Fibrosis is an exaggerated wound-healing response resulting in the thickening of the affected tissue, which can result in dysfunctional organs³⁰.

After inflammation, the tissue has most likely been damaged and needs repair. The normal end phase of inflammation and wound healing involves the release of essential growth factors and cytokines, such as TGF β . TGF β is released by macrophages and platelets at the infected site. TGF β is the main driving force of fibroblast differentiation to myofibroblasts. Myofibroblasts are responsible for the synthesis of collagen and extracellular matrix, which is important in wound healing³¹.

The myofibroblasts need high contractile ability to generate tissue contractures. α -smooth muscle actin (α SMA) is a globular multi-functional protein that can form microfilaments, which strengthens the contractures. α SMA is therefore commonly used as a marker of myofibroblast formation, indicating fibrosis³².

Well-known fibrotic diseases include pulmonary fibrosis, sclerosis, liver cirrhosis, cardiovascular fibrosis, and nephritis³³⁻³⁶.

2.3 Metabolism of PUFAs

PUFAs can be found in the body circulating as free fatty acids (FFA) but also incorporated in the cell membranes as glycerides. Upon stress or injury, the body will release the PUFAs from the cell membrane via enzymes such as phospholipase acetyltransferases (PLA). The PUFAs are released at the sn-2 position of the glycerol backbone of the phospholipids. When freed from the membranes, FFAs are readily metabolized by β -oxidation¹.

The regulation of the metabolic pathways of PUFAs is essential to maintain homeostasis and prevent disease¹. There are three main enzymes responsible for the non-catabolic metabolism of PUFAs, including the cyclooxygenases (COX), lipoxygenases, and cytochrome P 450s (CYP)³⁷. The different enzymatic pathways will result in diverse bioactive mediators¹.

2.3.1 Cyclooxygenases

One of the three main pathways of PUFA metabolism is through the COX enzymes. These enzymes are responsible for the conversion of AA to eicosanoids, such as prostaglandins, prostacyclins, and thromboxanes. The COX enzyme exists in two isoforms, namely COX-1 and COX-2. COX-1 produces the mediators associated with normal physiologic function. The main responsibilities of these mediators include vasodilatation, blood platelet suppression, reducing gastric acid secretion, and regulating smooth muscle contraction^{28, 38-40}. COX-2 on the other hand is induced by inflammation and produces mediators associated with pro-inflammatory properties, which can cause fever and pain⁴¹. Moreover, prostaglandins work as lipid mediators, causing a switch from pro- to anti-inflammatory and pro-resolving mediators³⁸⁻⁴⁰.

2.3.2 Lipoxygenases

LOX enzymes are enzymes catalyzing the dioxygenation of PUFAs into lipid mediators such as leukotrienes, hepoxilins, and SPMs. SPMs are composed of lipoxins, E-series and D-series resolvins, protectins, and maresins. Their precursors are AA, EPA, DHA, and DPA. These mediators are important in neutrophil recruitment to the inflammatory site and clearance of

bacteria and apoptotic cells, hence important in shortening and ending the inflammatory response⁴². The LIPCHEM group, in collaboration with groups led by Professor Serhan and by Dr. Jesmond Dalli, has contributed to several publications related to the synthesis and structural elucidations regarding SPMs⁴³⁻⁴⁵.

The leukotrienes are synthesized from AA through another group of LOX enzymes, especially LOX-5. Interaction with G-protein coupled receptors (GPCRs) on the cell surface of immunocompetent cells, such as leukocytes, results in pro-inflammatory responses. Biological actions of leukotrienes include improved vascular permeability, bronchoconstriction, and recruitment of eosinophils in asthma^{14, 23, 26}.

2.3.3 CYP450

CYP450 metabolizes PUFAs to EpFAs, primarily by the subfamilies CYP2C and CYP2J¹. Depending on their precursor, the resulting EpFAs are referred to as epoxyeicosatrienoic acids, epoxyeicosatrienoic acids (EEQ), and EpDPAs derived from AA, EPA, and DHA, respectively⁴⁶. These EpFAs have been proven to have beneficial effects on inflammation¹, fibrosis², pain³, and the cardio-vascular system⁴. The regulation of EpFAs mainly occurs by release from cell membranes, biosynthesis, and degradation. Among the various enzymes involved in their metabolism, the sEH enzyme is the major degradation route in most tissues. The sEH enzyme will be further described later on. Other degradative routes involve autooxidation, β -oxidation, and esterification^{46, 47}.

The CYP epoxygenases add a molecular oxygen atom to a double bond forming an epoxide. Only *cis*-epoxides are formed by the CYP450 enzymes⁴⁸. The epoxygenases can epoxidize each of the double bonds of the PUFA, but often a certain epoxygenase favors certain regioisomers. Preferentially, the ω -3 double bond of EPA and DHA are oxidized. Little information about selectivity is obtained from the epoxidation of DHA, therefore the isomerism of EET will be discussed further. Each of the EET regioisomers consists of both the *R/S* and the *S/R*⁴⁹. However, the enantiomeric distributions are different for each epoxygenase, and the same epoxygenase will often have a different enantiomeric distribution of the two regioisomers⁷. Studies of the CYP enzyme indicate that the main product often is the 11,12- and 14,15-EET. This information could be transferred to the understanding of EpDPA regioisomers⁸.

It has also been observed enantiomeric dependence for some EET functions^{50, 51}. For example, an experiment performed by Zou *et. Al* demonstrated that 11,12-EET-induced relaxation of rat renal microvessels is only mediated by the 11(*R*),12(*S*)-EET regioisomers⁵⁰. Another experiment carried out by Wong *et Al.* demonstrated that the 14(*R*),15(*S*)-EET had a higher affinity to the mononuclear cells of guinea pigs than its enantiomer⁵². The 14(*S*),15(*R*)-EET, in contrast, was more potent in activating smooth muscle calcium-activated potassium channels in smooth muscle and dilating bovine coronary arteries.

2.3.4 Endocannabinoids

Endocannabinoids (eCBs) are another group of lipid mediators derived from ω -6 and ω -3 PUFAs. The CYP-enzymes are also mediating the epoxidation of the olefins of eCBs. Two of the most studied eCBs are arachidonoyl ethanolamide (AEA) and 2-arachidonoyl glycerol (2-AG)⁵³, displayed in Figure 4. DHA is also metabolized to its corresponding endocannabinoid, docosahexanoyl ethanolamide (DHEA) by the CYP enzyme.

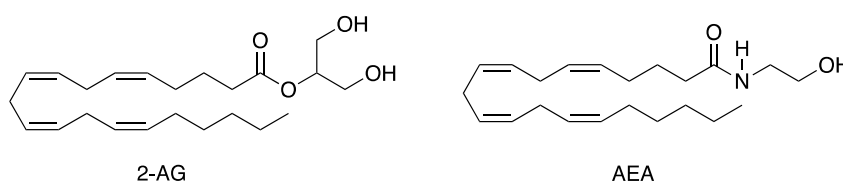


Figure 4 Outline of the chemical structure for 2-AG and AEA.

eCBs mimic the effects of Δ 9-tetrahydrocannabinol, the main psychotropic constituent of marijuana. The eCBs are ligands for the two GPCRs cannabinoid receptor (CB) 1 and 2. The first identified cannabinoid receptor is the CB1, and is the most abundant GPCR in the central nervous system⁵³. One of its most important roles is to mediate behavioral functions. However, it is also to a lesser extent found in the cardiovascular, pulmonary, intestinal, and reproductive tissues. CB2, on the other hand, is mostly expressed in the spleen and immune cells. B lymphocytes, macrophages, and natural killer cells are the immune cells with the highest level of CB2 receptors⁵³. Since CB2 is involved in neuroinflammation, it is of interest to generate selective agonists for CB2. The agonist could be of therapeutic value to diseases such as Alzheimer's disease, multiple sclerosis, and Parkinson's disease^{54, 55}. In addition, several studies have revealed that eCBs appear to reduce microglia-promoted neuroinflammation through CB2.

Hence, the discovery of selective CB2 agonists will be important in the means of moderating inflammatory pathologies⁵⁶⁻⁵⁸.

Further, DHEA is a substrate for the CYP epoxygenases resulting in the corresponding EpDPA-EA. Recent studies have reported that the terminal epoxide 19,20-EpDPA-EA exert dose-dependent inhibition of pro-inflammatory interleukin-6 (IL-6) cytokine and increase of anti-inflammatory IL-10⁵⁹. Both structures are displayed in Figure 5.

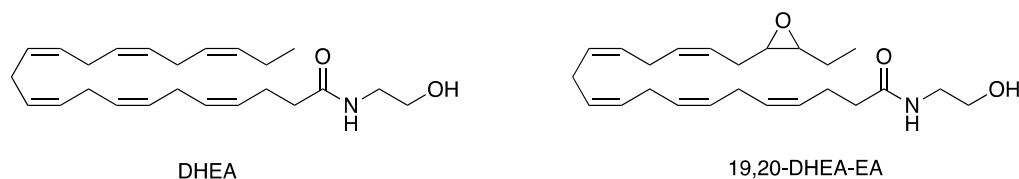
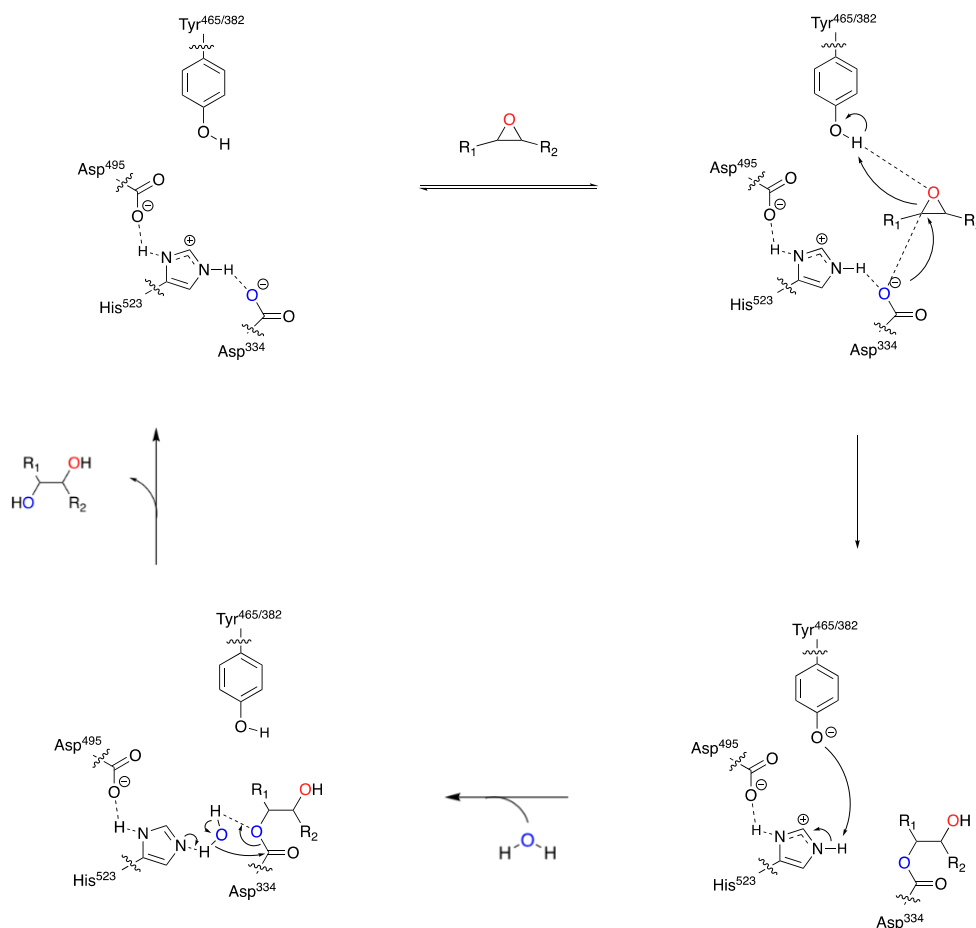


Figure 5 Chemical structures of DHEA and the metabolite 19,20-DHEA-EA regioisomer.

2.3.5 Soluble epoxide enzyme

EpFAs undergo metabolic transformation to their corresponding diols by the sEH enzyme. sEH enzymes are to be found in numerous tissues, but mainly in the liver and kidney tissue. The distribution can vary dramatically within the same organ among the different cell types⁶⁰.

The enzyme comprises a homodimer consisting of two subunits connected by a proline-rich peptide segment⁶¹. Herein, the epoxide hydrolase activity lies in the C-terminal domain, whereas the N-terminal domain is a catalytic site for phosphatase, with apparent specificity for fatty acid diol phosphates⁶². Within the epoxide hydrolase catalytic pocket, two tyrosine residues (Tyr381 and Tyr465) facilitate the ring opening. Through an S_N2-type reaction, the epoxide will be activated by forming a hydrogen bond with one of the tyrosines. Subsequently, a nucleophilic attack by Asp333 forms an acyl-enzyme intermediate, which is attacked by a water molecule activated by His523. The result is an unstable tetrahedral intermediate which finally collapses to form the diol product⁶³. The proposed catalytic mechanism is outlined in Scheme 3.



Scheme 3 Outline of the proposed catalytic mechanism of sEH⁶⁴.

These diols are considered less active than the EpFAs⁶⁵. Along with this, they are far more polar and rapidly conjugated than the EpFAs and will therefore diffuse out of the cells quicker⁶⁶.

Most of the ω -3 EpFAs are metabolized by sEH more rapidly than EETs, except for the 19,20-EpDPA. The low turnover and high biosynthesis make 19-20-EpDPA the most abundant ω -3 EpFA *in vivo*⁶⁷.

2.3.6 Soluble epoxide enzyme inhibitors

The biological properties of EpFAs have mainly been studied utilizing sEHIs to increase the concentrations of EpFAs in the body. Increasing EpFa concentrations have been shown to reduce the severity of a variety of diseases in laboratory settings¹⁰.

Structure-relationship studies (SAR) suggest that there are three central pharmacophores¹⁰. The primary pharmacophore mimics the oxygen atom of an EET epoxide interacting with Tyr383

and Tyr466 by a hydrogen bond. The hydrogen bond acceptor in the mimic is a carbonyl of either an amide or urea. As for the second structural feature, it involves the N-H group of an amide or urea group interacting with Asp335¹⁰. The polar functional group should be ~7 Å away from the urea carbonyl. This secondary pharmacophore was discovered after the study of 5-substituted piperazine, by the Long group¹⁴. Polar groups will also enhance the solubility and pharmacokinetic properties of the analogs. Additionally, a tertiary pharmacophore has been identified, in which the polar group should be 13 atoms or ~17 Å away from the urea carbonyl. Finally, the linker, connecting the pharmacophores, can be either a flexible alkyl or a restricted cyclic structure¹⁴. The sEH_i, with outlined pharmacophores, is displayed in Figure 6.

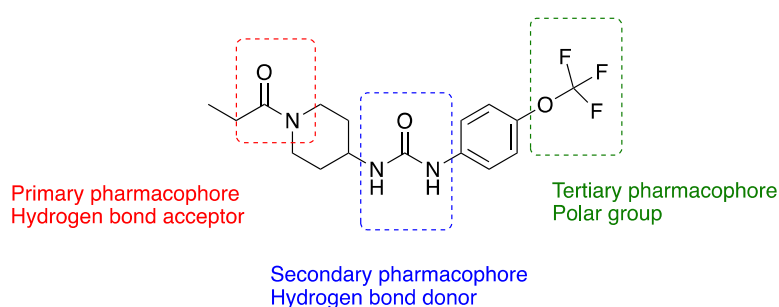


Figure 6 Outline of the different pharmacophores for the sEH_i TPPU.

One of the sEH_i, EC5026 (displayed in Figure 7), developed by Hammock *et al.*, has progressed to a human phase 1a study. It was investigated as an orally active analgesic resolving inflammation and neuropathic pain. The studies look promising for the advancement of EC5026 into multiple ascending dose Phase 1b studies⁶⁸. A recent animal study has also shown that the same drug candidate successfully relieved chemotherapy-induced peripheral neuropathy⁶⁹.

Another experiment found that levels of the sEH enzyme metabolite 19,20-dihydroxy-EpDPA in diabetic mouse retinas were increased. The sEH enzyme was hence identified as an important enzyme initiating pericyte loss and breakdown of endothelial barrier function by the generation of the pro-inflammatory metabolite. Treatment with the sEH inhibitor *t*-AUCB, displayed in Figure 7, prevented these effects⁷⁰.

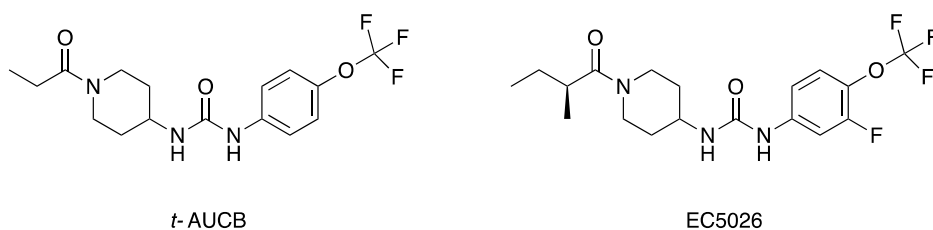


Figure 7 Chemical structures of the sEHIs, synthesized by Hammock and co-workers⁷⁰.

2.3.7 Biological actions of EpDPAs and EpDPA-EAs

Limited research has been devoted to EpDPAs, which makes the development of their mimics attractive. Notwithstanding the lack of research into EpDPAs, some projects have investigated their function as auto- and paracrine mediators, regulating both inflammation and vascular tone. More studies have on the other hand examined other EpFAs, especially EETs. Compared to the EETs, EpDPAs appear more potent acting as vasodilators and anti-inflammatory agents^{49, 67, 71, 72}.

Some studies have demonstrated the anti-inflammatory properties of 19,20-EpDPA. One of its bioactive properties is related to relaxing and anti-inflammatory effects on human pulmonary arteries⁷³. Another *in vivo* study demonstrated that the administration of 19,20-EpDPA alone was important in disease resolution of wet age-related macular degeneration in mice⁷⁴. In addition, other animal studies have revealed that the metabolite ameliorates hypertension, allergic intestinal inflammation, and kidney fibrosis⁷⁵. These findings together suggest a potential target of 19,20-EpDPA in anti-inflammatory therapy.

A research study from 2013 investigated the effects of the stable 19,20-EpDPA regioisomers on angiogenesis in mice. The most important findings were that the regioisomer reduces vascular endothelial growth factor (VEGF), the most important regulator of pathological angiogenesis, in mice⁷⁶. In addition, the same experiment demonstrated that the regioisomer significantly inhibited fibroblast growth factor 2 (FGF-2)-induced angiogenesis. These findings indicate that the 19,20-EpDPA regioisomer may exert its anti-cancer effects by inhibiting VEGF-mediated angiogenesis.

The 19,20-EpDPA-EA also exerts anti-inflammatory effects. An experiment carried out in the Das lab examined the EpDPA-EA's affinity to the CB receptors⁷⁷. They demonstrated that the

epoxygenation of the DHEA led to an altered CB1 and CB2 activity profile. Furthermore, they examined the anti-inflammatory effects of these molecules in an *in vitro* model of neuroinflammation. The 19,20-EpDPA-EA exerted the most potent dose-dependent reduction of pro-inflammatory markers. Additionally, the Das group demonstrated that the 19,20-EpDPA-EA exert vasodilatory and angiogenic effects⁷⁷.

2.3.8 Previous work on EpFA-mimics

EpDPA analogs are possible substrates for a range of different metabolic degradation routes. Including *beta*-, *omega*-, auto-oxidation, and epoxide hydrolysis executed by the sEH enzyme. By modifying these sites it is possible to enhance stability and improve biological activity. The thought metabolism and degradation of the 19,20-EpDPA are displayed in Figure 8.

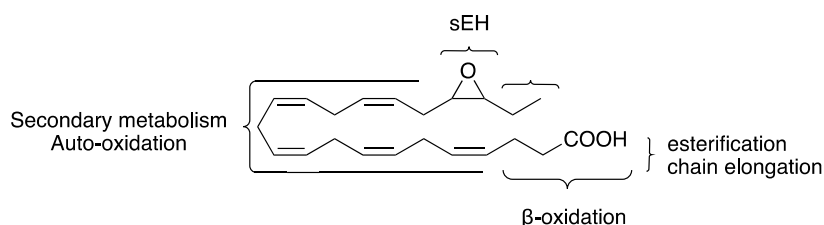


Figure 8 Outline of the possible metabolism and degradation of 19,20-EpDPA. Figure modified from J. R. Falck *et al.*⁴⁷.

As of today, no SAR studies have examined the EpDPA mimics, specifically. Studies have investigated the effects of exchanging the epoxide group of EETs and EEQs with bioisosteres^{47, 78}. Typical bioisosteric groups include but are not limited to, amides, *N*-hydroxyurea, oxamides, and alkoxy groups, similar to those applied for the sEHi. All of the mentioned bioisosteres have at least one hydrogen bond acceptor, similar to the epoxide group, implying they should have similar chemical properties. Most importantly, the bioisosteres are not subjected to hydrolysis by the sEH enzyme.

J. R. Falck and coworkers performed SAR studies on the 17,18-EET, revealing that a *cis*-11,12- or 14,15-olefin, in addition to the epoxide, were minimal structural features for anti-arrhythmic activity. They also found that the introduction of *N*-methyls onto the urea strongly dampened the anti-arrhythmic effect, while the 1,4-disubstituted oxamide was proven to be the most efficacious bioisostere⁷⁹. Two EET mimics with the current bioisosteres are displayed in Figure 9.

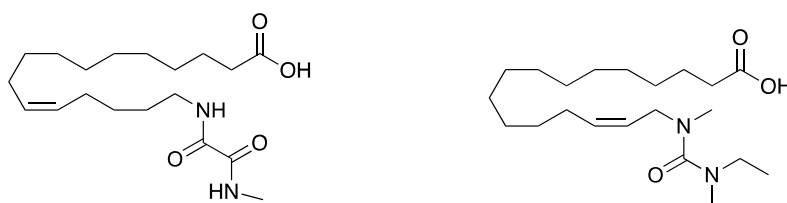


Figure 9 Chemical structure of previously reported 17,18-EET mimics ⁷⁹.

Since the olefins are subject to auto-oxidation, complete saturation should be avoided. Double bonds with *cis*-configuration are consistent with a shallow binding pocket. Thus, the double bonds should exhibit *cis*-configuration. Almost all of the EpFA mimics reported up until now have had one or several double bonds removed. Furthermore, the location of the kept double bonds seems to alter biological activity. For example, $\Delta^{11,12}$ - or $\Delta^{14,15}$ -olefins of the 17,18 EET analogs, displayed in Figure 9, are associated with agonist activity in relation to the anti-arrhythmic effects⁷⁹.

The carboxylic acid moiety can also be exchanged with bioisosteres. An experiment, from 2014 characterized an orally active antihypertensive 14,15-EET mimic (EET-A, displayed in Figure 10) protecting vascular endothelial function and lowering blood pressure⁸⁰. Here, aspartic acid was utilized as bioisostere in place of the carboxylic acid. Another experiment from 2019, demonstrated that the same EET analog exerts potent kidney protective and anti-inflammatory actions in mice⁸¹. More recently, EET-A has undergone further development by conjugating it to folic acid, resulting in the improved mimic EET-F01, displayed in Figure 10. A study from 2021 reports very promising protective effects of EET-F01 in cisplatin-induced nephrotoxicity in rats⁸². The EET-A and EET-F01 mimic are displayed in Figure 10.

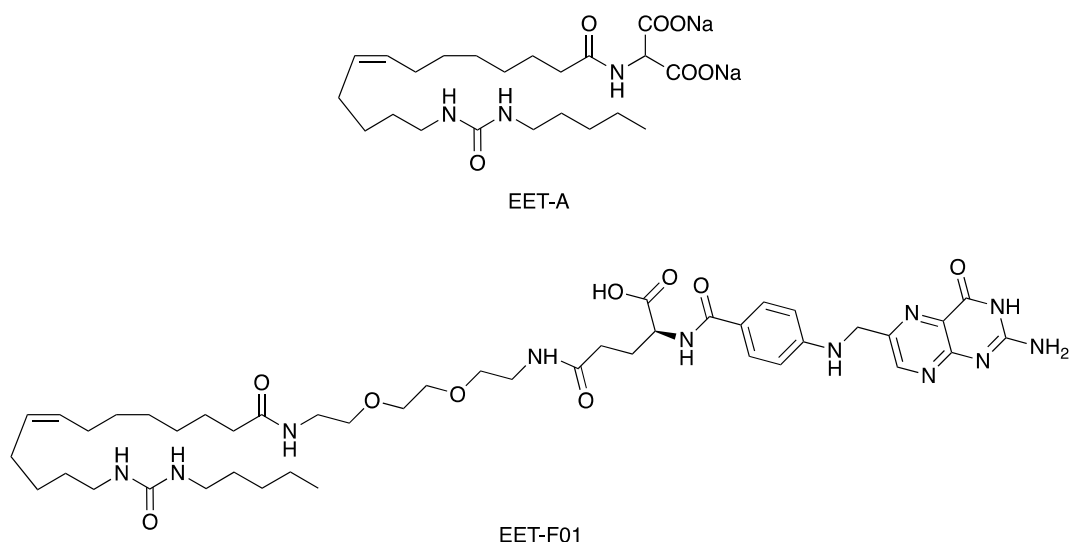


Figure 10 Outline of the chemical structures of EET-A and EET-F01^{81, 82}.

Shifting focus to the EEQ mimics, a SAR study from 2019 identified the carboxylic acid, *cis*-11,12-olefin, and 17(R),18(S)-epoxide as pharmacophores in the 17,18-EEQ as well. These structures were central in regard to exerting negative chronotropic effects. As for the EET mimics, oxamides and urea groups worked best as bioisosteres for the epoxide. Furthermore, the replacement of the *beta*-carbon with an oxygen atom abolished *beta*-oxidation. In the evaluated antiarrhythmic model, tetrazole was proven to be the most potent bioisostere for the carboxylic acid⁸³. Two third-generation 17,18-EEQ are displayed in Figure 11.

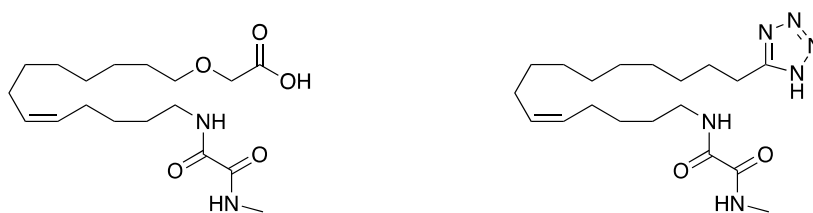


Figure 11 Chemical structure of previously reported 14,15-EEQ mimics⁸³.

A less investigated bioisostere for the epoxide is alkoxides. Incidentally, alkoxy groups were utilized as epoxide bioisosteres in compounds mimicking the juvenile hormones. Juvenile Hormone I (JH I) is important in the hormonal control of insect development. This discovery led to the initiative of discovering bioisosteres of its epoxide, which is readily metabolized by the insect epoxide hydrolase. Chemical modifications to the structure of JH I led to the discovery of alkyl and alkynyl dodecadienoates, such as methoprene. Both structures are

outlined in Figure 12. For decades, these compounds have been used as potent regulators for pest control⁶.



Figure 12 Outline of the structures for Methoprene and Juvenile hormone I.

An article written by Nalin *et Al.* compared different 17,18-EET alkoxy ether mimics regarding their effect on cytoprotection against high, acute cisplatin exposure. The alkoxy ethers consisted of a regioisomeric mixture. They concluded that all alkoxy ethers displayed bioisosteric activity but at different levels. Marginal effects were revealed for the methoxy, good for the *n*-propoxy and excellent for the ethoxy and *i*-propoxy⁷⁸. The ethoxy and *i*-propyl ether is displayed in Figure 13.

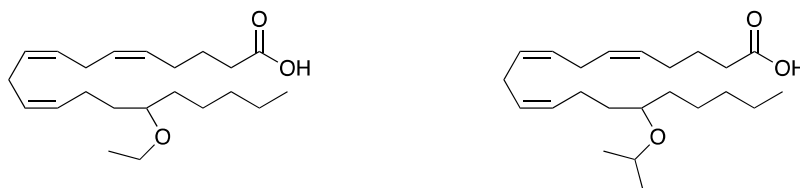


Figure 13 Outline of the chemical structure of previously reported 17,18-EET mimics⁷⁸.

An ongoing experiment carried out under the initiative of Dr. Hammock demonstrated through a mice model that EpDPAs are involved in the resolution of fibrosis. Two of the investigated mimics were designed and synthesized by our group. These preliminary studies demonstrated that the fibrosis was reduced by treatment with EpDPA mimics⁸⁴.

2.3.9 Mimics synthesized by the LIPCHEMA group

In September 2021, the LIPCHEMA group initiated their effort toward synthesizing new stable 19,20-EpDPA and ethanolamide mimics. Initially, the bioisosteres were either amide, urea, or oxamides. The six previously synthesized mimics displayed in Figure 14 have already been submitted for biological evaluation.

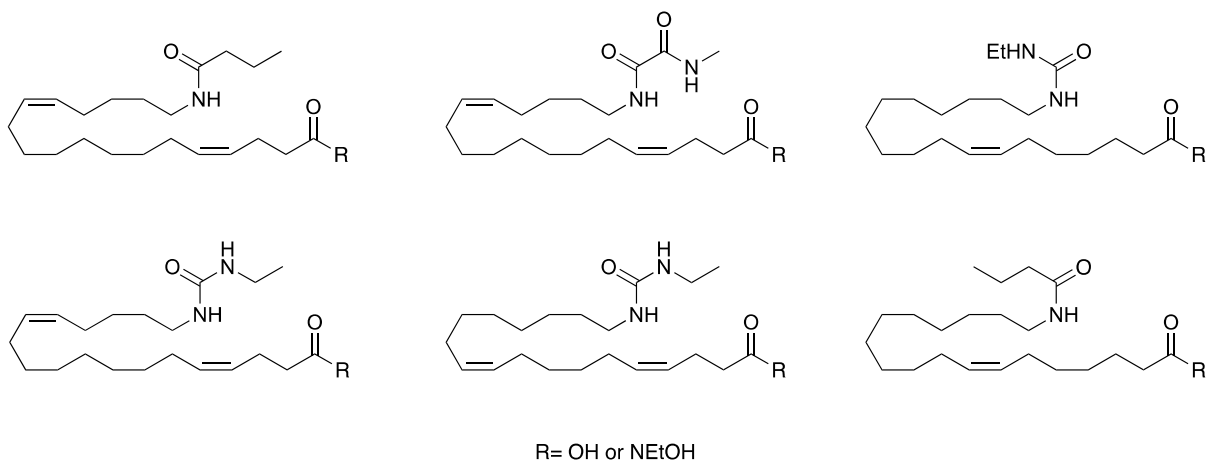


Figure 14 Outline of the previously synthesized 19,20-EpDPA and -EA mimics, prepared by the LIPCHEM group.

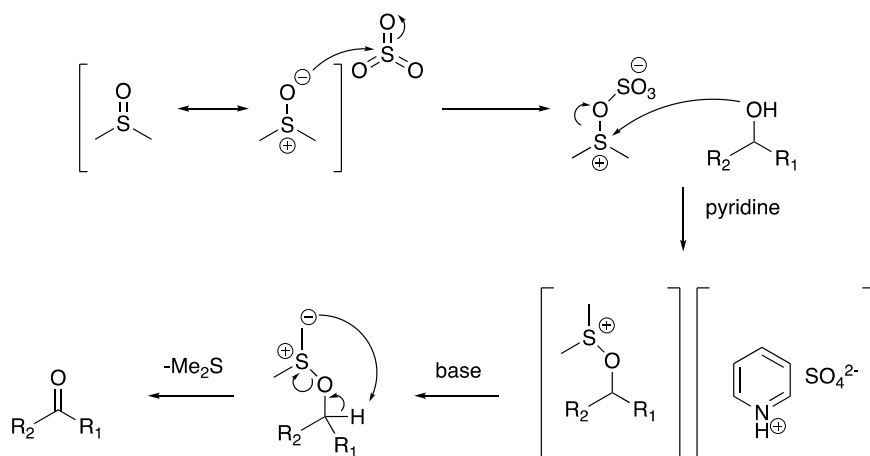
3 Synthetic methods

Herein, some of the key synthetic methods used in this thesis will be discussed.

3.1 Parikh-Doering oxidation

Aldehydes and ketones are important functionalities in a range of biologically active compounds. Additionally, they serve as essential reagents in modern organic chemistry. A central way of preparing these functional groups is by the oxidation of alcohols. The Parikh-Doering oxidation represents a modification of the commonly used Swern oxidation procedure. Compared to the Swern oxidation, the Parikh-Doering procedure exerts lower toxicity, is less sensitive toward water, and does not require low temperatures. It does however have some disadvantages. The byproduct methyl thiomethyl ether is negligible, but to a lesser extent than for the Swern oxidation. Additionally, the reaction is carried out very diluted, and sometimes larger amounts of dimethylsulfoxide (DMSO) are needed⁸⁵.

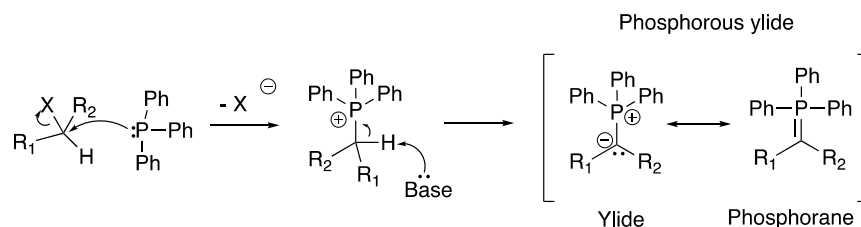
The Parikh-Doering procedure uses DMSO as the oxidant and cosolvent. Sulfur trioxide pyridine complex activates the oxidant in the presence of triethylamine (TEA). The mechanism, displayed in Scheme 4, starts with DMSO reacting with SO₃-pyridine to yield the intermediate. Thereafter, the alcohol performs a nucleophilic attack on the sulfur atom. An alkoxy sulfonium ion is formed, complexing with the anionic pyridinium sulfate complex. Next, at least two equivalents of the base must be added to deprotonate the alkoxy sulfonium ion to yield a sulfur ylide. Consequently, the pyridinium sulfate counterion is removed. Lastly, the ylide forms a five-membered ring in a transition state to yield the desired aldehyde/ketone⁸⁶.



Scheme 4 General outline of the Parikh-Doering oxidation mechanism⁸⁶.

3.2 Wittig reaction

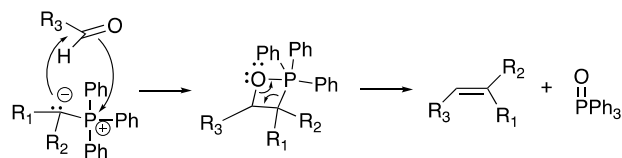
The German scientist Georg Wittig was in 1979 awarded the Noble Prize in chemistry for the valuable Wittig reaction. Wittig reactions are used to convert ketones and aldehydes into alkenes by forming a new C-C bond at the location of the carbonyl. The starting materials contain an aldehyde or ketone and a phosphorus ylide (phosphorane). An ylide is a neutral molecule that includes a negatively charged atom directly attached to a positively charged heteroatom. This ylide has a resonance structure that is free of any charges. Moreover, the phosphorus atom in the salt carries a positive charge making the adjacent proton acidic. Therefore, the ylide can easily be prepared by treating an alkyl halide with triphenylphosphine followed by a strong base deprotonating this acidic proton⁸⁷. The reaction is an SN₂-reaction, and is displayed in Scheme 5.



Scheme 5 Outline of the mechanism of the phosphorus ylide formation.

The full mechanism of the Wittig reaction is not fully understood. However, there is an agreement that an irreversible [2+2] cycloaddition of the phosphonium ylide to the electrophilic carbonyl compound forms a four-membered cyclic intermediate, a *syn*-oxaphosphetane. The

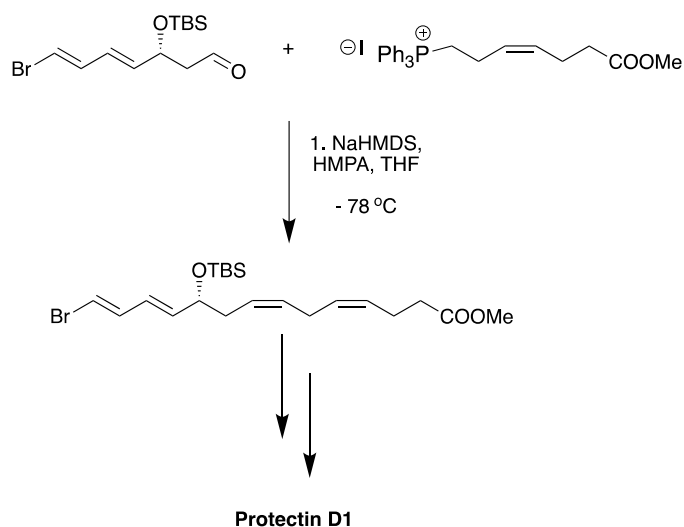
syn-oxaphosphetane then undergoes fragmentation to afford the alkene and forms triphenylphosphine oxide as a by-product⁸⁷. An outline of the mechanism is displayed in Scheme 6.



Scheme 6 Outline of a [2+2] cycloaddition mechanism for the Wittig reaction.

Stereoselectivity can be obtained by strategically choosing the properties of the ylide, counterion for the ylide formation, and type of carbonyl compound and solvent type⁸⁸. Stabilized ylides will result in alkenes with high to moderate (*E*)-selectivity. Stabilized ylides have at least one electron-withdrawing group adjacent to stabilize the negative charge. Moreover, polar aprotic solvents and the use of Lithium salts also favor (*E*)-alkenes. Unstabilized ylides will provide high (*Z*)-selectivity. These unstabilized ylides do not have the properties to stabilize the negative charge. Moreover, salt-free conditions in a dipolar aprotic solvent, as well as low temperature favor the (*Z*)-alkene. Semi-stabilized ylides will yield a mixture of the two isomers⁸⁸.

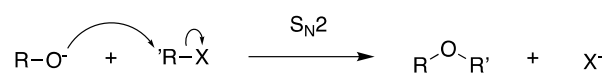
The Wittig reaction is one of the top C-C bond-forming reaction types in natural product chemistry⁸⁹. It has been frequently utilized in the LIPCHEM group to prepare polyunsaturated fatty acids and derivatives. For instance, a *Z*-selective Wittig reaction was applied in the preparation of the lipid mediator protectin D1, displayed in Scheme 7⁹⁰.



Scheme 7 Example of one of the *Z*-selective Wittig reactions utilized in the preparations of lipid mediator protectin D1⁹⁰.

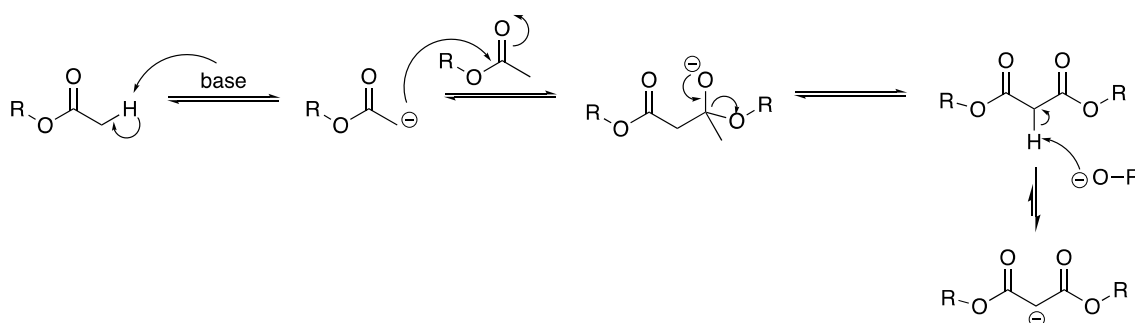
3.3 O-alkylation in the presence of an ester

The most common way of forming an ether from an organohalide and alkoxide is the Williamson ether synthesis. Alexander Williamson developed the reaction in 1850⁹¹. The reaction follows an S_N2 bimolecular nucleophilic substitution mechanism, where the alkoxide performs a nucleophilic backside attack of the electrophile, typically a halide or a tosylate. The reaction demands a good leaving group. Preferably the leaving site should be a primary or secondary carbon atom as tertiary carbon atoms prefer to proceed with elimination reactions. Protic and apolar solvents tend to slow the reaction, which restrains the availability of the free nucleophile. The common reaction is displayed in Scheme 8⁹¹.



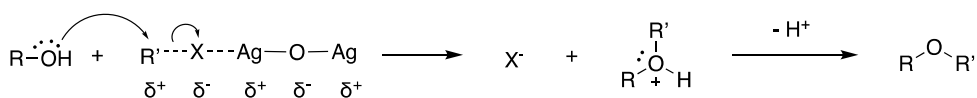
Scheme 8 Outline of the mechanism for the Williamson ether synthesis.

Strong bases such as NaH are commonly used to form alkoxides. This will however serve problems when other acidic protons, such as alpha protons relative to esters are present in the molecule. Since the product carbanion is resonance stabilized, alpha protons display unusual acidity with pK_a values of 19-20 instead of 40-50 for common C-H alkyl bonds⁸⁷. Deprotonation of the acidic alpha carbon atoms can result in unwanted side reactions, such as Claisen condensation, displayed in Scheme 9.



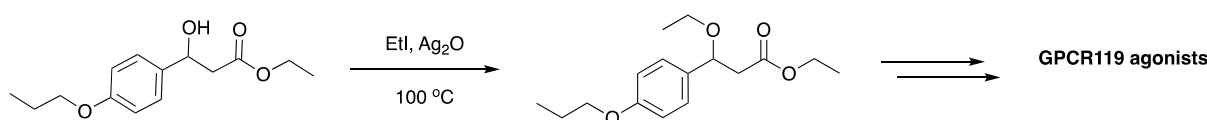
Scheme 9 General outline of the Claisen condensation mechanism.

In such cases, other conditions are demanded. Silver (I) oxide in the place of a strong base allows the reaction to proceed without the alkoxide intermediate and will not deprotonate the alpha protons. The positively charged silver withdraws the electron density from the halide, giving the adjacent carbon a partial positive charge allowing the alcohol to act as a nucleophile⁹² as displayed in Scheme 10 below.



Scheme 10 Outline of the mechanism for ether synthesis using silver oxide.

A British patent from 2012 reports the use of Silver (I) oxide in the preparation of a GPCR119 agonist⁹³. Since the starting material contains an ethyl ester, the mentioned conditions are applied. The procedure is outlined in Scheme 11.

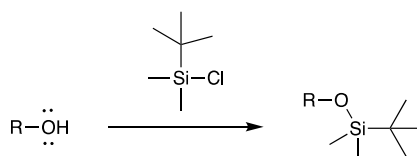


Scheme 11 Outline of the alkylation of one of the intermediate products in the synthesis of the GPCR119 agonist.

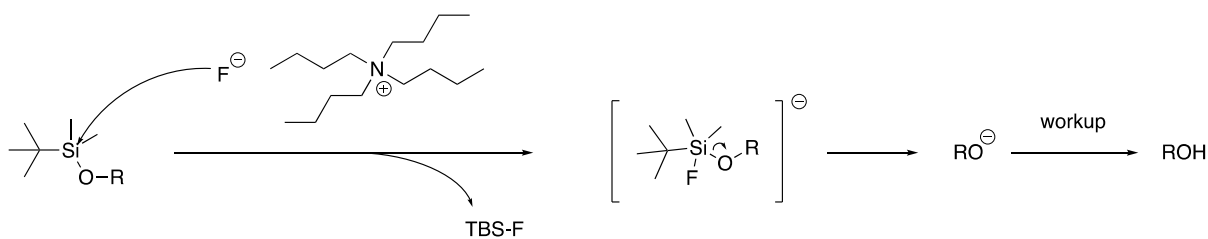
3.4 Protection of alcohols with silyl groups

Hydroxyl groups are present in several biological and synthetic compounds. They are subject to a range of different reactions. In polyfunctional molecules, it is often desired to protect the hydroxyl groups to avoid side reactions during synthesis.

Tert-butyldimethylsilyl (TBS) ethers are among the most known and widely used alcohol protective groups in organic chemistry. They are particularly useful since they are installed and removed by rather mild conditions and hydrolyze much slower than trimethyl ethers. TBS-protected alcohols are usually relatively stable under basic conditions and inert towards most nucleophiles. A general outline of TBS protection is displayed in Scheme 12. They are sensitive to acidic conditions, consequently often removed by employing catalytic amounts of acetyl chloride in dry methanol⁹⁴. Another common reagent used in the removal of TBS groups is tetraammonium fluoride (TBAF). Removal of TBS groups using fluoride conditions is displayed in Scheme 13.



Scheme 12 Outline of TBS-protection for alcohols.



Scheme 13 Outline of the mechanism for deprotection of alcohols under fluoride conditions.

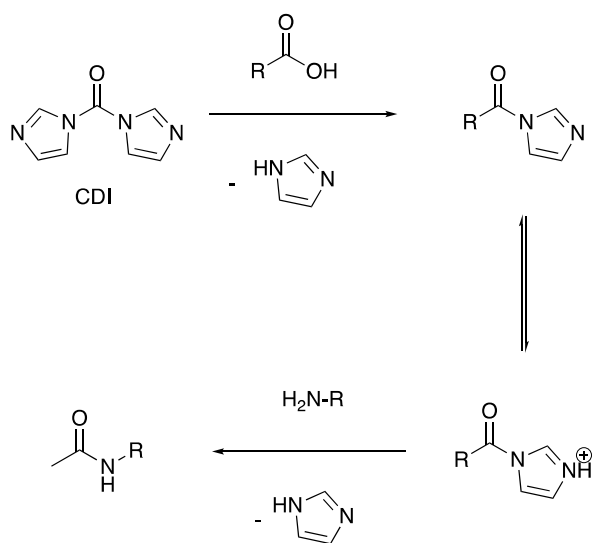
Common silylation of alcohols requires a silyl chloride and an amine base, such as imidazole. Reactions of alcohols with TBSCl and catalytic amounts of 4-dimethylaminopyridine (DMAP), instead of imidazole, have been shown to selectively protect primary alcohols over secondary alcohols in good yields⁹⁴. Common solvents are dimethylformamide (DMF) and dichloromethane (DCM). DCM will however result in a somewhat slower reaction but appears to be preferred when selectively protecting primary alcohol. When the excess reagent is used, flash column chromatography is required to remove silanol and siloxane⁹⁴.

3.5 Amide coupling with CDI

Amide groups are present in a range of different drug molecules. Two of the most applied methods for amide formation utilize coupling agents such as *N,N*-dicyclohexylcarbodiimide (DCC), and 1-(3-Dimethylaminopropyl)-3-ethylcarbodiimide hydrochloride (EDCI). Moreover, *N,N*-carbonyldiimidazole (CDI) is another frequently used coupling agent. CDI is cheaper, less toxic, and gives fewer toxic byproducts than the more endorsed DCC. Additionally, CDI is favored in the synthesis of fatty acid amides, which are known to be both sensitive and expensive compounds. An article from 2019 by Stenström *et al.*⁹⁵ prepared *N*-acyletanolamines of seven different fatty acids, including DHA, where all yields were over 95 %.

The current way is more expedient than traditional amidation, where an amine is assembled with a carboxylic acid. In the traditional reaction scheme, an acid-base reaction will initially occur, yielding the thermodynamically favored salt. Conversely, the mechanism of peptide coupling with CDI includes the formation of an activated ester intermediate. In this way, the intermediate salt species are voided. CDI reacts with the carboxylic acid of the fatty acid to produce the acyl intermediate, present as an imidazolium salt. This acyl is a much better leaving group and will undergo amide coupling under milder conditions. Usually, the reaction is carried

out under basic conditions, due to neutralization of the hydrogen chloride produced during the reaction⁹⁶. A general outline of amide formation by the use of CDI is displayed in Scheme 14.



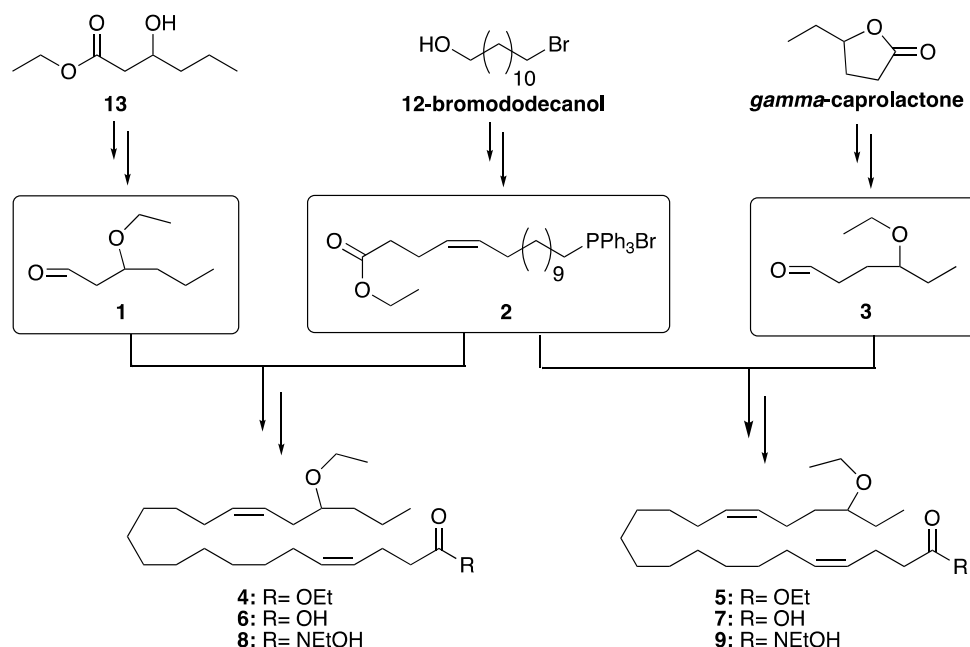
Scheme 14 General outline of amide formation by the use of CDI⁹⁶.

4 Results and discussion

4.1 Overview

This study aims to synthesize stable 19,20-EpDPA mimics and ethanolamides. Four stable mimics were successfully synthesized, where an ethyl ether takes place as a bioisosteric group for the epoxide in the 19,20-position. An overview of the synthetic strategy is outlined in Scheme 15.

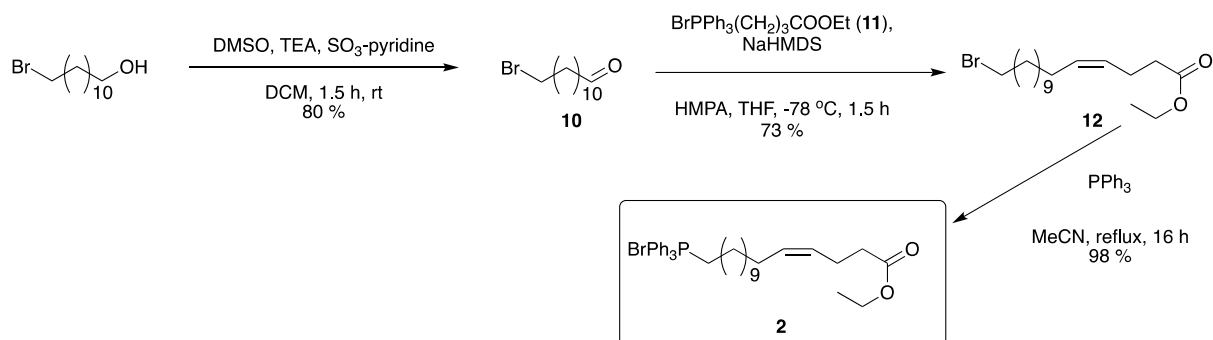
The first step of the syntheses was to synthesize Wittig salt **2**, which is the common intermediate for all the mimics. Thereafter two regioisomers, aldehyde **1** and **3**, were synthesized through two different routes. Wittig salt **2** was thereafter sequentially assembled with each of the two aldehydes yielding the two *Z*-alkenes **4** and **6**. Subsequently, the esters **4** and **6** were hydrolyzed to yield their corresponding carboxylic acids **5** and **7**. Lastly, the two carboxylic acids were converted to their corresponding ethanolamides **8** and **9**. Detailed descriptions for each of the substances' syntheses and characterizations are described in the following sections. All obtained NMR- and IR spectra and associated HRMS data are attached in Appendix 8.



Scheme 15 Simplified flowchart over the synthesis plan for target molecules 6-9.

4.2 Synthesis of Wittig salt 2

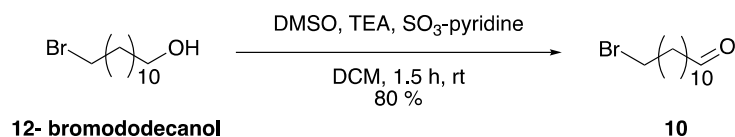
Wittig salt **2** was synthesized from 12-bromododecanol in three steps as outlined in Scheme 16. This procedure gave a total yield of 57 %.



Scheme 16 Outline of synthesis for Wittig salt **2**.

4.2.1 Synthesis of 12-bromododecanol 10

A Parikh-Doering oxidation was employed to oxidize 12-bromododecanol to its respective aldehyde **10** as outlined in Scheme 17. DMSO acts as a base and solvent. The oxidant is activated by the SO_3 -pyridine complex in the presence of TEA.



Scheme 17 Outline of synthesis for 12-bromododecanol **10**.

The alcohol, 12-bromododecanol, was dissolved in dry DCM, DMSO, TEA, and SO_3 -pyridine complex sequentially. After 1.5 hours of stirring at room temperature, thin layer chromatography (TLC) displayed full conversion of the starting material. Next, aqueous workup and purification by flash column chromatography afforded the desired aldehyde **10** in a yield of 80 %.

4.2.2 Characterization of 12-bromododecanal **10**

The recorded ^1H NMR spectrum exhibits a singlet at 9.76 ppm (t, $J = 1.9$ Hz, 1H) consistent with what is expected for aldehydes. Additionally, no signal corresponding to the protons of the carbinol was observed. These findings suggest a successful oxidation. The spectrum accounts for a total of 23 protons, in agreement with the molecular structure. As expected for protons adjacent to aldehydes, a signal arises at 2.41 ppm (td, $J = 7.3, 1.9$ Hz, 2H). The signal occurs as a triplet of a doublet since it couples with the adjacent aliphatic protons and the aldehyde proton. Furthermore, the triplet at 3.40 ppm (t, $J = 6.9$ Hz, 3H) originates from the protons adjacent to the electronegative bromine atom. Last, the rest of the signals appear at 1.90-1.26 ppm, with a total integral of 15 protons, which accounts for the remaining protons. A proposal of some chemical shifts is made in Figure 15.

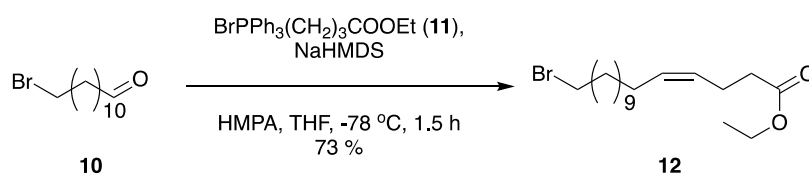


Figure 15 Assignment of ^1H NMR (left) and ^{13}C NMR (right) signals for 12-bromododecanal **10**.

The ^{13}C NMR spectrum displays 12 signals accounting for the 12 carbon atoms in molecule **10**. Aldehydes give a characteristic signal over 200 ppm, hence the peak at 203.1 ppm can be attributed to the aldehyde carbon. Moreover, the signal at 44.1 ppm originates from the carbon atom directly bound to the bromine atom, while the signal at 34.2 ppm most likely belongs to the carbon atom next to the aldehyde. The remaining nine signals between 33.0 and 22.2 ppm correspond to the rest of the nine carbon atoms. All spectroscopic data were in agreement with those previously reported by Porter *et al.*⁹⁷.

4.2.3 Synthesis of *Z*-alkene **12**

The second step in the synthesis of Wittig salt **2** was a *Z*-selective Wittig reaction between aldehyde **10** with commercially available Wittig salt **11**, displayed in Scheme 18.



Scheme 18 Outline of synthesis for *Z*-alkene **12**.

Firstly, the starting material **10** was dissolved in dry tetrahydrofuran (THF). Due to the reaction being sensitive to air/water, the solution was purged and degassed. Secondly, the Wittig salt **11** was dissolved in dry THF and hexamethylphosphoramide (HMPA), which was also purged and degassed. By subjecting the Wittig salt **11** to a very low temperature of $-78\text{ }^{\circ}\text{C}$ before adding the base sodium bis(trimethylsilyl)amide (NaHMDS), a non-stabilized ylide was obtained. Both the low temperature and the non-stabilized ylide encourage *Z*-selectivity. Afterward, the aldehyde **10** was added and the reaction mixture was stirred at $-78\text{ }^{\circ}\text{C}$ for 1.5 hours. After aqueous workup the crude was purified by flash chromatography, giving the desired *Z*-alkene **12** in 73 % yield. Obtained NMR spectra, found in Appendix **8**, indicate a successful Wittig reaction, with only one stereoisomer observed.

4.2.4 Characterization of *Z*-alkene **12**

The recorded ^1H NMR spectrum accounts for a total of 33 protons as expected for the structure. The most downfield multiplet at 5.46 – 5.25 ppm (m, 2H), is indicative of alkenes and is consistent with a successful Wittig reaction. Notably, none of the signals correspond to the aldehyde proton. In this case, (*Z*)-selectivity was not possible to confirm, due to the higher order multiplet and uncalculatable coupling constant (*J*). Considering the reaction conditions, it is improbable that the compound is the (*E*)-alkene. Additionally, ^1H NMR and ^{13}C NMR display only one stereoisomer. Furthermore, the quartet at 4.12 ppm (q, $J = 7.1\text{ Hz}$, 2H) corresponds nicely to the methylene protons in the ethoxy group of the ester. The triplet at 3.39 ppm (t, $J = 6.9\text{ Hz}$, 2H) corresponds well with the expected signal for the protons adjacent to the bromine atom. Next, the protons *alpha* and *beta* to the ester give rise to the multiplet at 2.40 – 2.27 ppm (m, 4H). Due to deshielding, the two remaining allylic protons are found at 2.02 ppm (q, $J = 6.9\text{ Hz}$, 2H). Additionally, the quintet at 1.83 ppm (p, $J = 6.9$, 2H) originates from the protons at C2, which are adjacent to two methylene groups and the closest to the electronegative bromine atom. Lastly, the big multiplet most upfield accounts for the 19 remaining aliphatic protons. Assignment of some chemical shifts are made in Figure **16** below.

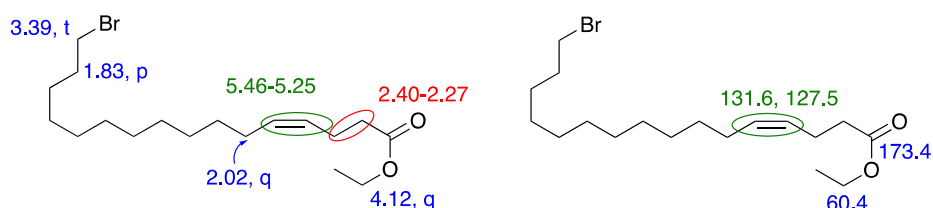
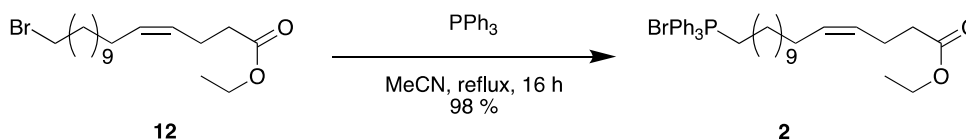


Figure 16 Assignment of ^1H NMR (left) and ^{13}C NMR (right) signals for *Z*-alkene **12**.

In the ^{13}C NMR spectrum, 18 signals were observed, corresponding to the 18 carbon atoms in **12**. As expected for alkenes, two peaks arise at 131.6 ppm and 127.5 ppm, thus also indicating a successful Wittig reaction. The absence of additional peaks in this region is consistent with a stereoselective Wittig reaction. Furthermore, the signal at 60.4 ppm arises from the carbon adjacent to the electronegative oxygen atom in the ethoxy moiety of the ester. Further characterization could not be made without evaluation from 2D spectra, which was not deemed necessary.

4.2.5 Synthesis of Wittig salt **2**

Wittig salt **2** was prepared by reacting bromine **12** with triphenylphosphine, as outlined in Scheme 19.



Scheme 19 Outline of synthesis for Wittig salt **2**

After TLC displayed full conversion, the solvent was removed by evaporation. Purification was performed by flash column chromatography on silica gel, starting with only DCM until excess triphenylphosphine had eluted, then the eluent was changed to 5 % MeOH in DCM. The procedure yielded the desired Wittig salt **2**, the common key fragment, in 98 % yield.

4.2.6 Characterization of Wittig salt **2**

The ^1H NMR spectrum integrates a total of 48 protons, nicely corresponding with the molecular structure. A multiplet arises at 7.83 – 7.62 ppm (m, 15H), corresponding to the protons of the three phenyl groups. Noteworthy, there is no longer a signal observed around 3.39 ppm which previously originated from the protons adjacent to the bromine atom. Additionally, the signal at 3.73-3.62 ppm (m, 2H) arises from the protons closest to the phosphorus atom in the aliphatic chain. These two findings indicate a successful reaction. The two olefinic protons resonate at 5.40 – 5.21 ppm (m, 2H). As expected for the ethylene protons in the ethyl ester, a quartet arises at 4.06 ppm (q, $J = 7.1$ Hz, 2H). Considering the coupling of these protons to the multiplet at 1.34 – 1.06 (m, 17H), as determined by analyzing the COSY spectrum, the methyl group must

be incorporated in this multiplet. Furthermore, the COSY-spectrum displays coupling between the multiplet at 3.73 – 3.62 ppm (m, 2H) and the signal at 1.57 ppm (m, Hz, 4H), hence the latter must correspond to the protons *beta* and *gamma* to the phosphorus atom. While the methyl group gives rise to the peak at 1.26 ppm, the protons *alpha* and *beta* to the ester give rise to the multiplet at 2.34 – 2.22 ppm (m, 4H). Next, the other allylic protons appear at 1.96 (q, $J = 7.0$ Hz, 2H). The remaining signals account for the rest of the 21 aliphatic protons. The proposed assignment of signals is given in Figure 17.

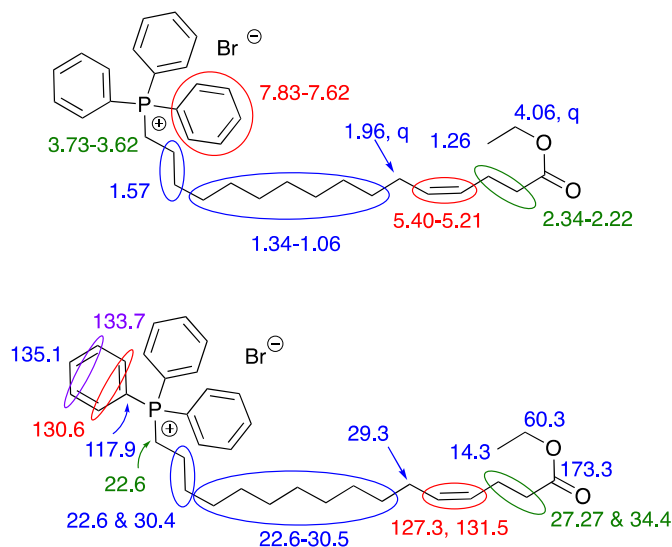
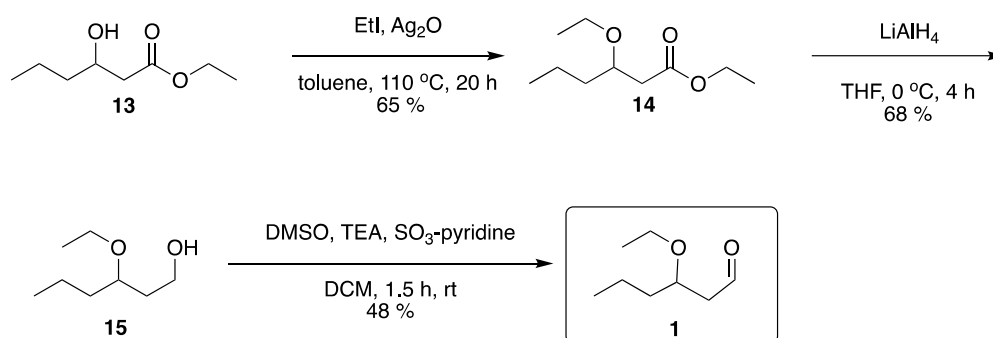


Figure 17 Assignment of ^1H NMR (above) and ^{13}C NMR (below) signals for Wittig salt **2**.

The ^{13}C NMR spectrum displayed four characteristic peaks accounting for the three phenyl groups in the aromatic area 135.1 to 117.9 ppm. The phosphorous atom has a spin of $I = 1/2$. ^{13}C atoms that spin-couple to the phosphorous atom will therefore appear as doublets. The doublets at 135.1 ppm with the lowest coupling constant of $J = 3.1$ Hz correspond to the three *para*-positioned carbon atoms. While the intense doublet at 133.7 ppm with a coupling constant of $J = 9.9$ Hz corresponds to the six carbon atoms in the *meta*-position. Next, the intense doublet with the second highest coupling constant of $J = 12.5$ Hz at 130.6 ppm accounts for the six carbon atoms in the *ortho*-position. Lastly, the doublet with the highest coupling constant of $J = 85.8$ Hz appearing at 118.3 ppm can be attributed to the three aromatic carbon atoms directly attached to the phosphorus atom. Furthermore, the doublet at 22.6 ppm ($J = 4.6$ Hz) accounts for the carbon between the phosphorus atom and the carbon chain. This is also indicating a successful conversion. COSY, HSQC, and HMBC spectra can be found in Appendix 8.1.

4.3 Synthesis of aldehyde 1

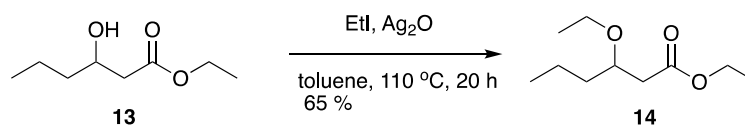
Aldehyde **1** was synthesized in three steps from commercially available ethyl 3-hydroxy hexanoate **13** as displayed in Scheme 20. The first two steps were first attempted on a small scale. The second time, the desired compound was yielded, but unexpectedly low yields were obtained from the oxidation step. A third attempt was performed before aldehyde **1** was synthesized in desirable amounts.



Scheme 20 Outline of synthesis for aldehyde **1**

4.3.1 Alkylation of alcohol **13**

The conventional Williamson ether synthesis procedure was not applicable for the alkylation of ethyl 3-hydroxy hexanoate **13**, due to the presence of acidic *alpha* protons. Deprotonation of these protons could make the compound acceptable to Claisen condensation. Therefore, a procedure with other conditions obtained from a British patent⁹³ was utilized instead (Scheme 21).



Scheme 21 Outline of synthesis for ether **14**.

Compound **13** was dissolved in toluene. Ag_2O and EtI in excess were added and the mixture was stirred at 110 °C. After 6 hours, TLC did not reveal a desirable conversion, and it was therefore decided to add another 4.9 equivalents of EtI . The mixture was left stirring overnight and upon examining the TLC the following day, a notable increase in conversion of the starting material was detected. The crude mixture was filtered through a Celite plug to get rid of the

silver dioxide, and the filtrate was concentrated *in vacuo*. Purification was performed by flash column chromatography yielding the desired product **14** in a moderate yield of 65 %.

A possible reason for the moderate yield can be due to an intramolecular bond making the hydroxy proton less available. The product of the intramolecular bond is a stable six-membered ring, displayed in Figure 18. However, when the same procedure was attempted for the regioisomer compound **18**, which does not have the possibility for this stable intramolecular bond, the yield was even lower. It is therefore likely that other factors are affecting the moderate yield.

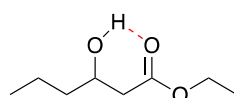


Figure 18 Possible intramolecular bond for compound 14.

4.3.2 Characterization of ether 14

The ^1H NMR spectrum integrates a total of 20 protons, as expected for the product, hence indicating a successful conversion. Three signals, accounting for five protons in total, are to be found in the area 4.14-3.45 ppm. This area is characteristic of protons deshielded by an oxygen atom. These findings agree well with the structure. Specifically, the signal at 3.77 – 3.66 ppm (m, 1H) can be attributed to the proton at the chiral center since this is the only single proton. Protons *alpha* to carbonyls usually occur in the area of 2.0-2.6 ppm. Due to the stereogenic center, the protons *alpha* of the carbonyl are diastereotopic. Therefore they give rise to two distinguished doublets of doublets. A further proposition of the remaining signals is shown in Figure 19 and supported by COSY, HSQC, and HMBC, found in Appendix 8.1.

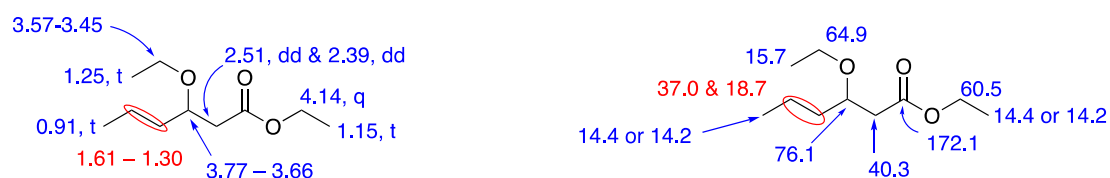


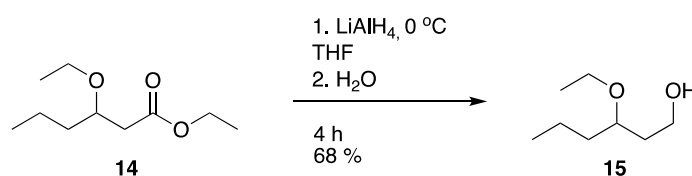
Figure 19 Assignment of ^1H NMR (left) and ^{13}C NMR (right) signals for ether 14.

The ^{13}C NMR spectrum displayed a total of 10 peaks and thereby accounts for all the carbon atoms in compound **14**. The peak at 64.9 ppm arises from the carbon directly connected to the oxygen atom in the ether moiety. In addition, there is a new peak at 15.7 ppm in the area

characteristic for aliphatic carbon atoms, belonging to the methyl in the ethoxy group. This also indicates that the ether synthesis was successful. The most downfield peak at 172.1 ppm corresponds to the carbonyl. A suggestion for the assignment of all shifts is shown in Figure 13 above. Propositions are based on COSY, HSQC, and HMBC spectra.

4.3.3 Reduction of ester 14

Alcohol 15 was prepared by reduction of ester 14 using LiAlH₄. The procedure is displayed in Scheme 22.



Scheme 22 Outline of synthesis for alcohol 15.

LiAlH₄ was added to a flask and stirred at 0 °C. The ester 14, dissolved in dry THF, was added in a dropwise manner under N₂-gas. After stirring at room temperature for four hours, the solution was again cooled to 0 °C. Reactions with LiAlH₄ tend to form AlOH upon aqueous quenching, which can result in emulsions. Hence, the Fieser workup was applied to get rid of the aluminum salt residues. The salts could easily be removed via a Büchner funnel. Lastly, the concentrate was purified by flash column chromatography, yielding the desired product alcohol 15 in 68 % yield.

4.3.4 Characterization of alcohol 15

The recorded ¹H NMR spectrum accounts for a total of 17 protons, which is as expected for the structure. The absence of the hydroxy signal can be due to the signal being too broad or incorporated into other signals. Three signals arise in the area 3.33 – 3.90 ppm, which can be attributed to the five protons geminal to the oxygen atoms. Furthermore, the signals in the most upfield area are accounting for a total of 12 protons. Additionally, no peak occurs in the area around 2 ppm, where signals from protons *alpha* to carbonyl groups typically resonate. These findings indicate a successful reduction. A proposition of the signals is displayed in Figure 20.

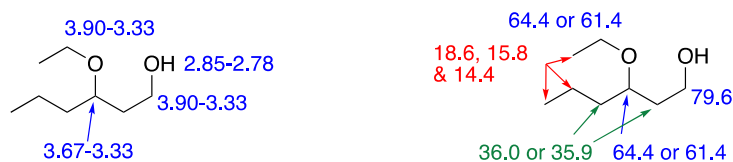


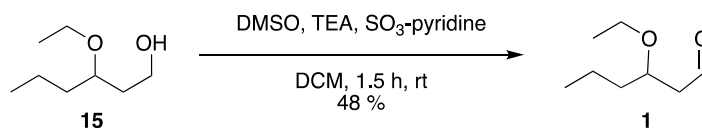
Figure 20 Assignment of ^1H NMR (left) and ^{13}C NMR (right) signals for alcohol **15**.

As expected, the ^{13}C NMR spectrum displayed a total of eight distinct peaks. Notably, the absence of a signal in the area around 170 ppm implies a successful reduction. Furthermore, the three farthest downfield peaks most likely belong to the carbon atoms directly bonded to the oxygen atoms. A proposition of the signals can be found in Figure 20.

4.3.5 Oxidation of alcohol **15**

Lastly, aldehyde **1** was prepared by oxidation of alcohol **15** to its corresponding aldehyde as displayed in Scheme 23. As for compound **10**, Parikh-Doering oxidation was utilized.

After stirring for 1.5 hours at room temperature, TLC displayed full conversion of the starting material. However, only 48 % was yielded after aqueous workup and purification by flash chromatography.



Scheme 23 Outline of synthesis for aldehyde **1**.

After the first attempt, it was theorized that the low yield could be attributed to evaporation of the compound while being subjected to the rotavator. Computational calculations using ChemDraw estimated a boiling point of 180 °C. In other words, this hypothesis was unlikely. In the second attempt, the reaction mixture was exposed to milder conditions while being evaporated, but a low yield was still obtained.

Another possible reason for the low yield could be explained by the water solubility of aldehyde **1**. Based on computational calculations using ChemDraw, the aldehyde being extracted was estimated a $\log P$ of 0.94. This suggests that considerable amounts of the aldehyde may have partitioned to the aqueous phase during the workup. Furthermore, since EtOAc was used as the extracting solvent, it is likely that the distribution coefficient is even more in favor of the

aqueous phase. This is due to EtOAc being even less polar than 1-octanol, which the estimate was based on. Therefore it could be favorable to utilize smaller extraction volumes and repeat the extraction several times. Even though a 48 % yield is considered very low for an oxidation reaction, it was decided not to optimize the reaction step, since enough aldehyde was obtained to carry on with the Wittig reaction.

4.3.6 Characterization of aldehyde 1

A new triplet arises at 9.79 ppm (t, $J = 2.3$ Hz, 1H) in the recorded ^1H NMR spectrum, indicative of an aldehydic proton. No peaks correspond to hydroxy or carbinol protons, reflecting a successful oxidation of the alcohol. As expected, only two signals accounting for a total of three protons, appear in an area of 3-4 ppm characteristic for protons bound to ether carbon atoms. The signals at 2.49 (ddd, $J = 16.0, 4.9, 1.9$ Hz, 1H) and 2.59 ppm (ddd, $J = 16.2, 7.1, 2.5$ Hz, 1H) most likely belong to the protons between the aldehyde and the chiral center. They exhibit doublets of doublets of doublets due to their diastereotopicity and coupling with the proton of the aldehyde and the proton in the stereogenic center. The remaining 10 protons are displayed in the multiplet most upfield. Hereby all protons have been accounted for.

However, the recorded spectrum displayed two protons too many, incorporated in the multiplet at 1.63 – 1.22 ppm. This likely arises from heptane residues, because of gentle evaporation due to the assumption that the aldehyde was volatile. Heptane residues are justified by it not influencing the next reaction step.

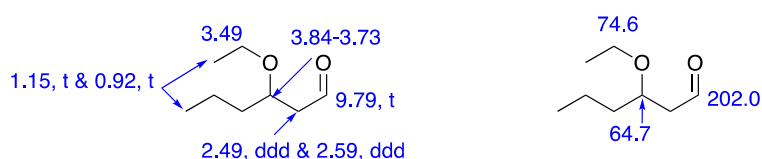


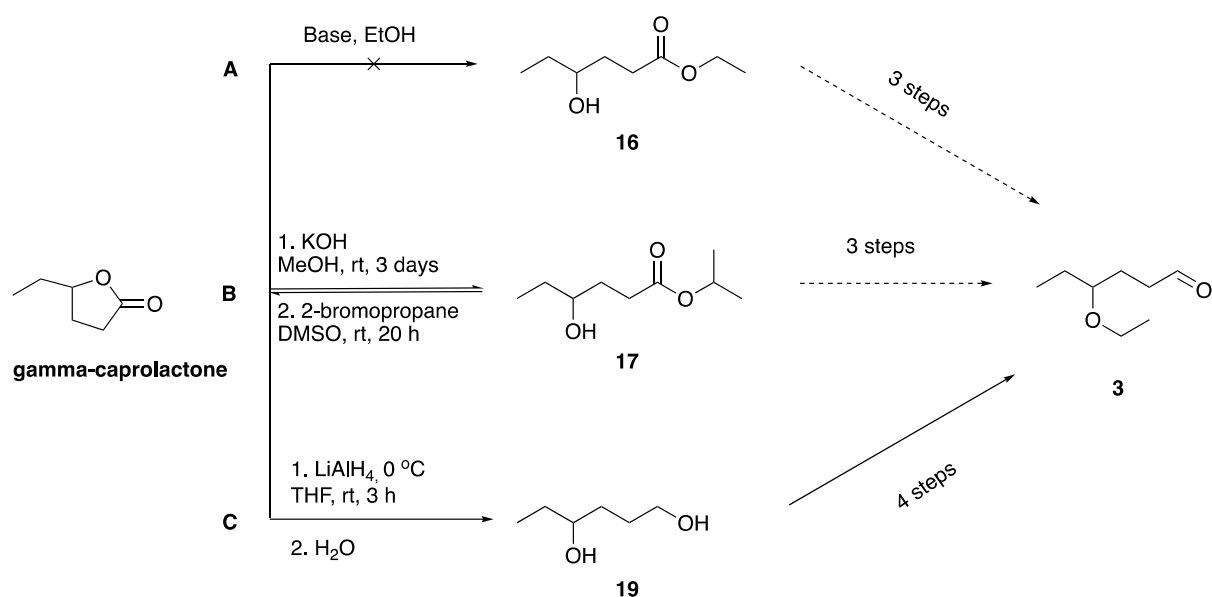
Figure 21 Assignment of ^1H NMR (left) and ^{13}C NMR (right) signals for aldehyde 1.

The recorded ^{13}C NMR spectrum displays eight peaks, as expected. The peak at 202.0 ppm is characteristic of aldehydes. Only two peaks are to be found in the area around 60-80 ppm, indicating successful oxidation. Notably, the signals of the impurities are only located in the most upfield area, further indicating heptane as the impurity. As no 2D spectrum was recorded it is not possible to assign all the signals, but some propositions are presented in Figure 21.

When the HRMS analysis was performed, it was not possible to obtain a good calibration for the measurements. Neither could the compound be stored and rerecorded at a later stage, due to the instability of the aldehyde. Hence, no HRMS or elemental analysis was obtained. It is however almost evident that the desired compound was yielded, based on the recorded NMR spectra, and the qualitative analyses of the target molecule **7**.

4.4 Synthesis of aldehyde **3**

Three different routes were attempted in the synthesis of aldehyde **3** before a successful method was developed, as displayed in Scheme 26. The initial plan (route **A**) was to perform a hydrolysis of *gamma*-caprolactone and thereafter continue with the same reaction steps as for the previous aldehyde **1**. Despite attempts with two distinct bases, both attempts proved to be unsuccessful. An alternative route **B** was therefore devised. After discovering problems related to the alkylation of the alcohol **17**, it was decided to attempt a third route **C**, not involving an ester as the substrate. The diol **19** in route **C** was protected before further alkylation and deprotection, and was at last oxidized to the desired aldehyde **3**. The first attempt in the last step of the synthesis resulted in way too little product to continue. Therefore, the whole synthesis via route **C** was repeated, on a larger scale, to gain a sufficient amount of aldehyde **3** to proceed.

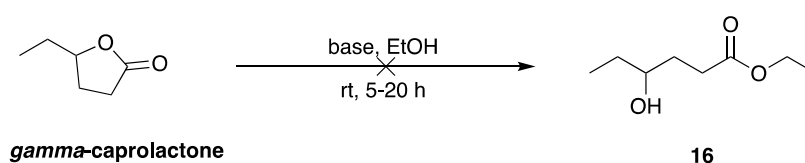


Scheme 24 Outline of the three simplified attempted syntheses for aldehyde **3**.

4.4.1 Hydrolysis of *gamma*-caprolactone

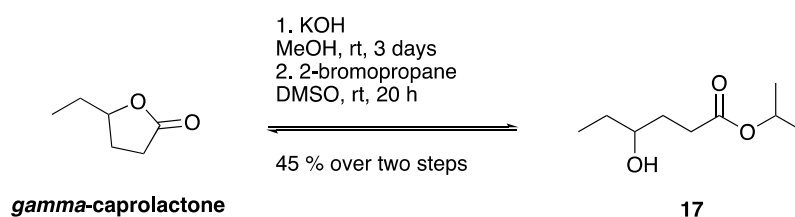
As mentioned, the first step in the initial plan of synthesizing aldehyde **3** was to perform a hydrolysis of *gamma*-caprolactone, as displayed in Scheme 27. Both KOH and Et₃N were tried as the base. However, none of the reactions were successful.

When the reaction was attempted with KOH, TLC displayed full conversion. However, after aqueous work-up and evaporation, a white unwanted salt was yielded. When changing to Et₃N as the base, minimal conversion of starting material was revealed on TLC after 24 hours and the experiment was therefore stopped.



Scheme 25 Outline of attempted synthesis for ester **16**.

An alternative route **B**, displayed in Scheme 28, was approached after discovering three articles describing the same principle⁹⁸⁻¹⁰⁰. A test reaction was first performed before upscaling. The articles suggested hydrolyzing the lactone with a strong base and trapping it as its carboxylate. Without further purification, the carboxylate would be alkylated to yield the ester **17**. Since the conversion of the lactone to its ester is an equilibrium, a bulkier ester was theorized to sterically hinder the conversion back to the starting material.



Scheme 26 Outline of synthesis for ester **17**.

Hydrolysis of the commercially available lactone was effected using KOH in MeOH. The solution was stirred at room temperature for three days which resulted in the specie trapped as its respective carboxylate. TLC displayed almost full conversion of the starting material. Thereafter, the carboxylate salt was transformed into the isopropyl ester **17** by adding DMSO and 2-bromopropane. TLC displayed almost full conversion after 20 hours of stirring at room temperature. Aqueous work-up and purification by flash column chromatography were

performed. A gradient eluent was employed to first eluate the excess 2-bromopropane, starting with pure DCM, changing to 5 % Et₂O in DCM to eluate the ester. The two steps resulted in a 45 % yield of compound **17**.

4.4.2 Characterization of ester **17**

The recorded ¹H NMR integrates a total of 18 protons, which agrees well with the structure. Two signals arise at 4.99 (sept, *J* = 6.3 Hz, 1H) and 3.58 – 3.48 (m, 1H), characteristic of protons geminal to oxygen, as expected for the structure. The septet at 4.99 (sept, *J* = 6.3 Hz, 1H) and the doublet at 1.22 (d, *J* = 6.3 Hz, 6H) correspond to the isopropyl moiety. This indicates a successful esterification. Moreover, a triplet of a doublet arises at 2.41 ppm (td, *J* = 7.3, 2.5 Hz, 2H). The splitting pattern suggests that the signal originates from the protons vicinal to the carbinol and *beta* to the ester. The rest of the seven protons are accounted for in the remaining signals. Hence, all 18 protons have been accounted for. An assignment of some chemical shifts is displayed in Figure 22.

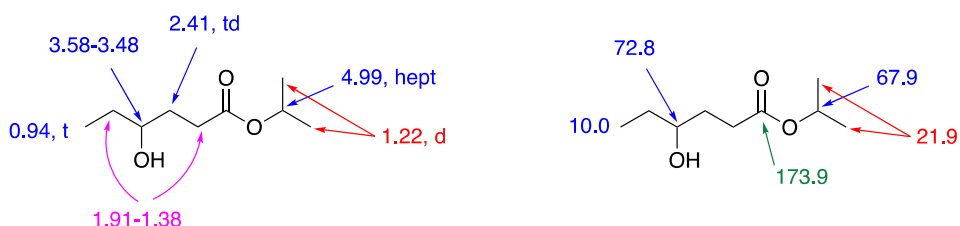


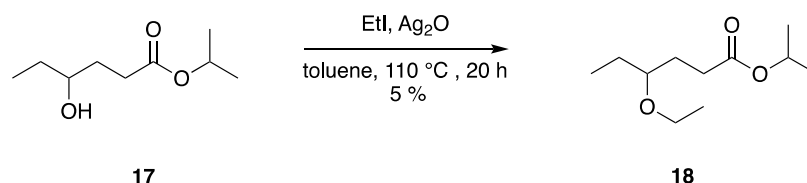
Figure 22 Assignment of ¹H NMR (left) and ¹³C NMR (right) signals for ester **17**.

The recorded ¹³C NMR spectrum displays a total of nine peaks, accounting for all of the carbon atoms in ester **17**. Two peaks arise at 72.8 ppm and 67.9 ppm, typical for carbon atoms single-bonded to an oxygen atom. While the carbonyl gives rise to the peak at 173.9 ppm. These three peaks together suggest a successful ring opening. A total of six peaks are seen in the area of 10.0-31.3 ppm, as expected of the structure. Hereby all nine carbon atoms have been accounted for.

4.4.3 Alkylation of alcohol **17**

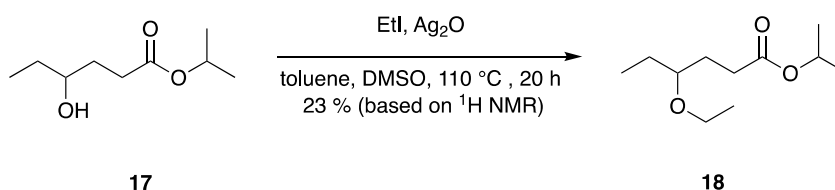
The procedure for synthesizing ether **14** was attempted for the synthesis of ethyl ether **18**, as displayed in Scheme 29. Alcohol **17** was dissolved in toluene. Ag₂O and EtI in excess were added and the mixture was stirred at 110 °C. First, it was attempted to only utilize 2.3

equivalents of Ag₂O compared to 4.9 equivalents used for the synthesis of compound **14**, due to a shortage of Ag₂O. After 19 hours TLC displayed a poor conversion of the starting material. It was therefore decided to add another 4.9 equivalents of EtI. Even after another 19 hours, the TLC revealed the poor conversion of the starting material. Hence, the reaction was stopped, and the mixture was filtrated over a Celite plug and concentrated *in vacuo*, which yielded ether **18** in a disappointing 5 % yield.



Scheme 27 Outline of the first attempted synthesis for compound **18**.

A second attempt with the same conditions was approached, but this time with 4.9 equivalents Ag₂O since more had been delivered. The second attempt is displayed in Scheme **30**. TLC once again revealed the poor conversion of the starting material. Consequently, 4.9 additional equivalents of EtI were added. After stirring for two more hours, it was decided to add 10 more equivalents of EtI. It was decided to try adding a polar aprotic solvent, which often favors S_N2 reactions. Therefore, some DMSO was added to achieve a solvent containing DMSO: toluene (1:4). After 19 hours of stirring at reflux, the reaction mixture was cooled down. Thereafter, the solvent was removed *in vacuo* and an aqueous workup was performed. The crude ¹H NMR revealed a 23 % conversion to yield the desired product. It was therefore decided to discard the attempted route.

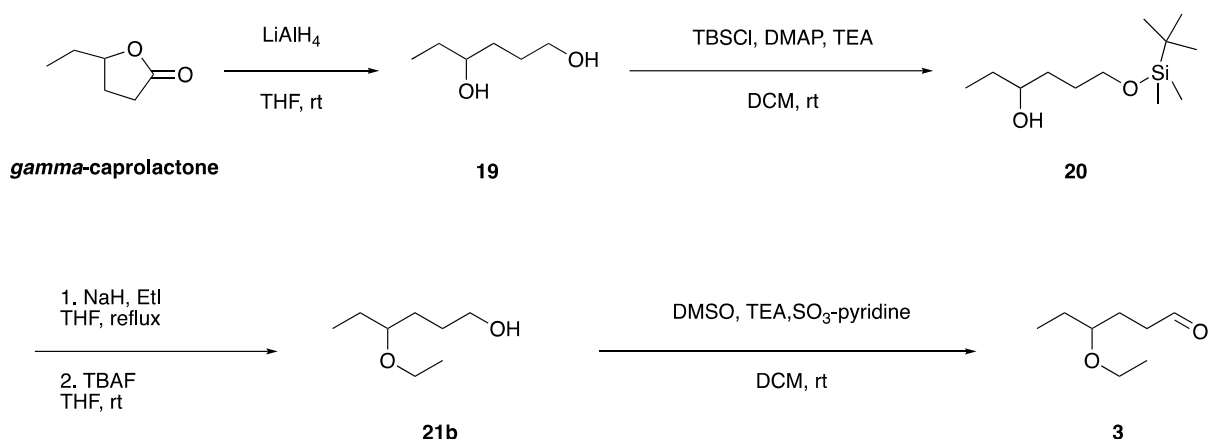


Scheme 28 Outline of the second attempted synthesis of compound **18**.

4.4.4 Reduction of *gamma*-caprolactone

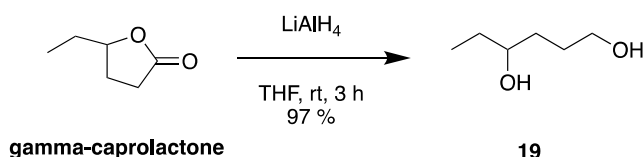
The reason why a common Williamson ether procedure could not be utilized for the alkylation step in the original plan is the presence of the acidic *alpha* protons of the ester. As mentioned

earlier, deprotonation of the alpha protons can lead to Claisen condensation. Even though the procedure involving Ag₂O did not result in unwanted condensation, it still did not result in sufficient yields of the desired product either. To circumvent the issue, a strategic decision was made to employ a starting material devoid of acidic *alpha* protons. In this way, a more predictable procedure could be applied in the alkylation step. The outline of the new strategy **C**, is displayed in Scheme 31.



Scheme 29 Outline of the planned synthesis for aldehyde **3**.

Ring-opening to yield the diol was accomplished by reducing the commercially available *gamma*-caprolactone with LiAlH₄, as outlined in Scheme 32. The procedure yielded the desired product **19** in 97 %.



Scheme 30 Outline of synthesis for compound **19**.

The lactone was dissolved in THF at 0 °C and LiAlH₄ was thereafter added. TLC displayed full conversion of the starting material, after stirring at room temperature for three hours. The Fieser method was utilized for the workup. Lastly, the crude mixture was purified through a silica plug with EtOAc to remove eventual salts and other more polar compounds.

4.4.5 Characterization of diol 19

The recorded ^1H NMR spectrum accounts for a total of 14 protons, which corresponds well with the structure. Data were in agreement with the literature^{101, 102}. Noteworthy, a singlet is observed most downfield, and can be assigned to the two hydroxy protons. All three carbinol protons are accounted for in the multiplet at 3.68 – 3.44 ppm (m, 3H). Lastly, the remaining nine aliphatic protons arise in the most upfield area. With the proposed assignment displayed in Figure 23, all 14 protons have been accounted for.

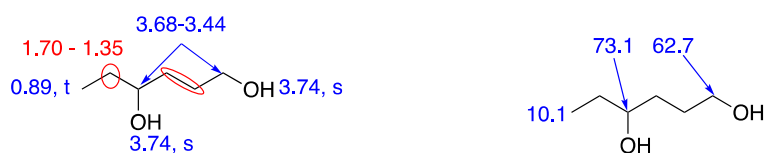
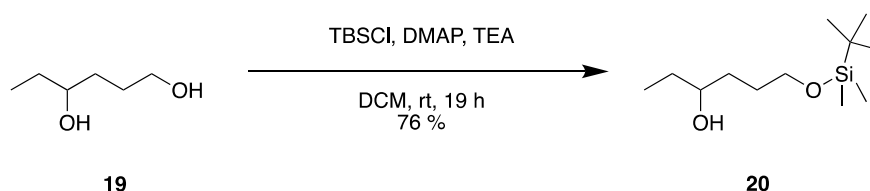


Figure 23 Assignment of ^1H NMR (left) and ^{13}C NMR (right) signals for diol 19.

The recorded ^{13}C NMR spectrum displays a total of six peaks. Data were consistent with those reported in the literature^{101, 102}. Two peaks arise within the expected range of 60 to 80 ppm, for carbinol carbon atoms. The signal with the highest shift most likely arises from the carbon of the secondary carbinol. Noteworthy, no peak corresponds to a carbonyl, consistent with a successful conversion.

4.4.6 Selective TBS-protection of diol 19

The next step in the synthesis was to selectively protect the primary alcohol of compound 19, as outlined in Scheme 33. In this way, the subsequent alkylation would only occur at the secondary alcohol. Selective protection of the primary alcohol was accomplished in one step by the use of a TBS-protection group, and DMAP as the catalyst. TEA was used to regenerate the catalyst.



Scheme 31 Outline of the synthesis for compound 20.

The diol was dissolved in DCM. DMAP, TEA, and TBSCl were added sequentially. TLC displayed small amounts of both starting material and over-protected starting material as well as the desired product **20** after 19 hours. After aqueous work-up and purification by flash chromatography, the desired TBS-protected alcohol **20** was afforded in 76 % yield.

4.4.7 Characterization of TBS-protected alcohol **20**

The signals in the recorded ^1H NMR spectrum integrate a total of 28 protons. This is an additional 14 protons, from the spectrum of the diol **19**, indicating the addition of the TBS group. A multiplet at 0.95-0.82 ppm (m, 12H) accounts for the *tert*-butyl moiety and the aliphatic methyl group. Furthermore, the singlet at 0.04 ppm (s, 6H) accounts for the two methyl groups directly bonded to silisium, with no neighboring protons. Hence, all the protons of the TBS group have been accounted for. Notably, only one signal, at 2.60 ppm (s, 1H) is consistent with those arising from hydroxy protons. This indicates the exchange of one hydroxylic proton with the TBS group. Hereby all 28 protons have been accounted for. A proposition for the assignment of the proton signals is made in Figure 24.

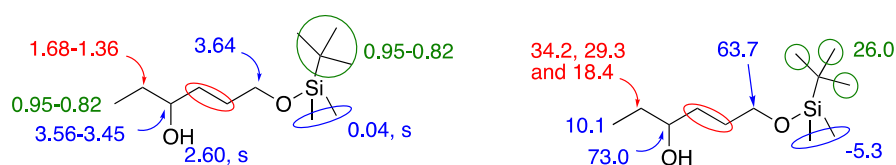
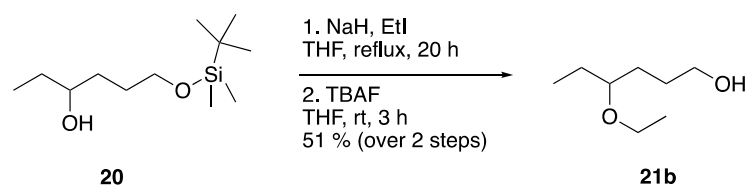


Figure 24 Assignment of ^1H NMR (left) and ^{13}C NMR (right) signals for compound **20**.

The recorded ^{13}C NMR spectrum displays eight peaks accounting for a total of eleven carbon atoms. Only three peaks arise from the TBS group, because of symmetry. The most intense peak at 26.0 ppm accounts for the three carbon atoms in the *tert*-butyl moiety. Next, the two carbon atoms in the methyl groups directly bound to silisium typically arise right below 0 ppm, in this case at -5.3 ppm. Hereby all eleven carbon atoms have been accounted for. A proposition for the assignment of the carbon signals is made in Figure 24.

4.4.8 Synthesis of ether **21b**

Finally, a conventional and more predictable procedure for alkylating the alcohol could be applied. A standard Williamson ether synthesis, outlined in Scheme 34 below, was utilized.



Scheme 32 Outline of the synthesis of ether **21b**.

Sodium hydride 60 % in mineral oil, was used as the base. Activation of the base was performed by washing it with THF. Thereafter, the base was added to the alcohol **20** and stirred for 30 minutes at room temperature. Even though TLC did not display full conversion it was decided to end the reaction after 20 hours at reflux. An aqueous workup was performed.

It was first attempted to perform purification by flash column chromatography between the alkylation- and deprotection steps. Starting with pure heptane, changing to 1 %, 2 %, 5 %, and lastly 10 % Et₂O. This gave a disappointing yield of 32 %. The low yield was likely due to the high lipophilicity ($R_f = 0.28$ in pure heptane) of the compound posing a challenge in terms of purification prior to deprotection. Clean fractions of compound **21a** (displayed in Figure 25) were obtained, but the product showed tailing over several fractions. As a result, it was decided to carry out the deprotection following alkylation without intermediate purification.

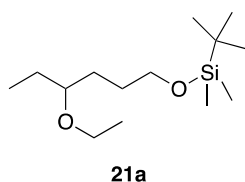


Figure 25 Outline of the chemical structure of compound **21a**.

For deprotection, TBAF was added to a solution of the crude mixture of ether **21a** at 0 °C. After 3 hours of stirring TLC displayed two distinguished spots, corresponding to both the diol **19** and the desired alcohol **21b**. Phosphate buffer was added and aqueous workup was performed. Lastly, purification was performed by flash column chromatography (40% EtOAc in heptane). This resulted in a much better yield of 51 % over two steps.

4.4.9 Characterization of ether **21a**

Since clean fractions were obtained when performing purification between the alkylation- and deprotection steps, both ¹H NMR and ¹³C NMR spectrum of **21a** was obtained.

The recorded ^1H NMR spectrum integrates a total of 32 protons, which agrees well with the structure. The three most downfield multiplets, ranging from 3.65 – 3.12 ppm, integrate the five deshielded protons geminal to the two oxygen atoms. Furthermore, the additional two protons in this area indicate a successful alkylation. Next, the multiplet at 1.67 – 1.39 ppm (m, 6H) accounts for the six aliphatic protons. Since the two methyl groups directly bonded to silisium have no coupling protons, the singlet at 0.93-0.82 ppm (s, 6H) must correspond to them. Lastly, the two multiplets integrating a total of 15 protons account for the five remaining methyl groups. Hence, all protons have been accounted for. A proposition for the assignment of the proton signals is made in Figure 26.

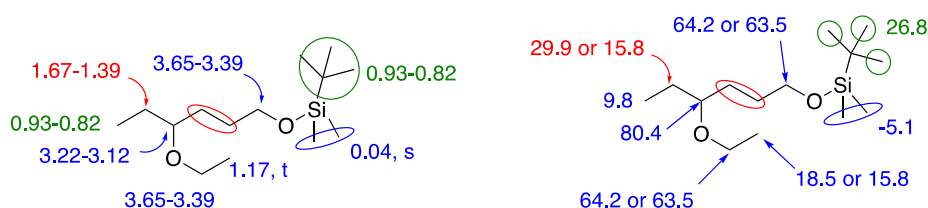


Figure 26 Assignment of ^1H NMR (left) and ^{13}C NMR (right) signals for protected ether **21a**.

The recorded ^{13}C NMR spectrum displays a total of 11 peaks accounting for all 14 carbon atoms. As mentioned earlier, the TBS moiety gives rise to only three peaks, and therefore only 11 peaks are to be seen. Three peaks arise in the area of 60-80 ppm, which are to be expected for carbon atoms directly bound to oxygen. This indicates a successful alkylation. Hereby all 14 carbon atoms have been accounted for.

4.4.10 Characterization of deprotected alcohol **21b**

The recorded ^1H NMR spectrum accounts for a total of 18 protons. Gratifiyngly, this is 14 protons less than the previous spectrum and demonstrates the absence of the TBS groups, thus a successful deprotection. Two signals integrating a total of six protons ranging from 3.68 – 3.40 ppm are to be found in the area characteristic of protons geminal to oxygen, which are as expected for the structure. Additionally, the hydroxy proton gives rise to the signal at 3.28-3.18 ppm (m, 1H). The rest of the spectrum is otherwise comparable to the spectrum of intermediate **21a**. Thus, the total number of protons in the spectrum is in accordance with the total of 18 protons in molecule **21b**. A proposition for the assignment of the proton signals is made in Figure 27 below.

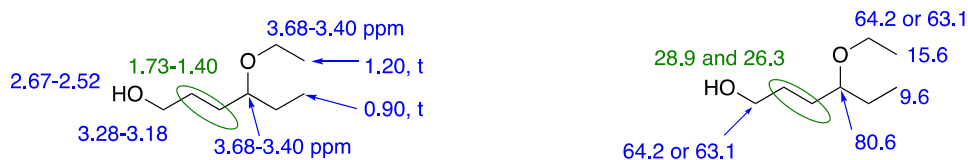
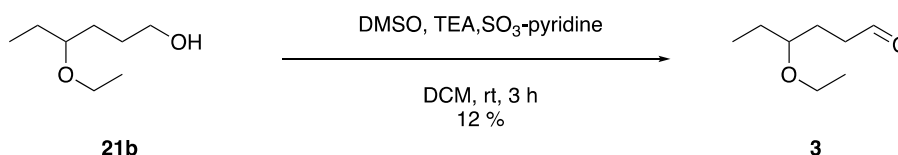


Figure 27 Assignment of ^1H NMR (left) and ^{13}C NMR (right) signals for protected ether **21b**.

The recorded ^{13}C NMR spectrum displays a total of eight peaks, accounting for eight carbon atoms of compound **21b**. That is six less and indicates the loss of the TBS groups, which contained six carbon atoms. The three most downfield peaks account for the carbon atoms directly bonded to oxygen. Hereby all eight carbon atoms have been accounted for. A proposition for the assignment of the carbon signals is made in Figure **27** above.

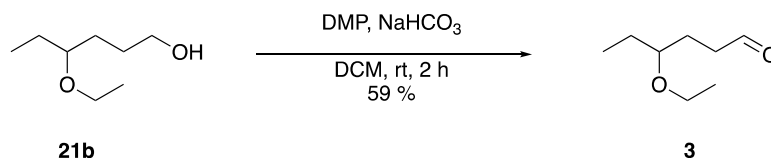
4.4.11 Oxidation of alcohol **21b**

Two different oxidation procedures were attempted for the synthesis of aldehyde **3**. First, the Parikh-Doering oxidation was attempted, displayed in Scheme **35**. TLC revealed full conversion after three hours. However, after aqueous workup and purification a disappointing yield of 12 % was obtained.



Scheme 33 Outline of the first attempt for the synthesis of aldehyde **3**.

It was theorized that the low yields of aldehyde **3** also was due to the product partitioning to the water layer. Computational calculation estimated a $clog P$ of 0.80 for 1-octanol, which is even lower than for the previous aldehyde **1**. A strategic choice was therefore made to attempt a Dess-Martin oxidation (Scheme **36**) since it requires smaller work-up volumes. This would be favorable if the low yield was due to the product partitioning to the aqueous layer. The synthesis, utilizing Dess-Martin periodinane (DMP), is displayed in Scheme **36** below.



Scheme 34 Outline of the second attempt of the synthesis for aldehyde **3**.

The alcohol **21b** was dissolved in DCM. Sequentially NaCHO₃ and DMP were added. TLC revealed full conversion of stirring at room temperature for three hours. For the workup, only 5 mL of water was utilized, compared to 50 mL for the Parikh-Doering procedure. Purification was performed by flash column chromatography. This procedure resulted in a much better yield of 59 %. Even though a 59 % yield is considered low for an oxidation reaction, it gave a sufficient amount of aldehyde **3** to proceed with the synthesis.

4.4.12 Characterization of aldehyde **3**

The recorded ¹H NMR spectrum displays a new triplet at 9.77 ppm (t, *J* = 1.9 Hz, 1H), accounting for the aldehydic proton. Since the signal is consistent with an aldehydic proton it is now also evident that the selective protection of diol **19** was successful. There is no longer a peak corresponding to a hydroxy proton, also indicating successful oxidation. Furthermore, the triplet of doublets at 2.49 ppm (td, *J* = 7.2 Hz, 2H) most likely belongs to the protons between the aldehyde and the chiral center. The remaining 10 protons are displayed in the multiplet most upfield. Hereby all protons have been accounted for. A proposition for the assignment of the proton signals is made in Figure **28** below.



Figure 28 Assignment of ¹H NMR (left) and ¹³C NMR (right) signals for protected aldehyde **3**.

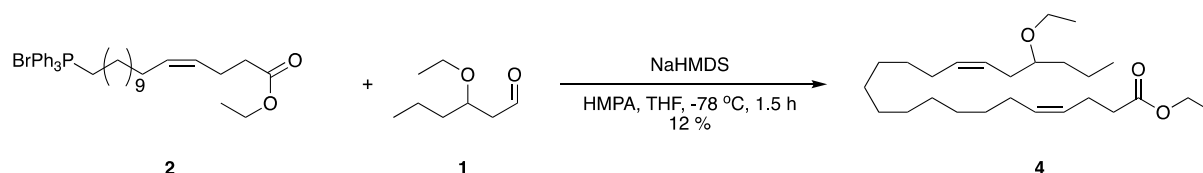
The recorded ¹³C NMR spectrum displays a total of eight peaks, as expected for the structure. The peak at 202.6 ppm is characteristic of carbon atoms in aldehydes, also indicating a successful oxidation. As no 2D spectrum was recorded it is not possible to assign all the signals, but some propositions are presented in Figure **28**.

4.5 Synthesis of target molecules

The convergent synthesis towards the four target molecules was at last unified by the assembly of each of the aldehydes **1** and **3** with the Wittig salt **2**. The following sections discuss the coupling of the key fragments and the final steps in preparation of the target molecules **6-9**.

4.5.1 Synthesis of Z-alkene **4**

Finally, after obtaining enough material of compound **2** the next step was to synthesize Z-alkene **4** as outlined in Scheme 24. The same conditions for synthesizing compound **11** were applied for this step.



Scheme 35 Outline of synthesis for compound **4**.

After aqueous workup, the crude was filtered through a silica plug and purified by flash column chromatography with 10 % Et₂O in heptane. The first attempt of purification failed and another attempt of purification by flash column chromatography, this time with 4 % Et₂O in heptane, yielded the desired Z-alkene **4** in a disappointing yield of 12 %. Obtained NMR spectra and HRMS analysis indicate a successful Z-selective Wittig reaction.

There are several possible explanations for the low yield. It is important to keep dry and inert conditions. Deviations from these conditions, whether in the form of non-optimal reagents or techniques, are likely to impact the reaction outcome. Additionally, full conversion of the starting material was not obtained before the workup and purification. In hindsight, it is possible that the reaction was ended too early. If the reaction had been allowed to stir for more hours, a higher conversion may have been obtained. Additionally, the solution was run through a silica plug once and twice through the flash chromatography column. Some product could have gone lost attaching to the silica, but not enough to justify the low yield.

4.5.2 Characterization of *Z*-alkene 4

In the recorded ^1H NMR spectrum a total of 48 proton signals are displayed, agreeing nicely with the structure. The multiplet at 5.46 – 5.23 ppm (m, 4H) accounts for the four vinylic protons, indicating that the Wittig reaction was successful. *Z*-selectivity could not be confirmed this time either, since the multiplet was of higher order and the coupling constant (J) could not be calculated. However, the reaction conditions favor *Z*-configuration. Four signals accounting for a total of five protons arise in the area characteristic of protons bound to ether carbon atoms, agreeing well with the structure. The signals observed between 1.94 – 2.36 ppm account for a total of 10 protons. These most likely arise from the eight allylic protons and the two protons neighboring the carbonyl, while the protons of methylene in the ether moiety give rise to the multiplet at 3.61-3.37 (m, 2H). The remaining 28 protons are accounted for in the three multiplets most downfield. Hereby all 48 protons have been accounted for. The assignment of chemical shifts is displayed in Figure 29 below.

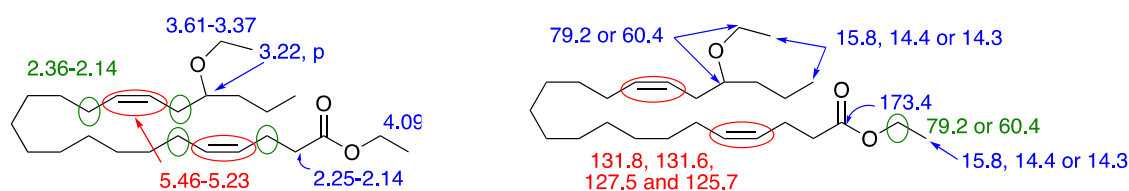
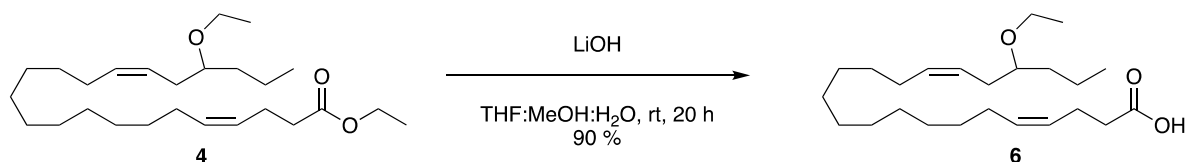


Figure 29 Assignment of ^1H NMR (left) and ^{13}C NMR (right) signals for *Z*-alkene 4.

The recorded ^{13}C NMR spectrum displays a total of 23 signals accounting for a total of 26 carbon atoms. Notably, four peaks are observed in the area 131.8 – 125.7 ppm, expected for alkenes. The absence of any additional signals in this area suggests the absence of the *E*-isomer, confirming a successful *Z*-selective Wittig reaction. The most downfield peak arises from the carbonyl. Moreover, three peaks appear in the area characteristic for carbon atoms directly connected to an oxygen atom, ranging from 79.2 – 60.4 ppm. The three most intensive peaks in the area 29.8 – 29.7 ppm can be attributed to the three terminal carbon atoms. Finally, the rest of the 13 signals accounts for the remaining carbon atoms. Hereby all 26 carbon atoms have been accounted for.

4.5.3 Synthesis of 19,20-EpDPA mimic 6

The final step to prepare target molecule **6** was hydrolyzing compound **4** to its corresponding carboxylic acid as displayed in Scheme 25.



Scheme 36 Outline of the synthesis for target molecule **5**.

Hydrolysis of the ester was performed by treating **4** with LiOH in aqueous THF-MeOH at 0 °C. TLC displayed low conversion after three hours. Hence, the solution was left stirring until full conversion was revealed the morning after. After acidic workup, the crude product was purified by flash column chromatography yielding target molecule **6** in 90 % yield.

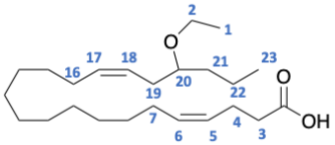
4.5.4 Characterization of 19,20-EpDPA mimic **6**

The recorded ¹H NMR spectrum integrates a total of 44 protons. Markedly, there is no longer a peak in the area around 4 ppm and one less apparent triplet in the alkane area, indicating the loss of the ethyl moiety. Additionally, it is now possible to observe the signal at 3.56-3.45 ppm (dq, $J = 9.3$, 2H), accounting for the diastereotopic protons, splitting into a doublet of quartets.

After the hydrolysis, the ¹³C NMR spectrum counts two peaks less. The absence of the two signals demonstrates the loss of the corresponding ethyl moiety. As for the signals of the ¹H NMR spectrum, the remaining signals agree well with the signals present in ester **4**.

A suggestion for the assignment of chemical shifts is shown in Table **1** below, demonstrated through the COSY- and HSQC spectrum displayed in Figure **30** and **31** respectively.

Table 1 Assignment of ^1H and ^{13}C chemical shifts of target molecule **6**.

Position: chemical shift (ppm)		
1: 1.18, t	1: 15.7	 <p style="text-align: center;">6</p>
2: 3.56, dq & 3.45, dq	2: 64.4	
3 & 4: 2.42 – 2.33, m	3 & 4: 34.3, 22.7	
5, 6, 17, 18: 5.49 – 5.29, m	5, 6, 17, 18: 132.0, 131.9, 127.1, 125.7	
7 & 16: 2.08 – 1.97, m	7 & 16: 27.5, 27.3	
19: 2.27 – 2.15, m	19: 32.0	
20: 3.26, p	20: 79.3	
21: 1.43, m	21: 18.9	
23: 0.90, t	23: 14.3	

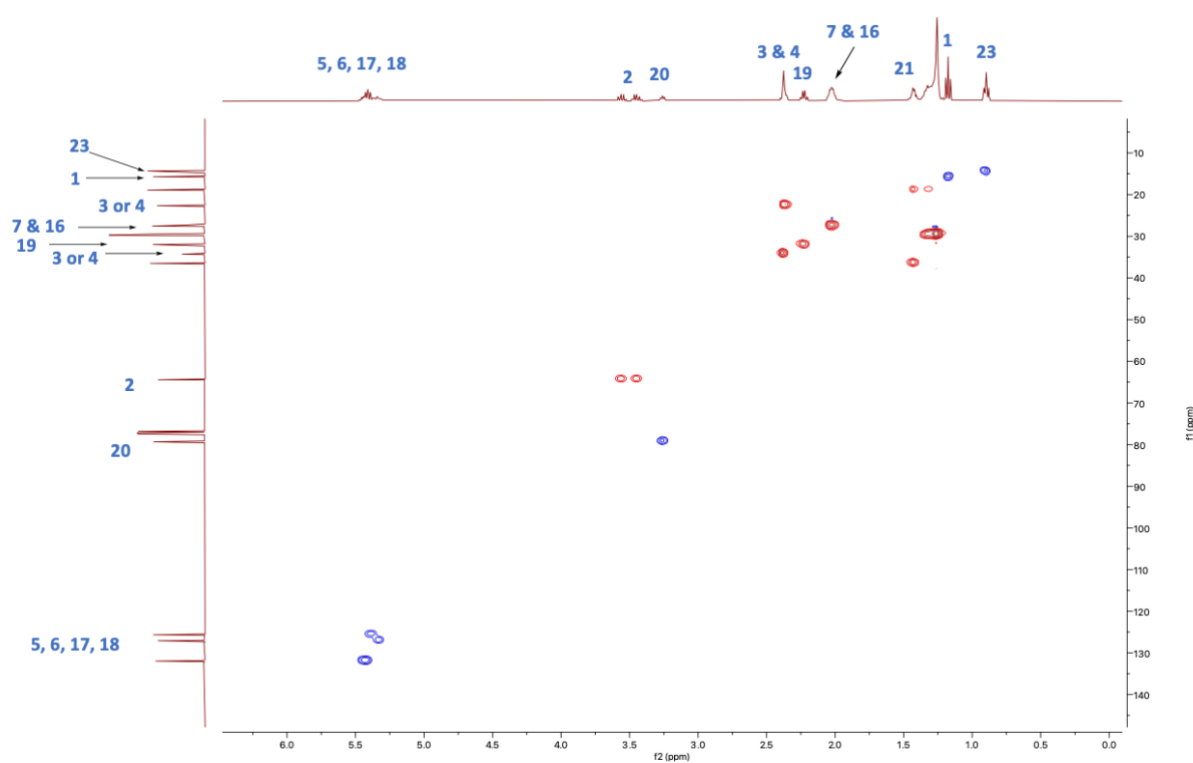


Figure 30 HSQC spectrum of compound **6**.

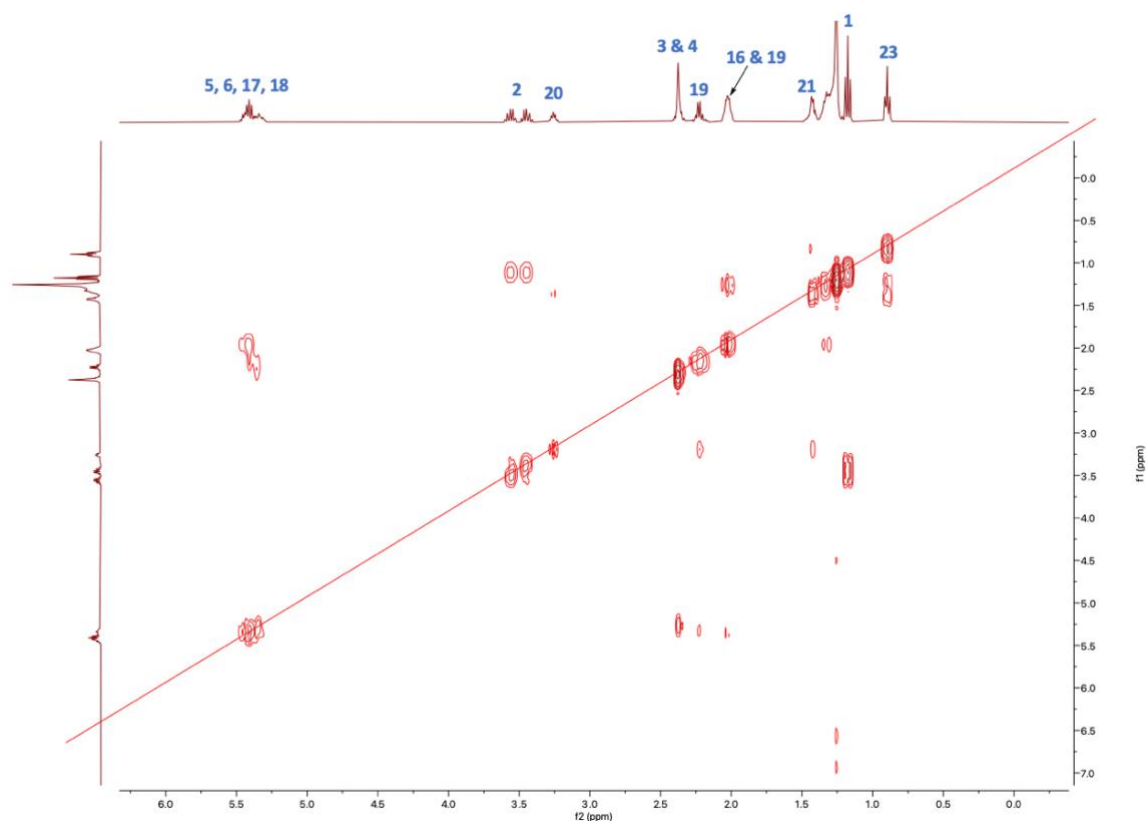
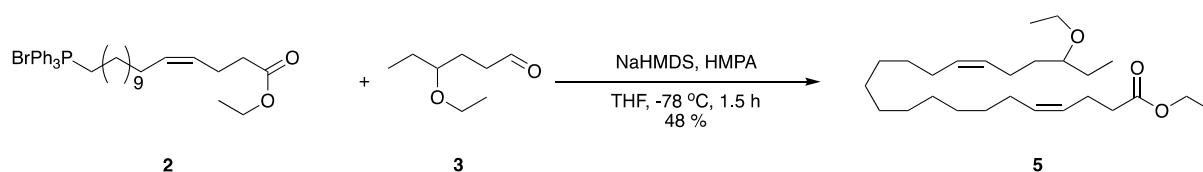


Figure 31 COSY spectrum of compound **6**.

In an IR spectrum, the C-H stretch is expected at around $3000\text{--}3100\text{ cm}^{-1}$. The recorded IR spectrum, found in Appendix **8.3**, displays a stretch at 3010 cm^{-1} , which could correspond to the C-H bonds of the alkenes in molecule **6**. Additionally, the obtained IR spectrum indicates the presence of a carboxylic acid with the presence of a wide O-H stretch at $3400\text{--}2400\text{ cm}^{-1}$ and the carbonyl at 1738 cm^{-1} .

4.5.5 Synthesis of *Z*-alkene **5**

After obtaining a sufficient amount of aldehyde **3**, the next step was to synthesize *Z*-alkene **5**. The same conditions for synthesizing compounds **12** and **4** were applied, as outlined in Scheme **37**.



Scheme 37 Outline of the synthesis for *Z*-alkene **5**.

Firstly, starting material **3** was dissolved in dry THF. Secondly, the Wittig salt **2** was dissolved in dry THF and HMPA. Both solutions were purged and degassed. To ensure *Z*-selectivity, the Wittig salt **2** was subjected to a very low temperature of $-78\text{ }^{\circ}\text{C}$ before adding the base. Afterward, the aldehyde **3** was added and the reaction mixture was stirred at a low temperature for 1.5 hours. After aqueous workup, the crude was filtered through a silica plug and purified by flash chromatography with 8 % Et₂O in heptane. Thereafter, purification by flash column chromatography was once again performed but with 4 % Et₂O in heptane. The desired *Z*-alkene **5** was yielded in 48 %. Obtained NMR spectra and HRMS analysis indicate a successful *Z*-selective Wittig reaction.

This reaction gave a four times higher yield, relative to the Wittig reaction for the regioisomer compound **4**. The increase can be due to more experience in the lab, resulting in better conditions. This time, there were also fewer purification steps. Even though the reactants are almost identical, the reacting aldehyde differs from the two reactions. The aldehydes will therefore to some degree have different reactivity. Although the two aldehydes are different, it is likely that the yield of the regioisomer of compound **5**, compound **4**, could be considerably increased.

4.5.6 Characterization of *Z*-alkene **5**

The recorded ¹H NMR spectrum exhibits signals accounting for a total of 49 protons. One proton too many is found in the alkane area spanning from 1.57 – 1.15 ppm, which integrates for a total of 27 protons. These multiplets, in addition to the most upfield triplet, integrate the 26 aliphatic protons. The multiplet at 5.45-5.28 ppm (m, 4H) accounts for the four vinylic protons, indicating that the Wittig reaction was successful. As for the previously synthesized alkenes, this ¹H NMR spectrum could not confirm *Z*-selectivity due to the higher-order multiplet and uncalculatable coupling constant (*J*). Nevertheless, the reaction conditions favor *Z*-configuration. Moreover, three peaks accounting for a total of five protons arise in the area 4.17 – 3.17 ppm and correspond to the protons adjacent to the oxygen atoms. The two multiplets in the area 2.39 – 2.13 ppm most likely belong to the eight allylic protons and the protons *alpha* to the carbonyl. Hereby all 48 protons have been accounted for. A proposition for the assignment of the proton signals is made in Figure **32**.

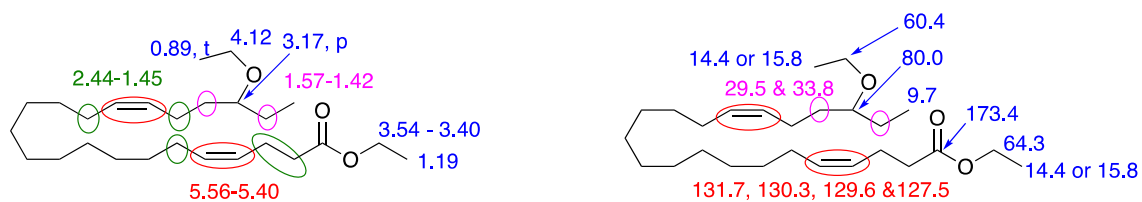
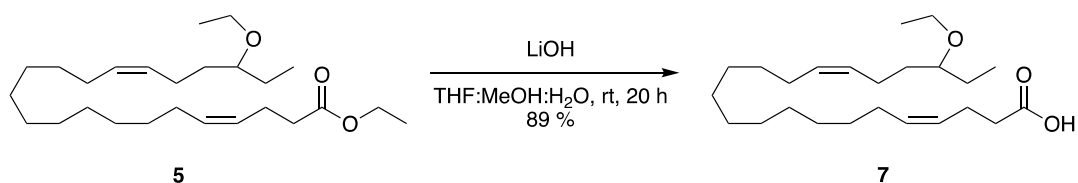


Figure 32 Assignment of ^1H NMR (left) and ^{13}C NMR (right) signals for protected *Z*-alkene **5**.

The recorded ^{13}C NMR spectrum displays a total of 21 peaks accounting for a total of 26 carbon atoms. Four peaks appear in the area 131.7 – 127.5 ppm, expected for alkenes. Since no additional signals arise in this area, it is unlikely that the *E*-isomer is present, confirming a successful *Z*-selective Wittig reaction. The most downfield peak arises from the carbonyl. Furthermore, three peaks appear in the area characteristic for carbon atoms directly connected to oxygen, from 80 ppm – 60.4 ppm. The rest of the 13 signals accounts for the remaining carbon atoms. Hereby all 26 carbon atoms have been accounted for. A proposition for the assignment of the carbon signals is made in the Figure above.

4.5.7 Synthesis of 19,20-EpDPA mimic **7**

The last step in synthesizing target molecule **7** was to hydrolyze the *Z*-alkene **5** to its corresponding carboxylic acid, as outlined in Scheme 38. As for compound **6**, LiOH was utilized to achieve the hydrolysis.



Scheme 38 Outline of the synthesis for target molecule **7**.

Full conversion was revealed on TLC after stirring at room temperature overnight. After acidic workup, the crude product was purified by flash column chromatography to yield the target molecule in 89 % yield.

4.5.8 Characterization of 19,20-EpDPA mimic **7**

The recorded ^1H NMR spectrum integrates a total of 45 protons. One proton too many is incorporated in the alkane area between 1.51 – 1.21 ppm, which integrates for a total of 20

protons. This small error is however acceptable. There is no longer a peak in the area of 4 ppm and the most upfield area integrates for three protons less. This indicates the loss of the ethyl moiety of the ester.

After the hydrolysis, the ^{13}C NMR spectrum counts two peaks less. The absent signals demonstrate the loss of the ethyl group corresponding to the ester moiety. As expected for the structure, the spectrum accounts for a total of 23 carbon atoms. The remaining signals agree well with the signals present in ester **5**.

A suggestion for the assignment of shifts is shown in Table 2 below, first demonstrated through the COSY spectrum (Figure 33). Based on these shifts and the HSQC spectrum (Figure 34), a further proposition for the ^{13}C was made.

Table 2 Assignment of ^1H and ^{13}C chemical shifts from of target molecule 7.

Position: chemical shift (ppm)		
1: 1.19, t 2: 3.56 – 3.40, m 3 & 4: 2.44 – 2.32, m 5, 6, 17, 18: 5.52 – 5.24, m 7, 16, 19: 2.14 – 1.96, m 20 & 22: 1.58 – 1.45, m 21: 3.18, p 23: 0.89, t	1: 15.6 2: 80 3 & 4: 34.1, 22.5 5, 6, 17, 18: 131.9, 130.2, 129.5, 126.9 7, 16, 19: 23.2, 27.2 20 & 22: 26.5, 33.6 21: 64.1 23: 9.6	<p style="text-align: center;">7</p>

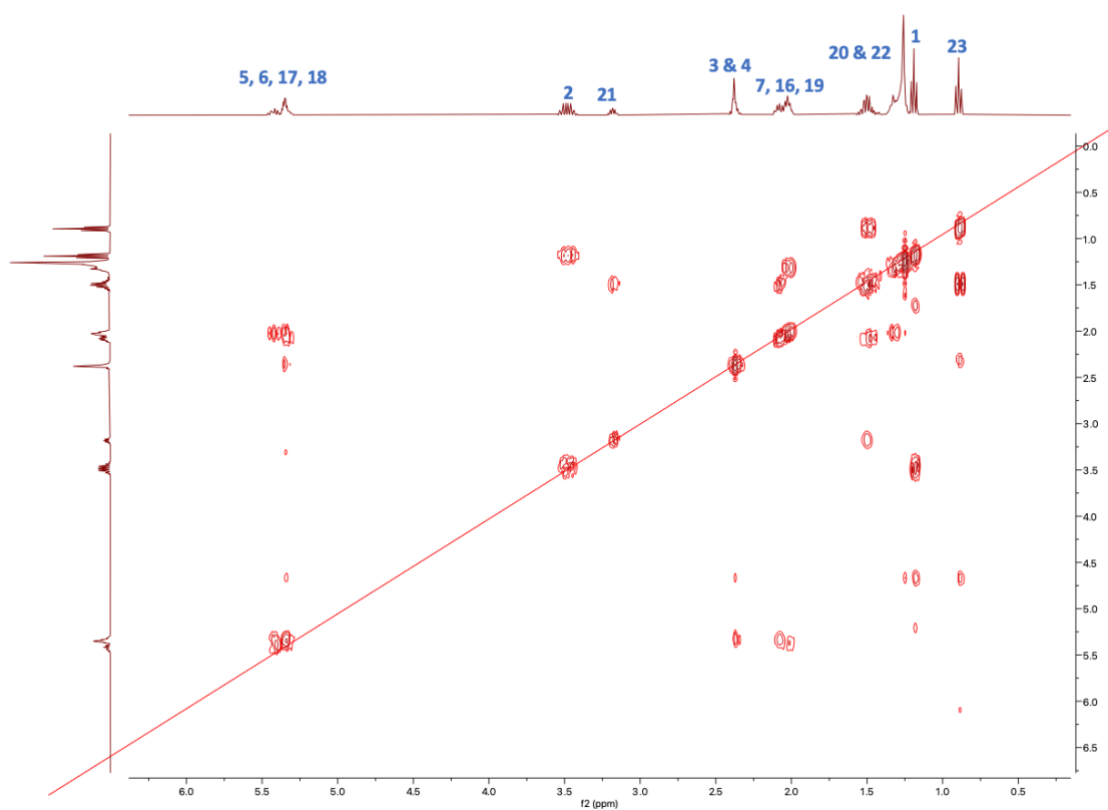


Figure 34 COSY spectrum of compound 7.

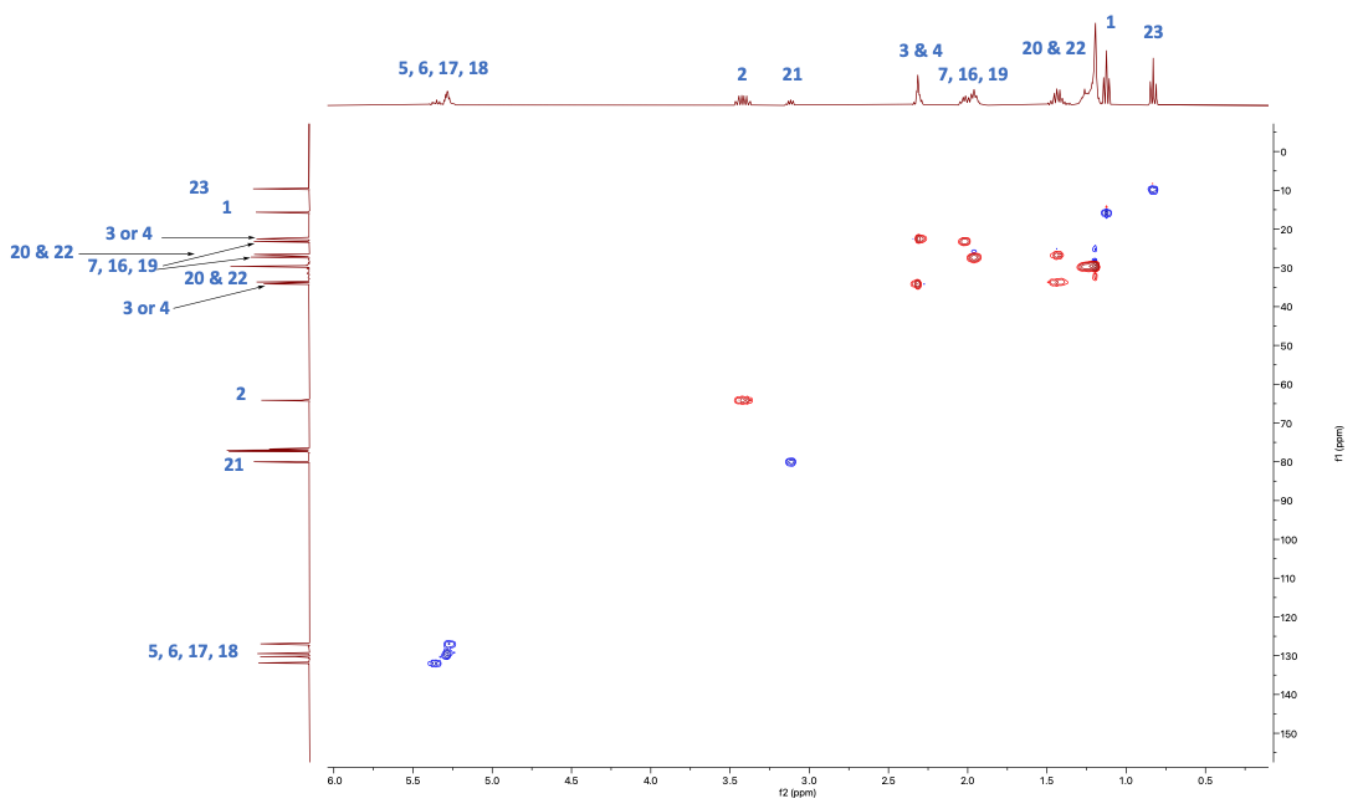
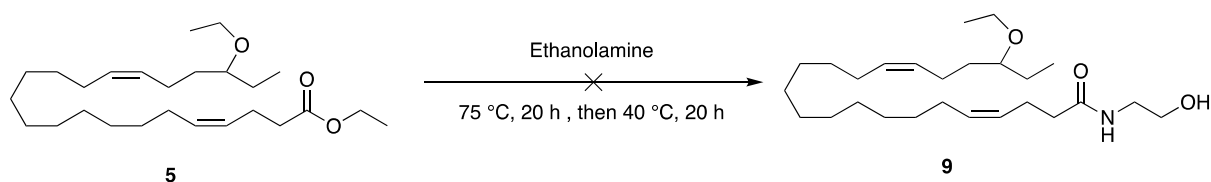


Figure 33 HSQC spectrum of compound 7.

In the recorded IR spectrum, a possible C-H stretch is visible at 3008 cm^{-1} . This peak could indicate the presence of double bonds. Furthermore, the IR spectrum indicates the presence of the carboxylic acid with an O-H stretch at $3400 - 2400\text{ cm}^{-1}$ and a C=O stretch at 1738 cm^{-1} . The obtained IR spectrum can be found in Appendix 8.3.

4.5.9 Synthesis of 19,20-EpDPA-EA 9

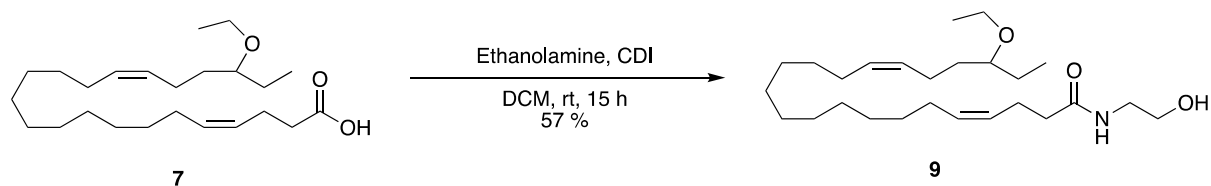
Theoretically, the 19,20-EpDPA-EA mimic **9** could be synthesized from both its corresponding ester and carboxylic acid. It was first attempted to assemble the ester **5** and ethanolamine neat at $75\text{ }^{\circ}\text{C}$, as displayed in Scheme 39 below.



Scheme 39 Outline of the first attempted synthesis for 19,20-EpDPA-EA **9**.

TLC displayed almost no conversion after 20 hours. The solution was then exposed to reduced pressure at $40\text{ }^{\circ}\text{C}$ to evaporate off the bi-product ethanol. Hopefully, this would force the reaction by shifting the equilibrium. After 20 hours under reduced pressure, TLC still displayed low conversion. It was therefore decided to attempt another procedure utilizing the carboxylic acid as starting material instead.

The carboxylic acid **7** was dissolved in DCM and added CDI and ethanolamine, as outlined in Scheme 40. TLC displayed almost full conversion after 15 hours of stirring at room temperature. Acidic work-up and purification by flash column chromatography were performed.



Scheme 40 Outline of the synthesis of compound **9**.

The purification of compound **9** was rather problematic. Despite TLC exhibiting favorable separation of the carboxylic acid **7** and the product **9**, clean fractions were not obtained after purification by flash column chromatography, using the same eluent of 5 % MeOH in DCM. A second attempt with EtOAc:heptane (1:1) was attempted, as TLC once again displayed good separation. Nevertheless, the fractions contained both substances. A third attempt using gradient eluent starting with 2,5 % changing to 5 % and lastly 10 % MeOH in DCM was required to obtain clean fractions. This procedure gave a yield of 57 %.

4.5.10 Characterization of 19,20-EpDPA-EA mimic **9**

The recorded ^1H NMR spectrum includes three new signals corresponding to an ethanolamide. Two signals, accounting for the four deshielded protons bonded to the carbon atoms of the ethanolamide are found at 3.70 ppm (t, 2H) and 3.58 – 3.28 ppm (m, 4H). The hydroxy proton gives rise to the most downfield singlet at 6.05 ppm. Even though the nitrogen proton is not visible in the spectrum it is still almost evident that the peptide coupling was successful. The remaining 43 protons align with the signals of the corresponding ester.

Two new peaks in the ^{13}C NMR arise at 62.6 ppm and 42.6 ppm corresponding nicely to the ethanolamide moiety. The rest of the 24 signals align with the previously recorded spectrum of the carboxylic acid **7**. Hereby all 26 carbon atoms have been accounted for.

A suggestion for the assignment of shifts is shown in Table 3, first demonstrated through the COSY spectrum (Figure 35) and then the HSQC spectrum (Figure 36).

Table 3 Assignment of ^1H and ^{13}C chemical shifts of target molecule **9**.

Position: chemical shift (ppm)		
1: 1.18, t	1: 15.8	<p style="text-align: center;">9</p>
2 & 4: 3.58 - 3.28, m	2: 64.3	
3: 3.70, t	3: 62.6	
5: 2.29-2.20, m	4: 42.6	
6: 2.37, q	23: 80.0	
7, 8, 19, 20: 5.58 – 5.28, m	5: 36.7,	
9, 18 & 21: 2.16 – 1.79, m	6: 23.3	
22 & 24: 1.62 – 1.39, m	7, 8, 19, 20: 132.0, 130.4, 129.6, 127.6	
23: 3.22 – 3.12, m	9, 18 & 21: 23.6, 27.4, 29.5	
25: 0.89, t	22 & 24: 26.5, 33.6	
	25: 9.7	

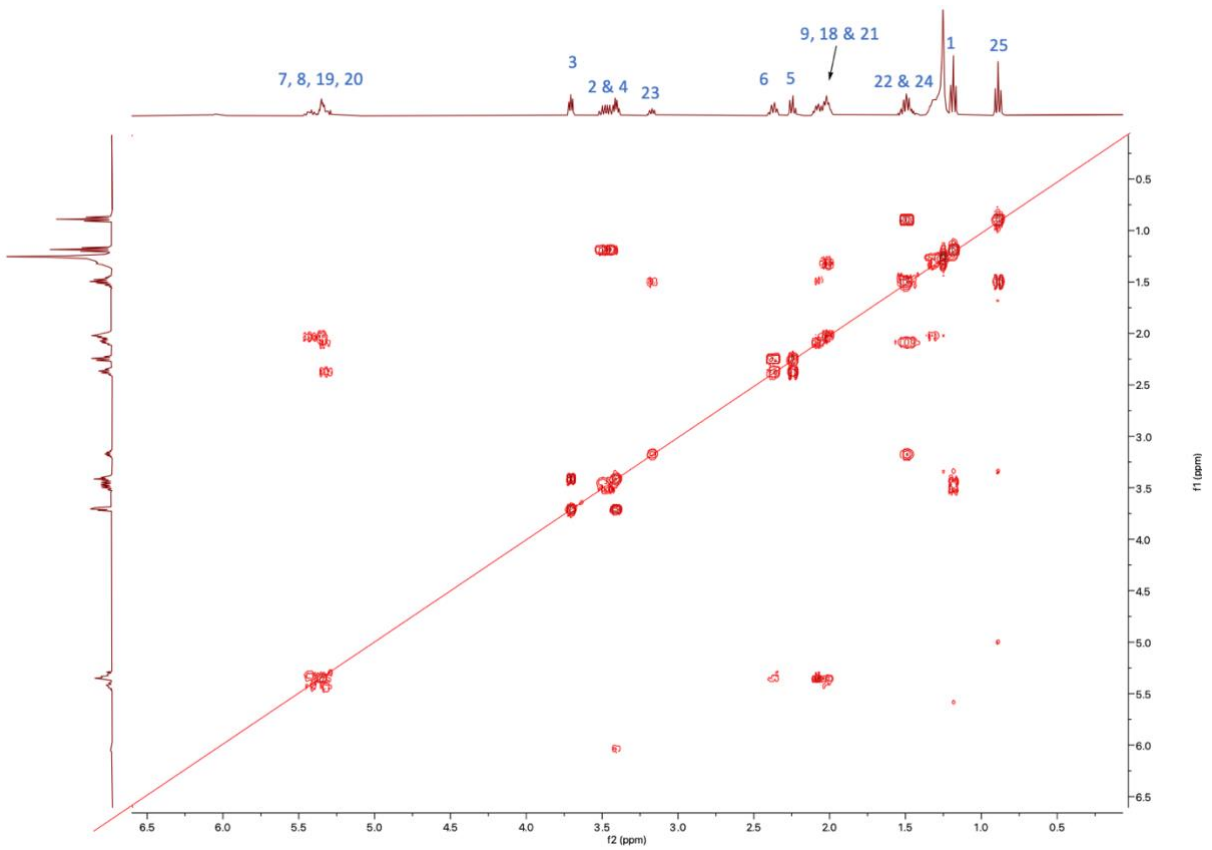


Figure 35 COSY spectrum for compound 9.

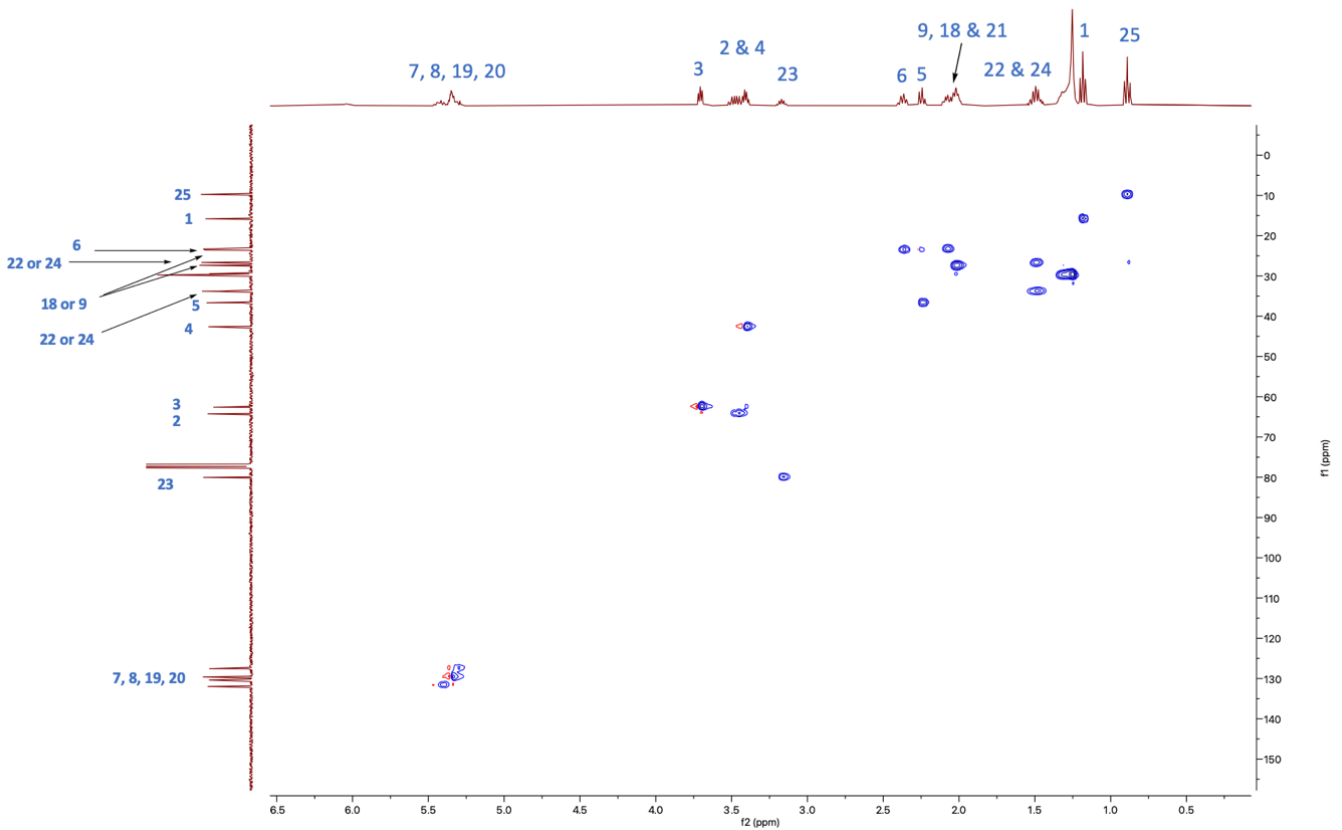


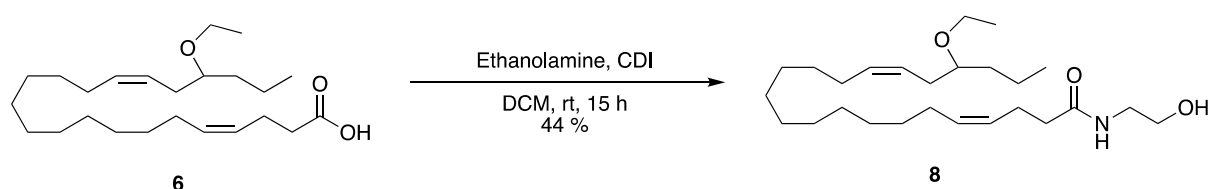
Figure 36 HSQC spectrum of compound 9.

In the IR spectrum of compound **9**, it is expected to observe a broad stretch in the area 3500 – 3200 cm^{-1} corresponding to the O-H bond. Additionally, N-H bonds are also expected in this area around 3300 cm^{-1} . The recorded IR spectrum displays a broad stretch at 3600 – 3000 cm^{-1} , which could correspond to both bonds. Furthermore, the carbonyl of the amide corresponds to the stretch at 1649 cm^{-1} . These findings are a further indication of the presence of an ethanolamide moiety. The obtained IR spectrum can be found in Appendix **8.3**.

4.5.11 Synthesis of 19,20-EpDPA-EA **8**

The same procedure as for preparing the 19,20-EpDPA mimic **9** was applied to synthesize mimic **8**, outlined in Scheme **41**. As expected, TLC displayed almost full conversion after 15 hours of stirring at room temperature. Acidic work-up and purification by flash column chromatography were performed.

Purification of compound **8** proved to be troublesome as well. It was first tried to start with 2.5 % MeOH in DCM, but impure fractions were quickly obtained. Two other attempts with different eluents, one time with EtOAc:heptane (1:1) and one time with 5% MeOH in DCM were necessary to at last obtain clean fractions. This procedure resulted in a yield of 44 %.



Scheme **41** Outline of the synthesis for compound **9**.

4.5.12 Characterization of 19,20-EpDPA-EA mimic **8**

As for mimic **9**, the recorded ^1NMR spectrum includes three new signals corresponding to an ethanolamide. One triplet arises at 3.72 ppm, corresponding to the protons of the carbinol. The protons of the carbon atom connected to the nitrogen atom give rise to the signal at 3.61– 3.37 ppm. The hydroxy proton gives rise to the most downfield singlet at 5.95 ppm. Nor in this spectrum is the amide proton visible. The remaining 43 protons align with the signals of the corresponding ester.

In the recorded ^{13}C NMR spectrum, the ethanolamide moiety gives rise to the peaks at 62.7 ppm and 42.7 ppm corresponding nicely to the ethanolamide moiety. The rest of the 24 signals align with the previously recorded spectrum of the carboxylic acid **6**. Hereby all 26 carbon atoms have been accounted for.

A suggestion for the assignment of shifts is shown in Table 3, first demonstrated through the COSY spectrum (Figure 37) and then the HSQC spectrum (Figure 38).

Table 3 Assignment of ^1H and ^{13}C chemical shifts of target molecule **8**.

Position: chemical shift (ppm)		
1: 1.18, t	1: 15.8	<p style="text-align: center;">8</p>
2 & 4: 3.61–3.37, m	2: 64.4	
3: 3.72, t	3: 62.7	
5 & 21: 2.29 – 2.16, m	4: 42.7	
6: 2.38, q	5: 36.7,	
7, 8, 19, 20: 5.50 – 5.27, m	6: 23.3	
9 & 18: 2.08 – 1.98, m	7, 8, 19, 20: 132.0, 131.9, 127.6, 125.7	
22: 3.26, p	22: 79.3	
23 & 24: 1.54 – 1.21, m	9, 18 & 21: 23.6, 27.4, 29.5	
25: 0.94- 0.86, m	23 & 24: 23.6, 36.7	
	25: 14.3	

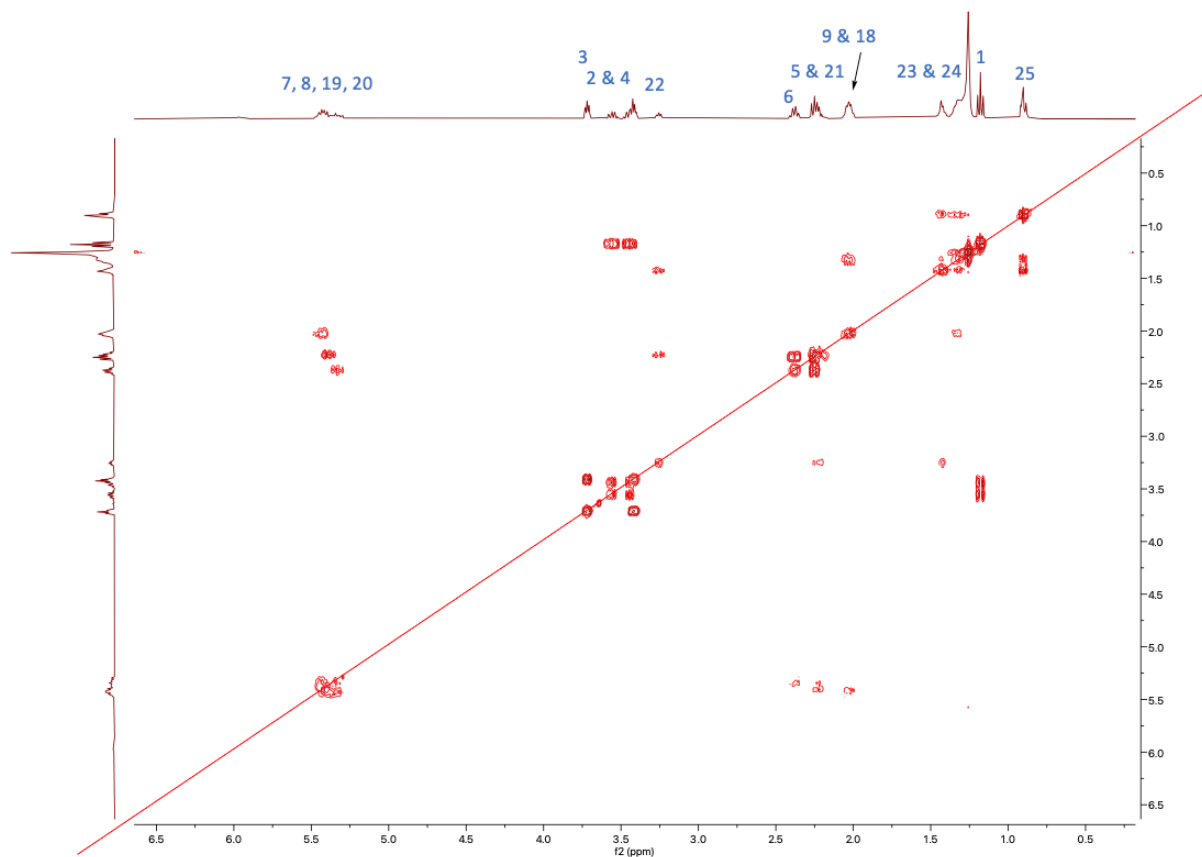


Figure 37 COSY spectrum of mimic 8.

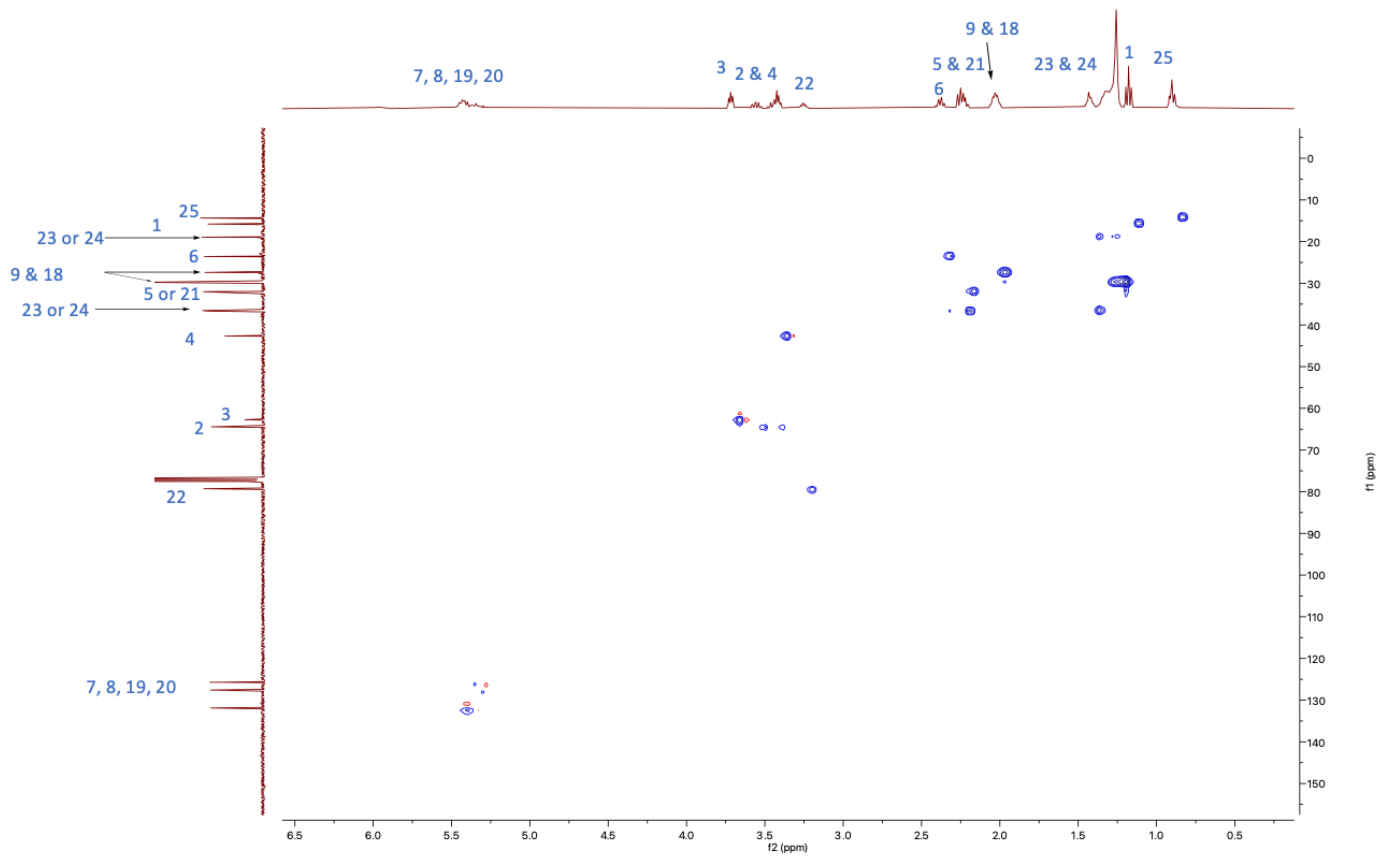


Figure 38 HSQC for compound 8.

As for ethanolamide **9**, the IR spectrum of compound **8** displays a broad stretch at 3600 – 3000 cm^{-1} , which could correspond to both the N-H and O-H bonds. Furthermore, the carbonyl of the amide corresponds to the stretch at 1651 cm^{-1} . These two stretches should correspond to the ethanolamide moiety. The obtained IR spectrum can be found in Appendix **8.3**.

5 Conclusion

Four stable mimics of the 19,20-EpDPA (**6** and **7**) and its ethanolamides (**8** and **9**) have been successfully synthesized. A total of 18 molecules were synthesized and characterized, of which 16 were previously not reported in the literature. Mimics **6** and **8** were prepared in six and seven steps, while the synthesis of **7** and **9** resulted in a total of seven and eight steps, respectively.

The obtained syntheses of molecules **6** and **8** were developed without encountering significant difficulties. The synthetic route toward target molecules **7** and **9** revealed that a reduction, instead of hydrolysis of the starting material *gamma*-caprolactone was more convenient. As the ring opening resulted in a diol rather than an ester, it was possible to employ a more conventional strategy. Despite additional steps of protection and deprotection, the new route **C** was more predictable and gave better yields than routes **A** and **B**. DMP oxidation, with smaller work-up volumes, turned out to result in the best yields of aldehyde **3**. By implementing the same strategy, there is a high possibility of achieving significantly higher yields of aldehyde **1** as well. The carboxylic acids **6** and **7** were prepared with Wittig reactions and hydrolysis. Lastly, ethanolamides **8** and **9** were successfully prepared by utilizing CDI in peptide coupling reactions.

These mimics should exhibit greater metabolic stability towards the sEH enzyme. To achieve this, the design strategy involved utilizing an ethyl ether as a bioisostere in place of the unstable epoxide. Additionally, the grade of unsaturation was reduced to lessen the incidence of oxidation of the double bonds. These modifications might result in a prolonged circulation time. In addition to being more metabolically stable, these mimics should reflect the biological properties of the 19,20-EpDPA and EAs, including anti-inflammatory, anti-fibrotic, antihyperalgesic, and cardioprotective effects. The target molecules **6-9** will shortly be submitted to biological studies at the group of Professor Bruce D. Hammock at the UC Davis, USA.

5.1 Future works

Given that these compounds exert some desired biological activity, additional 19,20-EpDPA and 19,20-EpDPA-EA mimics should be synthesized and evaluated. Other alkoxy groups of the bioisosteric ether, such as an isopropyl group, displayed in Figure 41 below, should be evaluated. Additionally, the grade of unsaturation of the lipid backbone can be altered. Bioisosteres in the place of the carboxylic acid, such as a tetrazole group, could also be evaluated. Preparing several compounds with these chemical alterations can make it possible to conduct a more comprehensive SAR study.

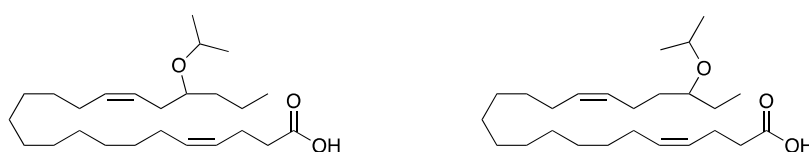


Figure 39 Proposed 19,20-EpDPA mimics with an isopropyl ether.

Another natural next step for future work is to prepare corresponding dopamine- and serotonin-based epoxide cannabinoids, displayed in Figure 42. These compounds can be synthesized from the carboxylic acids 6 and 7. Serotonin- and dopamine-based eCBs derived from AA have been reported to act as dual CB1/2 ligands and exhibit anti-inflammatory activity¹⁰³. Hence, the synthesis and biological evaluation of these DHA-derived compounds will be important in understanding the functions of eCBs and their potential therapeutical effects. Our group has been in contact with associate Professor Aditi Das at Georgia Tech, who is very interested in testing our compounds.

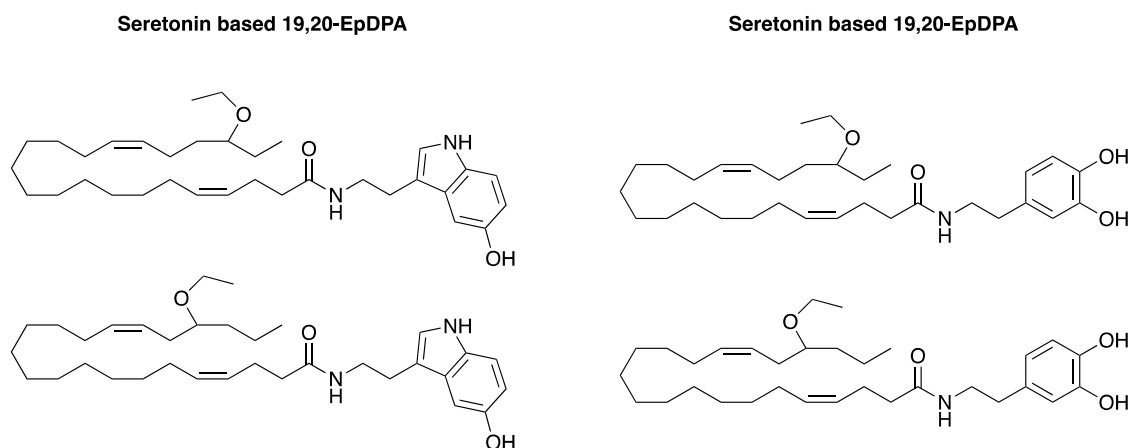


Figure 40 Outline of potential mimics with other structural modifications for the 19,20-EpDPAs.

6 Experimental

6.1 Material and apparatus

Unless stated otherwise, all commercially available solvents and reagents were used in the same form they were supplied without any further purification. The stated yields are based on isolated product unless stated otherwise. All sensitive reactions were performed under a nitrogen atmosphere using Schlenk techniques. Analytical TLC was performed on silica gel 60 F254 aluminum-backed plates (Merck). Depending on the reagents and products involved, different visualizing reagents were used, including KMnO_4 and cerium ammonium molybdate (CAM).

The primary purification method was flash chromatography performed on silica gel 60 (40-63 μm , Merck).

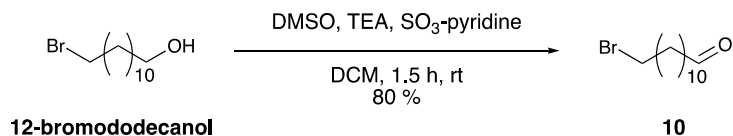
All NMR spectra were recorded on a Bruker AVI400 or AVNEO400 spectrometer at 400 MHz for ^1H NMR and 101 MHz for ^{13}C NMR. Chemical shifts are reported in parts per million (δ) relative to the central residual protium solvent resonance in ^1H NMR (CDCl_3 (7.27 ppm) and the central carbon solvent resonance in ^{13}C NMR ($\text{CDCl}_3 = 77.0$ ppm). Coupling constants (J) are reported in hertz.

High-resolution mass spectra were recorded at 70 eV at the Department of Chemistry, University of Oslo, on Water Prospec Q, using ESI as the method of ionization.

IR spectra were recorded on an Agilent 5500 Series FTIR instrument. All samples were first dissolved in Et_2O . All signals are described according to their intensity: w (weak), m (medium) and s (strong).

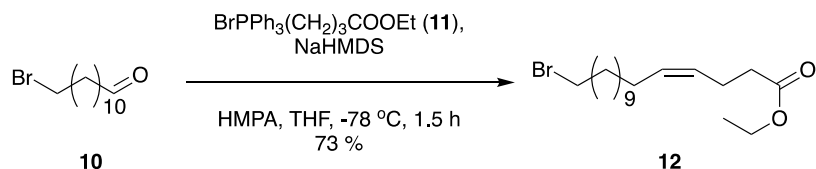
6.2 Experimental procedures

6.2.1 Synthesis of 12-bromododecanal **10**



To a round-bottom flask (100 mL) 12-bromododecanol (2.50 g, 9.43 mmol, 1.00 equiv.) was added to and dissolved in dry DCM (95 mL). Dry DMSO (23 mL), TEA (6.6 mL, 47 mmol, 5.0 equiv.), and SO₃ pyridine complex (4.50 g, 28.3 mmol, 3.00 equiv.) were added sequentially. After stirring for 1.5 hours at room temperature, water was added (100 mL) and the two phases were separated. Then, the aqueous phase was extracted Et₂O (2 x 50 ml). The combined organic phases were washed with brine and dried over Na₂SO₄. Thereafter, the filtrate was concentrated under reduced pressure. Purification was performed by flash column chromatography (heptane:Et₂O 95:5). The combined fractions containing the desired product were concentrated under reduced pressure. The reaction resulted in a colorless oil. **Yield:** 1.99 g, 7.56 mmol (80 %). **R_f:** 0.56 (EtOAc:heptane 1:1), visualized with KMnO₄-stain. **¹H NMR** (400 MHz, CDCl₃) δ 9.76 (t, *J* = 1.9 Hz, 1H), 3.40 (t, *J* = 7.0 Hz, 2H), 2.41 (td, *J* = 7.3, 1.9 Hz, 2H), 1.84 (p, *J* = 7.0 Hz, 2H), 1.62 (p, *J* = 7.3 Hz, 2H), 1.47 – 1.26 (m, 14H). **¹³C NMR** (101 MHz, CDCl₃) δ 203.1, 44.1, 34.2, 33.0, 29.6, 29.5, 29.5, 29.5, 29.3, 28.9, 28.3, 22.2. All spectroscopic data were in agreement with those reported in the literature ⁹⁷.

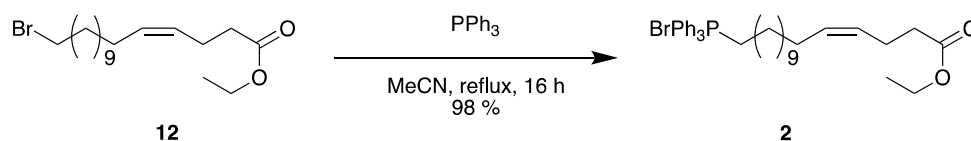
6.2.2 Synthesis of *Z*-alkene **12**



The Wittig salt **11** (4.12 g, 9.00 mmol, 1.20 equiv.) was dissolved in dry THF (18.6 mL) and HMPA (2.8 mL). Thereafter, the aldehyde **10** (1.97 g, 7.50 mmol, 1.00 equiv.) was dissolved in dry THF (1 mL). Both solutions were purged with N₂ three times. The reaction mixture containing the Wittig salt **11** was cooled down to -78 °C and NaHMDS (1.90 mL, 1.63 mmol, 1.05 equiv., 1.00 M in THF) was added. Next, the solution was stirred at room temperature for

30 minutes and thereafter cooled to $-78\text{ }^{\circ}\text{C}$. Aldehyde **10** was added in a dropwise manner and the mixture was stirred for 1.5 hours. Next, the solution was slowly warmed up to $0\text{ }^{\circ}\text{C}$. NH_4Cl (sat. aq., 20 ml) was added to quench the reaction, and the two phases were separated. The aqueous phase was extracted with Et_2O (2 x 15 ml). Thereafter, the combined organic extracts were washed with brine and dried over NaSO_4 . The crude mixture was concentrated under reduced pressure. The concentrate was purified by flash column chromatography (EtOAc : heptane 4:96). The combined fractions containing the desired product were concentrated under reduced pressure, which resulted in a colorless oil. **Yield:** 1.90 g, 5.50 mmol (73 %). **R_r:** 0.52 (EtOAc :heptane 1:2), visualized with KMnO_4 -stain. **$^1\text{H NMR}$** (400 MHz, CDCl_3) δ 5.46 – 5.25 (m, 2H), 4.12 (q, $J = 7.1$ Hz, 2H), 3.39 (t, $J = 6.9$ Hz, 2H), 2.40 – 2.27 (m, 4H), 2.02 (q, $J = 6.9$ Hz, 2H), 1.83 (p, $J = 6.9$, 2H), 1.47 – 1.17 (m, 19H). **$^{13}\text{C NMR}$** (101 MHz, CDCl_3) δ 173.4, 131.6, 127.5, 60.4, 34.5, 34.13, 33.0, 29.7, 29.7, 29.6, 29.5 (2C), 29.4, 28.9, 28.3, 27.3, 22.9, 14.4. **HRMS (ESI-TOF)** Exact mass calculated for $\text{C}_{18}\text{H}_{33}\text{O}_2\text{BrNa}$ $[\text{M} + \text{Na}]^+$: 383.1556; found 383.1555.

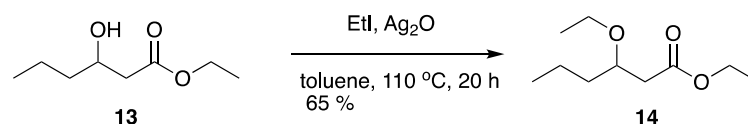
6.2.3 Synthesis of Wittig salt 2



Compound **12** (1.89 g, 5.12 mmol, 1.00 equiv.) was dissolved in dry acetonitrile (11 mL) and triphenylphosphine (5.37 g, 20.5 mmol, 4.00 equiv.) was then added. The solution was purged three times, then refluxed overnight (16 h). The next morning it was cooled to room temperature. The solvent was removed by evaporation. Purification was performed by flash column chromatography on silica gel, starting with only DCM until excess triphenylphosphine had eluted, then the eluent was changed to 5 % MeOH in DCM. The fractions were thereafter concentrated under reduced pressure at $50\text{ }^{\circ}\text{C}$. this resulted in a slightly red-colored oil. **Yield:** 3.12 g, 5.02 mmol (98 %). **$^1\text{H NMR}$** 400 MHz, CDCl_3) δ 7.83 – 7.62 (m, 15H), 5.40 – 5.21 (m, 2H), 4.06 (q, $J = 7.1$ Hz, 2H), 3.73 – 3.62 (m, 2H), 2.34 – 2.22 (m, 4H), 1.96 (q, $J = 7.0$ Hz, 2H), 1.57 (m, 4H), 1.34 – 1.06 (m, 17H). **$^{13}\text{C NMR}$** 101 MHz, CDCl_3) δ 173.3, 135.1 (d, $J = 3.1$ Hz, 3C), 133.7 (d, $J = 9.9$ Hz, 6C), 131.5, 130.6 (d, $J = 12.5$ Hz, 6C), 127.3, 118.8, 117.9, 60.3, 34.4, 30.5, 30.4, 29.6, 29.5, 29.5, 29.5, 29.3, 29.2, 29.2, 27.2, 22.8, 22.7, 22.6, 14.3.

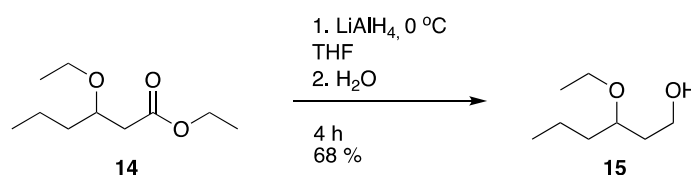
HRMS (ESI-TOF): Exact mass calculated for C₃₆H₄₈O₂P 543.3385 [M - Br]⁻ 383.1556; found 543.3385.

6.2.4 Synthesis of ether 14



Ethyl 3-hydroxy hexanoate **13** (3.00 mL, 18.2 mmol, 1.00 equiv.), ethyl iodide (7.30 mL, 89.3 mmol, 4.90 equiv.), silver(I)oxide (20.9 g, 89.3 mmol, 4.90 equiv.) and toluene (150 mL) were added. The mixture was stirred at 110 °C for 6 hours before ethyl iodide once again was added (7.30 mL, 89.3 mmol, 4.90 equiv.). After stirring for 16 hours at reflux, the reaction mixture was filtrated through a Celite plug. The filtrate was concentrated under low pressure. The concentrate was purified by flash column chromatography (pentane:Et₂O 95:5) and the combined fractions were concentrated under low pressure resulting in a colorless liquid. **Yield:** 1.40 g, 11.8 mmol (65 %) **R_r:** 0.61(EtOAc:heptane 1:1), visualized with KMnO₄-stain. **¹H NMR** (400 MHz, CDCl₃) δ 4.14 (q, *J* = 7.1 Hz, 2H), 3.77 – 3.66 (m, 1H), 3.57 – 3.45 (m, 2H), 2.51 (dd, *J* = 14.9, 7.3 Hz, 1H), 2.39 (dd, *J* = 14.9, 5.6 Hz, 1H), 1.61 – 1.30 (m, 4H), 1.25 (t, *J* = 7.1 Hz, 3H), 1.15 (t, *J* = 7.0 Hz, 3H), 0.91 (t, *J* = 7.2 Hz, 3H). **¹³C NMR** (101 MHz, CDCl₃) δ 172.1, 76.1, 64.9, 60.5, 40.3, 37.0, 18.7, 15.7, 14.4, 14.2. **HRMS (ESI-TOF)** Exact mass calculated for C₁₀H₂₀O₃Na [M + Na]⁺: 211.1305; found 211.1305.

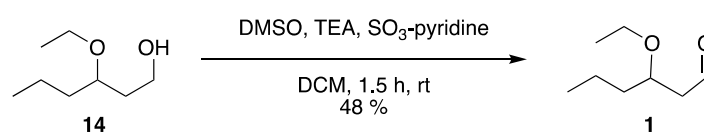
6.2.5 Reduction of ester 14



Compound **14** (1.38 g, 11.6 mmol, 1.00 equiv.) was dissolved in THF (5 mL) and added to a round-bottomed flask with LiAlH₄ (58.0 ml, 58.1 mmol, 5.00 equiv., 1.00 M in THF) at 0 °C. The solution was thereafter allowed to reach room temperature and stir for 4 hours. Next, the solution was again cooled to 0 °C. Water (2.2 mL) was added in a dropwise manner. Thereafter, NaOH (2.2 mL, aq. 15%) and distilled water (6.6 mL) were added sequentially. The mixture was diluted with Et₂O (5 mL) and dried with MgSO₄. Filtration was performed on a Büchner

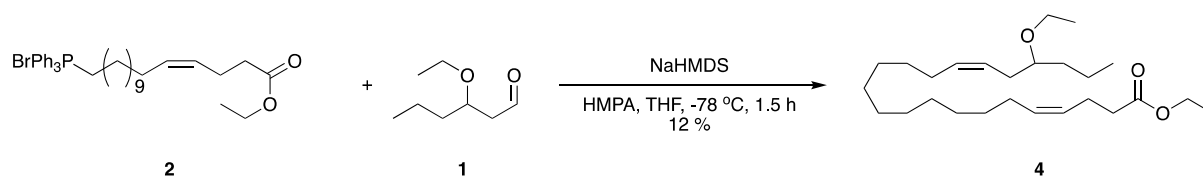
funnel. The filtrate was concentrated at low pressure resulting in a colorless oil. **Yield:** 0.901 g, 6.18 mmol (68 %) **Rr:** 0.28 (EtOAc:heptane 1:1.5) visualized with KMnO₄-stain. ¹H NMR (400 MHz, CDCl₃) δ 3.90 – 3.68 (m, 2H), 3.67 – 3.33 (m, 3H), 2.85 – 2.78 (m, 1H), 1.87 – 1.11 (m, 9H), 1.01 – 0.80 (m, 3H). ¹³C NMR (101 MHz, CDCl₃) δ 79.6, 64.4, 61.4, 36.0, 35.9, 18.6, 15.8, 14.4. **HRMS (ESI-TOF)** Exact mass calculated for C₆H₁₈O₂Na [M + Na]⁺: 169.1200; found 169.1199.

6.2.6 Synthesis of aldehyde 1



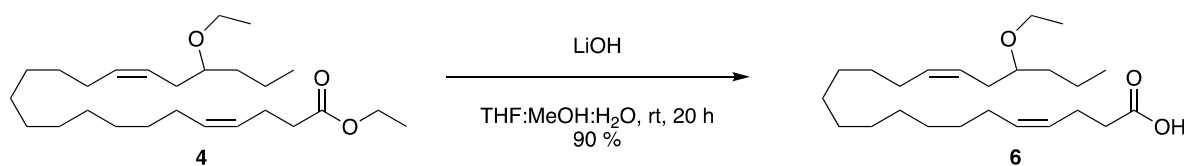
To a round-bottom flask (250 mL) the alcohol **14** (0.901 g, 6.18 mmol, 1.00 equiv.) was added and dissolved in dry DCM (62 mL). Dry DMSO (15 mL), TEA (4.3 mL, 31.0 mmol, 5.0 equiv.), and SO₃ pyridine complex (2.96 g, 18.61 mmol, 3.00 equiv.) were added sequentially. After stirring for 1.5 hours at room temperature, water was added (100 mL) and the two phases were separated. The aqueous phase was extracted with Et₂O (2 x 50 mL) and combined organic extracts were washed with brine and dried over Na₂SO₄ and filtrated. The filtrate was concentrated under reduced pressure. Purification was performed by flash column chromatography (heptane: Et₂O 95:5) and the combined fractions containing the desired product were added and concentrated under reduced pressure. The reaction resulted in a colorless oil. **Yield:** 0.432 g, 2.96 mmol (48 %) **Rr:** 0.48 (EtOAc:heptane 1:1) visualized with KMnO₄-stain. ¹H NMR (400 MHz, CDCl₃) δ 9.79 (t, *J* = 2.3 Hz, 1H), 3.84 – 3.73 (m, 1H), 3.49 (m, 2H), 2.59 (ddd, *J* = 16.2, 7.1, 2.5 Hz, 1H), 2.49 (ddd, *J* = 16.0, 4.9, 1.9 Hz, 1H), 1.63 – 1.22 (m, 6H), 1.15 (t, *J* = 7.0 Hz, 3H), 0.92 (t, *J* = 7.2 Hz, 3H). ¹³C NMR (101 MHz, CDCl₃) δ 202.0, 74.6, 64.7, 48.6, 36.8, 18.6, 15.6, 14.2.

6.2.7 Synthesis of Z-alkene 4



Aldehyde **1** (0.403 g, 2.77 mmol, 1.00 equiv.) was dissolved in dry THF (2 mL). In a separate flask, the Wittig salt **2** (2.10 g, 3.30 mmol, 1.20 equiv.) was dissolved in dry THF (15 mL) and HMPA (5.00 mL) was added. Both solutions were purged with N₂ three times each. The reaction solution containing the Wittig salt **2** was cooled down to -78 °C and NaHMDS (2.90 mL, 2.91 mmol, 1.05 equiv., 1.00 M in THF) was added. The solution was removed from the dry ice/acetone bath for 30 minutes. The solution containing the aldehyde was added in a dropwise manner and thereafter stirred for 1.5 hours at -78 °C. Thereafter the reaction was slowly allowed to reach 0 °C. NH₄Cl (50 mL, sat. aq.) was added. The two phases were separated. The aqueous phase was extracted with Et₂O (2 x 25 mL). The combined organic extracts were washed with brine (2 x 10 mL), dried over Na₂SO₄, and filtrated through a silica plug. The filtrate was purified by flash column chromatography (heptane:Et₂O 96:4). The combined fractions containing the desired product were added and concentrated under reduced pressure to a round-bottom flask. **Yield:** 0.14 g, 0.34 mmol (12 %) **R_r:** 0.25 (heptane: Et₂O 2:1) visualized with KMnO₄-stain. **¹H NMR** (400 MHz, CDCl₃) δ 5.46 – 5.23 (m, 4H), 4.09 (q, J = 7.1 Hz, 2H), 3.61-3.37 (m, 2H), 3.22 (p, 1H), 2.36 – 2.25 (m, 4H), 2.25 – 2.14 (m, 2H), 2.04 – 1.94 (m, 4H), 1.46 – 1.18 (m, 24H), 1.14 (t, J = 7.0 Hz, 3H), 0.89 – 0.82 (m, 3H). **¹³C NMR** (101 MHz, CDCl₃) δ 173.4, 131.8, 131.6, 127.5, 125.7, 79.2, 64.4, 60.4, 36.5, 34.6, 32.0, 29.8, 29.8, 29.7, 29.7, 29.7, 29.5, 29.4, 27.6, 27.3, 23.0, 18.9, 15.8, 14.4, 14.3. **HRMS (ESI-TOF)** Exact mass calculated for C₂₆H₄₈O₃Na [M + Na]⁺: 431.3495; found 431.3496.

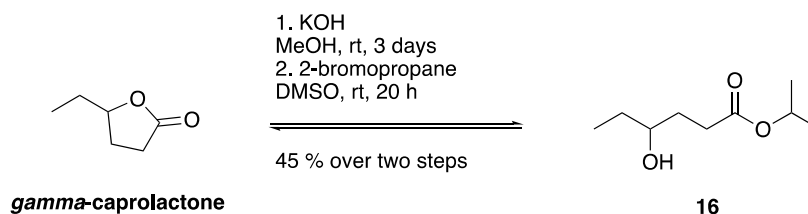
6.2.8 Synthesis of target molecule 6



In a round bottom flask (100 mL) the ester **4** (0.14 g, 0.30 mmol, 1.00 equiv.) was dissolved in THF:MeOH:H₂O (2:2:1) and stirred for three hours at 0 °C. Anhydrous LiOH (0.21 g, 8.85

mmol, 30.00 equiv.) was added in one portion. The solution was thereafter stirred overnight at room temperature. After 20 hours, NaH₂PO₄ (50 mL, sat. aq.) was added. The two phases were separated. And the aqueous phase was reextracted with EtOAc (2 x 30 mL). The combined organic phases were dried over Na₂SO₄, filtered, and concentrated under reduced pressure. The crude was purified by flash column chromatography two times. The first time with 50% EtOAc in heptane and a second time with gradient from 5% to 30% EtOAc in heptane. The combined fractions containing the desired product were added and concentrated under reduced pressure to a round-bottom flask. This resulted in target molecule **6** in a colorless oil. **Yield:** 97 mg, 0.30 mmol (90 %) **R_f:** 0.33 (EtOAc:heptane 1:1) visualized with KMnO₄-stain. **¹H NMR** (400 MHz, CDCl₃) δ 5.49 – 5.29 (m, 4H), 3.56 (dq, J = 9.3, 7.0 Hz, 1H), 3.45 (dq, J = 9.3, 7.0 Hz, 1H), 3.26 (p, J = 5.4 Hz, 1H), 2.42 – 2.33 (m, 4H), 2.27 – 2.15 (m, 2H), 2.08 – 1.97 (m, 4H), 1.51 – 1.22 (m, 20H), 1.18 (t, J = 7.0 Hz, 3H), 0.90 (t, J = 7.0 Hz, 3H). **¹³C NMR** (101 MHz, CDCl₃) δ 179.3, 132.0, 131.9, 127.1, 125.7, 79.3, 64.4, 36.5, 34.3, 32.0, 29.8, 29.8, 29.7 (2C), 29.7, 29.7, 29.5, 29.4, 27.5, 27.3, 22.7, 18.9, 15.7, 14.3. **HRMS (ESI-TOF)** Exact mass calculated for C₂₆H₄₈O₃Na [M + Na]⁺: 431.3495; found 431.3496. **IR (ATR, cm⁻¹)** v: 3010 (w), 2960 (m), 1738 (m).

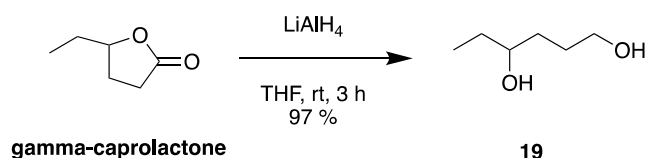
6.2.9 Hydrolysis of *gamma*-caprolactone



To a stirred solution of the *gamma*-caprolactone (5.0 mL, 45 mmol, 1.0 equiv.) in MeOH (90 mL) KOH (2.48 g, 44.8 mmol, 1.00 equiv.) was added. The mixture was stirred at room temperature for 3 days. The solvent was removed under reduced pressure to yield a white solid. DMSO (120 mL) was added to the white solid with heating, which gave a light brown mixture. Thereafter the solution was cooled to 0 °C and 2-bromopropane (15.0 mL, 160 mmol, 3.70 equiv.) was added. After stirring at room temperature for 20 hours, the solution was diluted with water (100 mL) and extracted with Et₂O (3 x 75 mL). The combined organic extracts were washed with water (3 x 100 mL), dried over Na₂SO₄, filtrated, and concentrated under reduced pressure. The resulting oil was purified by flash chromatography starting with pure DCM and changing to 5% Et₂O in DCM. The combined fractions containing the desired product were

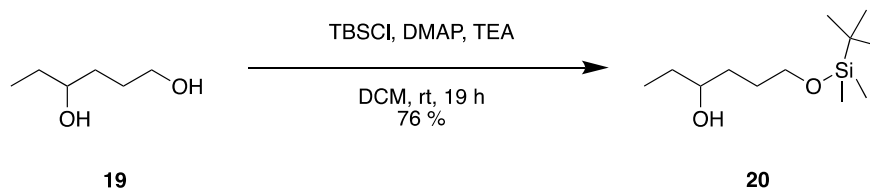
added and concentrated under reduced pressure yielding compound **16** as a colorless oil. **Yield:** 3.40 g, 19.5 mmol (45 %) **R_f:** 0.09 (5% Et₂O in DCM) visualized with KMnO₄-stain. **¹H NMR** (400 MHz, CDCl₃) δ 4.99 (sept, J = 6.3 Hz, 1H), 3.58 – 3.48 (m, 1H), 2.41 (td, J = 7.3, 2.5 Hz, 2H), 1.91 – 1.59 (m, 2H), 1.58 – 1.38 (m, 3H), 1.22 (d, J = 6.3 Hz, 6H), 0.94 (t, J = 7.5 Hz, 3H). **¹³C NMR** (101 MHz, CDCl₃) δ 173.9, 72.8, 67.9, 31.8, 31.3, 30.4, 21.9, 21.9, 10.0. **HRMS (ESI-TOF)** Exact mass calculated for C₉H₁₈O₃Na [M + Na]⁺: 197.1147; found 197.1148.

6.2.10 Reduction of *gamma*-caprolactone



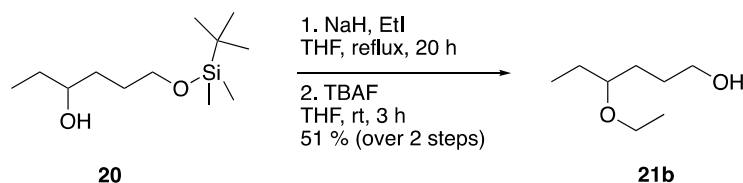
To a stirred solution of *gamma*-caprolactone (2.2 mL, 20 mmol, 1.0 equiv.) in THF (24 mL) at 0 °C was added LiAlH₄ (40 mL, 40 mmol, 2.0 equiv., 1.0 M in Et₂O) slowly. The solution was thereafter allowed to reach room temperature. After stirring for 3 hours the reaction was cooled to 0 °C. Water (1.5 mL) was added in a dropwise manner. Thereafter NaOH (1.5 mL, aq. 15%) and distilled water (4.5 mL) were added sequentially. The mixture was dried with MgSO₄. Filtration was performed on a Büchner funnel. The filtrate was concentrated at low pressure and purified through a silica plug (EtOAc) and concentrated under reduced pressure. This resulted in the desired compound **19** as a colorless oil. **Yield:** 2.08 g, 17.9 mmol (89 %) **R_f:** 0.15 (EtOAc), visualized with KMnO₄-stain. **¹H NMR** (400 MHz, CDCl₃) δ 3.74 (s, 2H), 3.68 – 3.44 (m, 3H), 1.70 – 1.54 (m, 3H), 1.51 – 1.35 (m, 3H), 0.89 (t, J = 7.5 Hz, 3H). **¹³C NMR** (101 MHz, CDCl₃) δ 73.1, 62.7, 33.9, 30.3, 29.1, 10.1. **HRMS (ESI-TOF)** Exact mass calculated for C₆H₁₄O₂Na [M + Na]⁺: 141.0886; found 141.0887. All spectroscopic data were in agreement with those reported in the literature^{101, 102}.

6.2.11 Selective TBS-protection of compound 19



To a stirred solution of compound **19** (1.99 g, 17.5 mmol, 1.00 equiv.) in DCM (50 mL), DMAP (0.086 g, 0.70 mmol, 0.040 equiv.) TEA (2.23 g, 21.0 mmol, 1.20 equiv.) and TBSCl (2.90 g, 19.3 mmol, 1.10 equiv.) were added. The solution was stirred at room temperature for 19 hours. Water (10 mL) and NH₄Cl (30 mL, sat. aq.) were added, and the two phases were separated. The aqueous phase was reextracted with DCM (3 x 30 mL). The combined organic extracts were washed with NH₄Cl (3 x 30 mL, sat. aq.), dried with NaSO₄, filtrated, and concentrated under reduced pressure. The concentrate was purified by flash column chromatography (Et₂O:heptane 1:10). The combined fractions containing the desired product were added and concentrated under reduced pressure yielding compound **20** as a colorless oil. **Yield:** 3.09 g, 13.3 mmol (76 %). **R_f:** 0.21(EtOAc), visualized with KMnO₄-stain. **¹H NMR** (400 MHz, CDCl₃) δ 3.64 (m, 2H), 3.56 – 3.45 (m, 1H), 2.60 (s, 1H), 1.68 – 1.56 (m, 3H), 1.51 – 1.36 (m, 3H), 0.95 – 0.82 (m, 12H), 0.04 (s, 6H). **¹³C NMR** (101 MHz, CDCl₃) δ 73.0, 63.7, 34.2, 29.3, 26.0 (3C), 18.4, 10.1, -5.3 (2C). **HRMS (ESI-TOF)** Exact mass calculated for C₁₂H₂₈O₂SiNa [M + Na]⁺: 255.1749; found 255.1751.

6.2.12 Alkylation and deprotection of compound 20

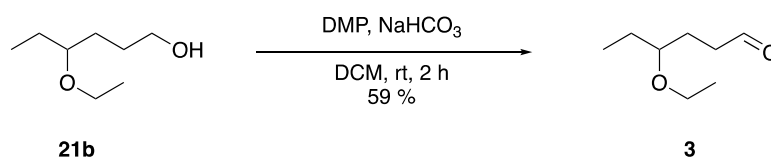


NaH (0.251 g, 2.08 mmol, 3.00 equiv., 60 % in mineral oil) was washed with THF (2 x 20 mL) and added a solution of alcohol **20** in THF (5 mL) at 0 °C. After stirring for 30 minutes, EtI (0.25 mL, 3.2 mmol, 3.0 equiv.) was added and the mixture was heated to reflux under nitrogen for 20 hours. Et₂O (50 mL) and water (50 mL) were added. The two phases were separated and the aqueous phase was reextracted with Et₂O (2 x 50 mL). The combined organic extracts were washed with water (2 x 50 mL) and once with brine (50 mL). Dried over NaSO₄, filtrated, and concentrated under reduced pressure. This resulted in a colorless oil, which was used in the

subsequent reaction without any further purification. **R_f**: 0.28 (heptane), visualized with KMnO₄-stain. **¹H NMR** (400 MHz, CDCl₃) δ 3.65 – 3.55 (m, 2H), 3.51 – 3.39 (m, 2H), 3.22 – 3.12 (m, 1H), 1.67 – 1.39 (m, 6H), 1.17 (t, *J* = 7.0 Hz, 3H), 0.93 – 0.82 (m, 6H), 0.04 (s, 6H). **¹³C NMR** (101 MHz, CDCl₃) δ 80.4, 64.2, 63.5, 29.9, 28.9, 26.8, 26.1, 18.5, 15.8, 9.8, - 5.1. **HRMS (ESI-TOF)** Exact mass calculated for C₁₄H₃₂O₂SiNa [M + Na]⁺: 283.2064; found 283.2064.

Next, the residue from the previous step was dissolved in dry THF (200 mL) and cooled to 0 °C. TBAF (2.8 mL, 2.8 mmol, 2.5 equiv., 1.0 M in THF) was slowly added to the solution, which was stirred for 3 hours. Thereafter, phosphate buffer (30 mL), EtOAc (30 mL), and water (30 mL) were added. The two phases were separated and the aqueous phase was reextracted with EtOAc (3 x 30 mL). The combined organic extracts were washed with water (2 x 30 mL) and once with brine (30 mL). Dried with NaSO₄, filtrated, and concentrated under reduced pressure. The concentrate was purified by flash column chromatography (EtOAc:heptane 4:6). The combined fractions containing the desired product were added and concentrated under reduced pressure yielding compound **21b** as a colorless oil. **Yield**: 0.64 g, 2.6 mmol (51 % over two steps). **R_f**: 0.25 (EtOAc: heptane 1:1), visualized with KMnO₄-stain. **¹H NMR** (400 MHz, CDCl₃) δ 3.68 – 3.40 (m, 4H), 3.28 – 3.18 (m, 1H), 2.67 – 2.52 (m, 1H), 1.73 – 1.40 (m, 6H), 1.20 (t, *J* = 7.0 Hz, 3H), 0.90 (t, *J* = 7.5 Hz, 3H). **¹³C NMR** (101 MHz, CDCl₃) δ 80.6, 64.2, 63.1, 30.4, 28.9, 26.3, 15.6, 9.6. **HRMS (ESI-TOF)** Exact mass calculated for C₈H₁₈O₂SiNa [M + Na]⁺: 169.1199; found 169.1201.

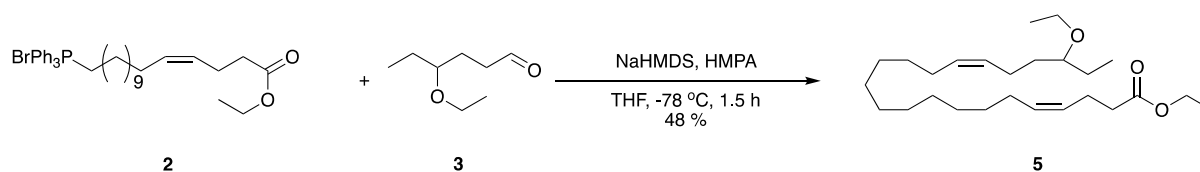
6.2.13 DMP oxidation of alcohol **21b**



Compound **21b** (0.683 g, 4.67 mmol, 1.00 equiv.) was dissolved in DCM (37 mL) and added NaHCO₃ (0.782 g, 9.24 mmol, 2.00 equiv.) and Dess-Martin periodinane (3.07 g, 6.53 mmol, 1.40 equiv.). The mixture was stirred at room temperature for 2 hours before NaHCO₃ (10 mL, sat. aq.) was added and the two phases were separated. The aqueous phase was extracted with DCM (2 x 5 mL). The combined organic layers were washed with water (5 mL) once, dried over MgSO₄, filtrated, and concentrated at reduced pressure. Purification was performed by flash column chromatography (5 % Et₂O in DCM). The combined fractions containing the

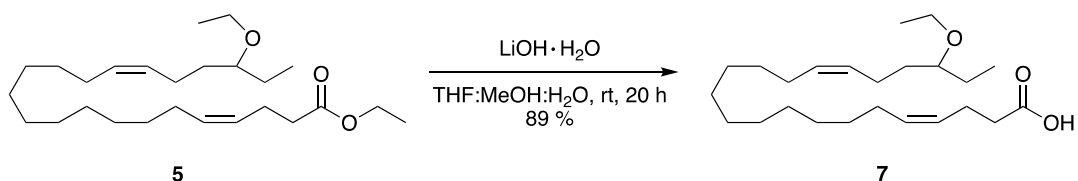
desired product were added and concentrated under reduced pressure yielding compound **3** as a colorless oil. **Yield:** 0.33 g, 2.3 mmol (59 %) **R_f:** 0.33 (5 % Et₂O in DCM). **¹H NMR** (400 MHz, CDCl₃) δ 9.77 (t, *J* = 1.9 Hz, 1H), 3.56 – 3.33 (m, 2H), 3.24 – 3.14 (m, 1H), 2.49 (td, *J* = 7.3, 1.9 Hz, 2H), 1.91 – 1.68 (m, 2H), 1.64 – 1.37 (m, 2H), 1.16 (t, *J* = 7.0 Hz, 3H), 0.90 (t, *J* = 7.5 Hz, 3H). **¹³C NMR** (101 MHz, CDCl₃) δ 202.6, 79.5, 64.3, 40.2, 26.5, 26.2, 15.5, 9.5. **HRMS (ESI-TOF)** Exact mass calculated for C₈H₁₆O₂Na [M + Na]⁺:167.1043; found 167.1043.

6.2.14 Synthesis of *Z*-alkene **5**



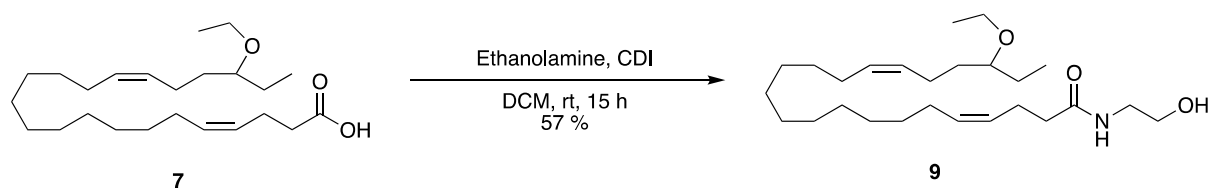
Aldehyde **3** (0.280 g, 1.92 mmol, 1.00 equiv.) was dissolved in dry THF (2 mL). In a separate flask, the Wittig salt **2** (1.20 g, 1.92 mmol, 1.00 equiv.) was dissolved in dry THF (8.7 mL) and HMPA (2.9 mL) was added. Both solutions were purged with N₂ and degassed three times each. The reaction solution containing the Wittig salt **2** was cooled down to -78 °C and NaHMDS (2.00 mL, 2.02 mmol, 1.05 equiv., 1.00 M in THF,) was added and put to room temperature for 15 minutes. The solution containing the aldehyde was added in a dropwise manner at -78 °C and thereafter stirred for 1.5 hours. Thereafter the reaction was slowly allowed to reach 0 °C. NH₄Cl (30 mL, sat. aq.) was added and the two phases were separated. The aqueous phase was extracted with Et₂O (2 x 15 mL). Next, the combined organic extracts were washed with brine (2 x 10 mL), dried over Na₂SO₄, and filtrated through a silica plug (8 % EtOAc in heptane). The filtrate was purified by flash column chromatography (heptane:Et₂O 96:4). The combined fractions containing the desired product were added and concentrated under reduced pressure yielding compound **5** as a colorless oil. **Yield:** 0.38 g, 0.93 mmol (48 %) **R_f:** 0.58 (EtOAc: heptane 1:1) visualized with KMnO₄-stain. **¹H NMR** (400 MHz, CDCl₃) δ 5.45 – 5.28 (m, 4H), 4.17 – 4.07 (m, 2H), 3.54 – 3.40 (m, 2H), 3.17 (p, *J* = 5.9 Hz, 1H), 2.39 – 2.29 (m, 1H), 2.13 – 1.98 (m, 6H), 1.57 – 1.42 (m, 4H), 1.38 – 1.15 (m, 23H), 0.89 (t, *J* = 7.0 Hz, 3H). **¹³C NMR** (101 MHz, CDCl₃) δ 173.4, 131.7, 130.3, 129.6, 127.5, 80.0, 64.3, 60.4, 34.6, 33.8, 29.9, 29.8, 29.8, 29.7, 29.5, 29.5, 23.3, 23.0, 15.8, 14.4, 9.7 **HRMS (ESI-TOF)** Exact mass calculated for C₂₆H₄₈O₃Na [M + Na]⁺:431.3496; found 431.3496.

6.2.15 Synthesis of target molecule 7



Ester **5** (0.12 g, 0.29 mmol, 1.00 equiv.) was dissolved in THF:MeOH:H₂O (2:2:1) and stirred for 3 hours at 0 °C. LiOH monohydrate (0.37 g, 8.8 mmol, 30 equiv.) was added in one portion. The solution was thereafter stirred overnight at room temperature. NaH₂PO₄ (60 mL, sat. aq.) was added after 20 hours, and the two phases were separated. The aqueous phase was reextracted with EtOAc (2 x 30 mL) and the combined organic phases were dried over Na₂SO₄, filtrated, and concentrated under reduced pressure. The crude was purified by flash column chromatography (EtOAc:heptane 1:1). This resulted in target molecule **7** as a colorless oil. **Yield:** 0.10 g, 0.28 mmol (89 %) **Rr:** 0.18 (EtOAc: heptane 1:1) visualized with KMnO₄-stain. **¹H NMR** (400 MHz, CDCl₃) δ 5.52 – 5.24 (m, 4H), 4.12 (q, *J* = 7.1 Hz, 1H), 3.56 – 3.40 (m, 2H), 3.18 (p, *J* = 5.7 Hz, 1H), 2.44 – 2.32 (m, 4H), 2.14 – 1.96 (m, 6H), 1.58 – 1.45 (m, 4H), 1.39 – 1.14 (m, 20H), 0.89 (t, *J* = 7.4 Hz, 3H). **¹³C NMR** (101 MHz, CDCl₃) δ 173.4, 131.9, 130.2, 129.5, 126.9, 80.0, 64.1, 34.1, 33.6, 29.8, 29.6, 29.6, 29.6, 29.5, 29.3, 29.3, 27.2, 27.2, 26.5, 23.2, 22.5, 15.6, 9.6. **HRMS (ESI-TOF)** Exact mass calculated for C₂₄H₄₃O₃Na [M + Na]⁺:379.3218; found 379.3217. **IR (ATR, cm⁻¹) v:** 3008 (w), 2964 (m), 1738 (m).

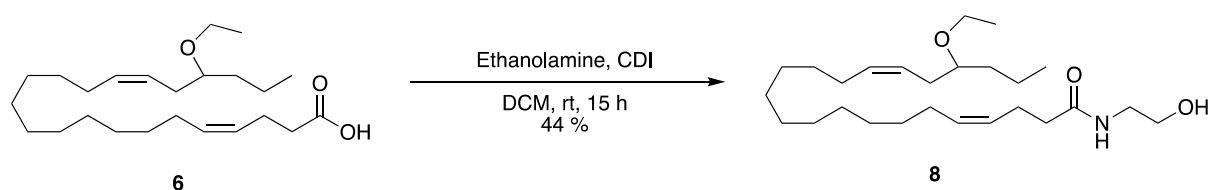
6.2.16 Synthesis of 19,20-EpDPA-EA mimic 9



The ester **7** (30 mg, 0.070 mmol, 1.0 equiv) was dissolved in DCM (1 mL) and added CDI (15 mg, 0.081 mmol, 1.1 equiv.). The solution was stirred at room temperature for 30 minutes before ethanalamine (5.0 μL, 0.081 mmol, 1.1 equiv.) was added. Thereafter, the solution was stirred for 15 hours before DCM (5 mL) and NH₄Cl (5 mL, sat. aq.) were added. HCl (1.0 M) was added until pH < 2. The two phases were separated. Thereafter, the aqueous layer was reextracted with DCM (3 x 5 mL). Combined organic layers were dried over Na₂SO₄, filtrated, and concentrated under reduced pressure. Purification was performed by flash column

chromatography first time with 5% MeOH in DCM. Second time with EtOAc:heptane (1:1) and lastly with 2.5% MeOH in DCM, changing to 5% and lastly 10% MeOH in DCM. The combined fractions containing the desired product were added and concentrated under reduced pressure to a round-bottom flask. The procedure yielded compound **9** as a colorless oil. **Yield:** 18 mg, 0.042 mmol (57 %). **R_f:** 0.12 (5% MeOH in DCM) **¹H NMR** (400 MHz, CDCl₃) δ 6.05 (s, 1H), 5.58 – 5.23 (m, 4H), 3.70 (t, *J* = 4.4 Hz, 2H), 3.58 – 3.28 (m, 4H), 3.22 – 3.12 (m, 1H), 2.37 (q, *J* = 7.2 Hz, 2H), 2.29 – 2.20 (m, 2H), 2.16 – 1.79 (m, 6H), 1.62 – 1.39 (m, 4H), 1.37 – 1.21 (m, 16H), 1.18 (t, *J* = 7.0 Hz, 3H), 0.89 (t, *J* = 7.5 Hz, 3H). **¹³C NMR** (101 MHz, CDCl₃) δ 174.0, 132.0, 130.4, 129.6, 127.6, 80.0, 64.3, 62.6, 42.6, 36.7, 33.8, 29.9, 29.8, 29.8 (2 C), 29.7 (2 C), 29.5 (2 C), 27.4, 27.4, 26.7, 23.6, 23.3, 15.8, 9.7. **HRMS (ESI-TOF)** Exact mass calculated for C₂₆H₄₉NO₃Na [M + Na]⁺:446.3605; found 446.3600. **IR (ATR, cm⁻¹) v:** 3310 (w), 1651 (m).

6.2.17 Synthesis of 19,20-EpDPA-EA mimic **8**



The ester **6** (39 mg, 0.092 mmol, 1.0 equiv.) was dissolved in DCM (1 mL) and added CDI (18 mg, 0.10 mmol, 1.1 equiv.). The solution was stirred at room temperature for 30 minutes before ethanolamine (6.5 μL, 0.10 mmol, 1.1 equiv.) was added. Thereafter, the solution was stirred for 15 hours before DCM (5 mL) and NH₄Cl (5 mL, sat. aq.) were added. HCl (1.0 M) was added until pH < 2. The two phases were separated. Thereafter, the aqueous layer was reextracted with DCM (3 x 5 mL). Combined organic layers were dried with NaSO₄, filtrated, and concentrated under reduced pressure. Purification was performed by flash column chromatography, first with 2.5% MeOH in DCM. Purification was performed a second time with EtOAc:heptane (1:1) and a third time with 5% MeOH in DCM. The combined fractions were concentrated *in vacuo* which resulted in the desired product **8** as a colorless oil. **Yield:** 19 mg, 0.044 mmol (44 %) **R_f:** 0.13 (5% MeOH in DCM) **¹H NMR** (400 MHz, CDCl₃) δ 5.95 (s, 1H), 5.50 – 5.27 (m, 4H), 3.72 (t, 2H), 3.61– 3.37 (m, 4H), 3.26 (p, *J* = 5.8 Hz, 1H), 2.38 (q, *J* = 7.3 Hz, 2H), 2.29 – 2.16 (m, 4H), 2.08 – 1.98 (m, 4H), 1.54 – 1.21 (m, 22H), 1.18 (t, *J* = 7.0 Hz, 3H), 0.94 – 0.86 (m, 3H). **¹³C NMR** (101 MHz, CDCl₃) δ 174.0, 132.0, 131.9, 127.6, 125.7, 79.3, 64.4, 62.7, 42.7, 36.7, 36.5, 32.0, 29.8, 29.8, 29.7, 29.5, 29.5, 27.6, 27.4, 23.6, 18.9, 15.8,

14.3. **HRMS (ESI-TOF)** Exact mass calculated for $C_{26}H_{49}NO_3Na$ $[M + Na]^+$:446.3605; found 446.3604. **IR (ATR, cm^{-1})** ν : 3309 (w), 1649 (m).

7 References

1. C. McReynolds, C. Morisseau, K. Wagner and B. Hammock, *Adv. Exp. Med. Biol.*, 2020, **1274**, 71-99.
2. A. Sharma, M. A. Hye Khan, S. P. Levick, K. S. Lee, B. D. Hammock and J. D. Imig, *Int. J. Mol. Sci.*, 2016, **17**, 406-410.
3. Y. Wang, K. M. Wagner, C. Morisseau and B. D. Hammock, *J. Pain Res.*, 2021, **14**, 61-72.
4. J. D. Imig, *Physiol. Rev.*, 2012, **92**, 101-130.
5. R. Pahwa, A. Goyal and I. Jialal, in *StatPearls*, StatPearls Publishing, Treasure Island, 2023, Available from: <https://www.ncbi.nlm.nih.gov/books/NBK493173/> pp- 1-12.
6. C. A. Henrick, G. B. Staal and J. B. Siddall, *J. Agric. Food. Chem.*, 1973, **21**, 354-359.
7. V. Sudhahar, S. Shaw and J. D. Imig, *Curr. Med. Chem.*, 2010, **17**, 1181-1190.
8. L. R. B. Dos Santos and I. Fleming, *Prostaglandins Other Lipid Mediat.*, 2020, **148**, 106407-106450.
9. B. Inceoglu, A. Bettaieb, F. G. Haj, A. V. Gomes and B. D. Hammock, *Prostaglandins Other Lipid Mediat.*, 2017, **133**, 68-78.
10. C. Morisseau and B. D. Hammock, *Annu. Rev. Pharmacol. Toxicol.*, 2013, **53**, 37-58.
11. C. Westphal, A. Konkell and W. H. Schunck, *Adv. Exp. Med. Biol.*, 2015, **851**, 151-187.
12. I. Djuricic and P. C. Calder, *Nutrients*, 2021, **13**, 2421-2429
13. A. Vik and T. V. Hansen, in *From Biosynthesis to Total Synthesis: Strategies and Tactics for Natural Products*, Hoboken, John Wiley & Sons, Inc., Hoboken, NJ, 2016, DOI: 10.1002/9781118754085.ch3, pp. 130-161.
14. J. Li, B. L. R. Pora, K. Dong and J. Hasjim, *Food Sci. Nutr.*, 2021, **9**, 5229-5243.
15. R. Medzhitov, *Nature*, 2008, **454**, 428-435.
16. H. Sprecher, D. L. Luthria, B. S. Mohammed and S. P. Baykousheva, *J. Lipid Res.*, 1995, **36**, 2471-2477.
17. X. Qiu, *Prost. Leukot. Fatty Acids*, 2003, **68**, 181-186.
18. L. Ferrero-Miliani, O. H. Nielsen, P. S. Andersen and S. E. Girardin, *Clin. Exp. Immunol.*, 2007, **147**, 227-235.
19. T. A. Wynn, *J. Pathol.*, 2008, **214**, 199-210.
20. D. R. Germolec, K. A. Shipkowski, R. P. Frawley and E. Evans, *Methods Mol. Biol.*, 2018, **1803**, 57-79.
21. K. G. Primdahl, no. 1911, University of Oslo, Faculty of Mathematics and Natural Sciences, School of Pharmacy, 2017.
22. C. N. Serhan, C. B. Clish, J. Brannon, S. P. Colgan, N. Chiang and K. Gronert, *J. Exp. Med.*, 2000, **192**, 1197-1204.
23. S. Hong, K. Gronert, P. R. Devchand, R.-L. Moussignac and C. N. Serhan, *J. Biol. Chem.*, 2003, **278**, 14677-14687.
24. V. L. Marcheselli, S. Hong, W. J. Lukiw, X. H. Tian, K. Gronert, A. Musto, M. Hardy, J. M. Gimenez, N. Chiang, C. N. Serhan and N. G. Bazan, *J. Biol. Chem.*, 2003, **278**, 43807-43817.
25. C. N. Serhan, S. Hong, K. Gronert, S. P. Colgan, P. R. Devchand, G. Mirick and R. L. Moussignac, *J. Exp. Med.*, 2002, **196**, 1025-1037.
26. D. W. Gilroy, P. R. Colville-Nash, D. Willis, J. Chivers, M. J. Paul-Clark and D. A. Willoughby, *Nat. Med.*, 1999, **5**, 698-701.

27. I. Zahoor and S. Giri, *Clin. Rev. Allergy Immunol.*, 2021, **60**, 147-163.
28. A. Mellor, *Journal*, 2012, **87**, 77-77.
29. B. Favaloro, N. Allocati, V. Graziano, C. Di Ilio and V. De Laurenzi, *Aging*, 2012, **4**, 330-349.
30. T. A. Wynn, *Nat. Rev. Immunol.*, 2004, **4**, 583-594.
31. N. Frangogiannis, *J. Exp. Med.*, 2020, **217**, 1-10.
32. B. Hinz, *J. Biomech.*, 2010, **43**, 146-155.
33. J. Varga and D. Abraham, *J. Clin. Invest.*, 2007, **117**, 557-567.
34. R. Bataller and D. A. Brenner, *J. Clin. Invest.*, 2005, **115**, 209-218.
35. S. C. Tyagi, *Clin. Exp. Hypertens.*, 1999, **21**, 181-198.
36. D. A. Zisman, M. P. Keane, J. A. Belperio, R. M. Strieter and J. P. Lynch, *Methods Mol. Med.*, 2005, **117**, 3-44.
37. R. Chrystelle, S.-S. Colin Peter, K. John, C. Eleanor, B. Stuart Edward, M. Trevor, B. James Charles, M. Angus, H. Patrick Eric, S. Donald and B. Jason, *Journal*, 2013.
38. E. Ricciotti and G. A. FitzGerald, *Arterioscler. Thromb. Vasc. Biol.*, 2011, **31**, 986-1000.
39. R. J. Gryglewski, *Agents Actions Suppl.*, 1980, **7**, 247-251.
40. S. Virtue, M. Masoodi, B. A. de Weijer, M. van Eijk, C. Y. Mok, M. Eiden, M. Dale, A. Pirraco, M. J. Serlie, J. L. Griffin and A. Vidal-Puig, *Int. J. Obes.*, 2015, **39**, 1151-1160.
41. M. E. Yeager, M. G. Frid, E. Nozik-Grayck and K. R. Stenmark, in *Muscle*, eds. J. A. Hill and E. N. Olson, Academic Press, Boston/Waltham, 2012, DOI: <https://doi.org/10.1016/B978-0-12-381510-1.00103-4>, pp. 1347-1358.
42. C. N. Serhan and N. A. Petasis, *Chem Rev*, 2011, **111**, 5922-5943.
43. J. I. Nesman, O. Chen, X. Luo, R.-R. Ji, C. N. Serhan and T. V. Hansen, *Org. Biomol. Chem.*, 2021, **19**, 2744-2752.
44. A. F. Reinertsen, K. G. Primdahl, A. E. Shay, C. N. Serhan, T. V. Hansen and M. Aursnes, *J. Org. Chem*, 2021, **86**, 3535-3545.
45. J. E. Tungen, M. Aursnes, S. Ramon, R. A. Colas, C. N. Serhan, D. E. Olberg, S. Nuruddin, F. Willoch and T. V. Hansen, *Org. Biomol. Chem.*, 2018, **16**, 6818-6823.
46. J. R. Falck, U. M. Krishna, Y. K. Reddy, P. S. Kumar, K. M. Reddy, S. B. Hittner, C. Deeter, K. K. Sharma, K. M. Gauthier and W. B. Campbell, *Am. J. Physiol. Heart Circ. Physiol.*, 2003, **284**, 337-349.
47. J. R. Falck, R. Kodela, R. Manne, K. R. Atcha, N. Puli, N. Dubasi, V. L. Manthathi, J. H. Capdevila, X.-Y. Yi, D. H. Goldman, C. Morisseau, B. D. Hammock and W. B. Campbell, *J. Med. Chem*, 2009, **52**, 5069-5075.
48. J. H. Capdevila, J. R. Falck and R. C. Harris, *J. Lipid Res.*, 2000, **41**, 163-181.
49. D. Ye, D. Zhang, C. Oltman, K. Dellsperger, H. C. Lee and M. VanRollins, *J Pharmacol Exp Ther*, 2002, **303**, 768-776.
50. A. P. Zou, J. T. Fleming, J. R. Falck, E. R. Jacobs, D. Gebremedhin, D. R. Harder and R. J. Roman, *Am. J. Physiol.*, 1996, **270**, F822-832.
51. T. Lu, M. VanRollins and H. C. Lee, *Mol. Pharmacol.*, 2002, **62**, 1076-1083.
52. P. Y. K. Wong, P.-S. Lai and J. R. Falck, *Prostaglandins Other Lipid Mediat.*, 2000, **62**, 321-333.
53. R. G. Pertwee, *Br. J. Pharmacol.*, 2006, **147**, S163-170.
54. I. Brown, M. G. Cascio, K. W. J. Wahle, R. Smoum, R. Mechoulam, R. A. Ross, R. G. Pertwee and S. D. Heys, *Carcinogenesis*, 2010, **31**, 1584-1591.
55. I. Brown, M. G. Cascio, D. Rotondo, R. G. Pertwee, S. D. Heys and K. W. J. Wahle, *Prog. Lipid Res.*, 2013, **52**, 80-109.

56. J. C. Ashton and M. Giass, *Curr. Neuropharmacol.*, 2007, **5**, 73-80.
57. C. Benito, R. M. Tolon, M. R. Pazos, E. Nunez, A. I. Castillo and J. Romero, *Br. J. Pharmacol.*, 2008, **153**, 277-285.
58. P. Nagarkatti, R. Pandey, S. A. Rieder, V. L. Hegde and M. Nagarkatti, *Future Med. Chem.*, 2009, **1**, 1333-1349.
59. L. N. Carnevale and A. Das, in *The Role of Bioactive Lipids in Cancer, Inflammation and Related Diseases*, eds. K. V. Honn and D. C. Zeldin, Springer International Publishing, Cham, 2019, DOI: 10.1007/978-3-030-21735-8_17, pp. 219-232.
60. C. Morisseau and B. D. Hammock, *Pest Manag Sci*, 2008, **64**, 594-609.
61. K. M. Wagner, C. B. McReynolds, W. K. Schmidt and B. D. Hammock, *Pharmacol. Ther.*, 2017, **180**, 62-76.
62. J. W. Newman, C. Morisseau and B. D. Hammock, *Prog. Lipid Res.*, 2005, **44**, 1-51.
63. A. K. Ghosh and M. Brindisi, *J. Med. Chem.*, 2020, **63**, 2751-2788.
64. C. Morisseau and B. D. Hammock, *Annu. Rev. Pharmacol. Toxicol.*, 2005, **45**, 311-333.
65. A. Ulu, K. S. Stephen Lee, C. Miyabe, J. Yang, B. G. Hammock, H. Dong and B. D. Hammock, *J. Cardiovasc. Pharmacol.*, 2014, **64**, 87-99.
66. T. Yang, R. Peng, Y. Guo, L. Shen, S. Zhao and D. Xu, *Lipids Health Dis.*, 2013, **12**, 151-155.
67. C. Morisseau, B. Inceoglu, K. Schmelzer, H. J. Tsai, S. L. Jinks, C. M. Hegedus and B. D. Hammock, *J. Lipid Res.*, 2010, **51**, 3481-3490.
68. B. D. Hammock, C. B. McReynolds, K. Wagner, A. Buckpitt, I. Cortes-Puch, G. Croston, K. S. S. Lee, J. Yang, W. K. Schmidt and S. H. Hwang, *J. Med. Chem.*, 2021, **64**, 1856-1872.
69. A. A. Takeshita, B. D. Hammock and K. M. Wagner, *Front. Pain. Res.*, 2022, **3**, 1-13.
70. J. Hu, S. Dziumbala, J. Lin, S. I. Bibli, S. Zukunft, J. de Mos, K. Awwad, T. Frömel, A. Jungmann, K. Devraj, Z. Cheng, L. Wang, S. Fauser, C. G. Eberhart, A. Sodhi, B. D. Hammock, S. Liebner, O. J. Müller, C. Glaubitz, H. P. Hammes, R. Popp and I. Fleming, *Nature*, 2017, **552**, 248-252.
71. K. Node, Y. Huo, X. Ruan, B. Yang, M. Spiecker, K. Ley, D. C. Zeldin and J. K. Liao, *Science*, 1999, **285**, 1276-1279.
72. B. Fisslthaler, R. Popp, L. Kiss, M. Potente, D. R. Harder, I. Fleming and R. Busse, *Nature*, 1999, **401**, 493-497.
73. W.-H. Schunck, A. Konkel, R. Fischer and K.-H. Weylandt, *Pharmacol. Ther.*, 2018, **183**, 177-204.
74. R. Yanai, L. Mulki, E. Hasegawa, K. Takeuchi, H. Sweigard, J. Suzuki, P. Gaissert, D. G. Vavvas, K.-H. Sonoda, M. Rothe, W.-H. Schunck, J. W. Miller and K. M. Connor, *Proc. Natl. Acad. Sci. U. S. A.*, 2014, **111**, 9603-9608.
75. J. Kunisawa, M. Arita, T. Hayasaka, T. Harada, R. Iwamoto, R. Nagasawa, S. Shikata, T. Nagatake, H. Suzuki, E. Hashimoto, Y. Kurashima, Y. Suzuki, H. Arai, M. Setou and H. Kiyono, *Sci. Rep.*, 2015, **5**, 9750-9750.
76. G. Zhang, D. Panigrahy, L. M. Mahakian, J. Yang, J. Y. Liu, K. S. Stephen Lee, H. I. Wettersten, A. Ulu, X. Hu, S. Tam, S. H. Hwang, E. S. Ingham, M. W. Kieran, R. H. Weiss, K. W. Ferrara and B. D. Hammock, *Proc. Natl. Acad. Sci. U. S. A.*, 2013, **110**, 6530-6535.
77. D. R. McDougle, J. E. Watson, A. A. Abdeen, R. Adili, M. P. Caputo, J. E. Krapf, R. W. Johnson, K. A. Kilian, M. Holinstat and A. Das, *Proc. Natl. Acad. Sci. U. S. A.*, 2017, **114**, 6034-6043.

78. N. Singh, A. Vik, D. B. Lybrand, C. Morisseau and B. D. Hammock, *Chem. Res. Toxicol.*, 2021, **34**, 2579-2591.
79. J. R. Falck, G. Wallukat, N. Puli, M. Goli, C. Arnold, A. Konkel, M. Rothe, R. Fischer, D. N. Müller and W. H. Schunck, *J. Med. Chem.*, 2011, **54**, 4109-4118.
80. M. A. Hye Khan, T. S. Pavlov, S. V. Christain, J. Neckář, A. Staruschenko, K. M. Gauthier, J. H. Capdevila, J. R. Falck, W. B. Campbell and J. D. Imig, *Clin. Sci. (Lond.)*, 2014, **127**, 463-474.
81. M. A. Hye Khan, A. Stavniichuk, M. A. Sattar, J. R. Falck and J. D. Imig, *Front. Pharmacol.*, 2019, **10**, 512-526.
82. J. D. Imig, M. A. Hye Khan, A. Burkhan, G. Chen, A. M. Adebessin and J. R. Falck, *Int. J. Mol. Sci.*, 2021, **22**, 2793-2799.
83. A. M. Adebessin, T. Wesser, J. Vijaykumar, A. Konkel, M. P. Paudyal, J. Lossie, C. Zhu, C. Westphal, N. Puli, R. Fischer, W. H. Schunck and J. R. Falck, *J. Med. Chem.*, 2019, **62**, 10124-10143.
84. B. Hammock, 2023, unpublished work.
85. T. T. Tidwell, in *Organic Reactions*, John Wiley and Sons, Inc., 2004, DOI: <https://doi.org/10.1002/0471264180.or039.03>, pp. 297-555.
86. A. Hassner and I. Namboothiri, Elsevier, 3rd Edition edn., 2012, pp. 1-1.
87. D. R. Klein and D. R. Klein, *Organic chemistry*, Wiley, Singapore, Global edition. edn., 2018.
88. R. W. Holman, *J. Chem. Educ.*, 2005, **82**, 1780-1789.
89. D. G. Brown and J. Boström, *J. Med. Chem.*, 2016, **59**, 4443-4458.
90. M. Aursnes, J. E. Tungen, A. Vik, J. Dalli and T. V. Hansen, *Org. Biomol. Chem.*, 2014, **12**, 432-437.
91. O. T. Benfey, *J. Chem. Educ.*, 1960, **37**, 552.
92. S. F. Dietmar Kennepohl, *Journal*, 2020, 1111-1112.
93. Bradley SE, GPRP119 agonist useful in the treatment of type II diabetes patent GB2498976. 2012.
94. R. A. Gibbs, *Am. J. Pharm. Educ.*, 2000, **64**, 108-120.
95. S. J. R. Johansson, T. Johannessen, C. F. Ellefsen, M. S. Ristun, S. Antonsen, T. V. Hansen, Y. Stenstrøm and J. M. J. Nolsøe, *Synlett*, 2019, **30**, 213-217.
96. C. A. G. N. Montalbetti and V. Falque, *Tetrahedron*, 2005, **61**, 10827-10852.
97. N. A. Porter, V. H. T. Chang, D. R. Magnin and B. T. Wright, *J. Am. Chem. Soc.*, 1988, **110**, 3554-3560.
98. R. C. Cooke, D. L. Capone, K. A. van Leeuwen, G. M. Elsey and M. A. Sefton, *J. Agric. Food Chem.*, 2009, **57**, 348-352.
99. E. Brenna, F. Dalla Santa, F. G. Gatti, G. Gatti and D. Tessaro, *Org. Biomol. Chem.*, 2019, **17**, 813-821.
100. K. L. Wilkinson, G. M. Elsey, R. H. Prager, T. Tanaka and M. A. Sefton, *Tetrahedron*, 2004, **60**, 6091-6100.
101. Y.-Q. Zhang, N. Funken, P. Winterscheid and A. Gansäuer, *Angew. Chem. Int. Ed.*, 2015, **54**, 6931-6934.
102. L. Bettoni, S. Gaillard and J.-L. Renaud, *Chem. Commun.*, 2020, **56**, 12909-12912.
103. W. R. Arnold, L. N. Carnevale, Z. Xie, J. L. Baylon, E. Tajkhorshid, H. Hu and A. Das, *Nat. Commun.*, 2021, **12**, 926-931.

8 Appendix

8.1 ^1H NMR and ^{13}C NMR spectra of the synthesized compounds

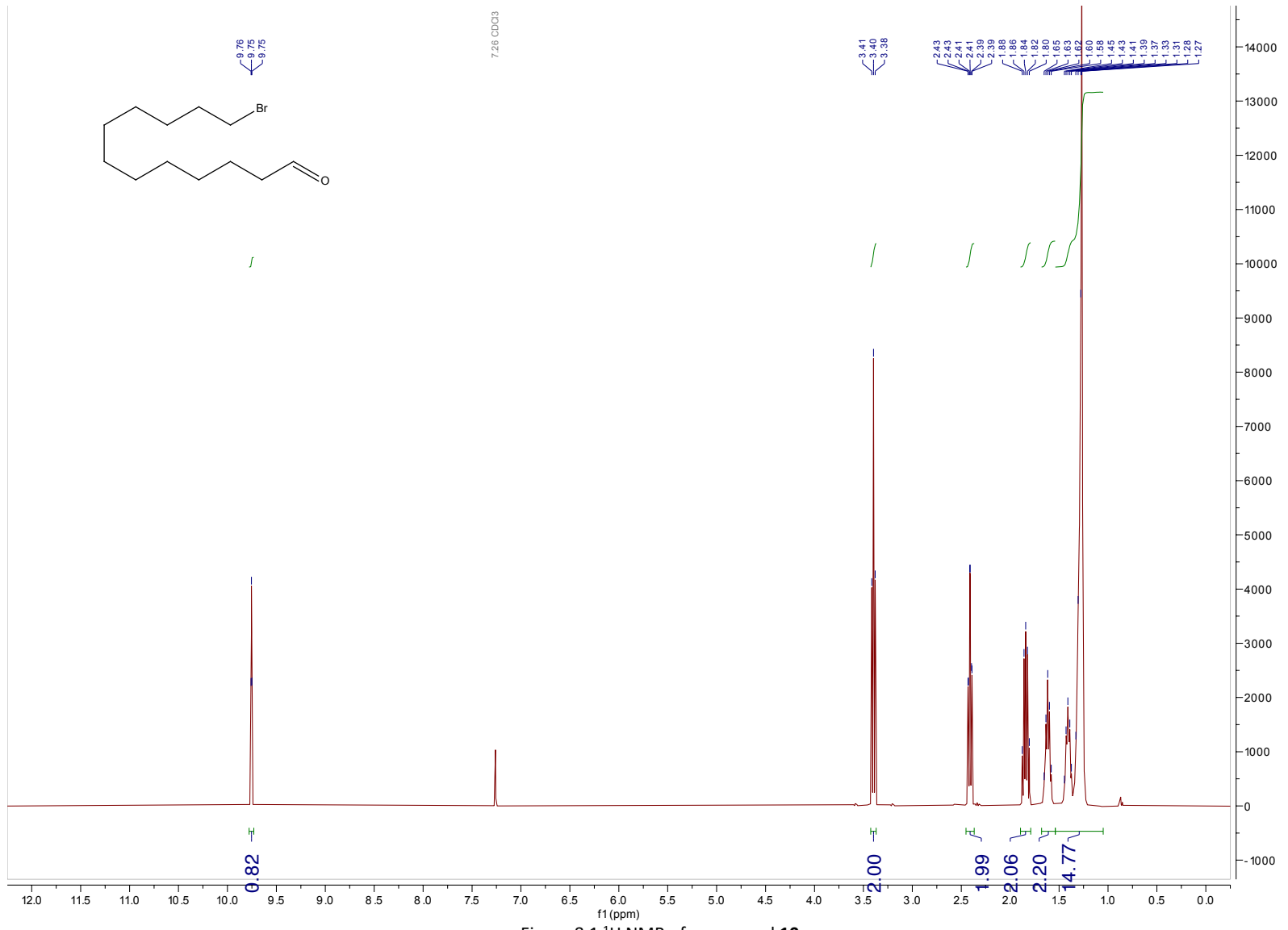


Figure 8.1 ¹H NMR of compound 10.

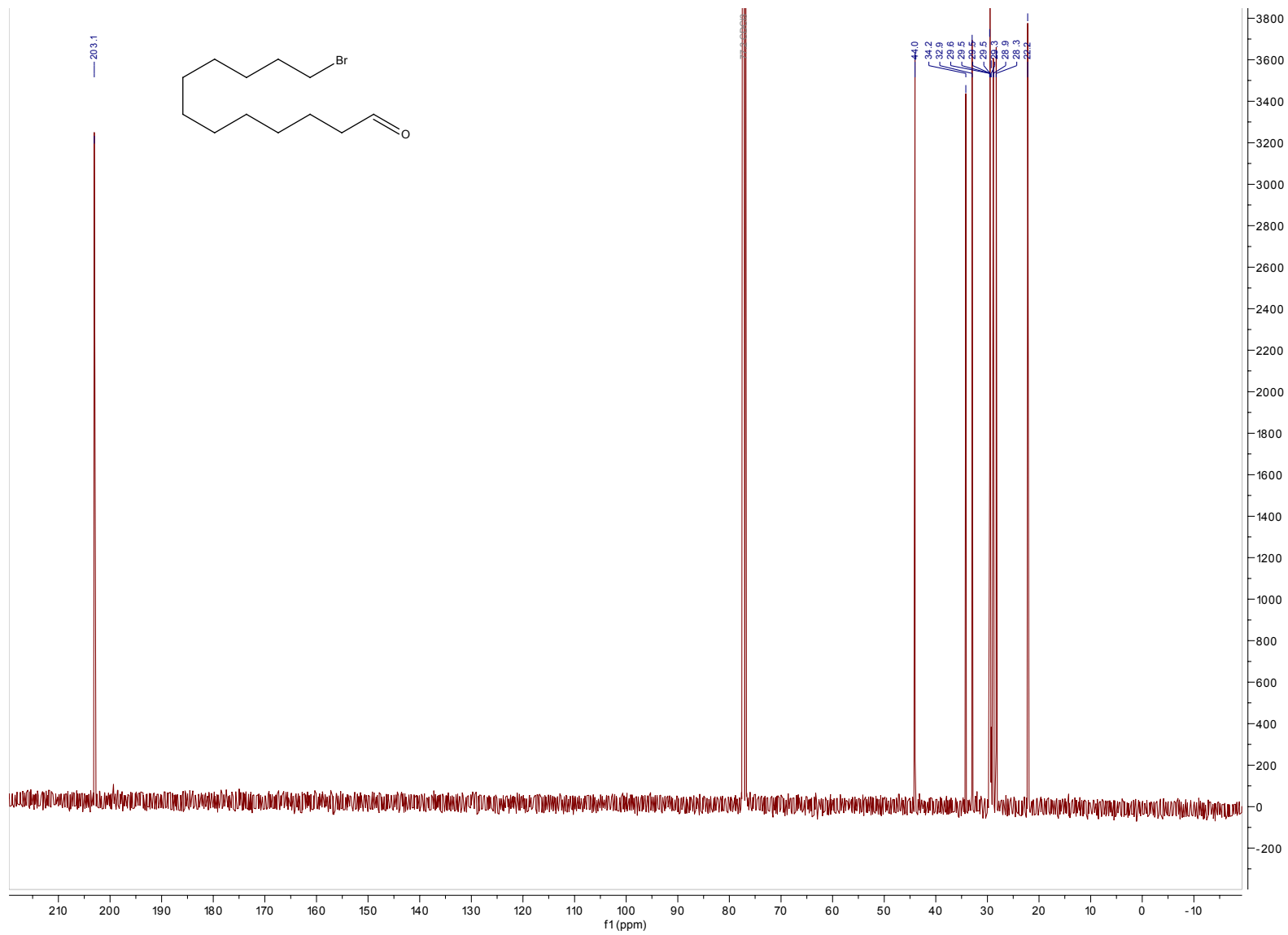


Figure 8.2 ¹³C NMR of compound 10.

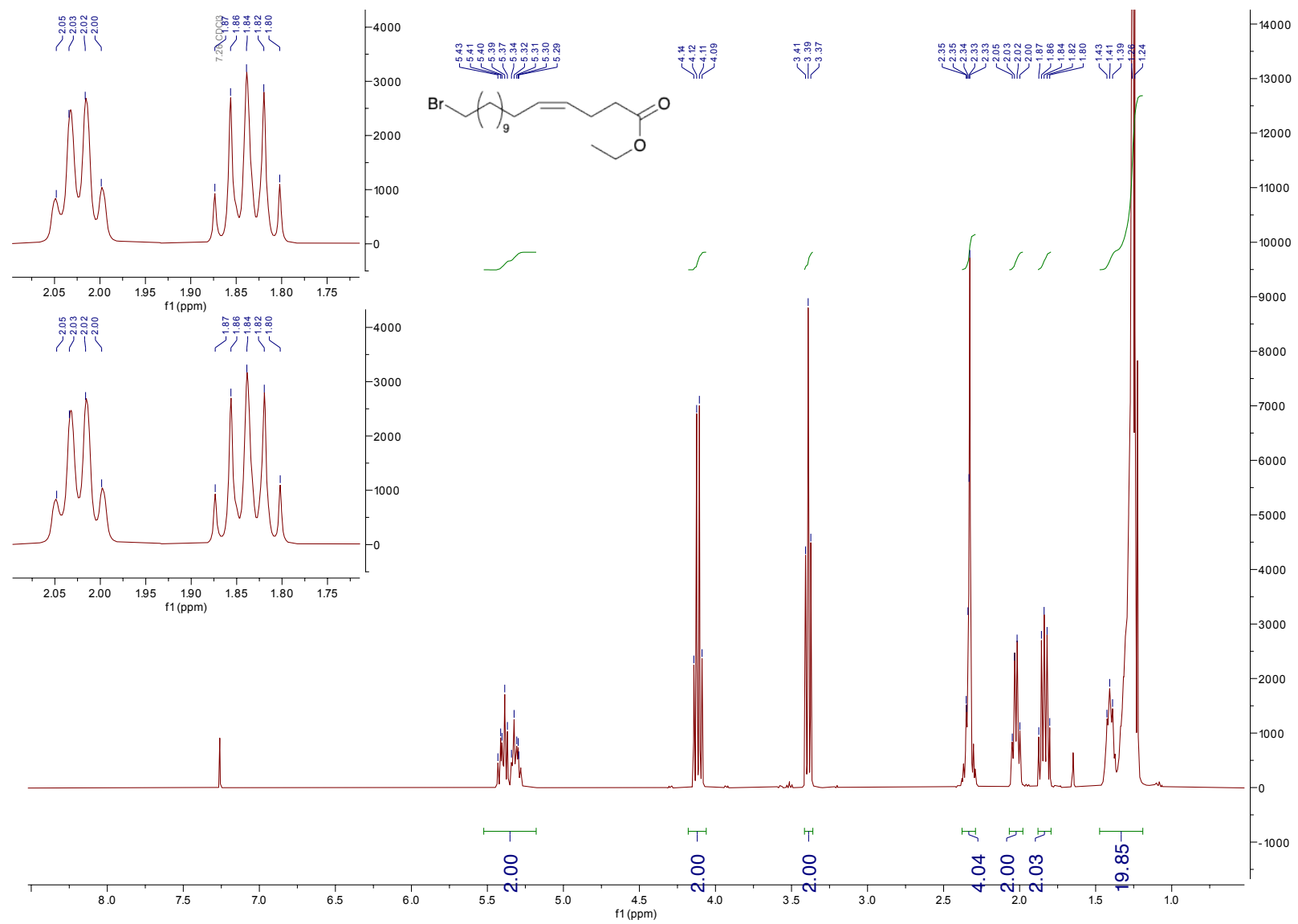


Figure 8.3 ¹H NMR of compound 12.

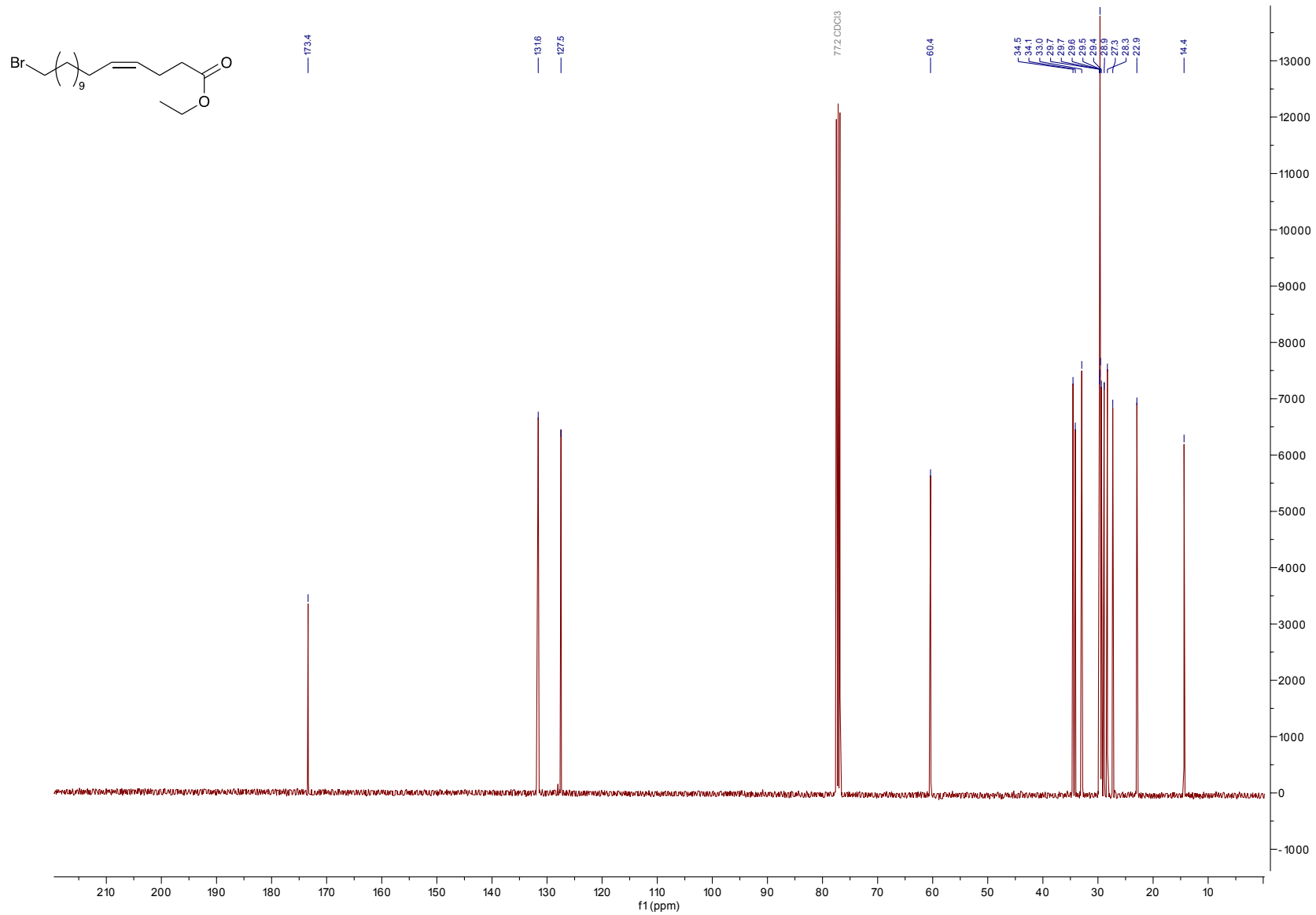


Figure 8.4 ^{13}C NMR of compound 12

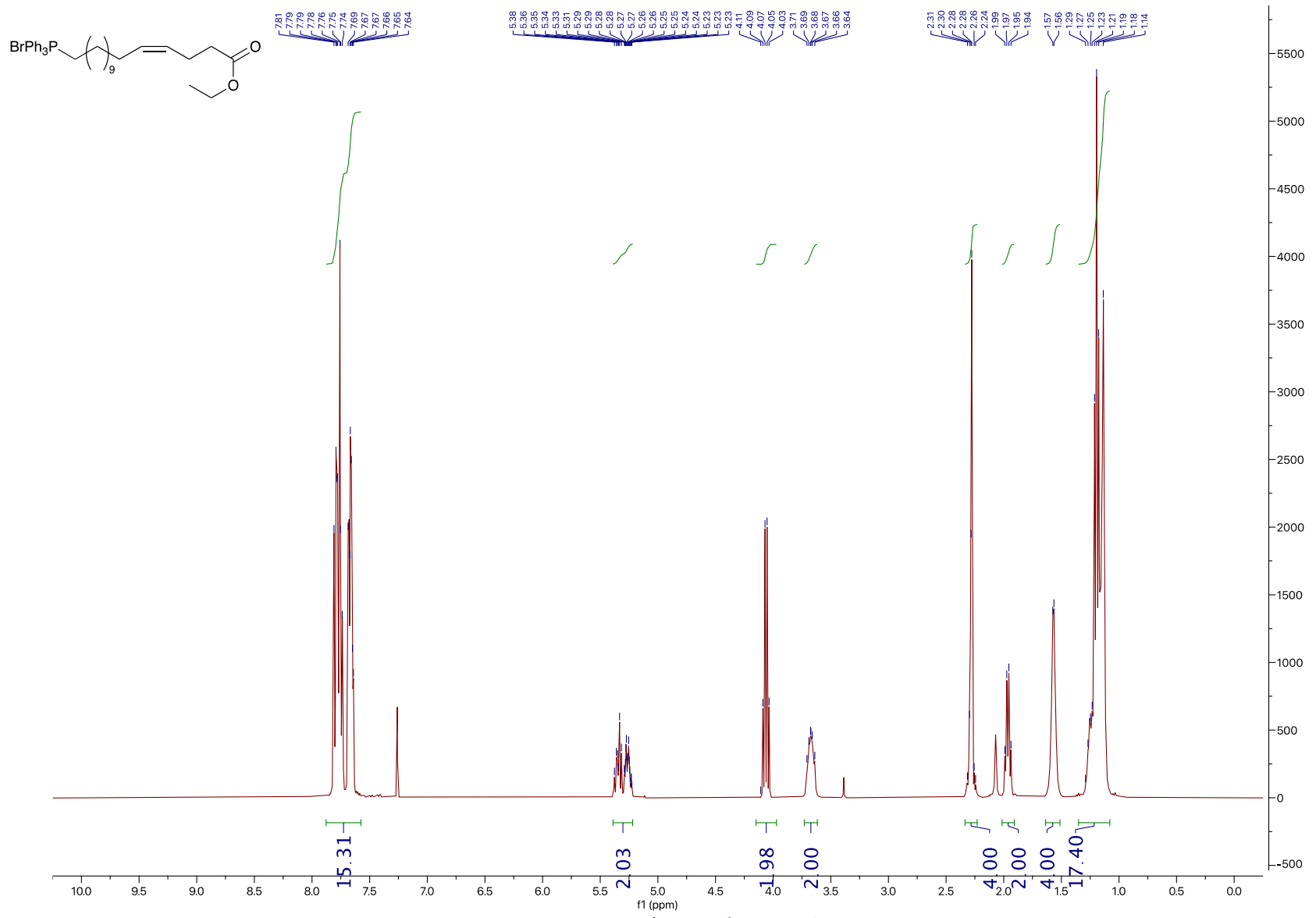


Figure 8.5 ¹H NMR of compound 2

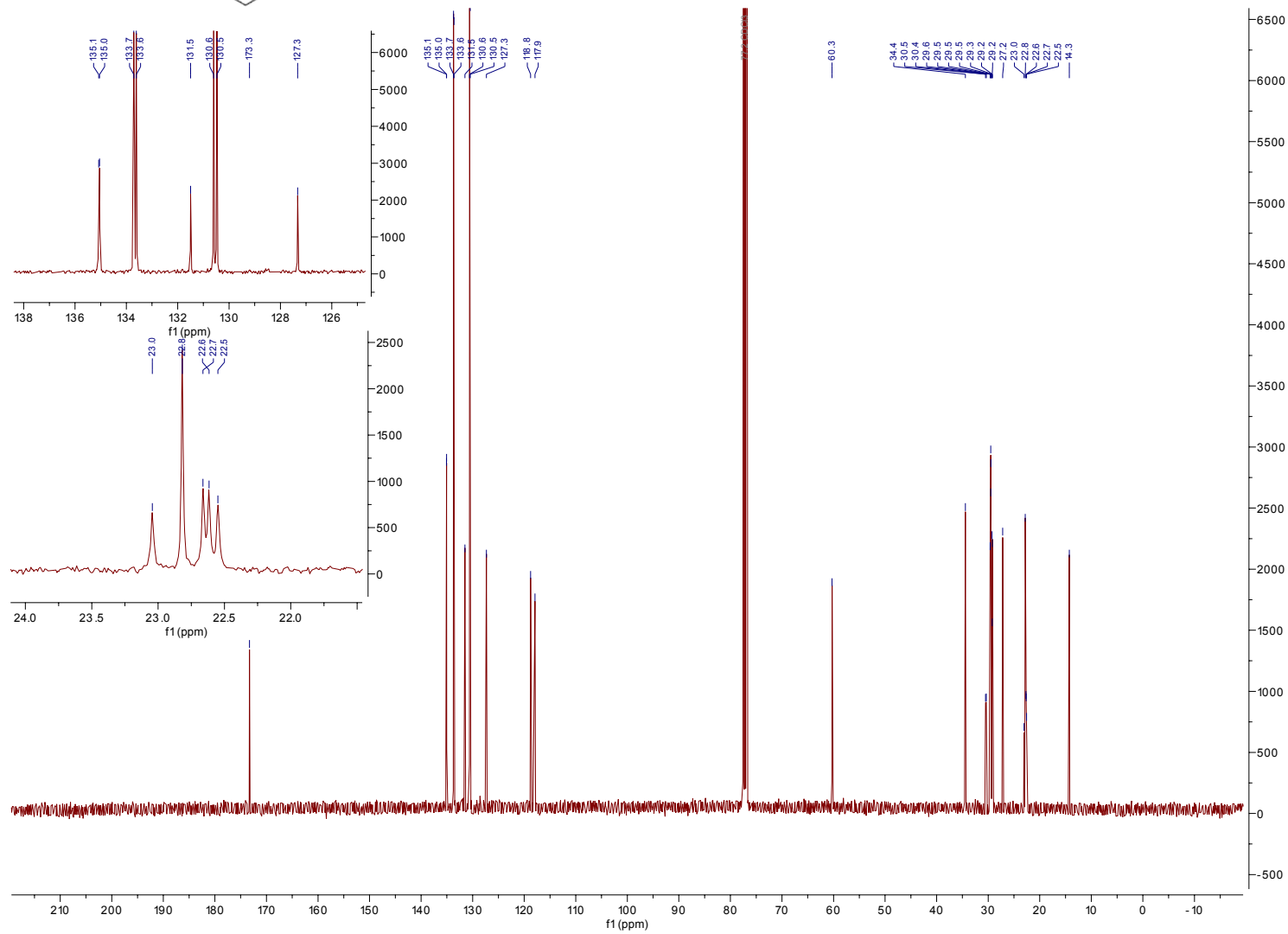
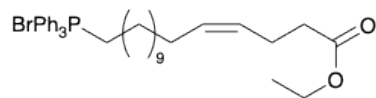


Figure 8.6 ^{13}C NMR of compound 2.

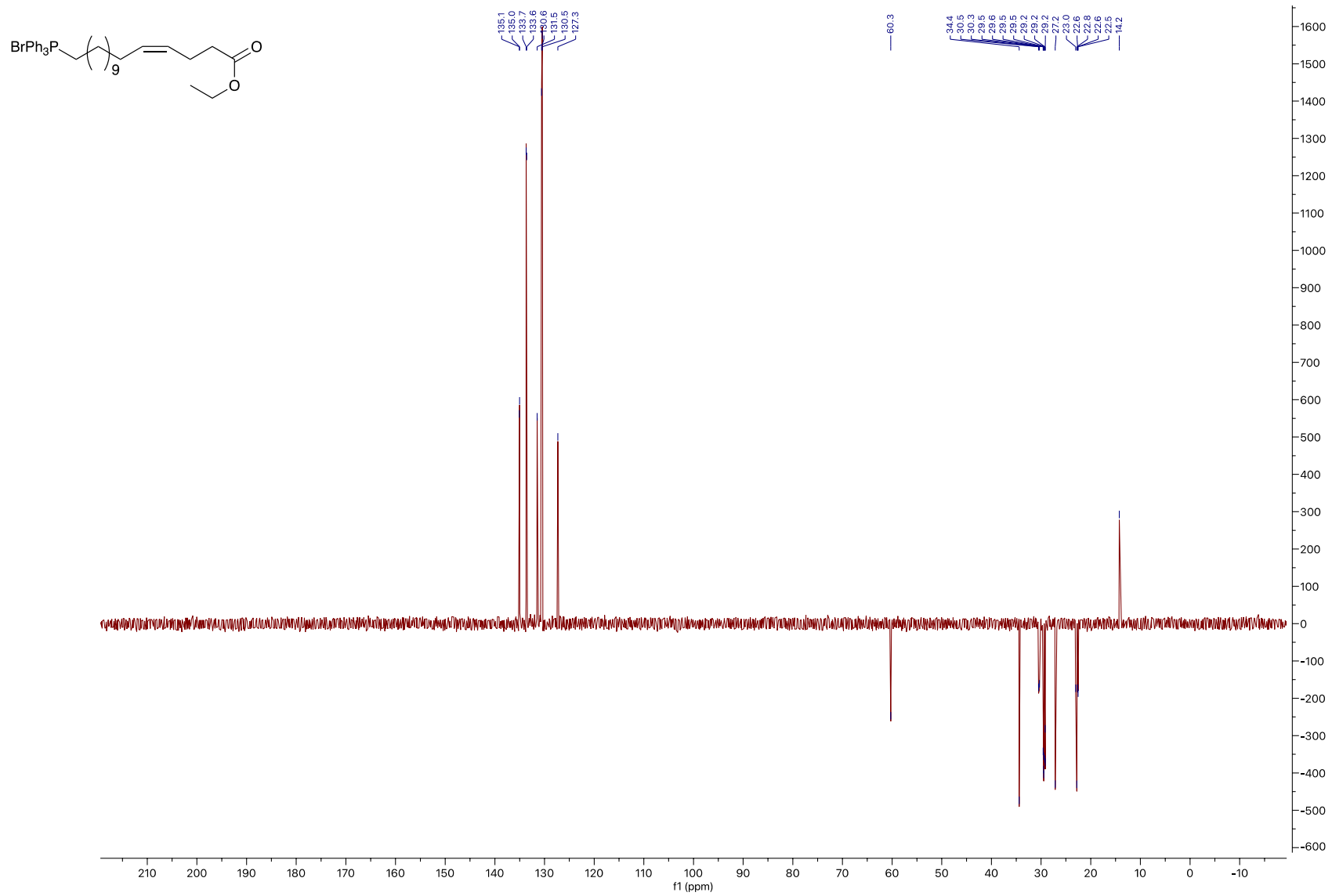


Figure 8.7 DEPT-135 of compound 2.

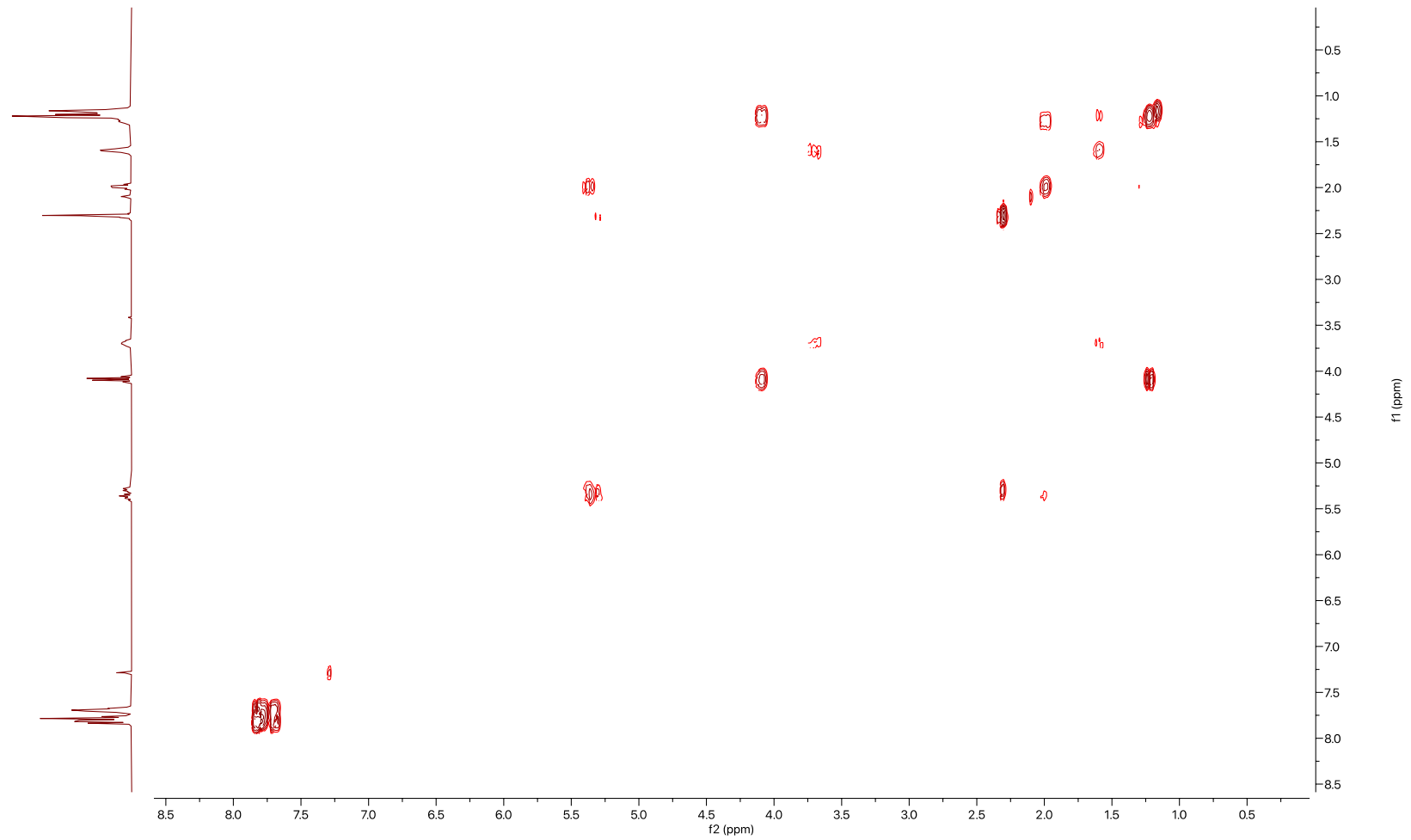
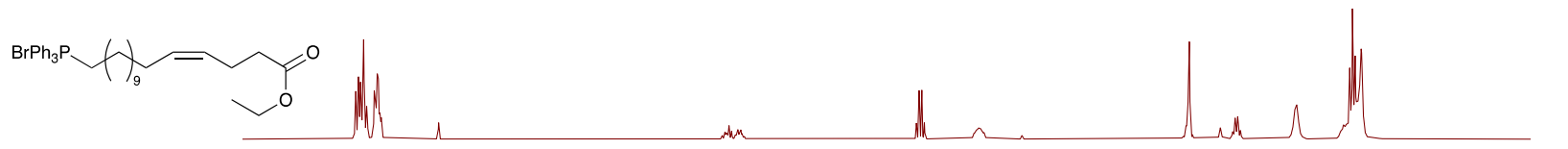
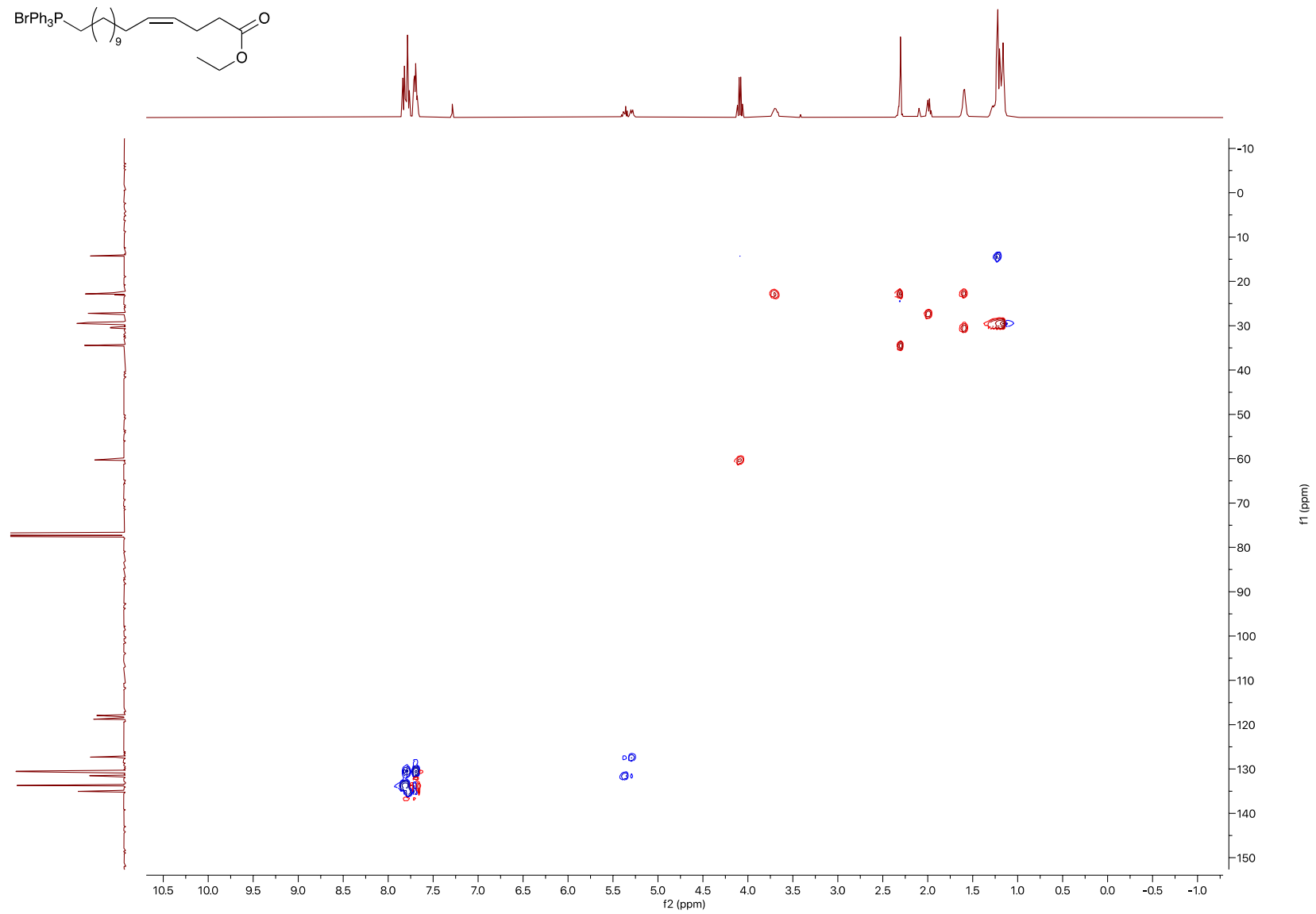
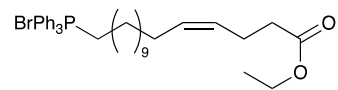


Figure 8.8 COSY of compound 2.



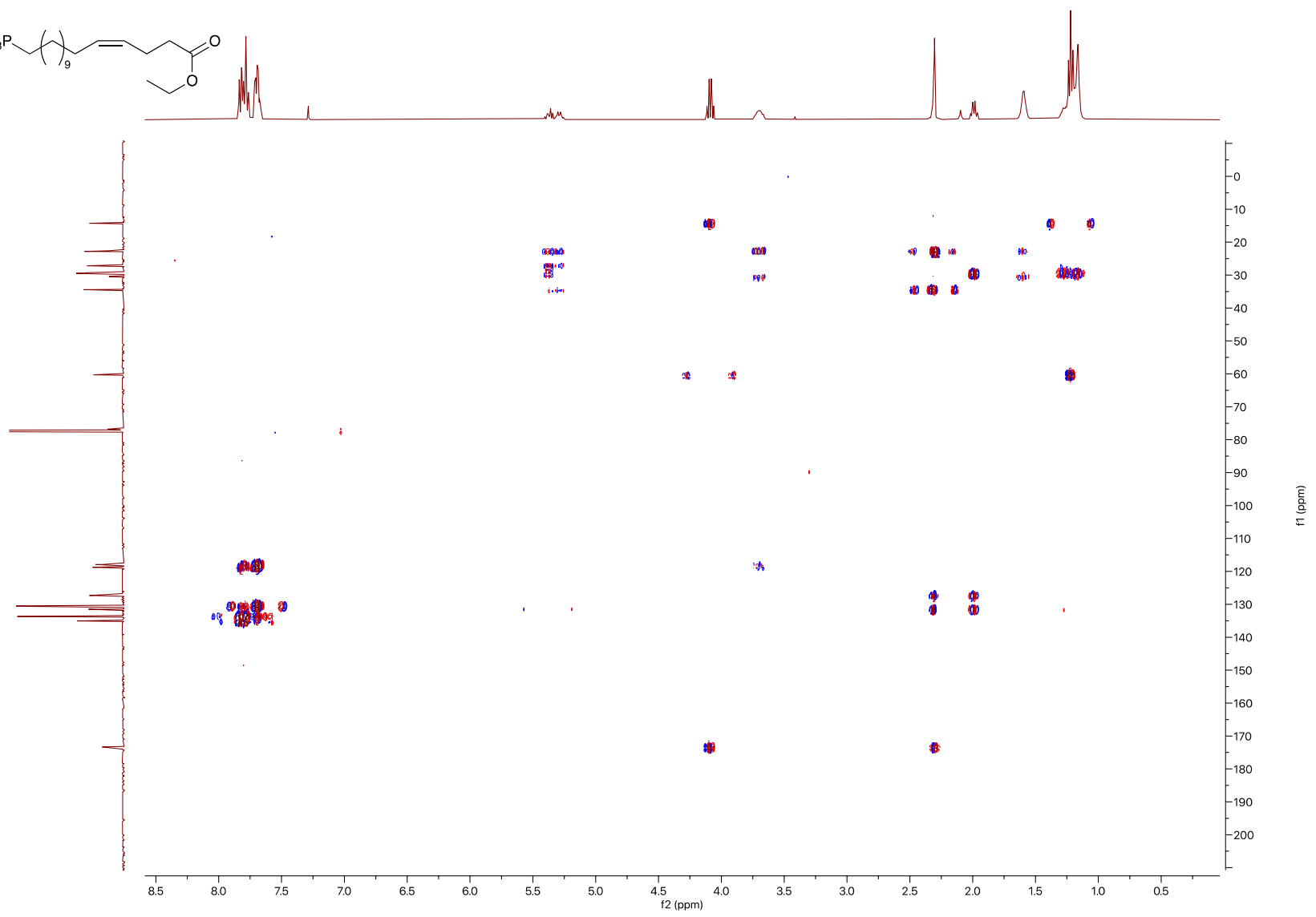
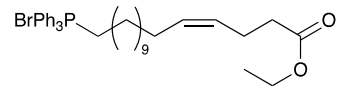


Figure 8.10 HMBC of compound 2.

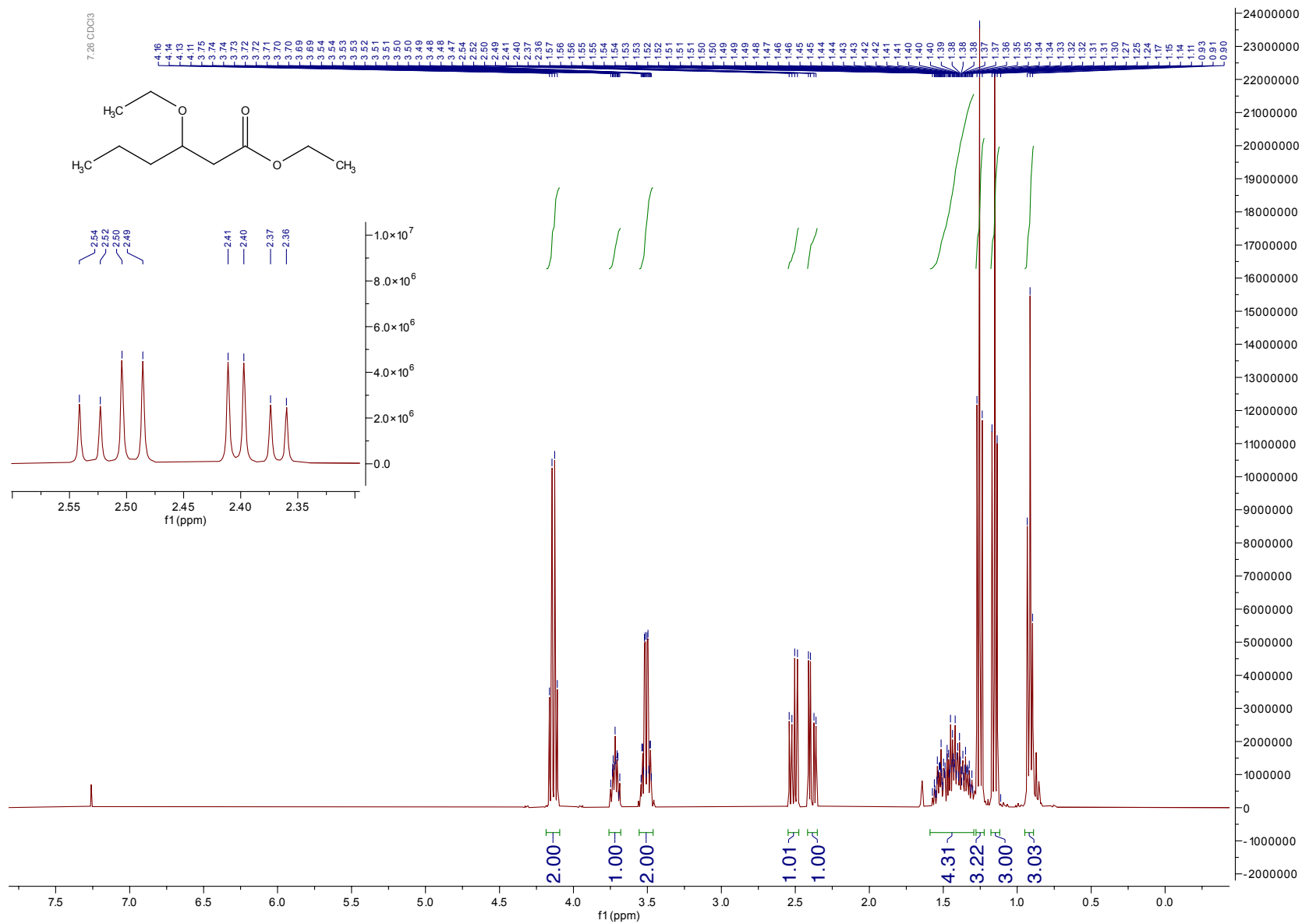


Figure 8.11 ^1H NMR of compound **14**

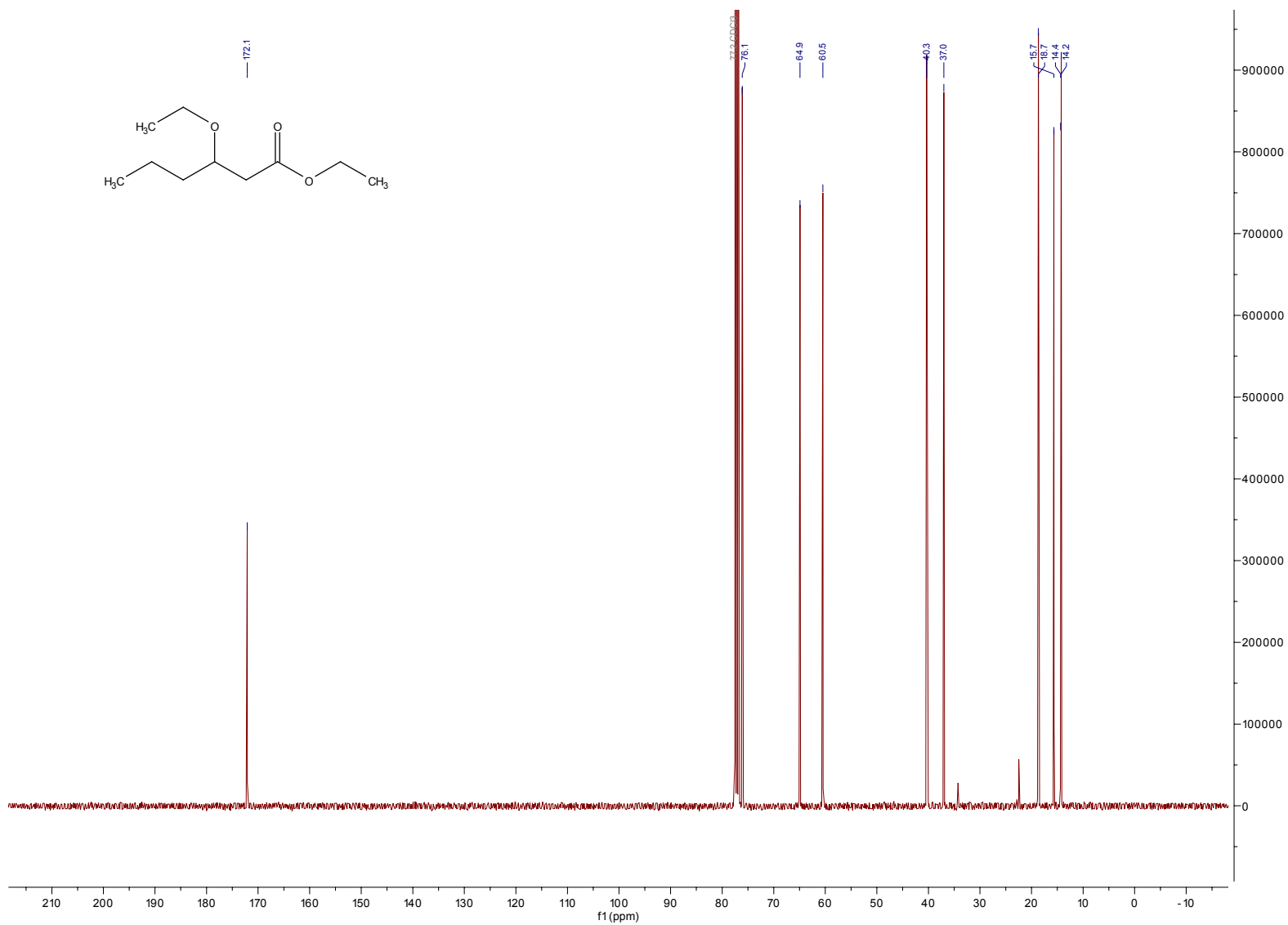


Figure 8.12 ¹³CNMR of compound 14

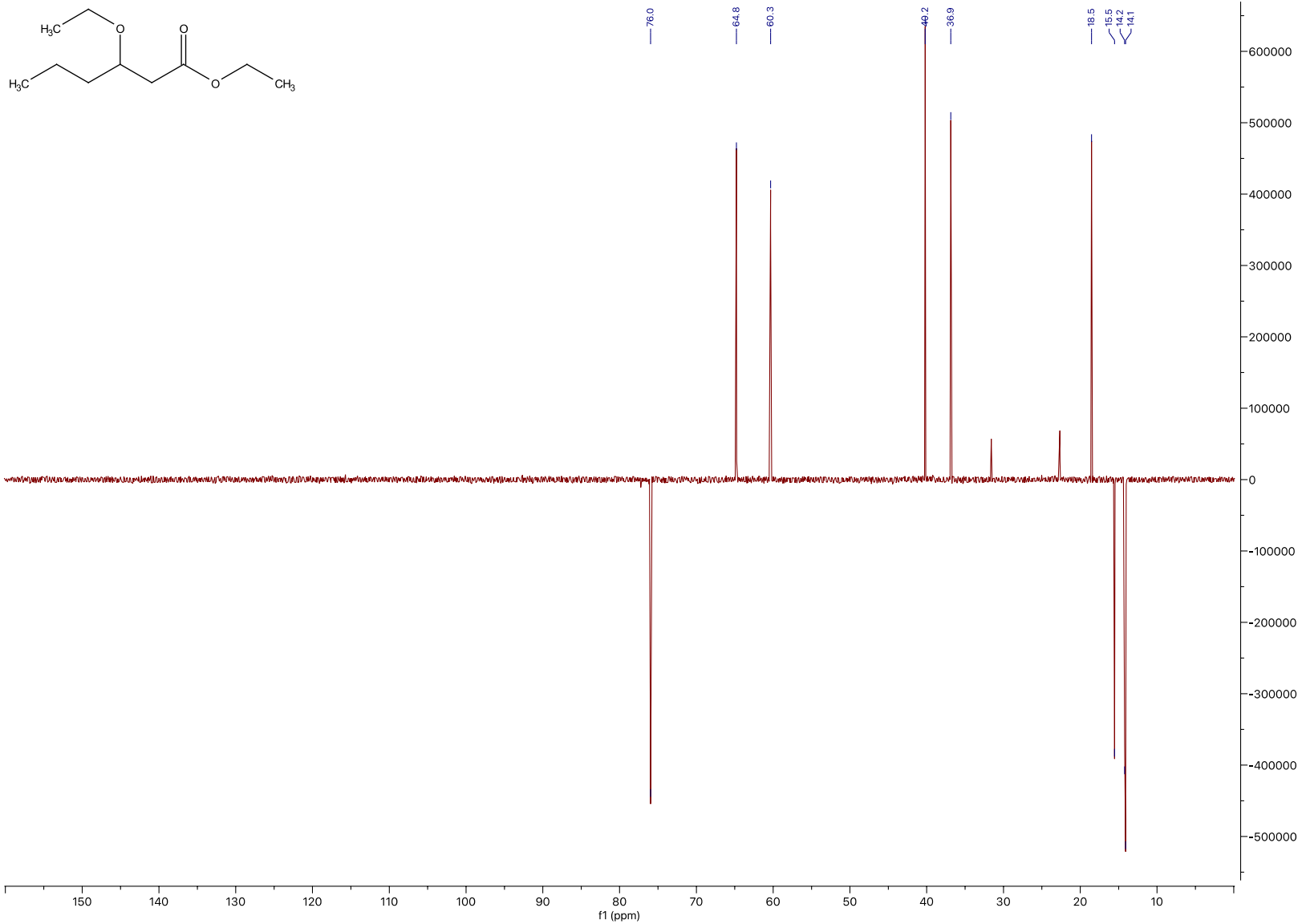


Figure 8.13 DEPT-135 of compound 14.

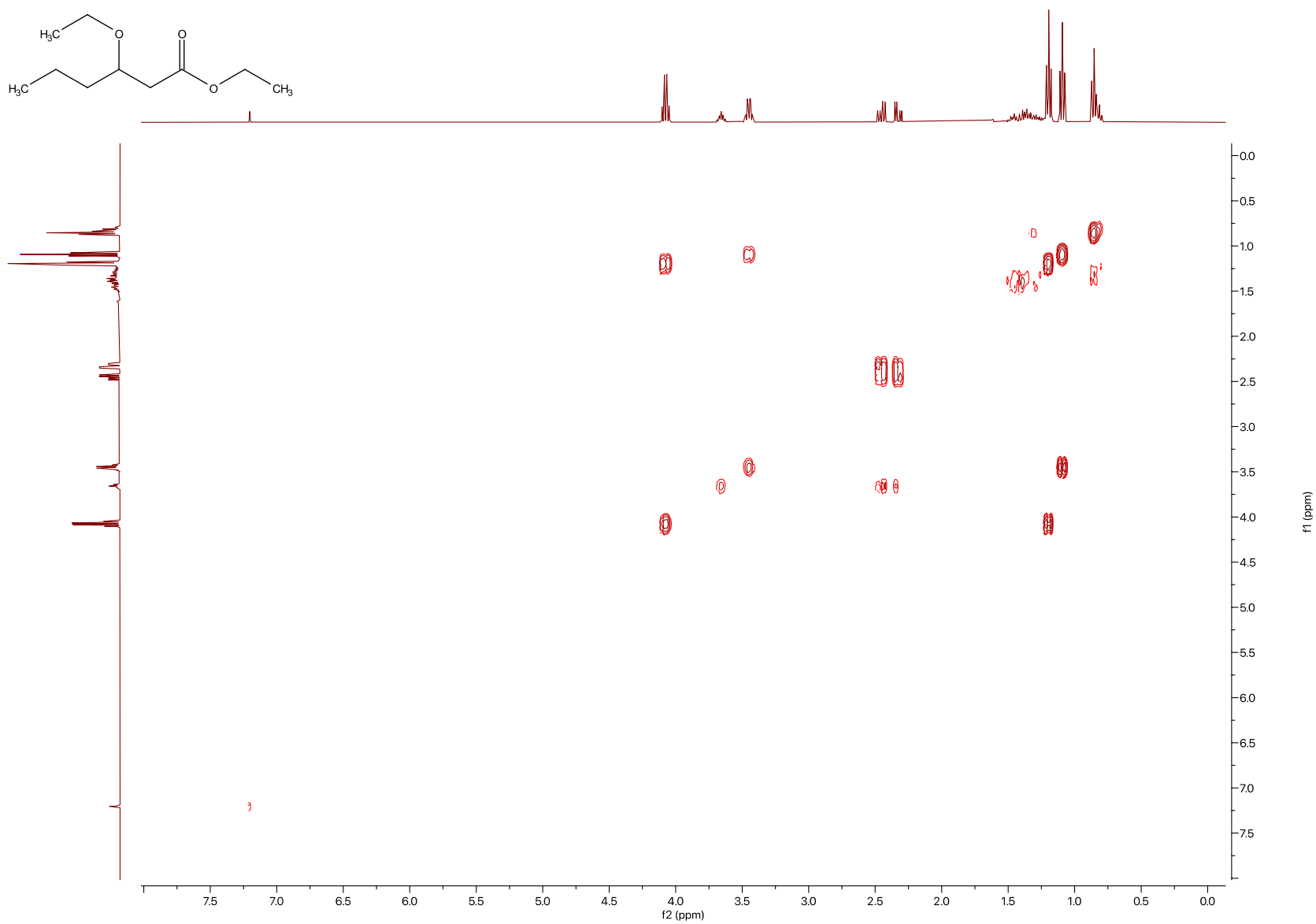
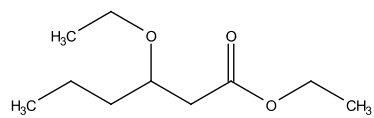


Figure 8.14 COSY of compound 14

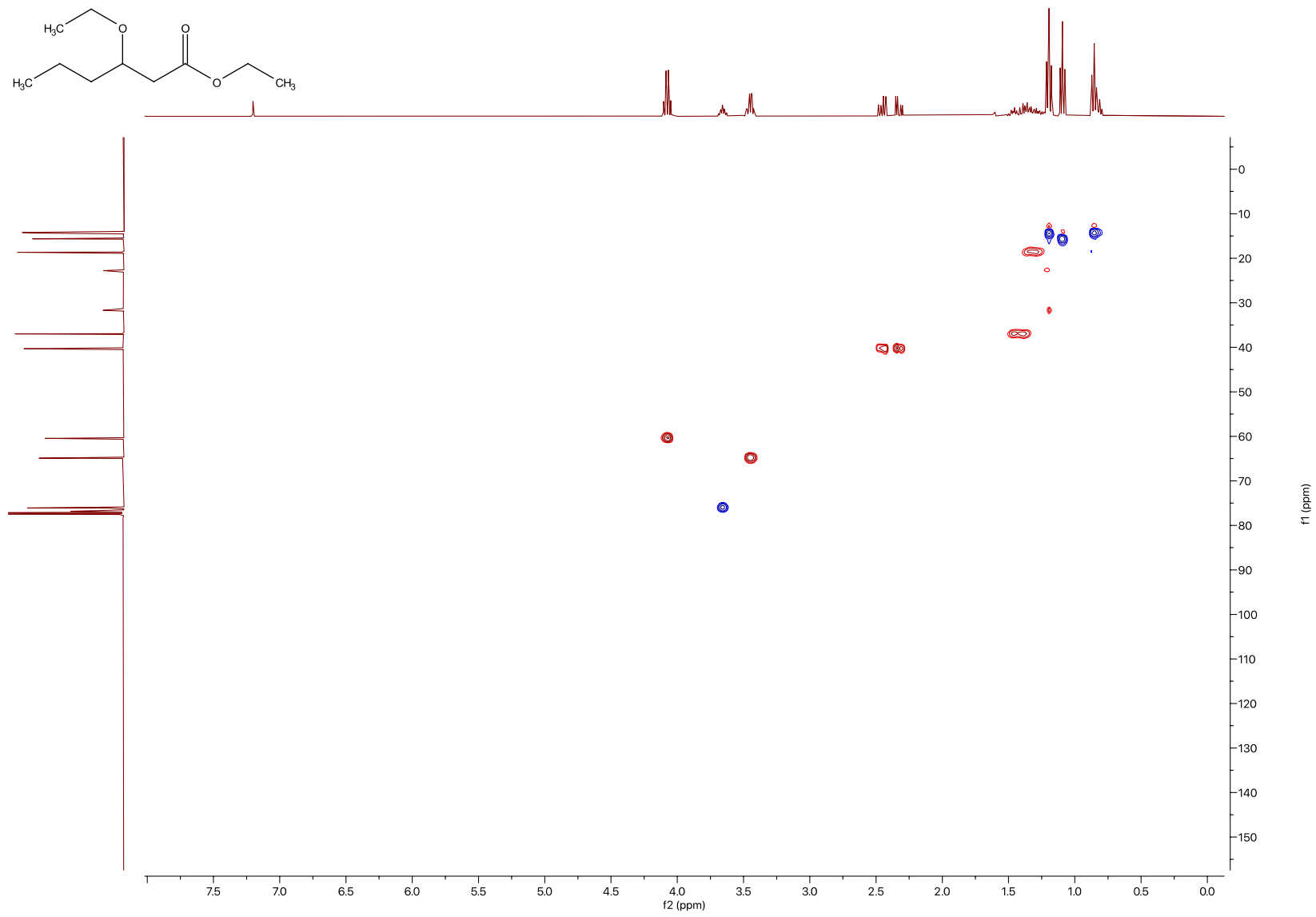
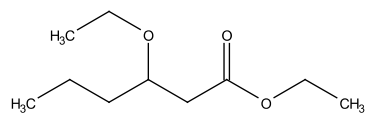


Figure 8.15 HSQC of compound 14

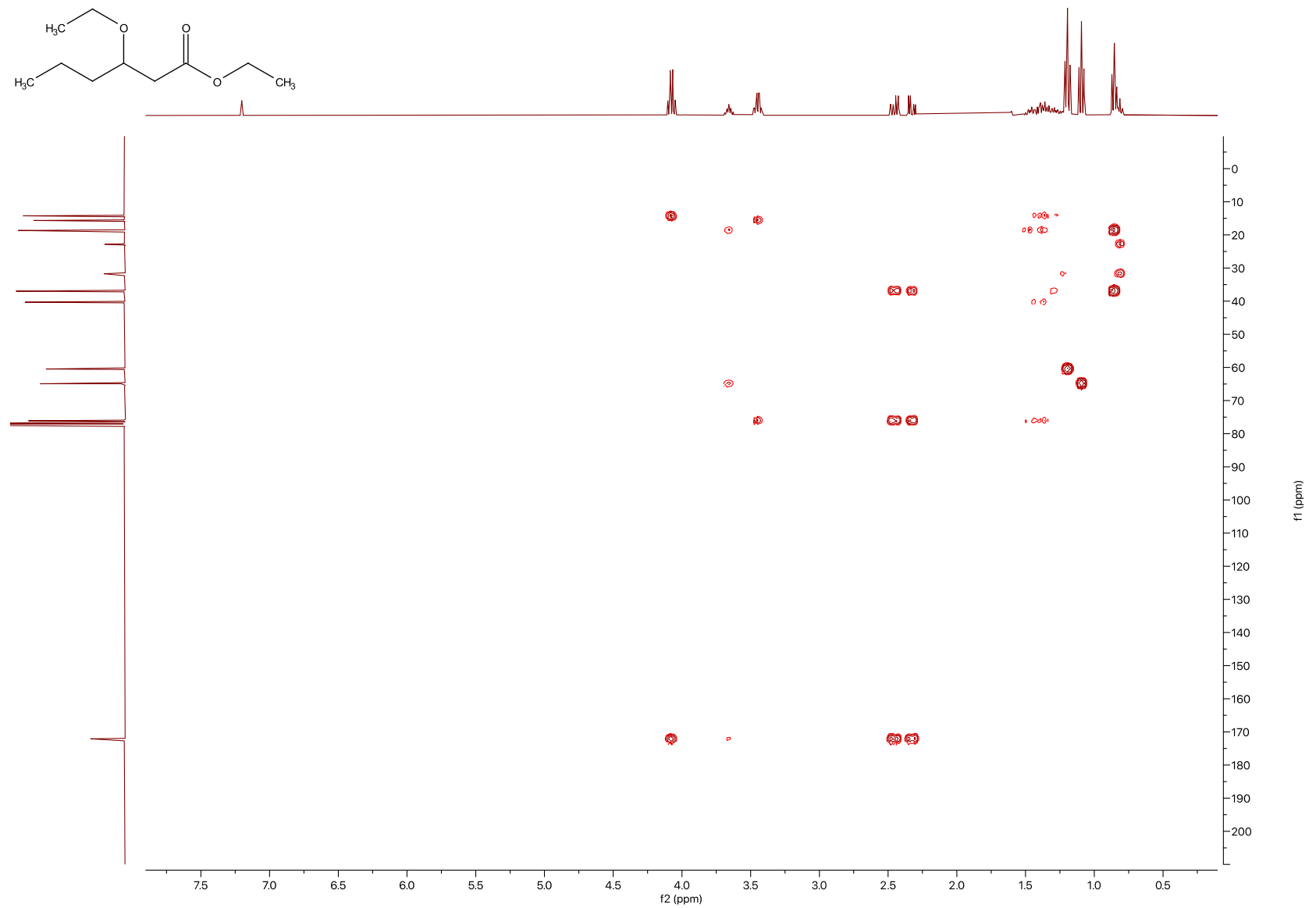
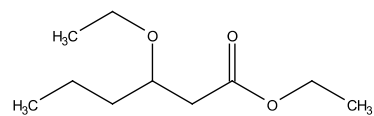


Figure 8.16 HMBC of compound 14.

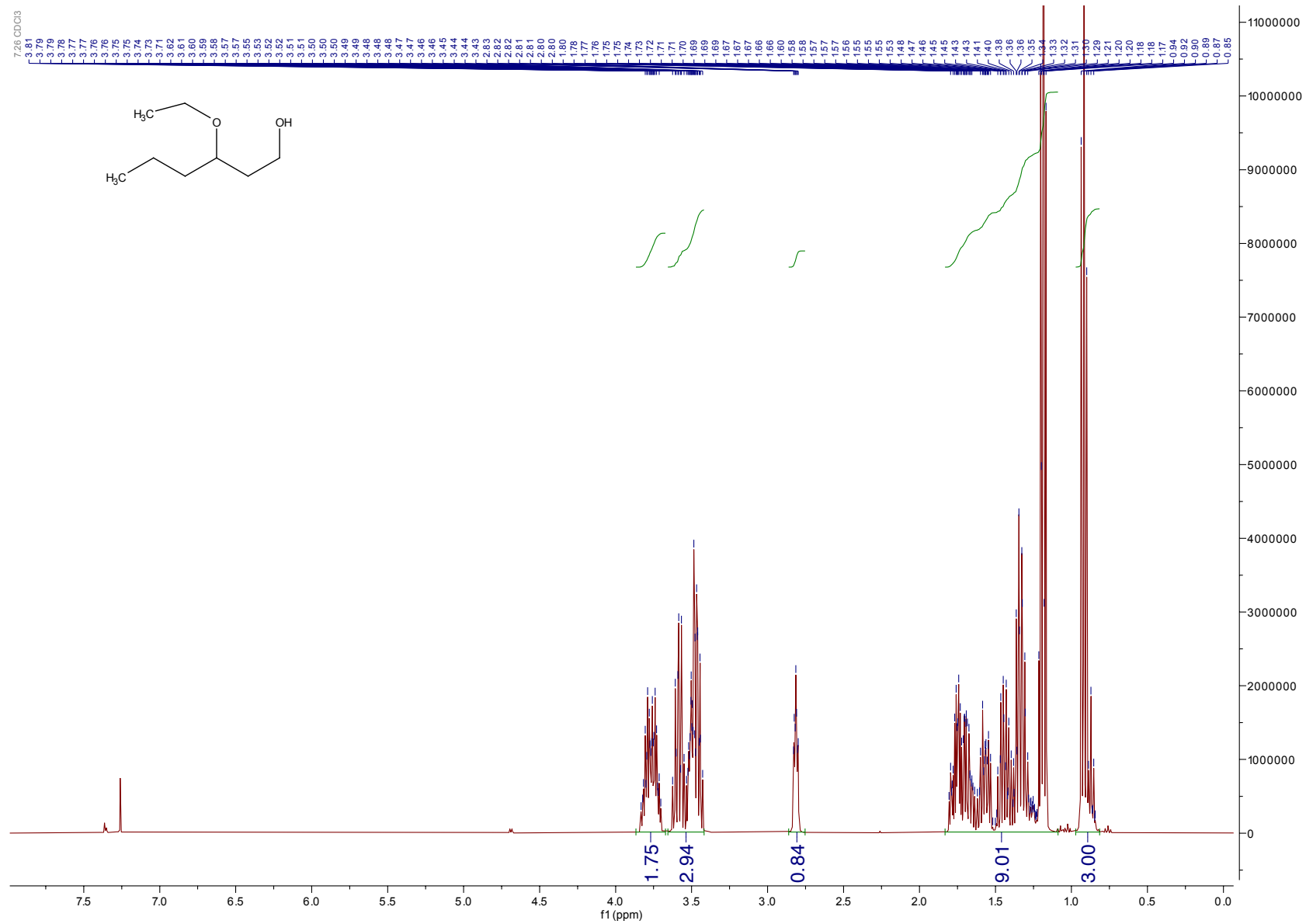


Figure 8.17 ¹H NMR of compound 15.

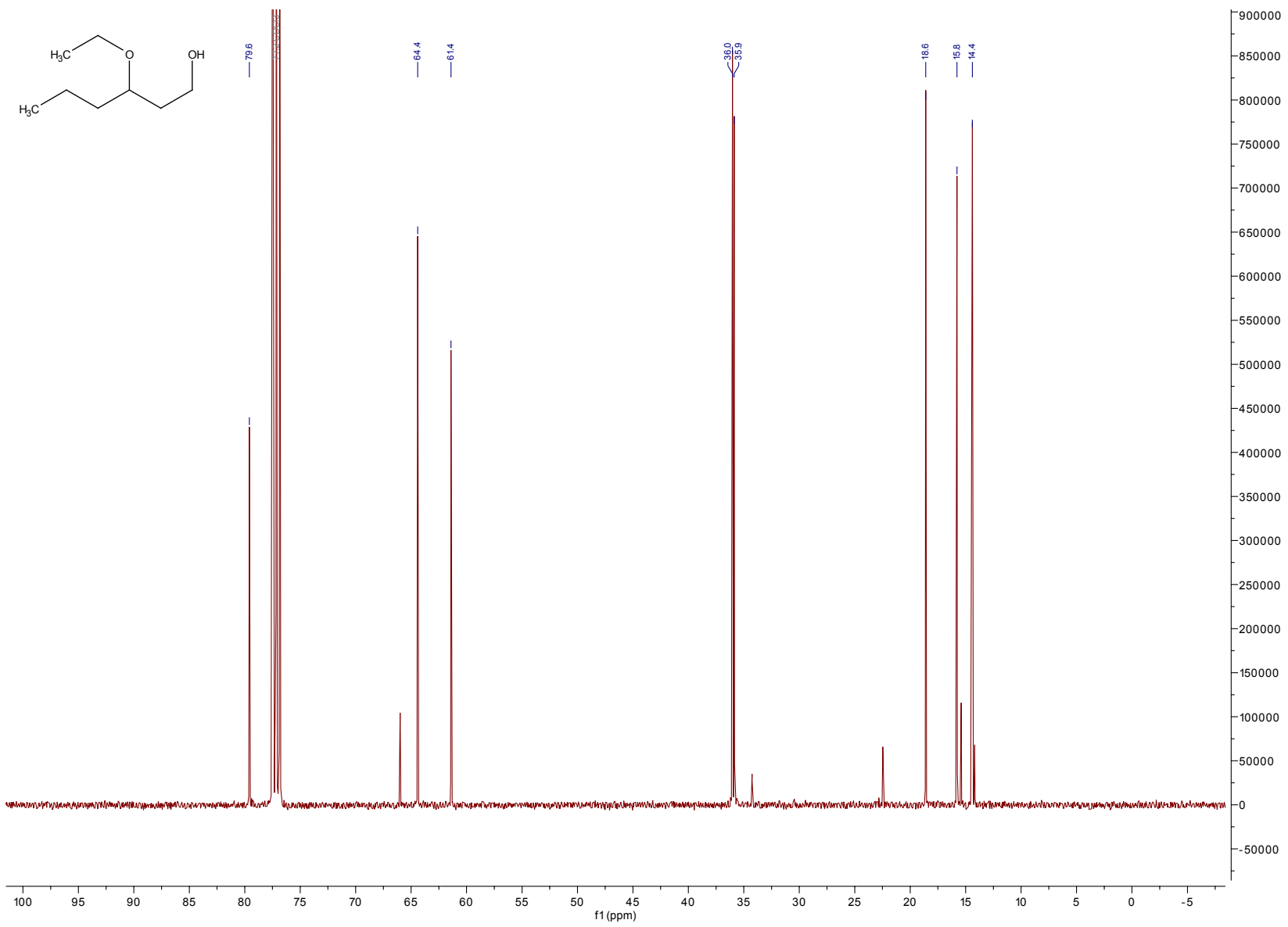


Figure 8.18 ^{13}C NMR of compound 15.

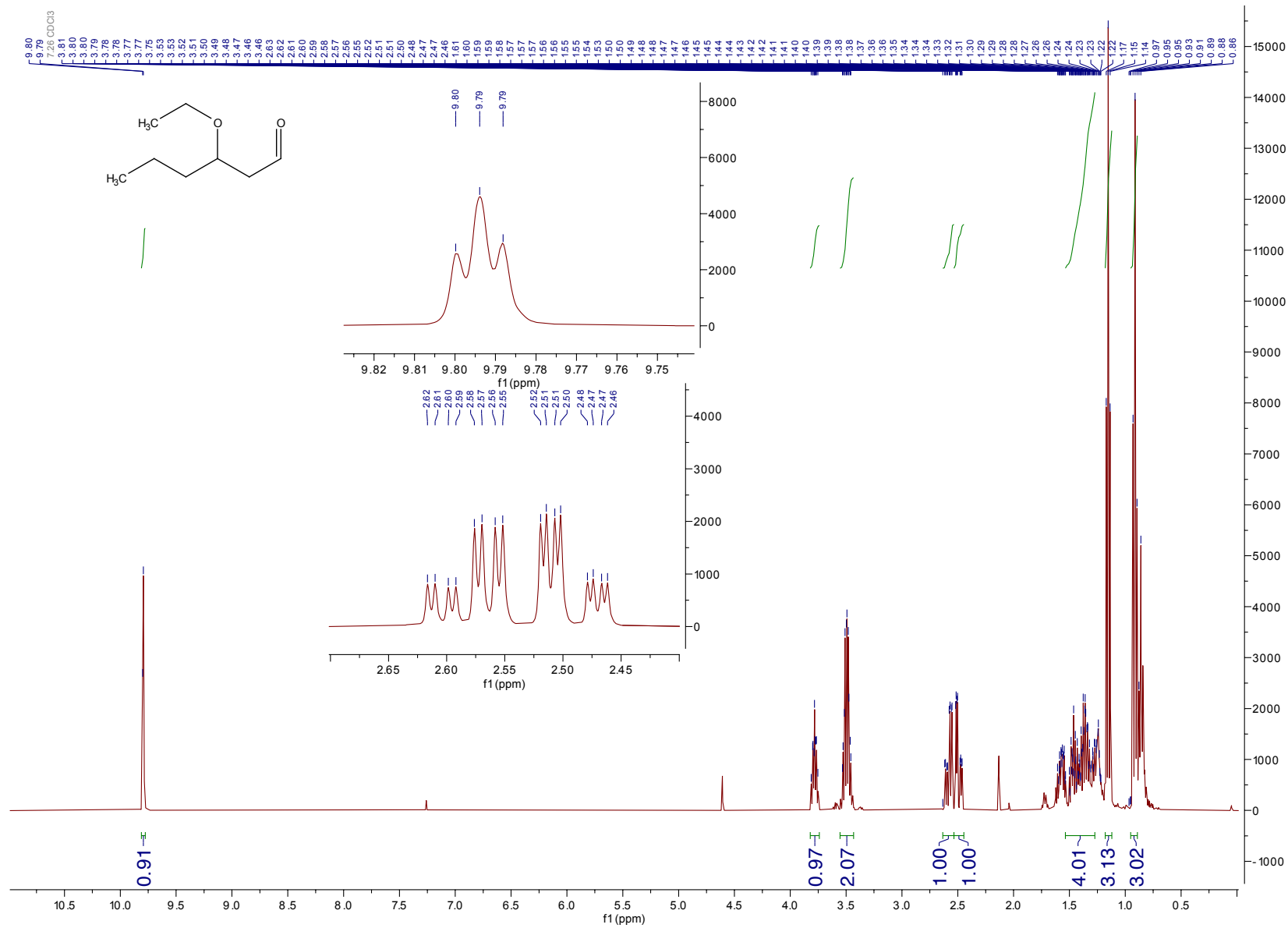


Figure 8.19 ¹H NMR of compound 1.

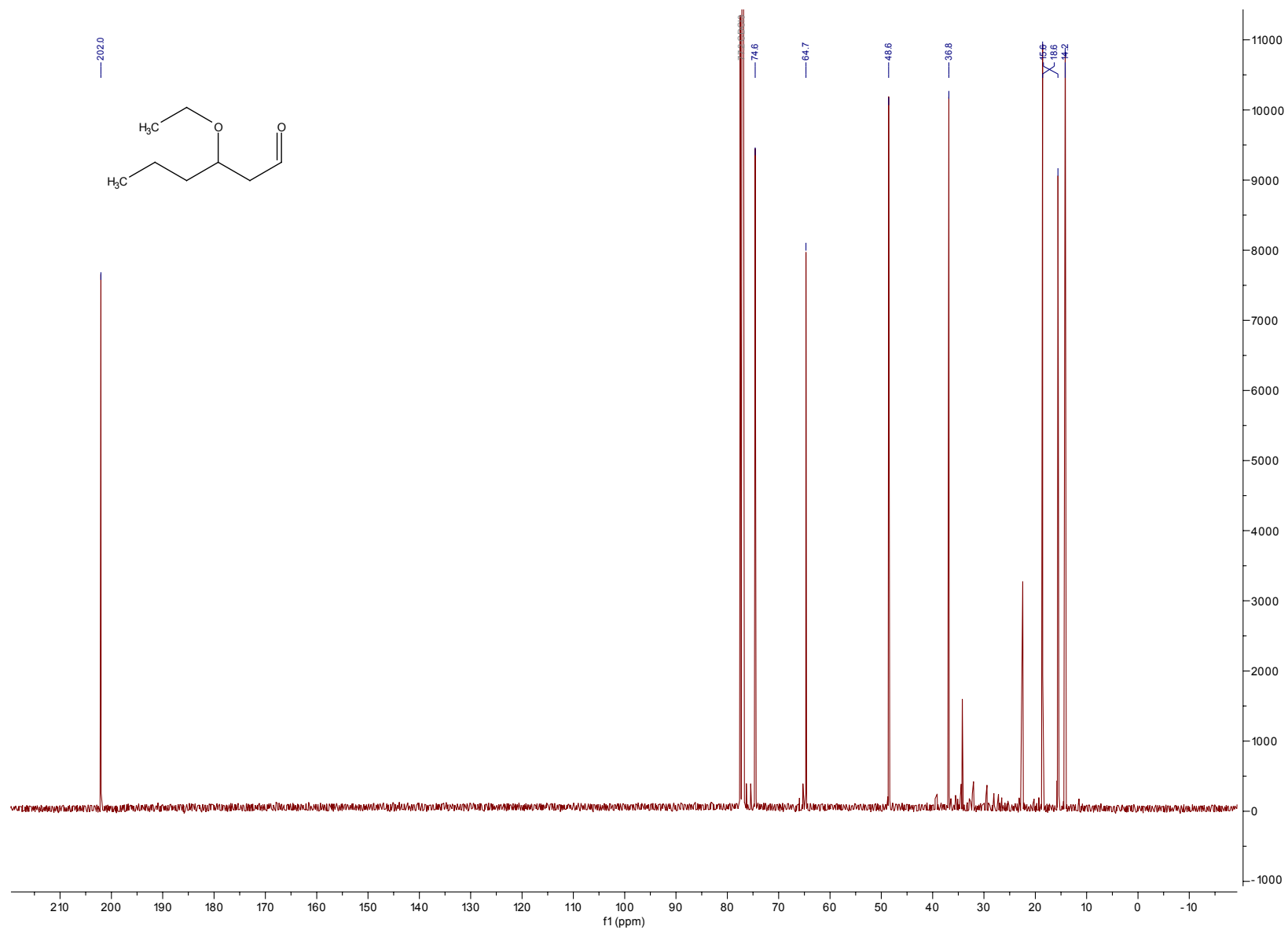


Figure 8.20 ^{13}C NMR of compound 1.

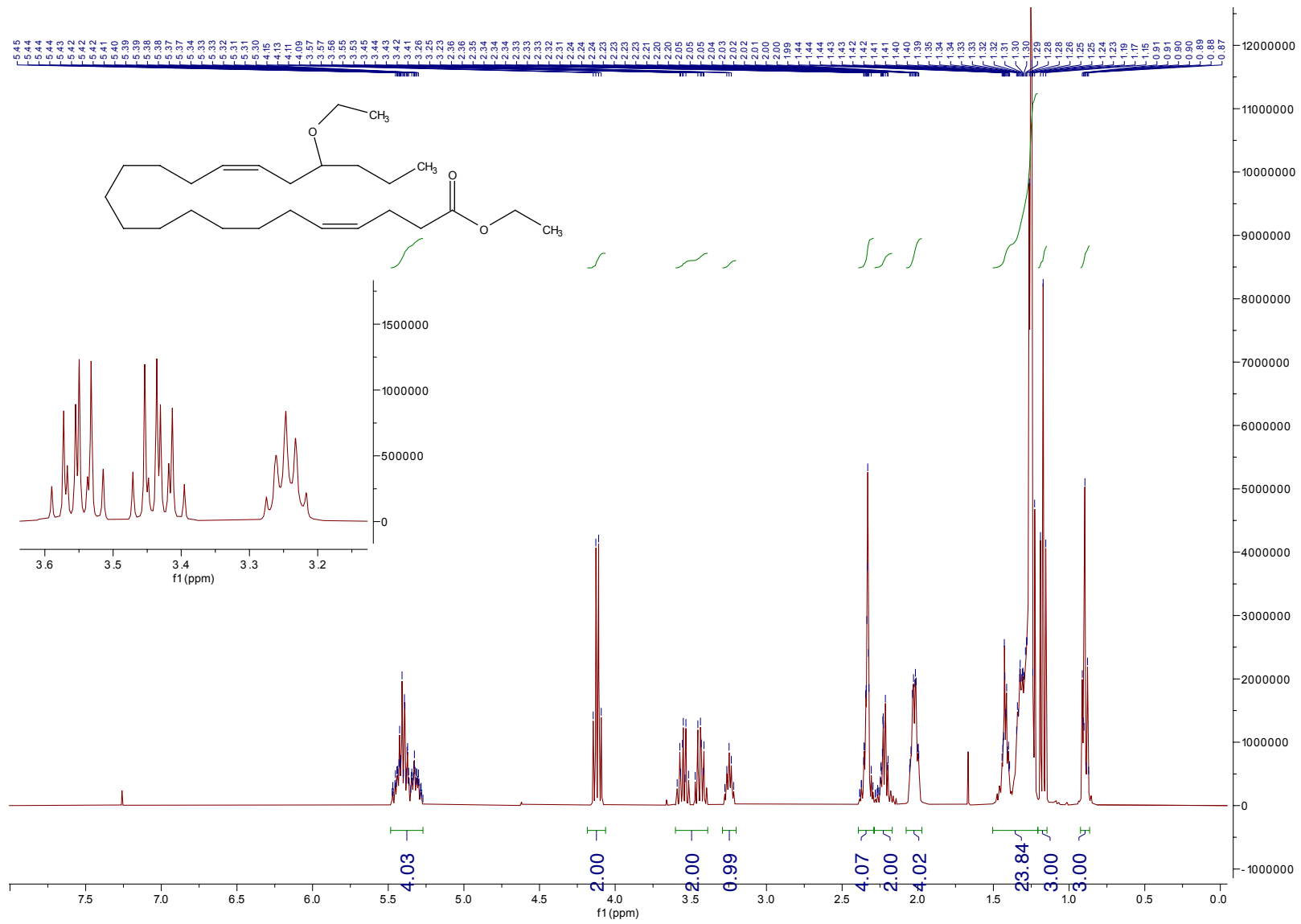


Figure 8.21 ¹H NMR of compound 4.

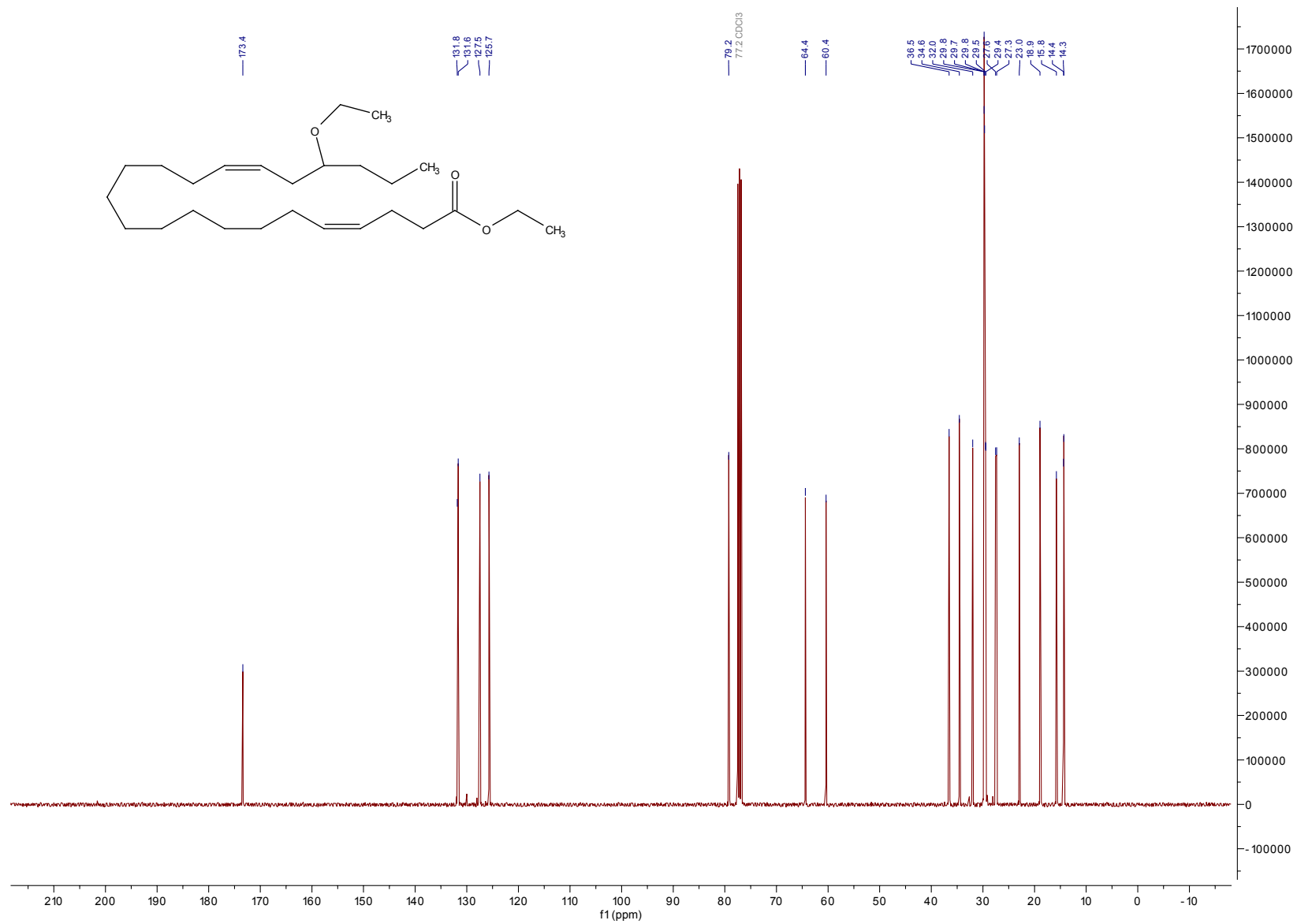


Figure 8.22 ¹³C NMR of compound 4.

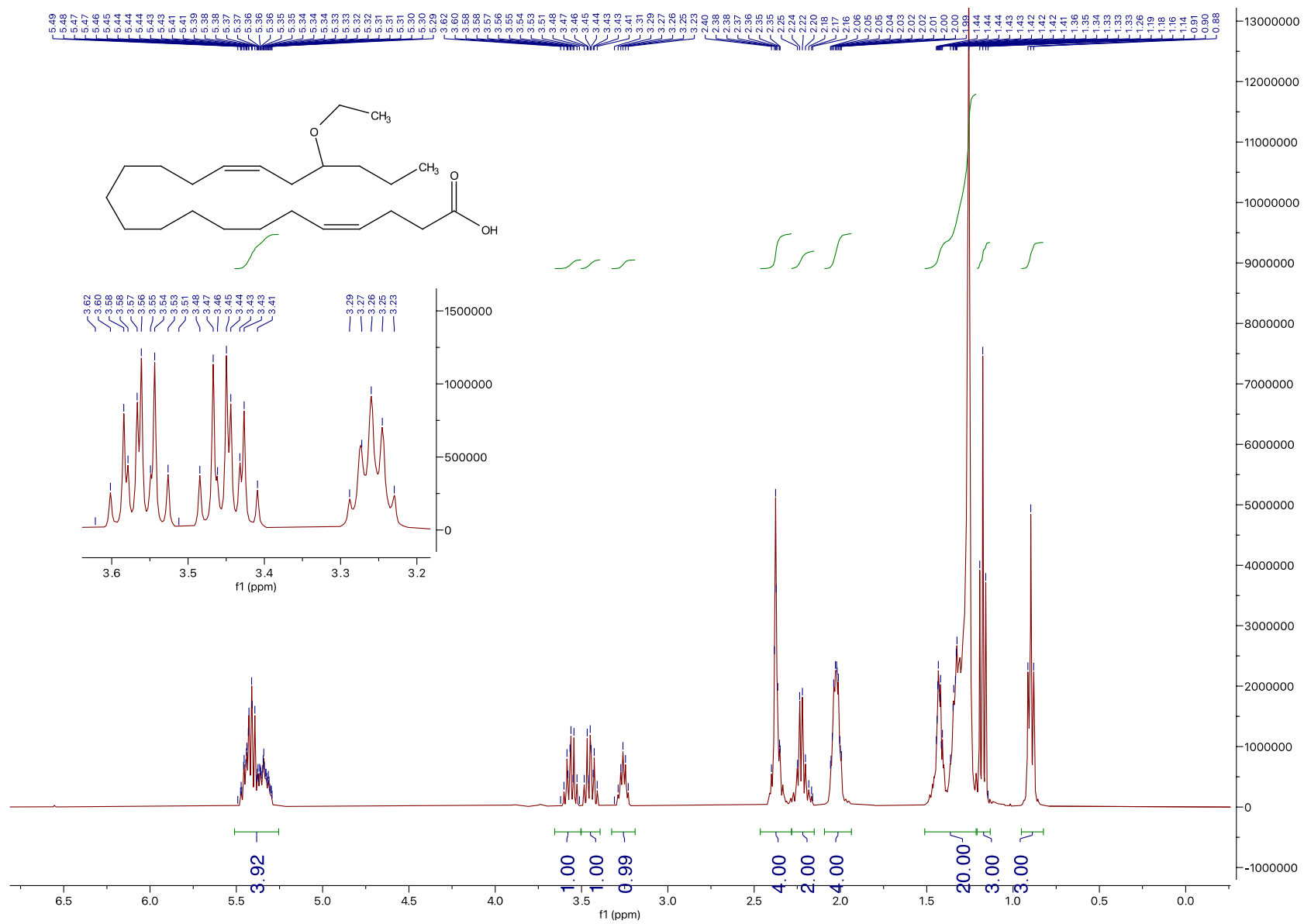


Figure 8.23 ^1H NMR of compound 6.

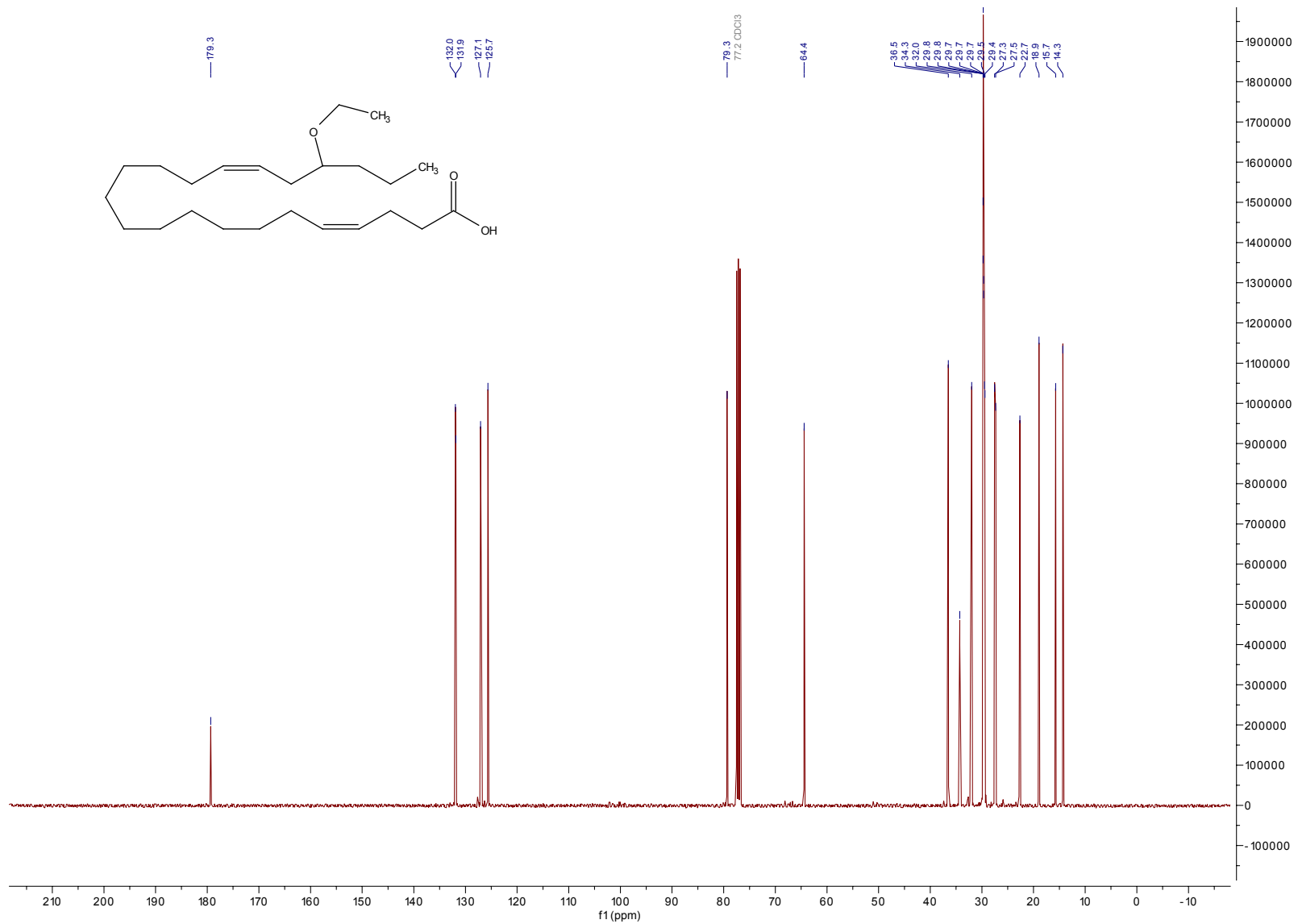


Figure 8.24 ¹³C NMR of compound 6.

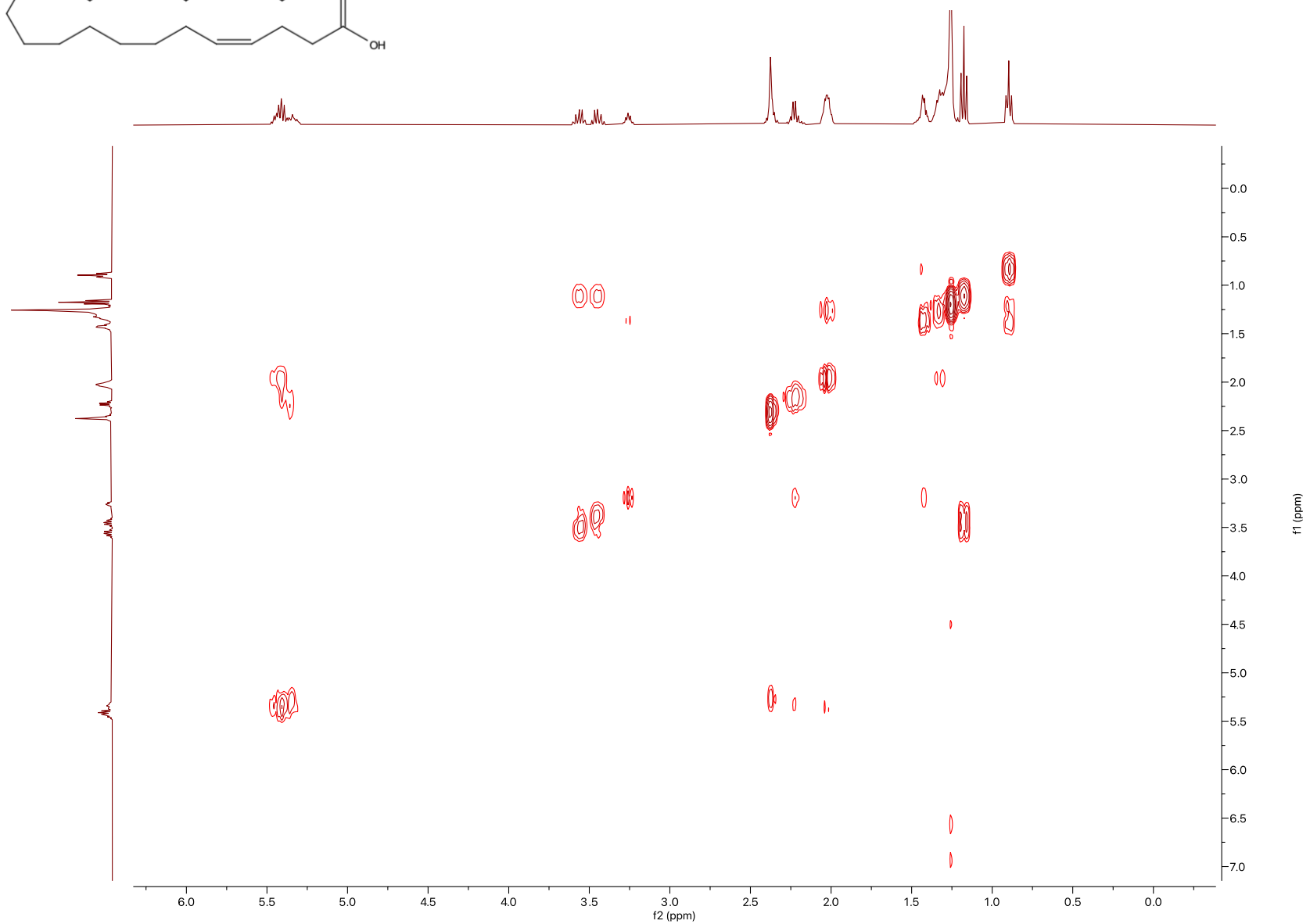
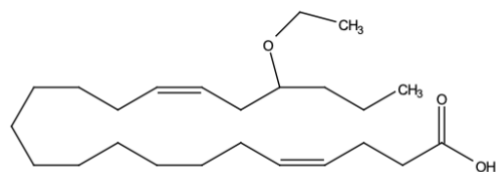


Figure 8.25 COSY of target molecule 6.

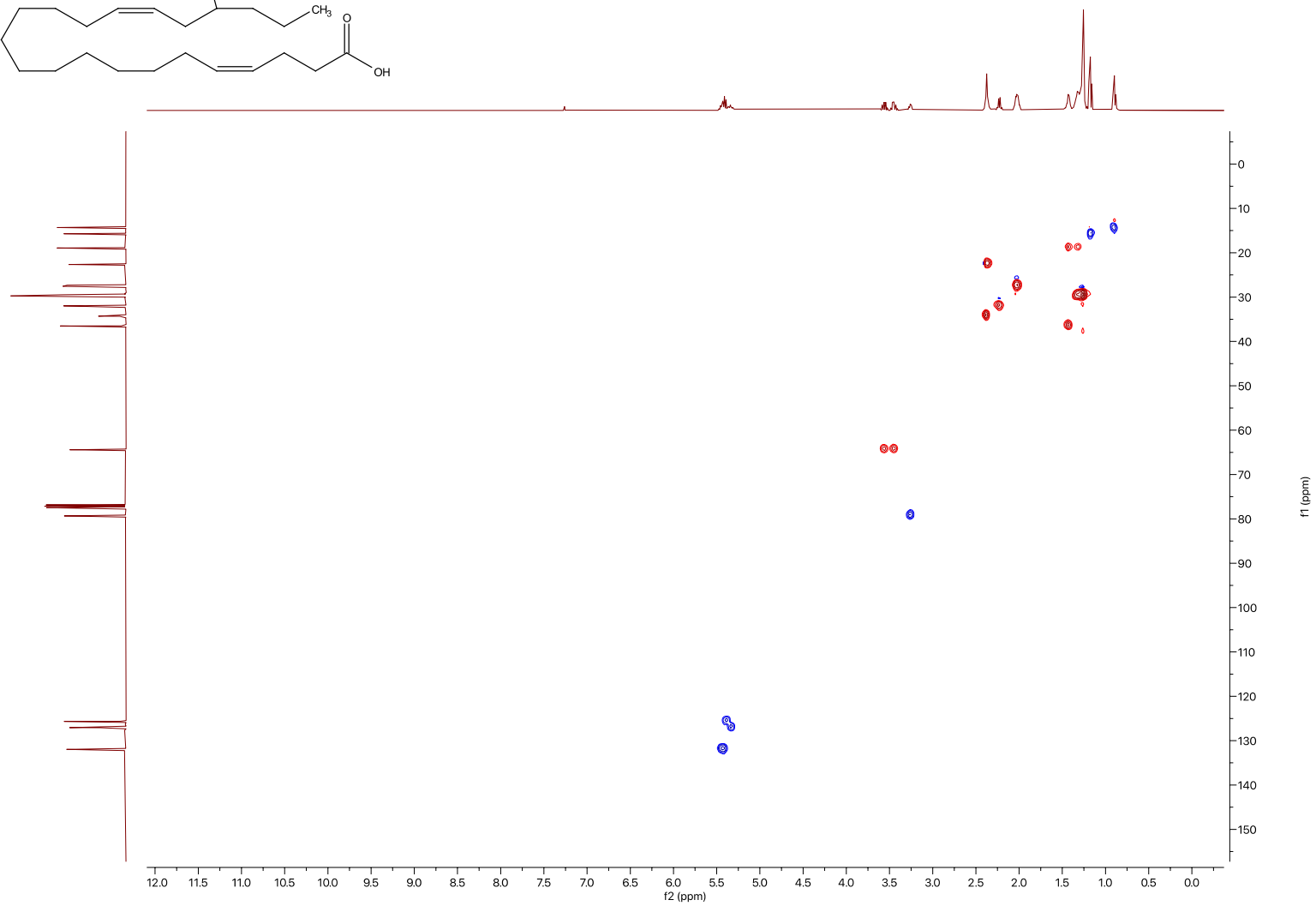
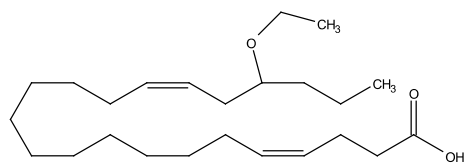


Figure 8.26 HSQC of target molecule 6.

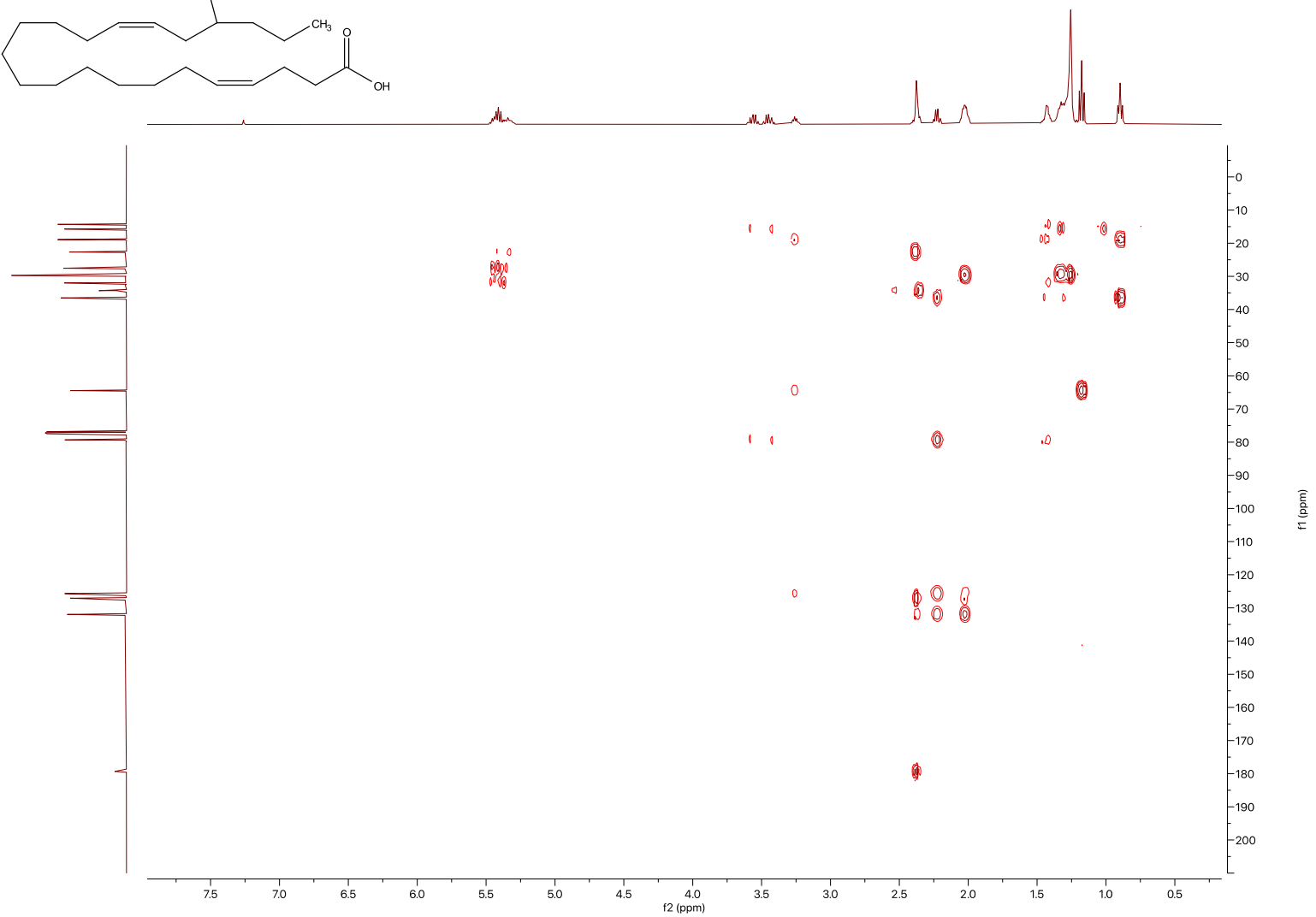
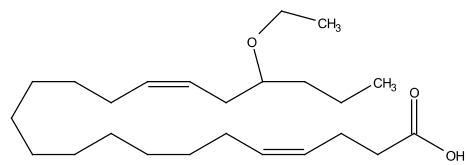


Figure 8.27 HMBC of target molecule 6.

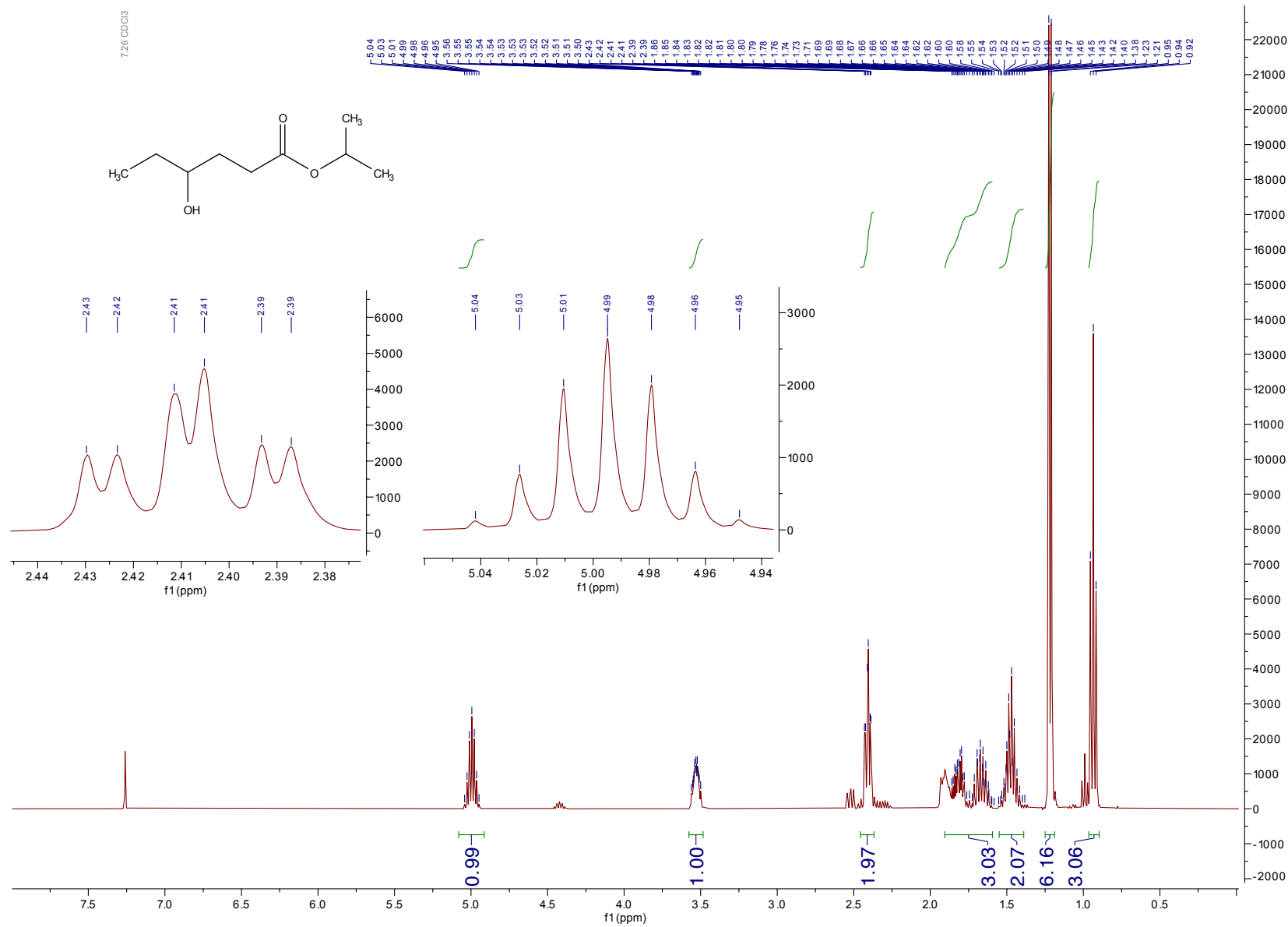


Figure 8.28 ¹H NMR of compound 17.

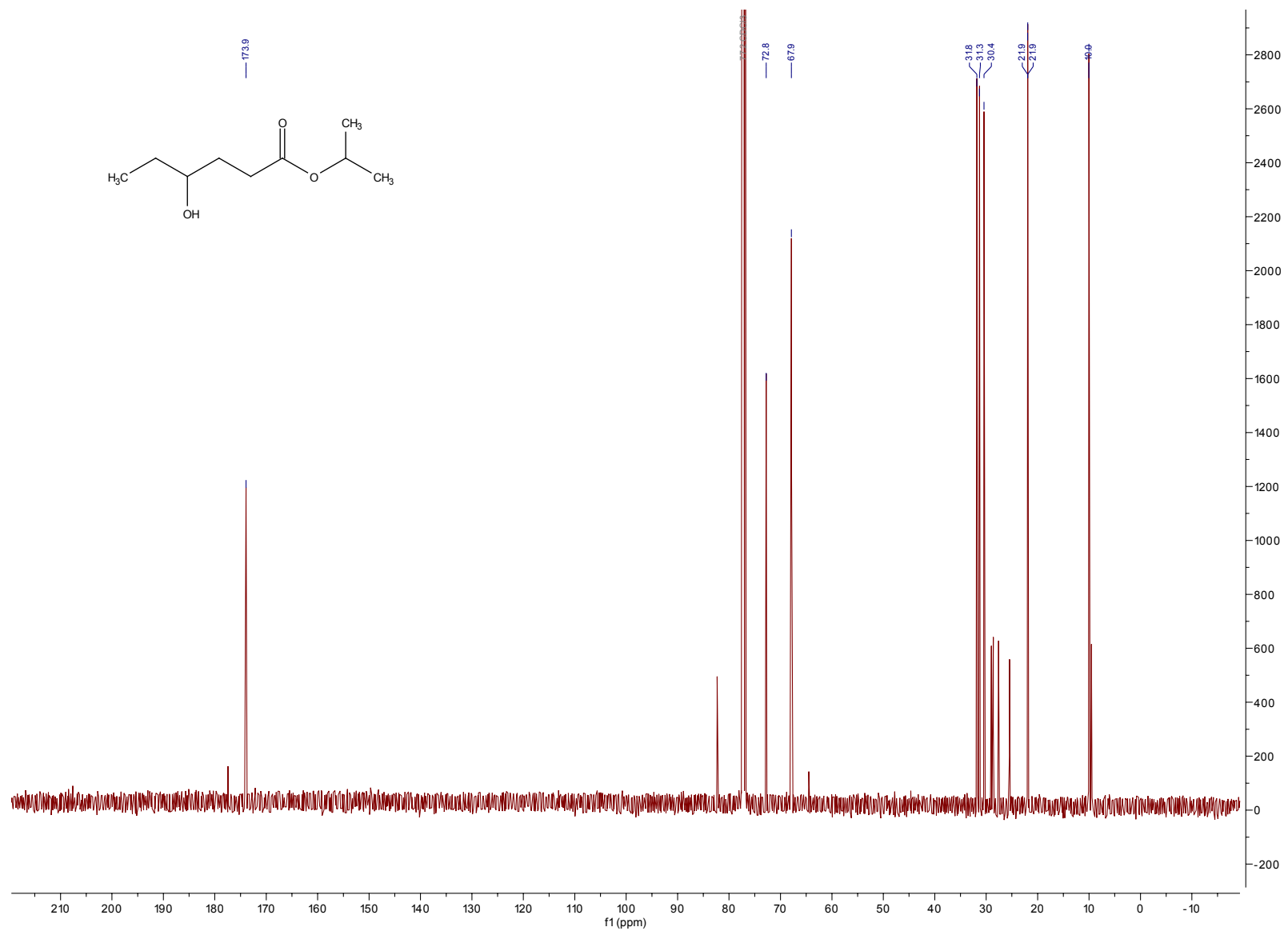
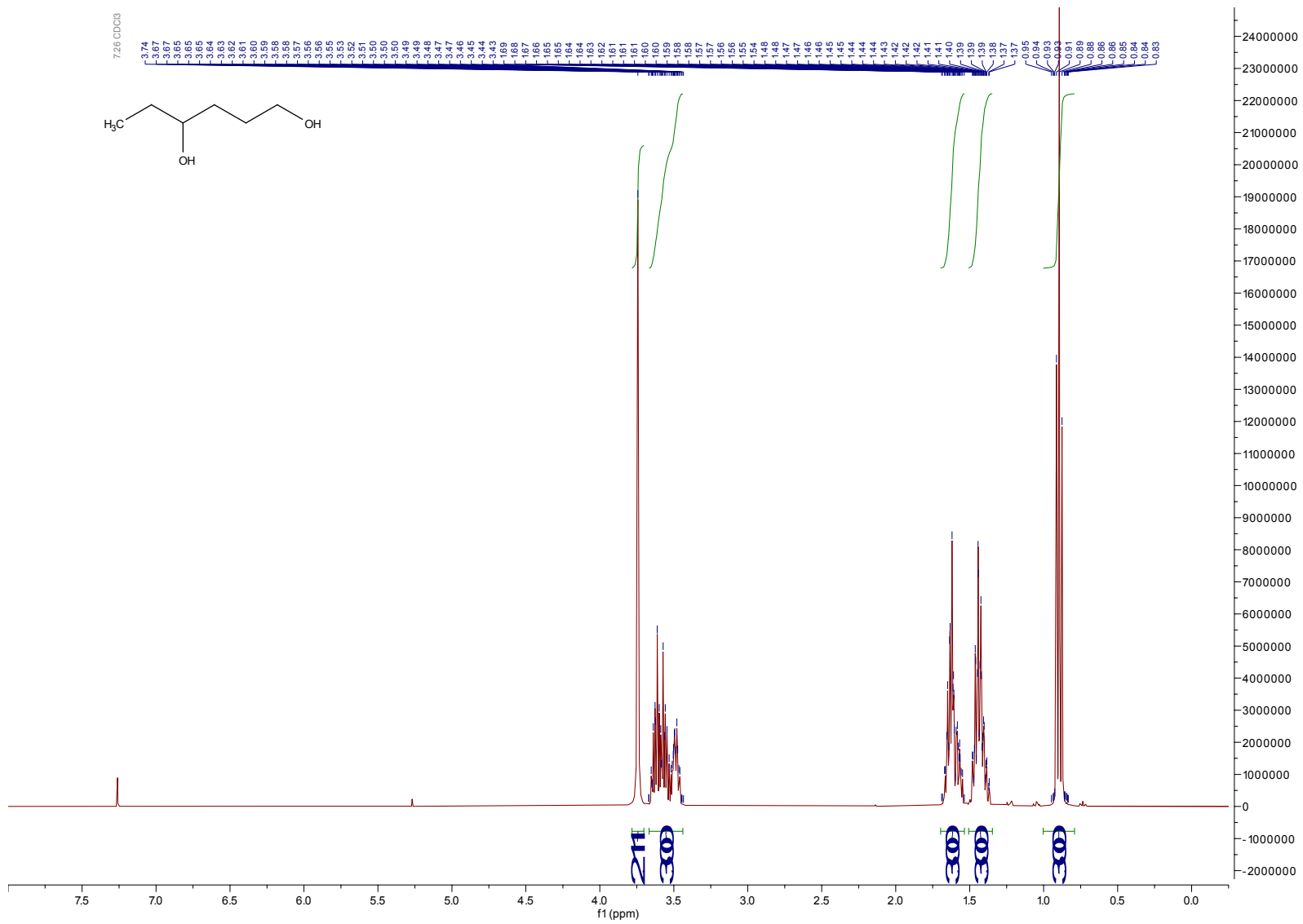


Figure 8.29 ¹³C NMR of compound 17.



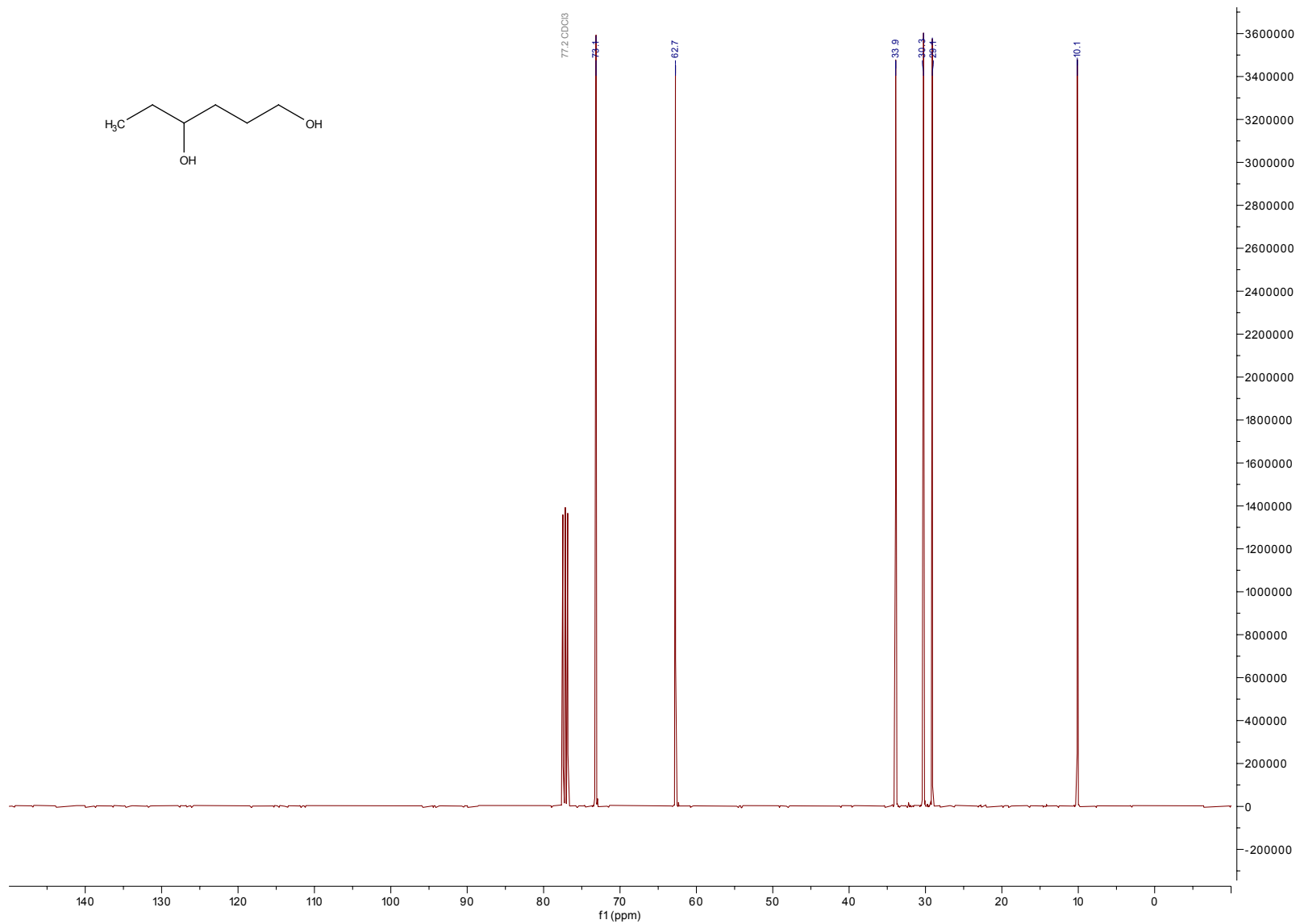
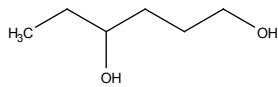


Figure 8.31. ¹³C NMR of compound **19**.

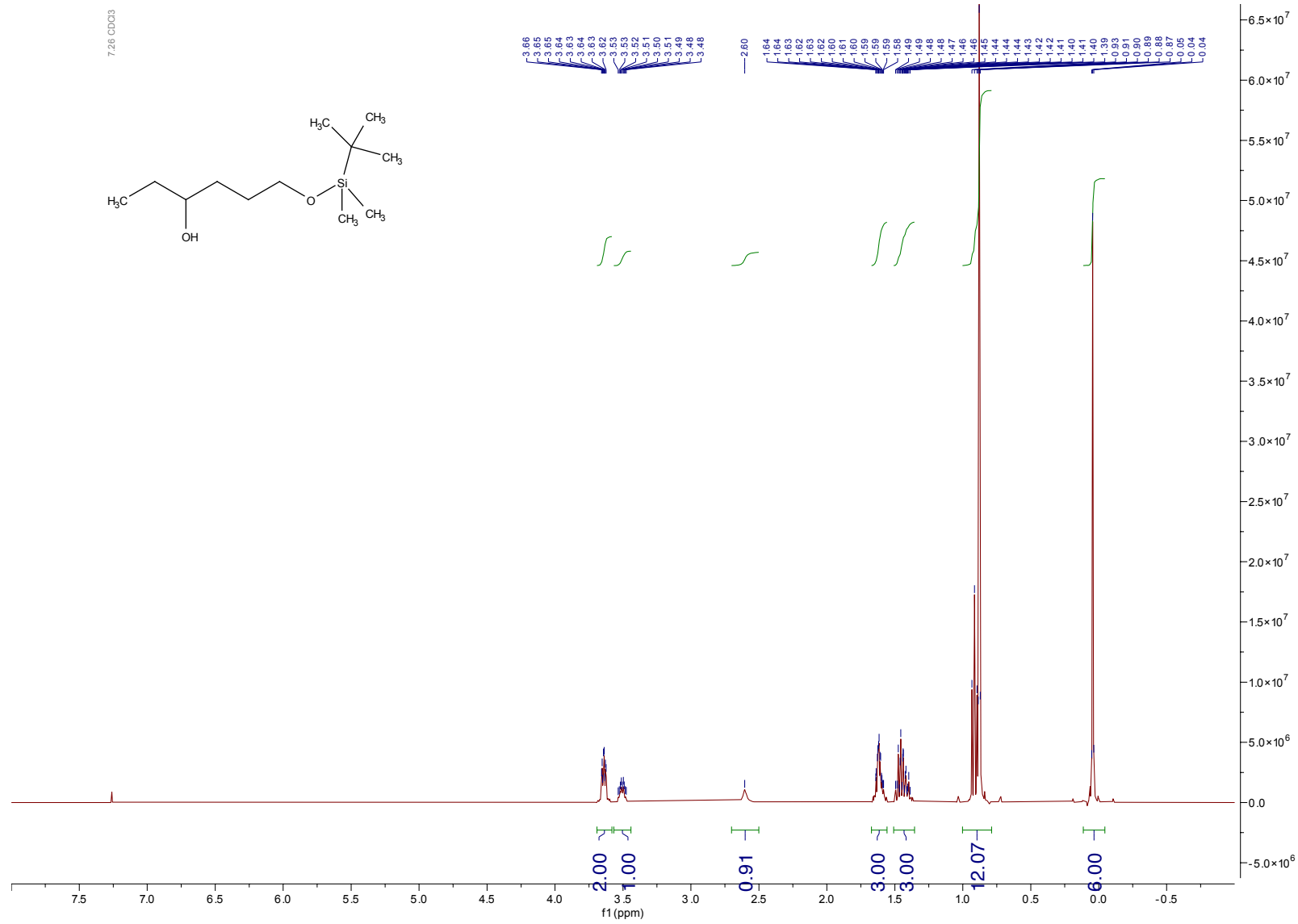


Figure 8.32 ¹H NMR of compound 20.

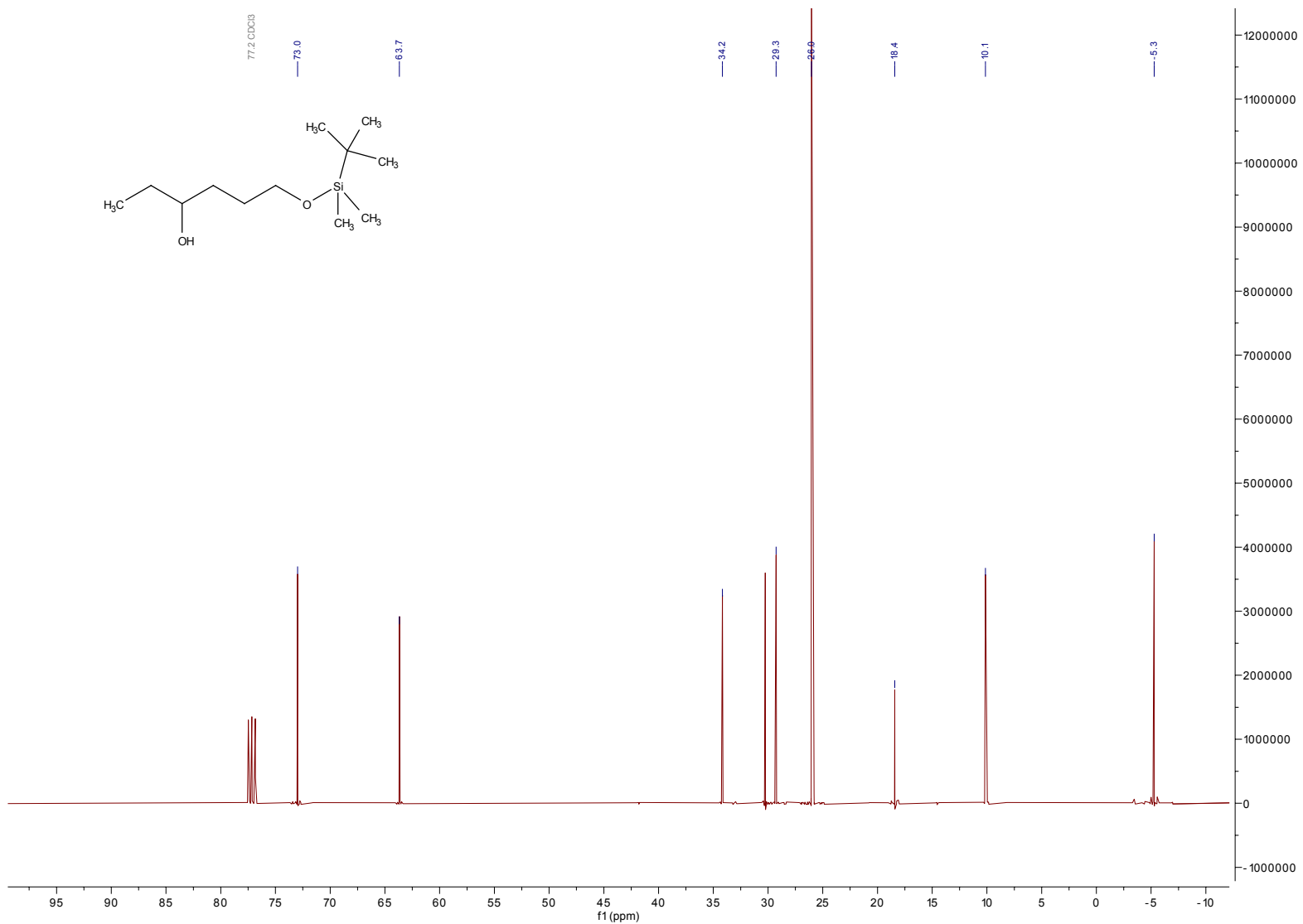


Figure 8.33 ^{13}C NMR of compound 20.

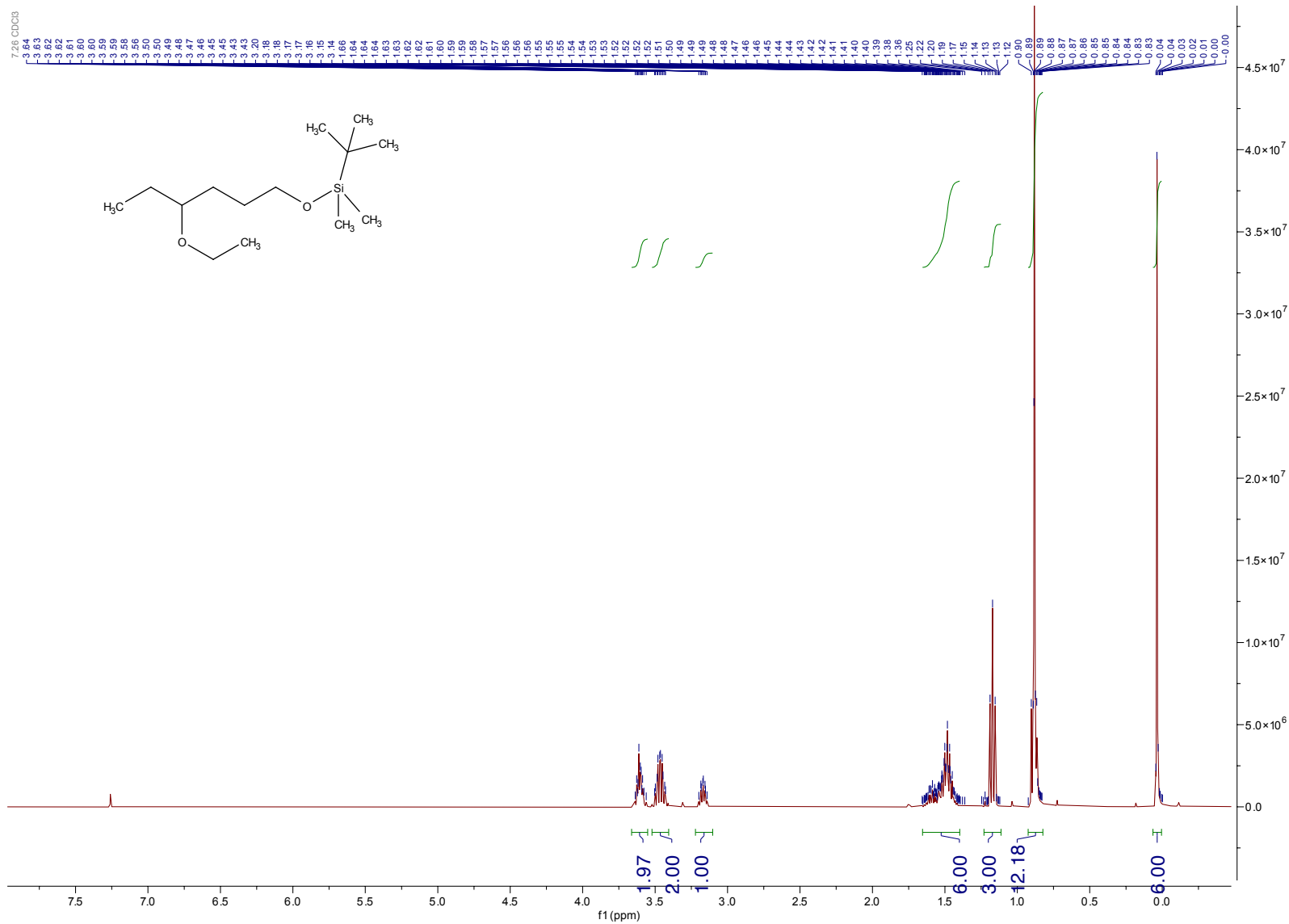


Figure 8.34 ¹H NMR of compound 21a.

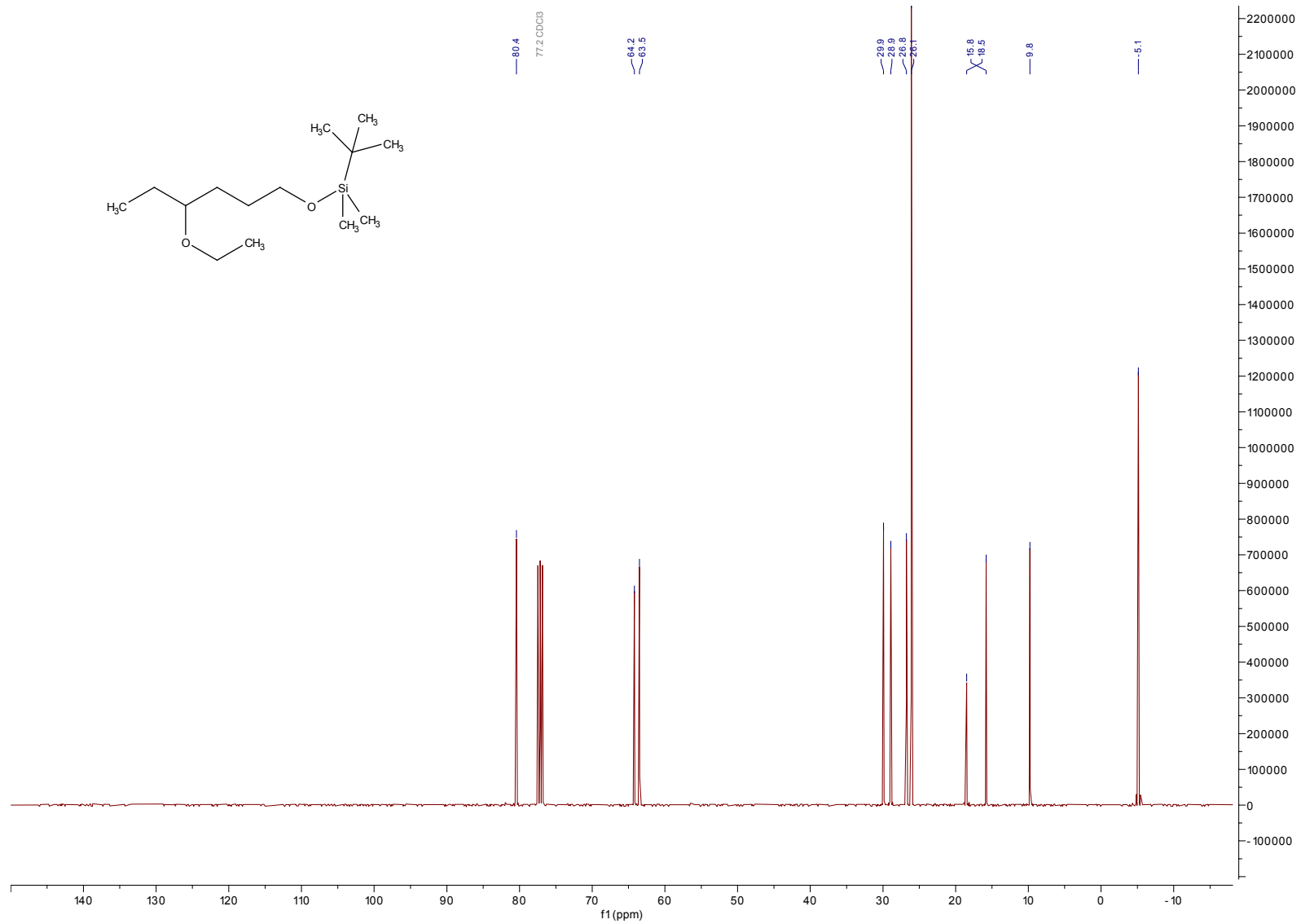


Figure 8.35 ^{13}C NMR of compound **21a**.

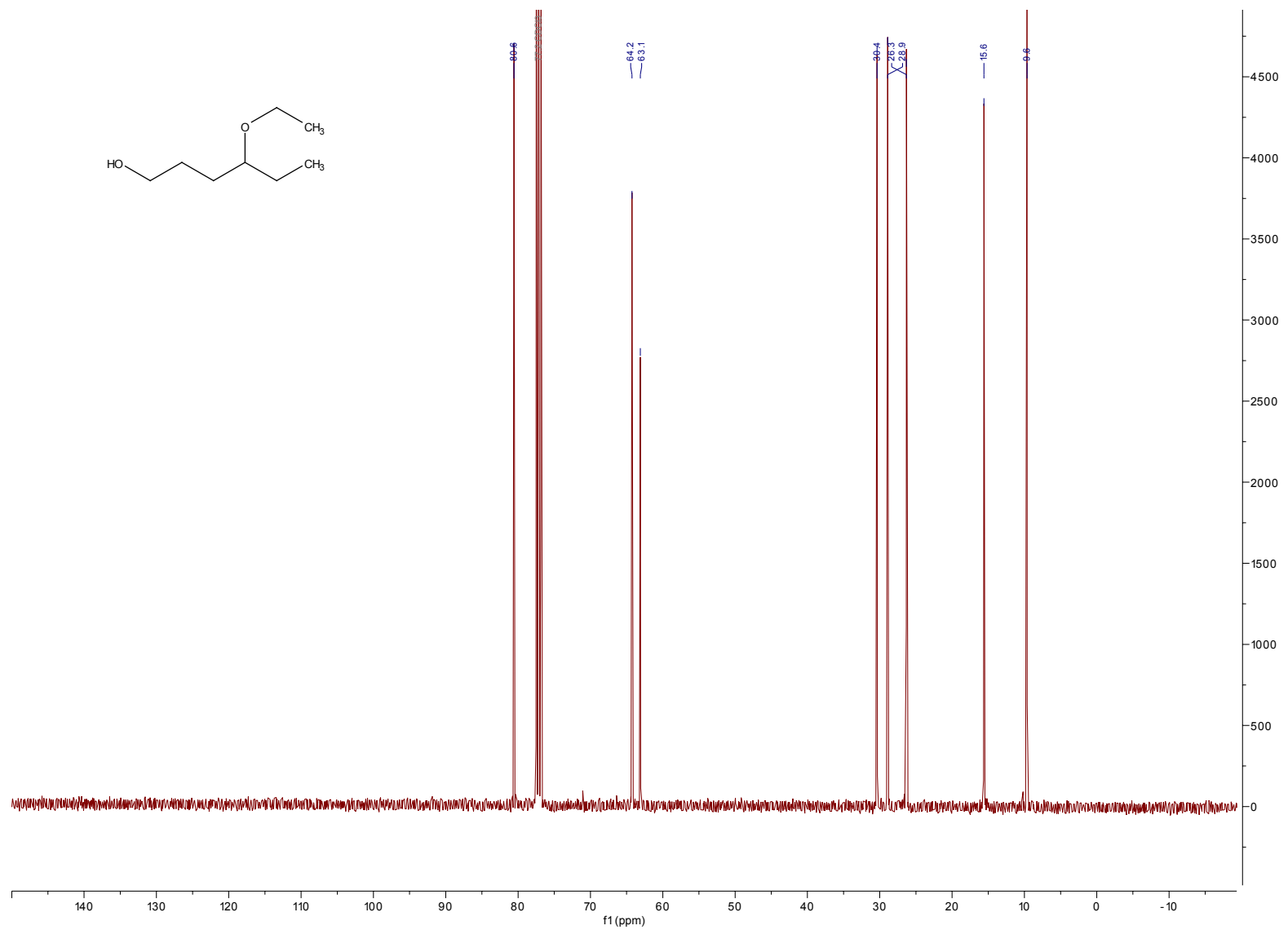


Figure 8.37 ^{13}C NMR of compound **21b**.

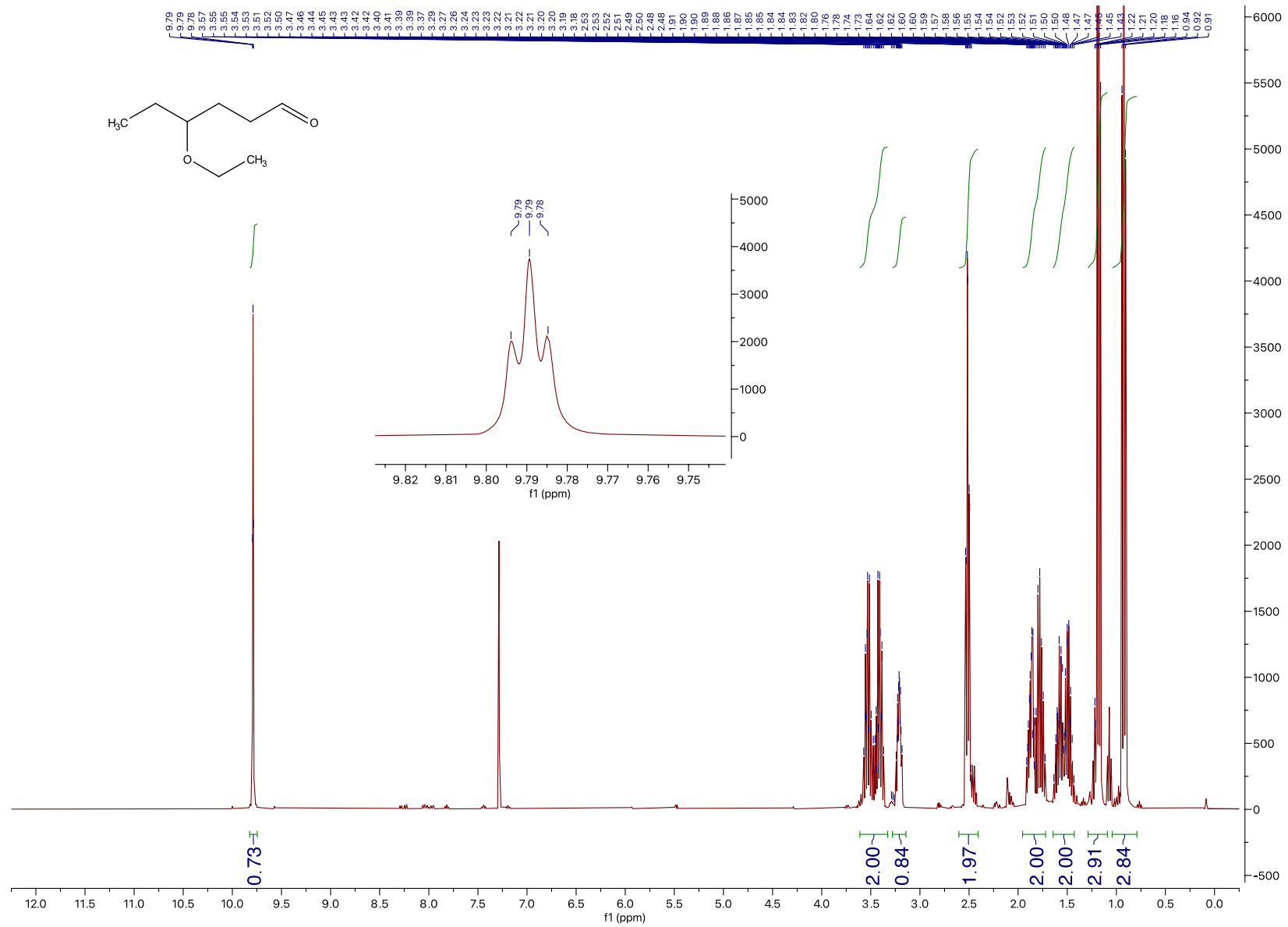


Figure 8.38 ¹H NMR of compound 3.

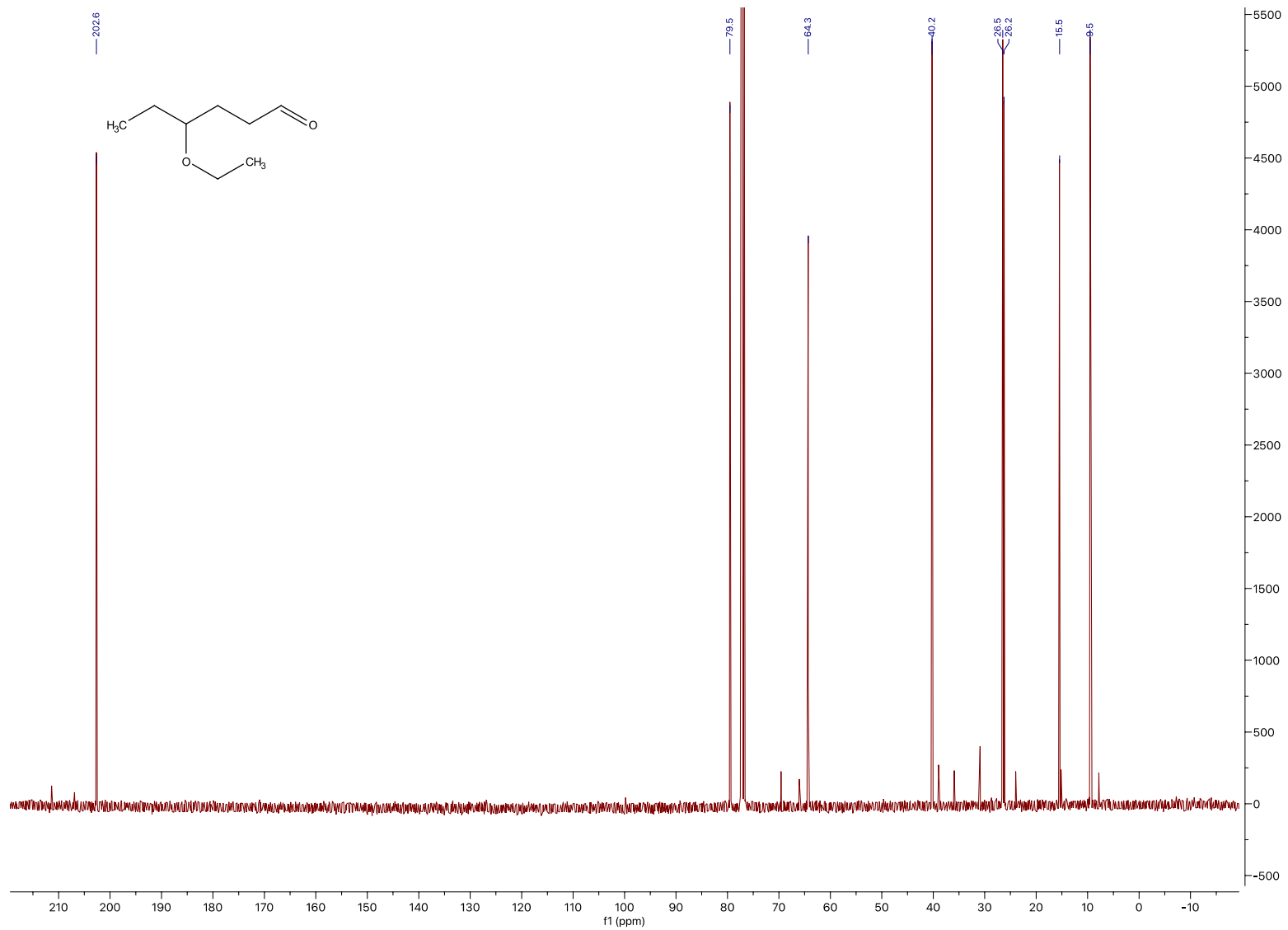


Figure 8.39 ¹³C NMR of compound 3.

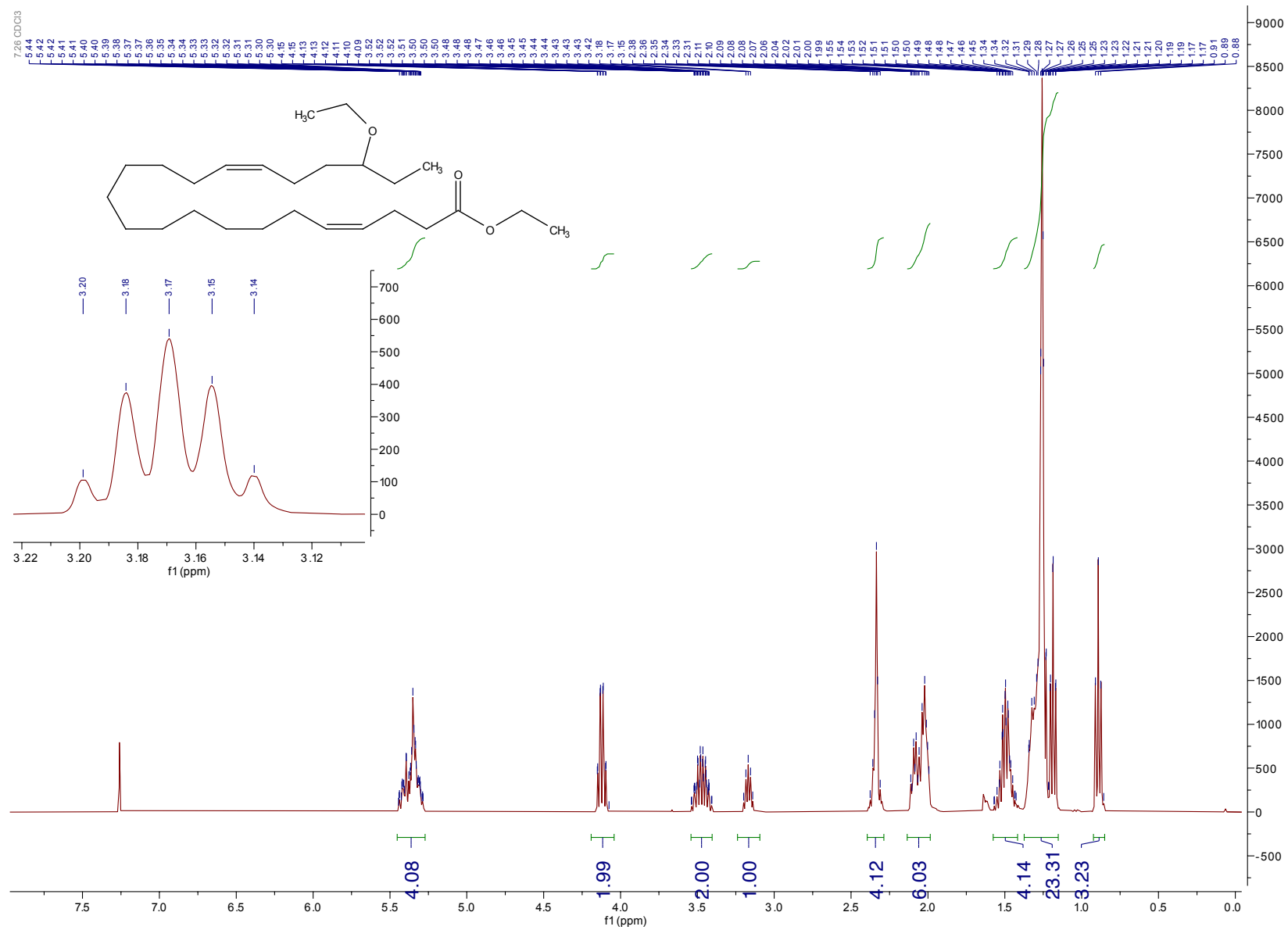


Figure 8.40 ¹H NMR of compound 5.

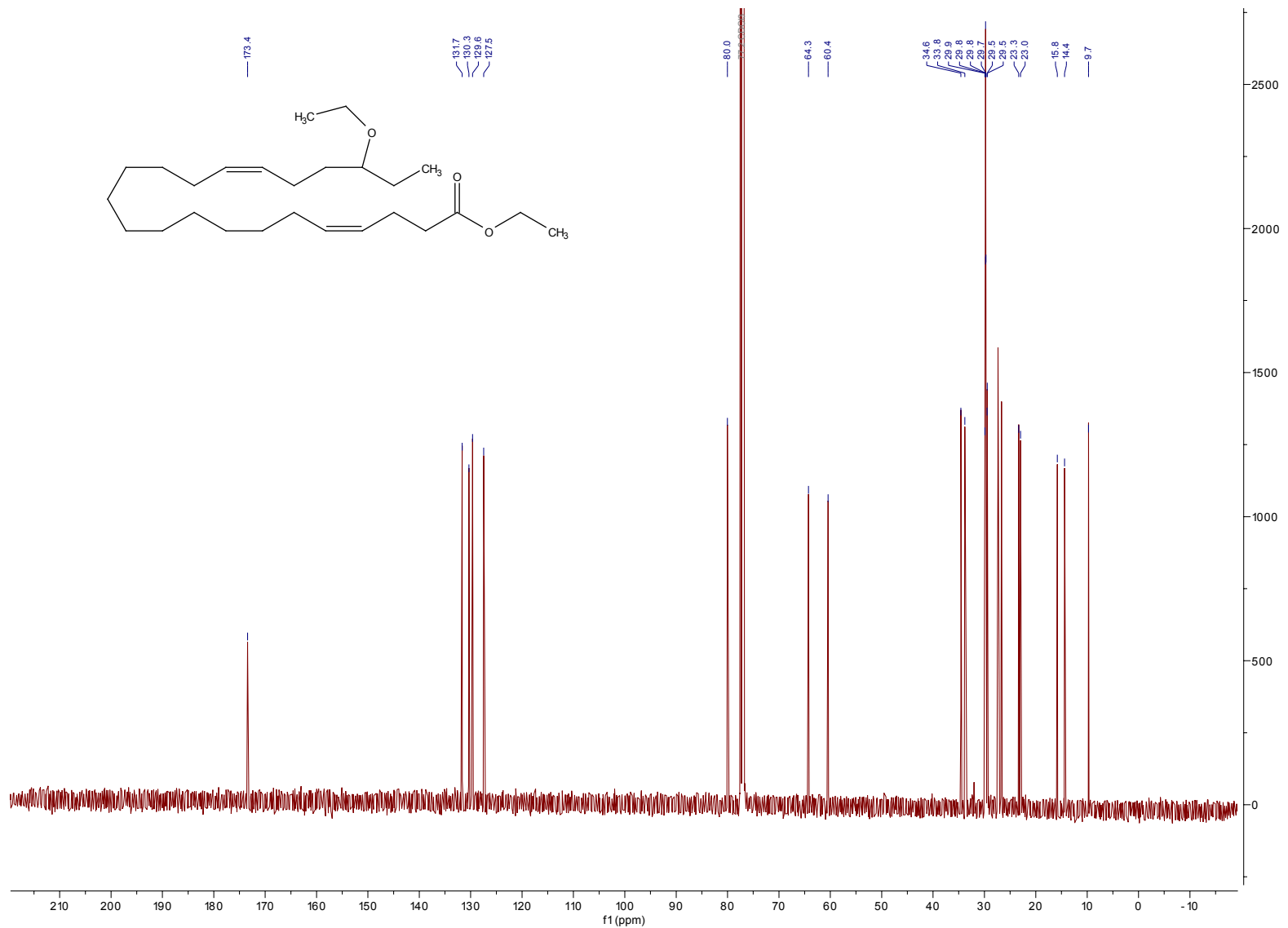


Figure 8.41 ¹³C NMR of compound 5.

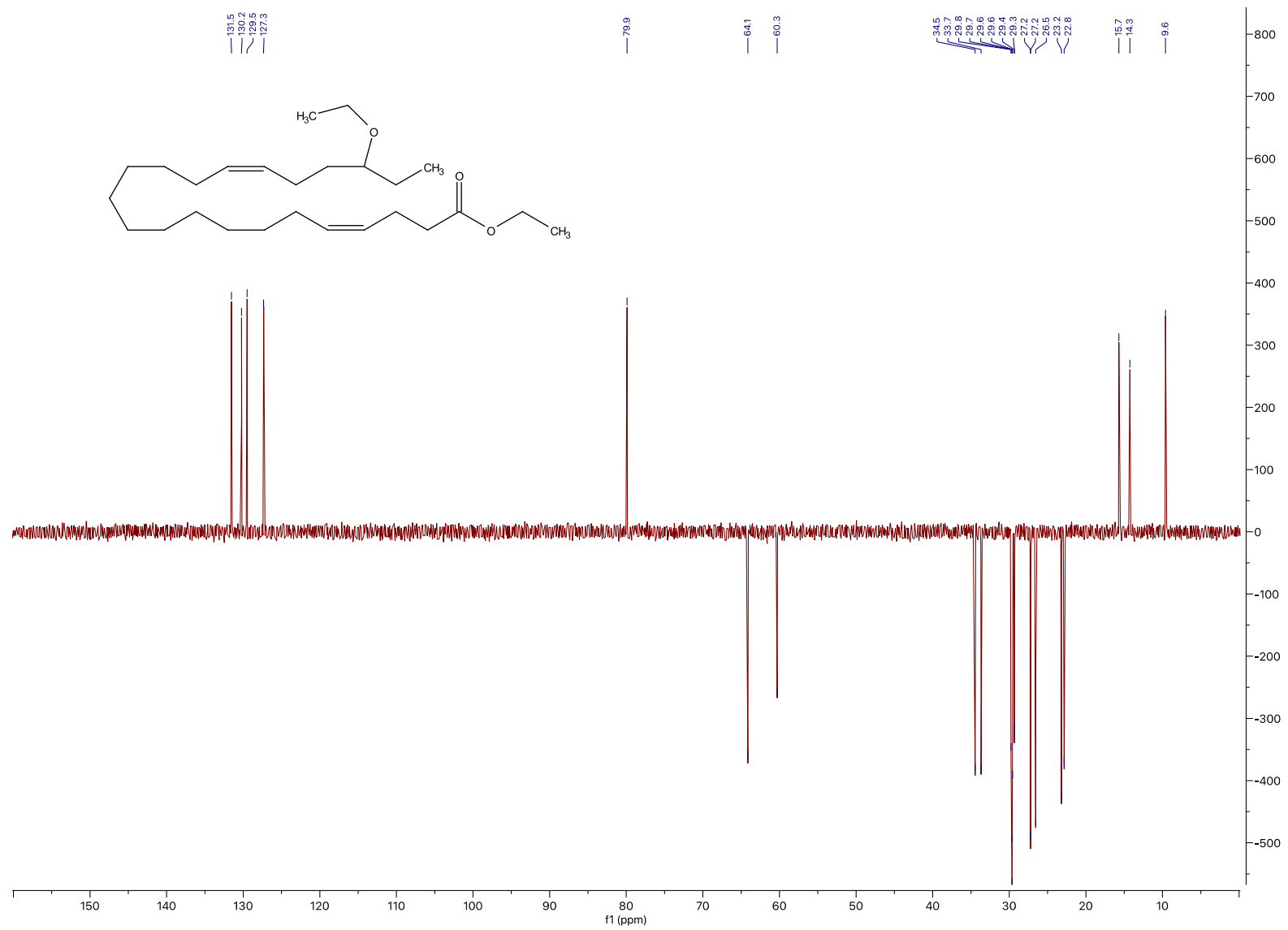


Figure 8.42 DEPT-135 of compound 5.

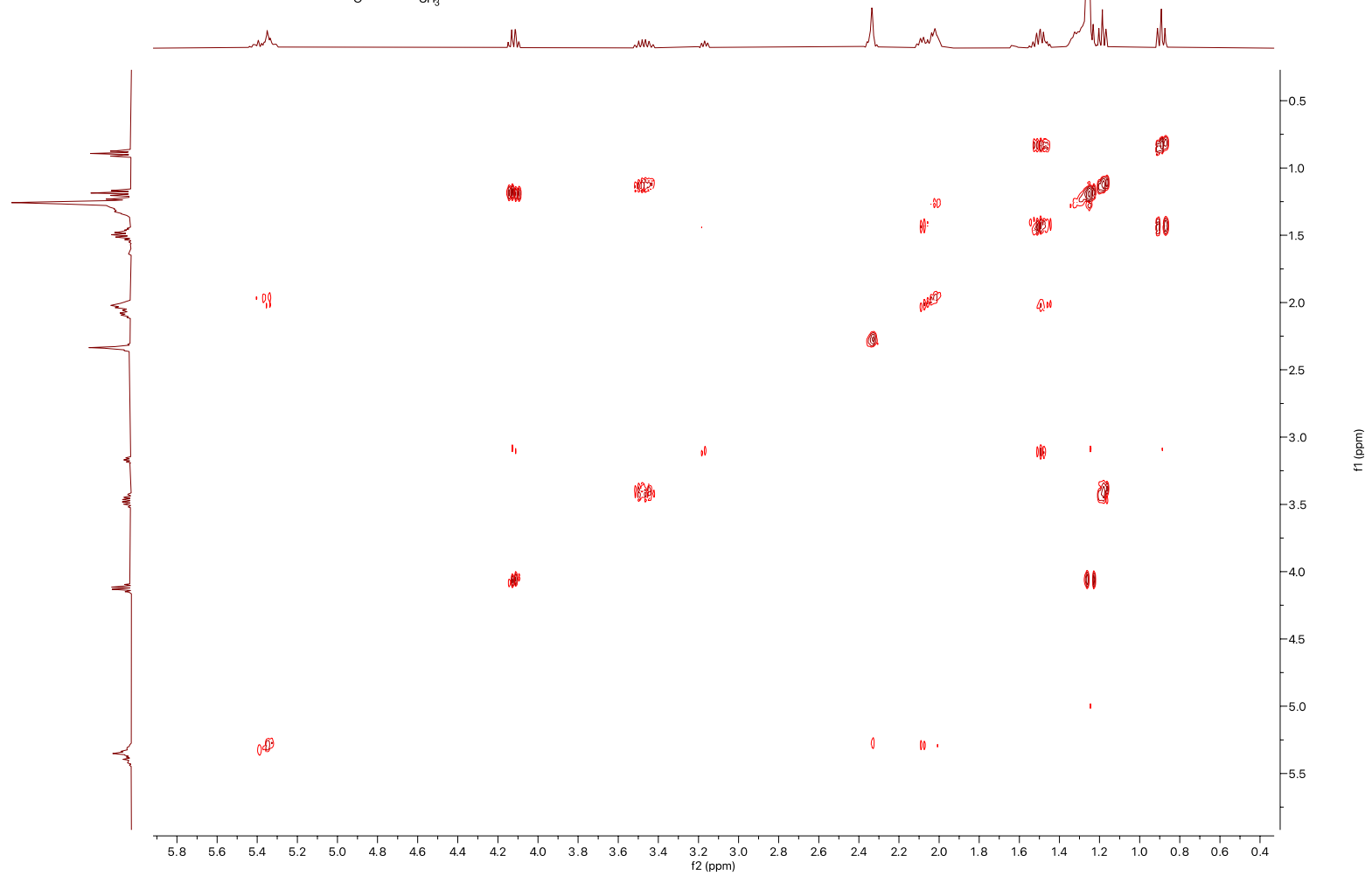
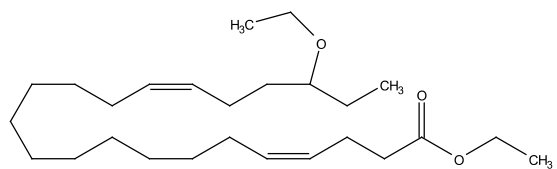


Figure 8.43 COSY of compound 5.

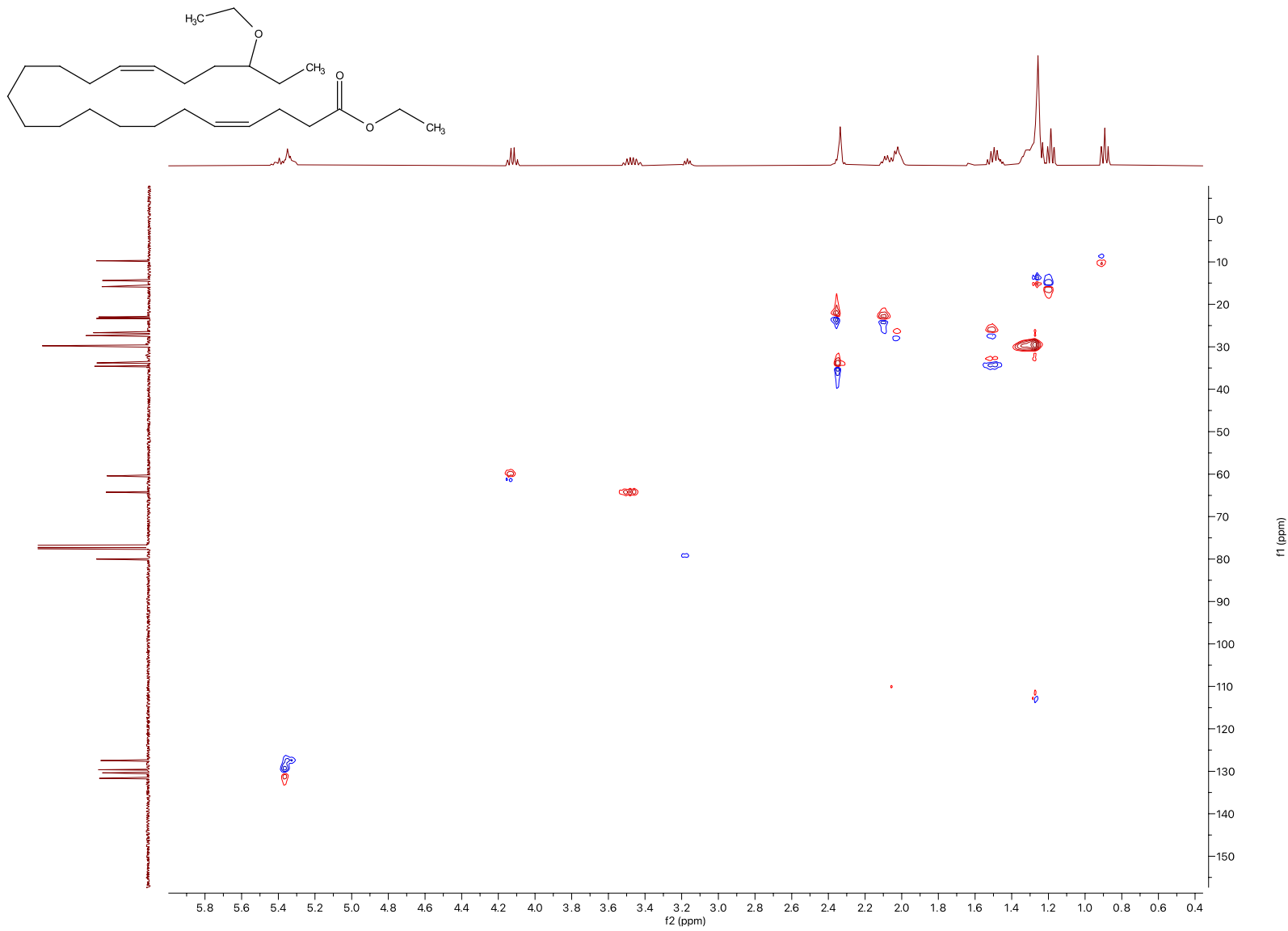


Figure 8.44 HSQC of compound 5.

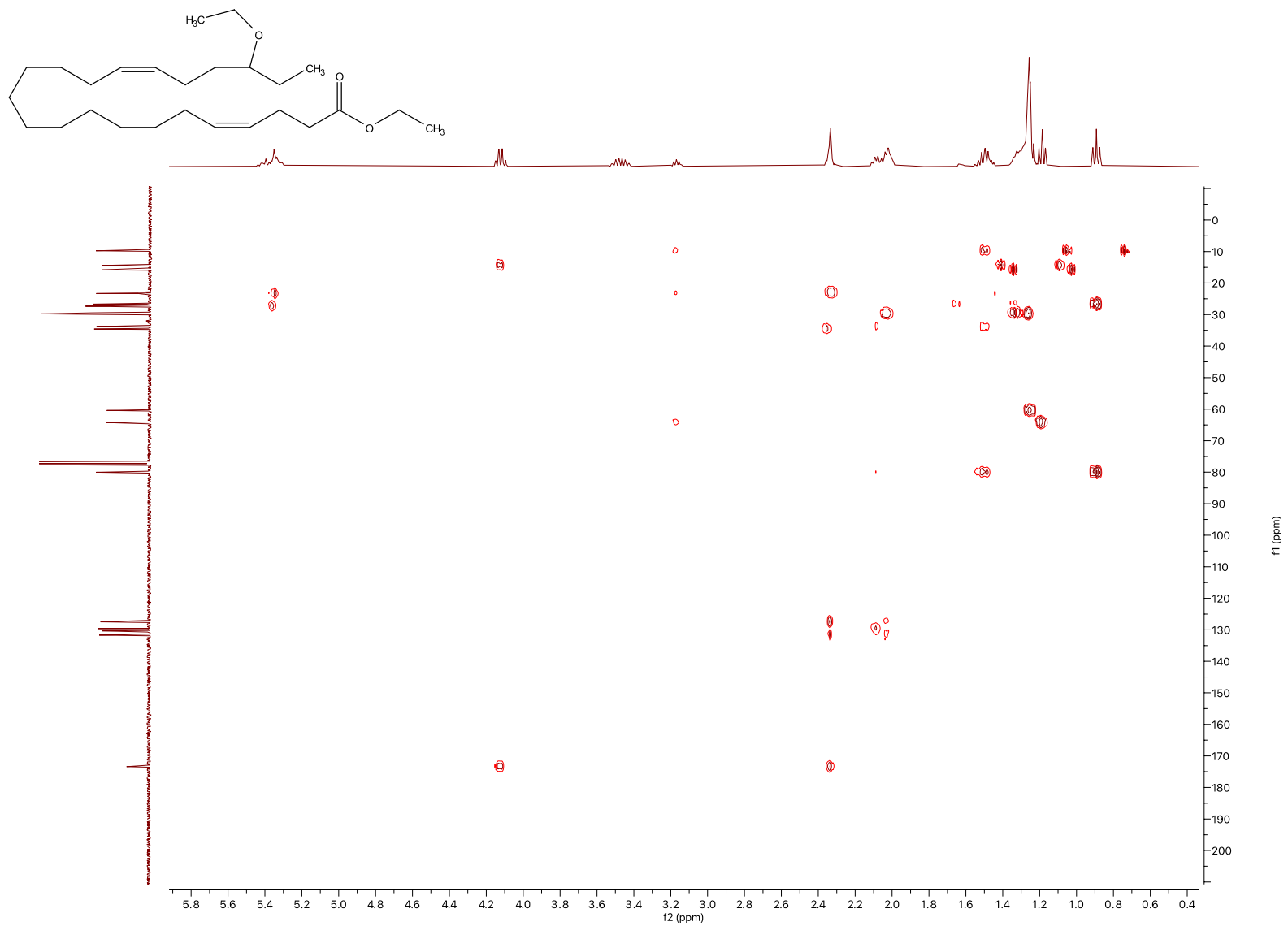


Figure 8.45 HMBC of compound 5.

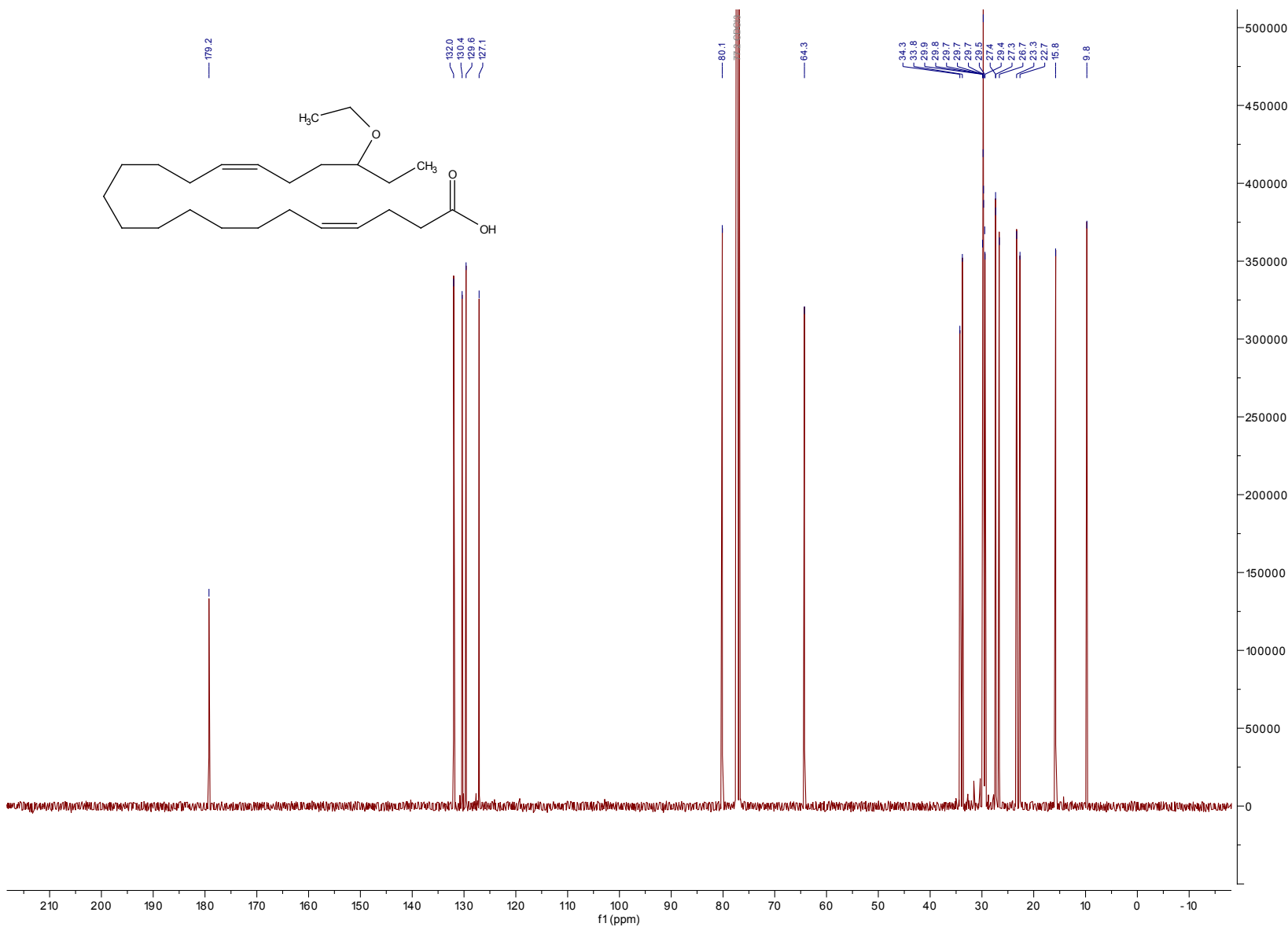


Figure 8.47 ^{13}C of compound 7.

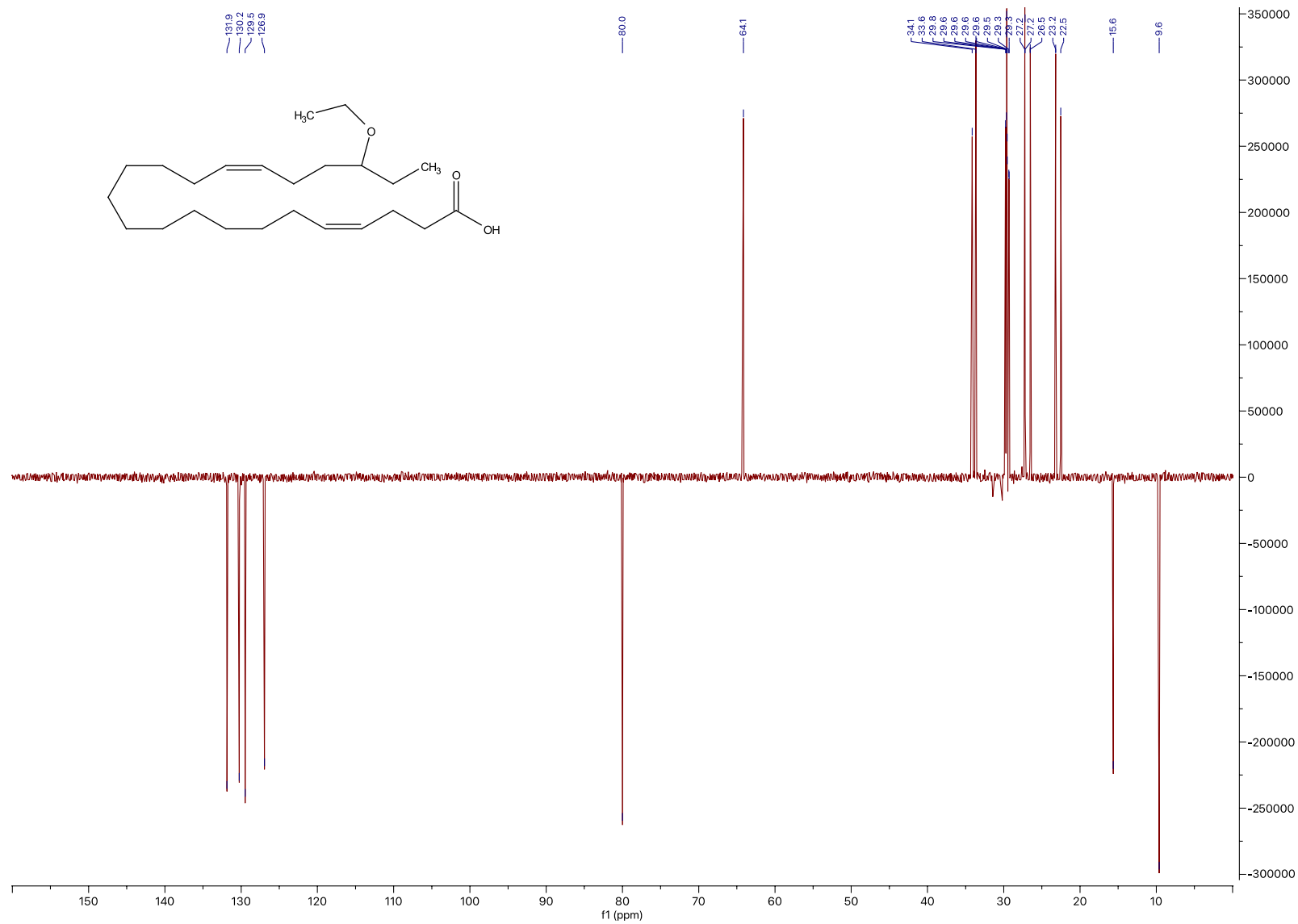


Figure 8.48 DEPT-135 for compound 7.

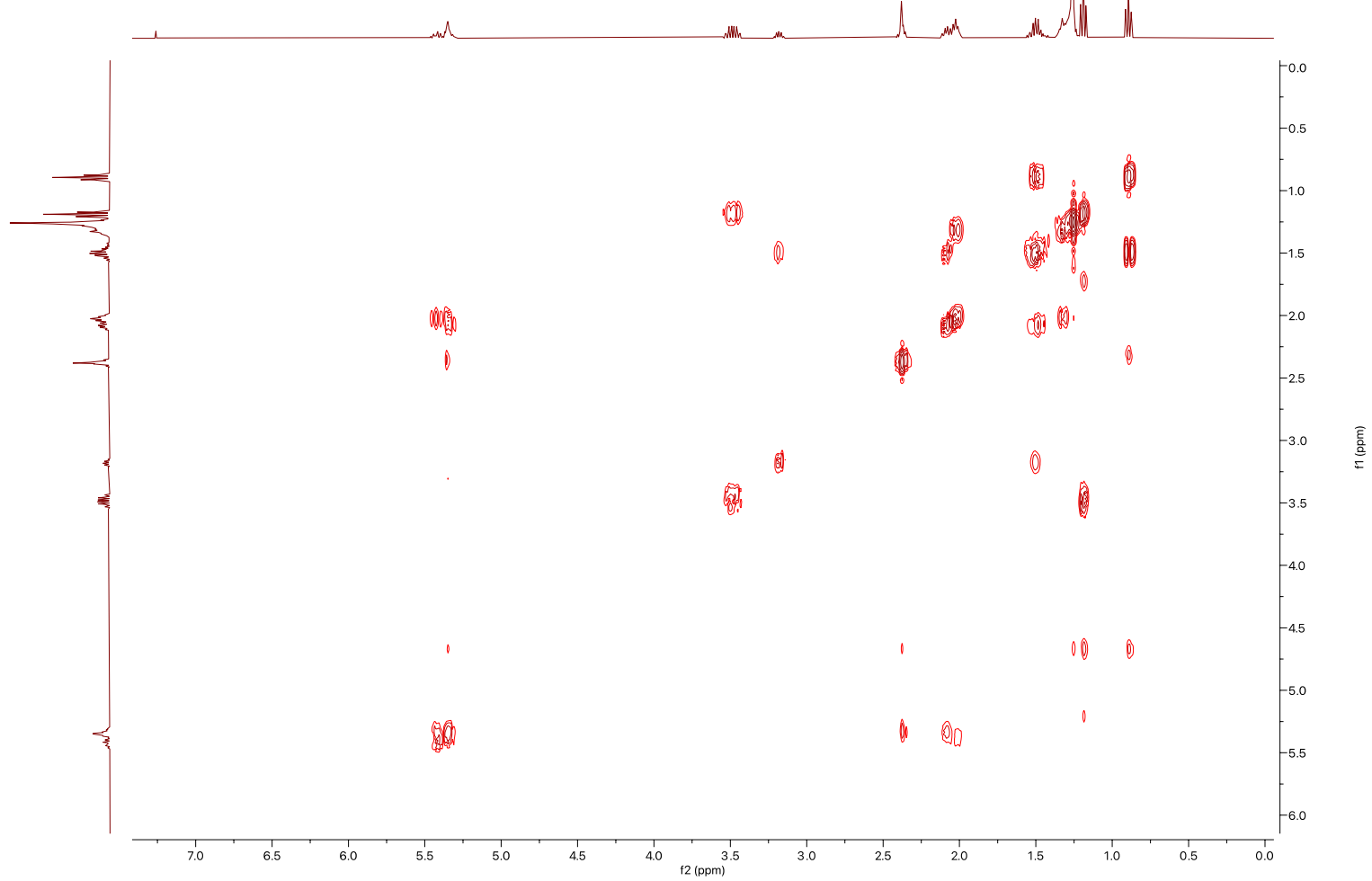
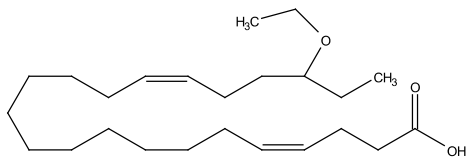


Figure 8.49 COSY for compound 7.

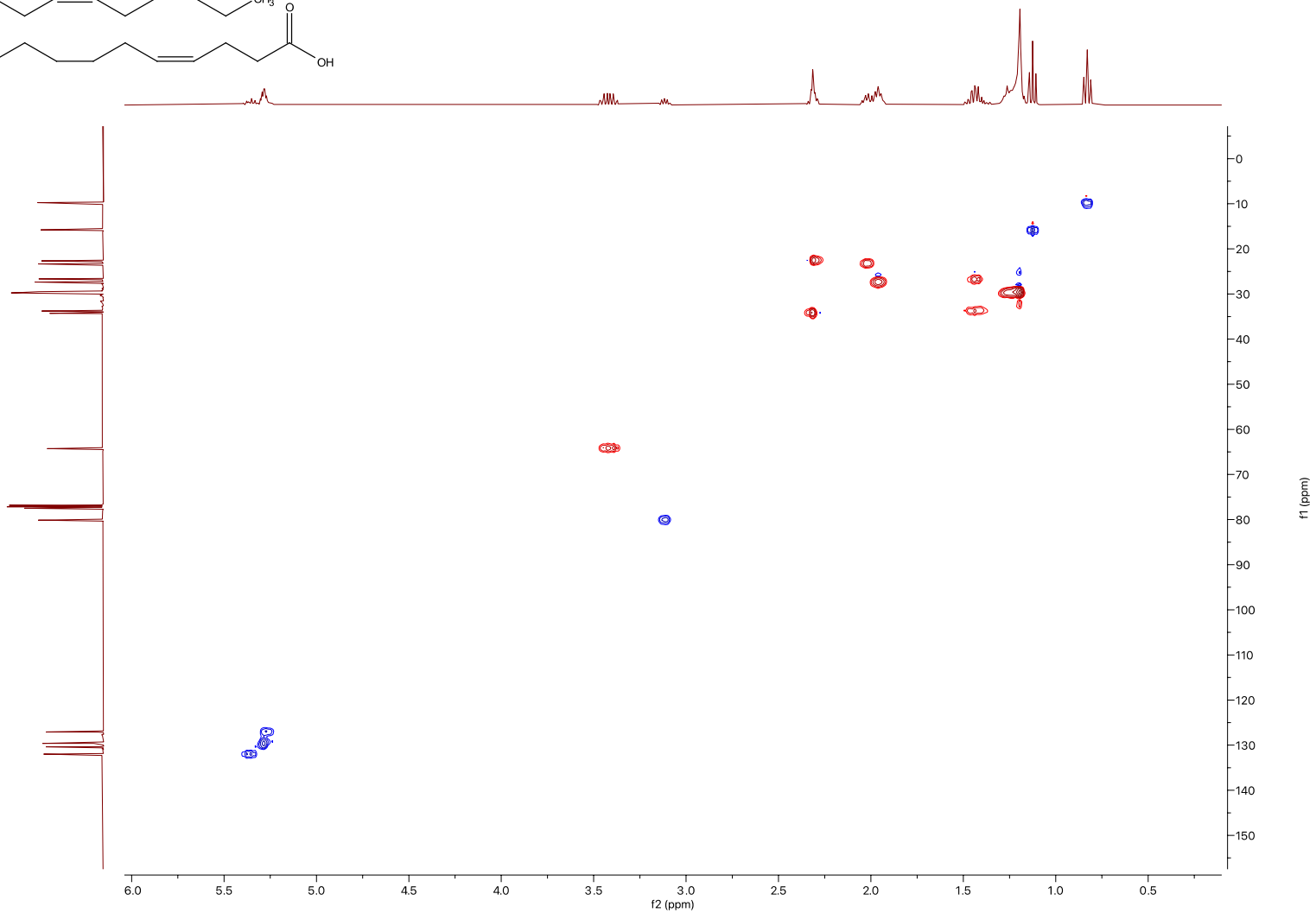
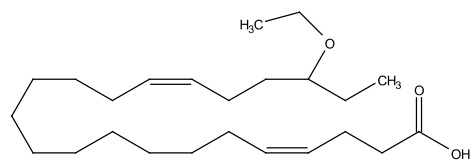


Figure 8.50 HSQC compound 7.

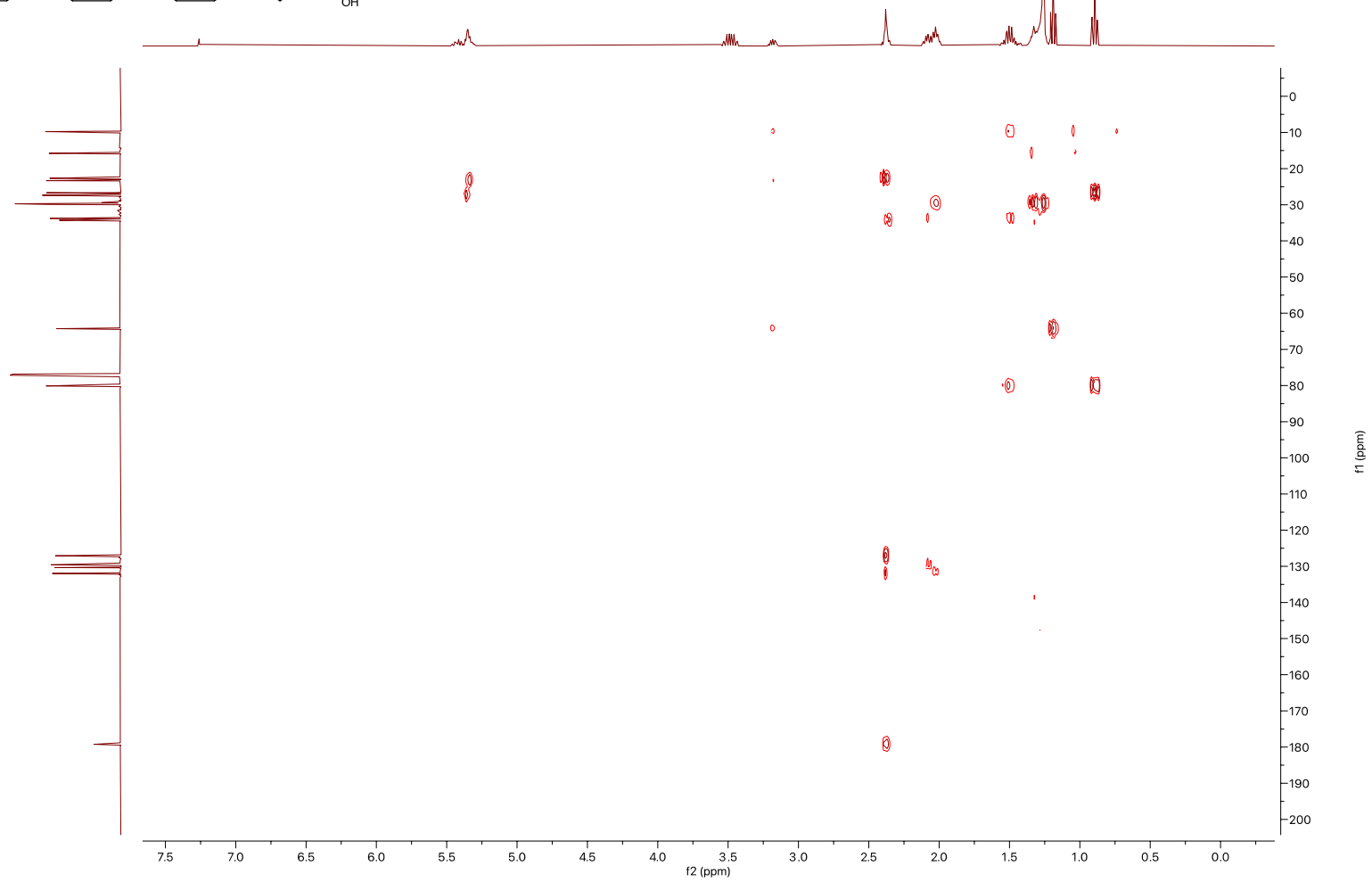
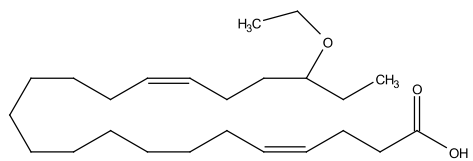


Figure 8.51 HMBC compound 7.

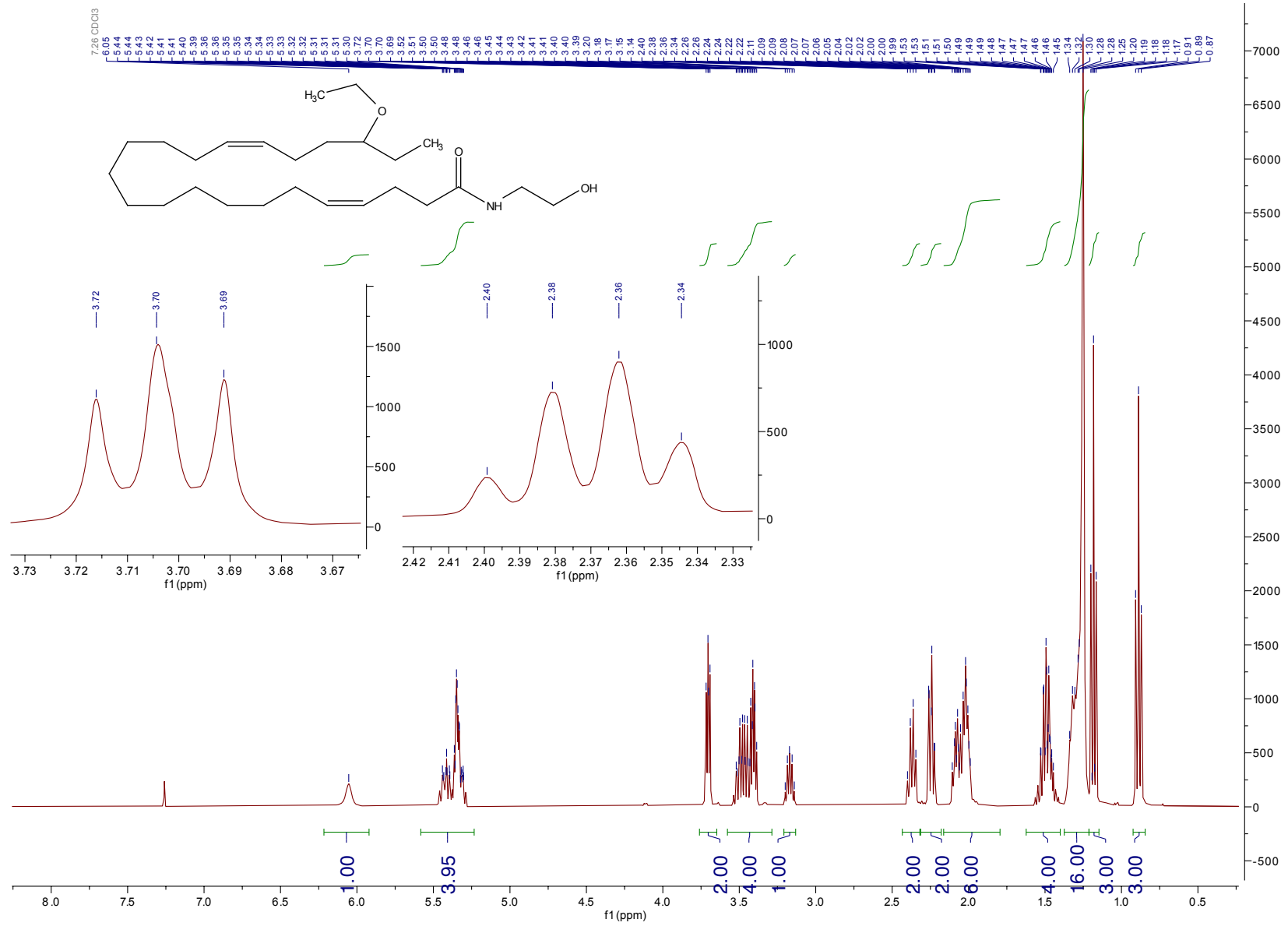


Figure 8.52 ^1H NMR of compound 9.

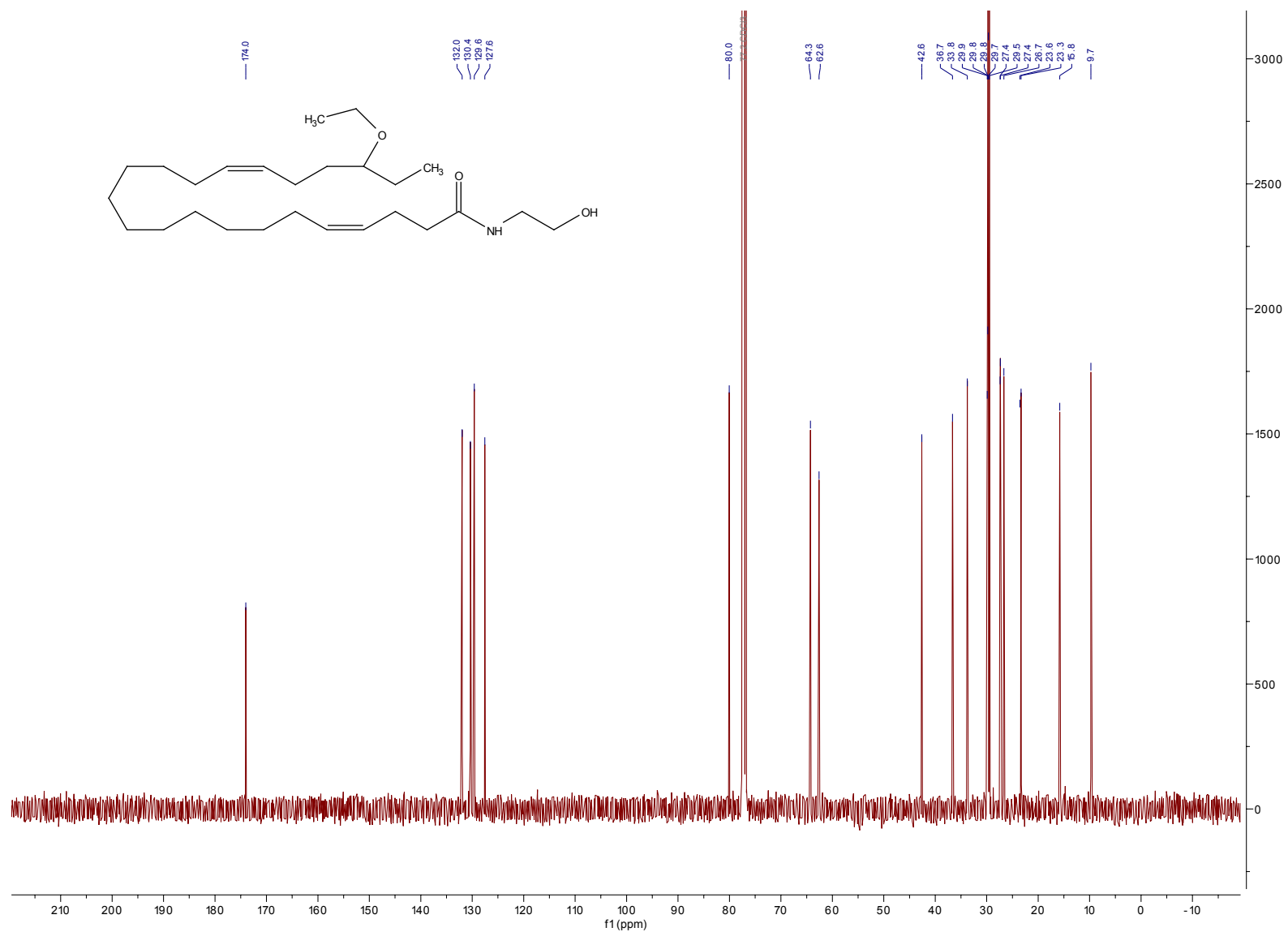


Figure 8.53 HSQC compound 9.

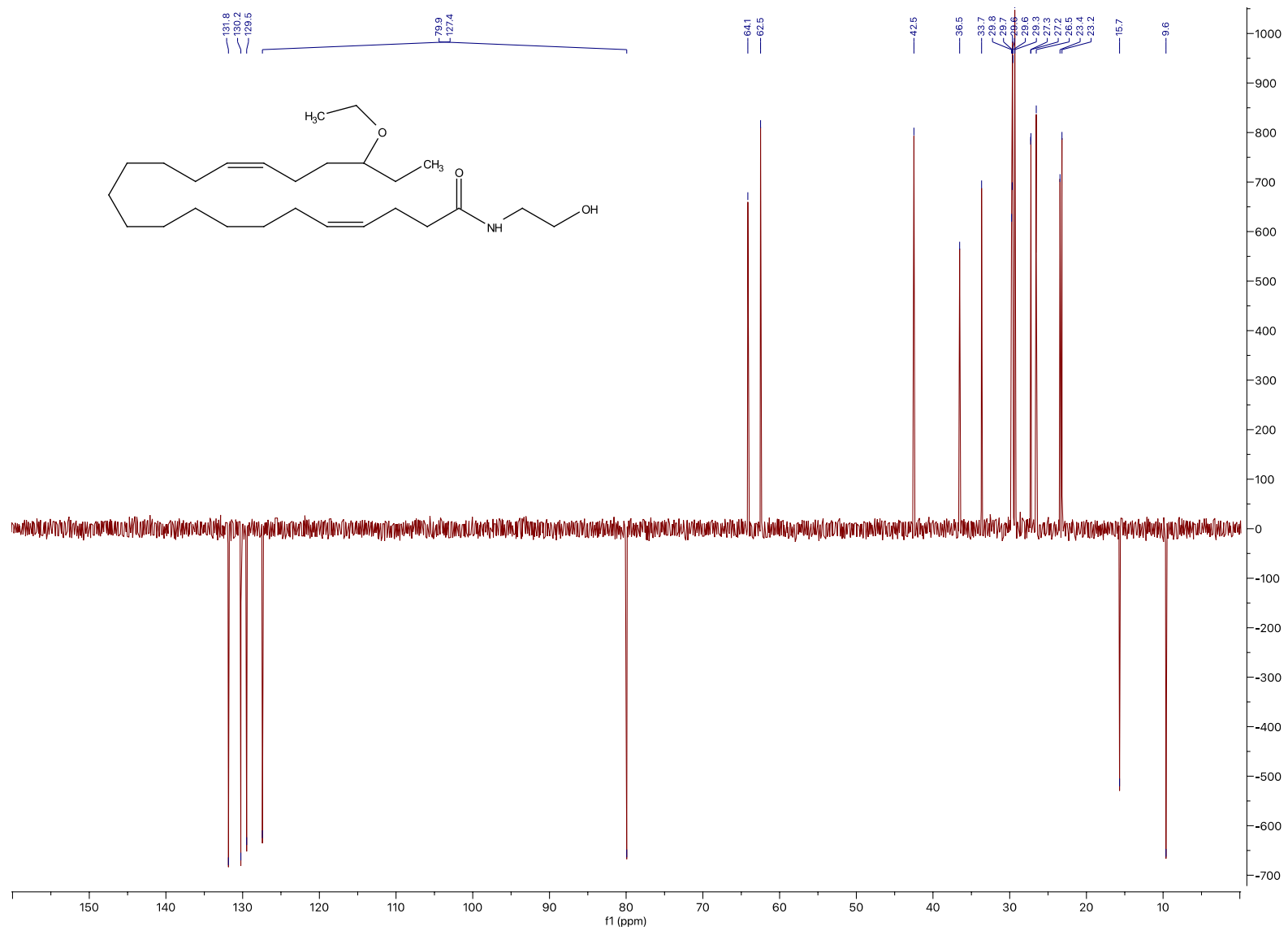


Figure 8.54 DEPT-135 of compound 9.

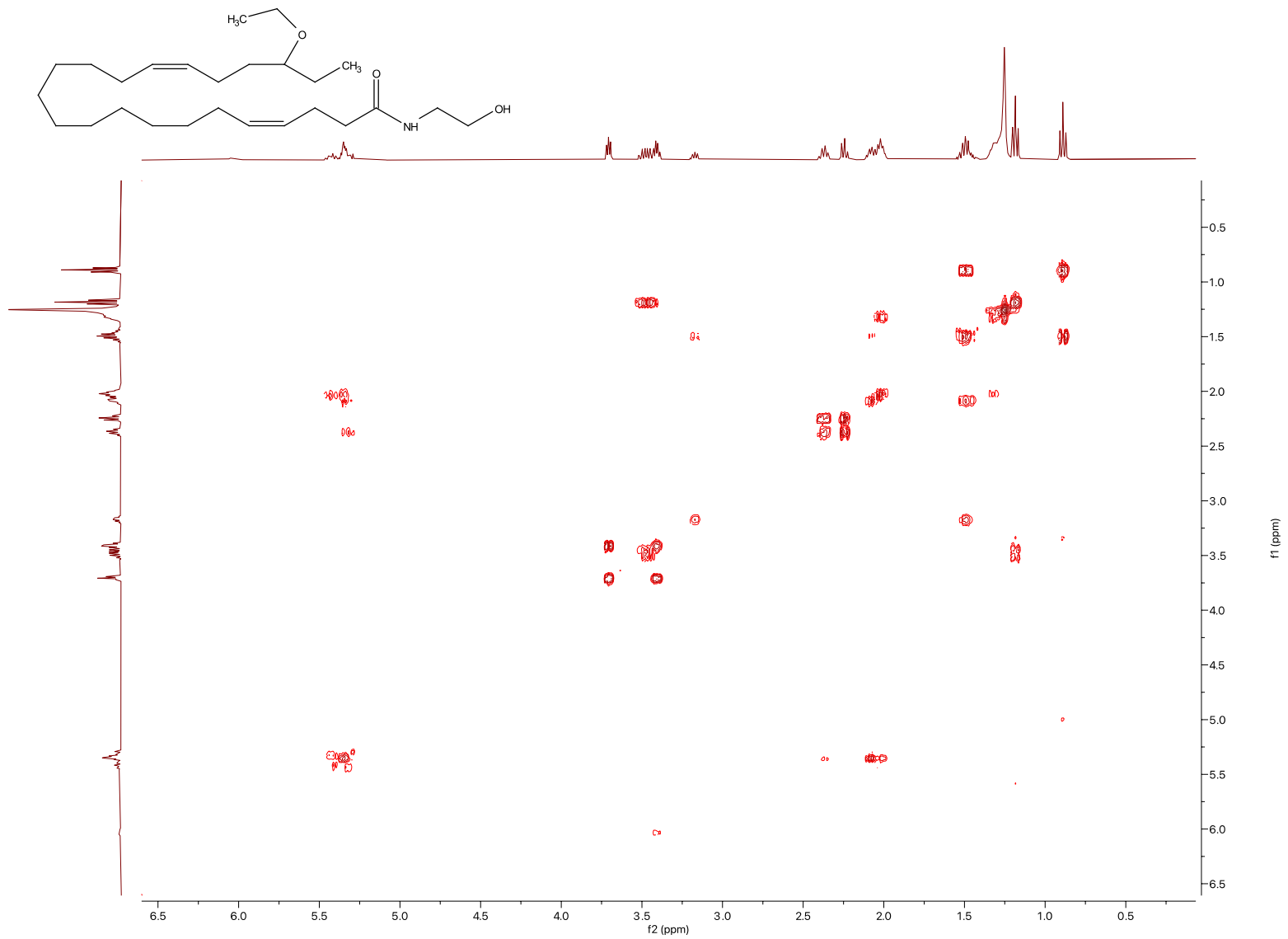


Figure 8.55 COSY of compound 9.

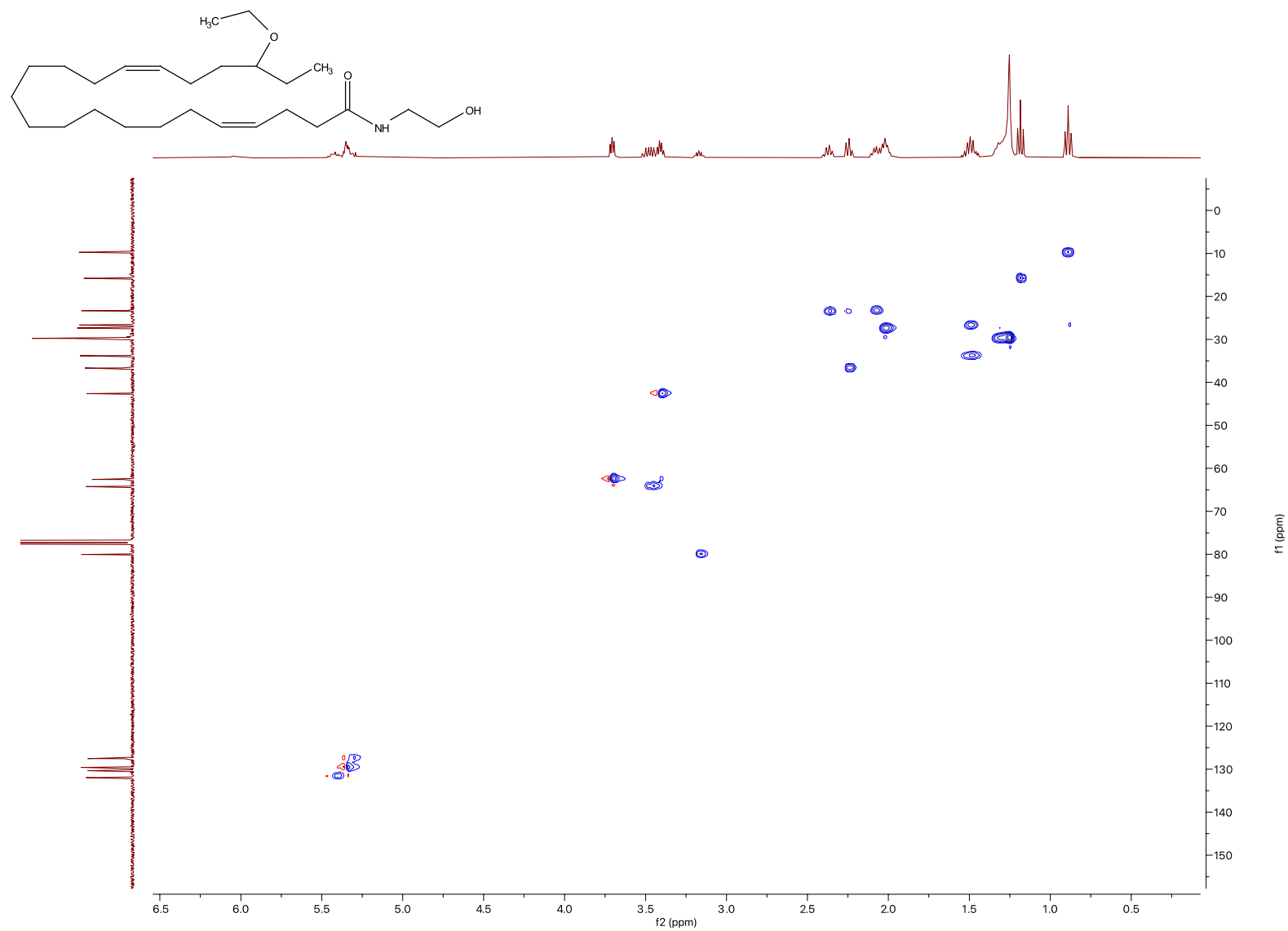


Figure 8.56 HSQC for compound 9.

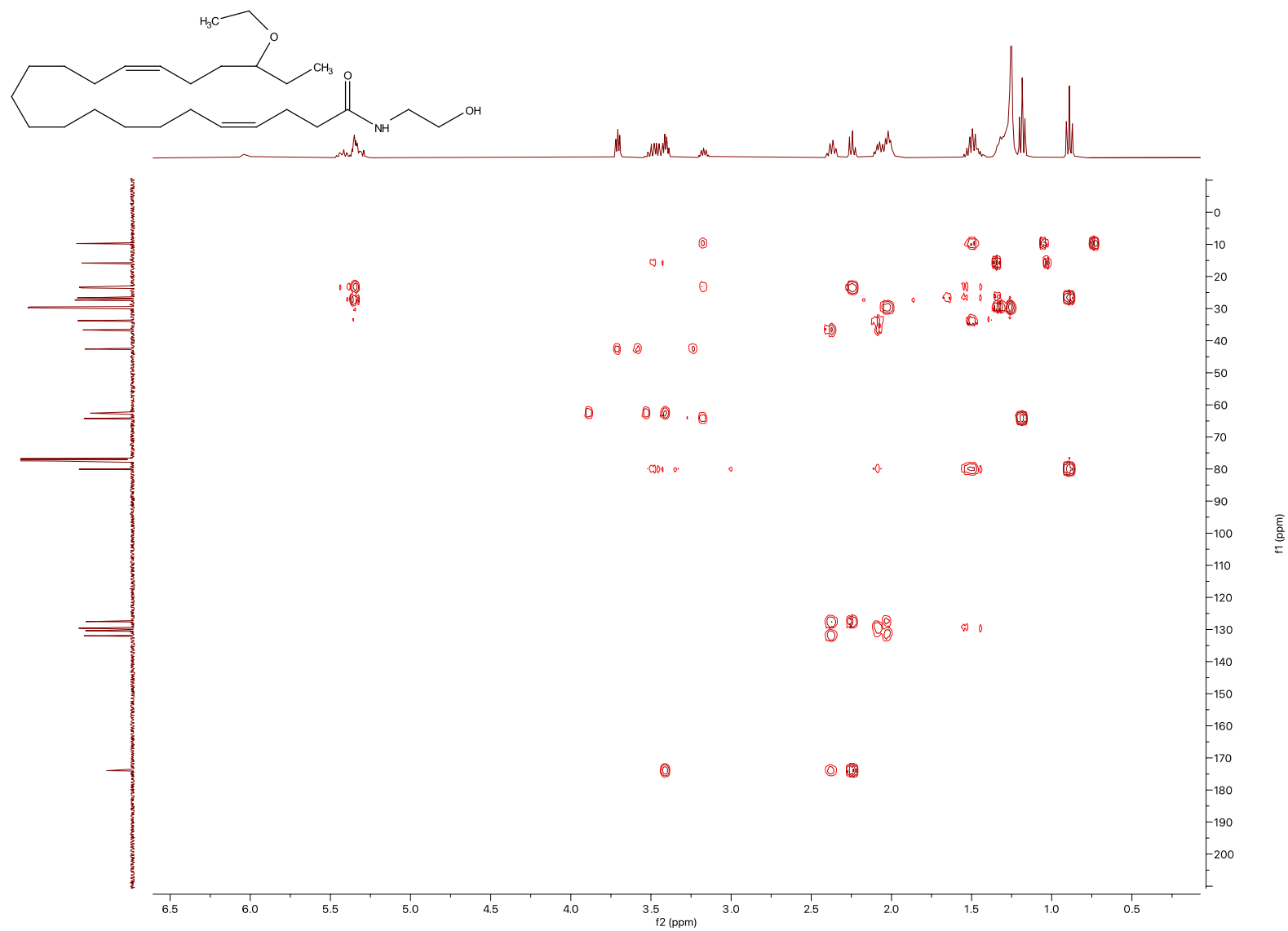


Figure 8.57 HMBC for compound 9.

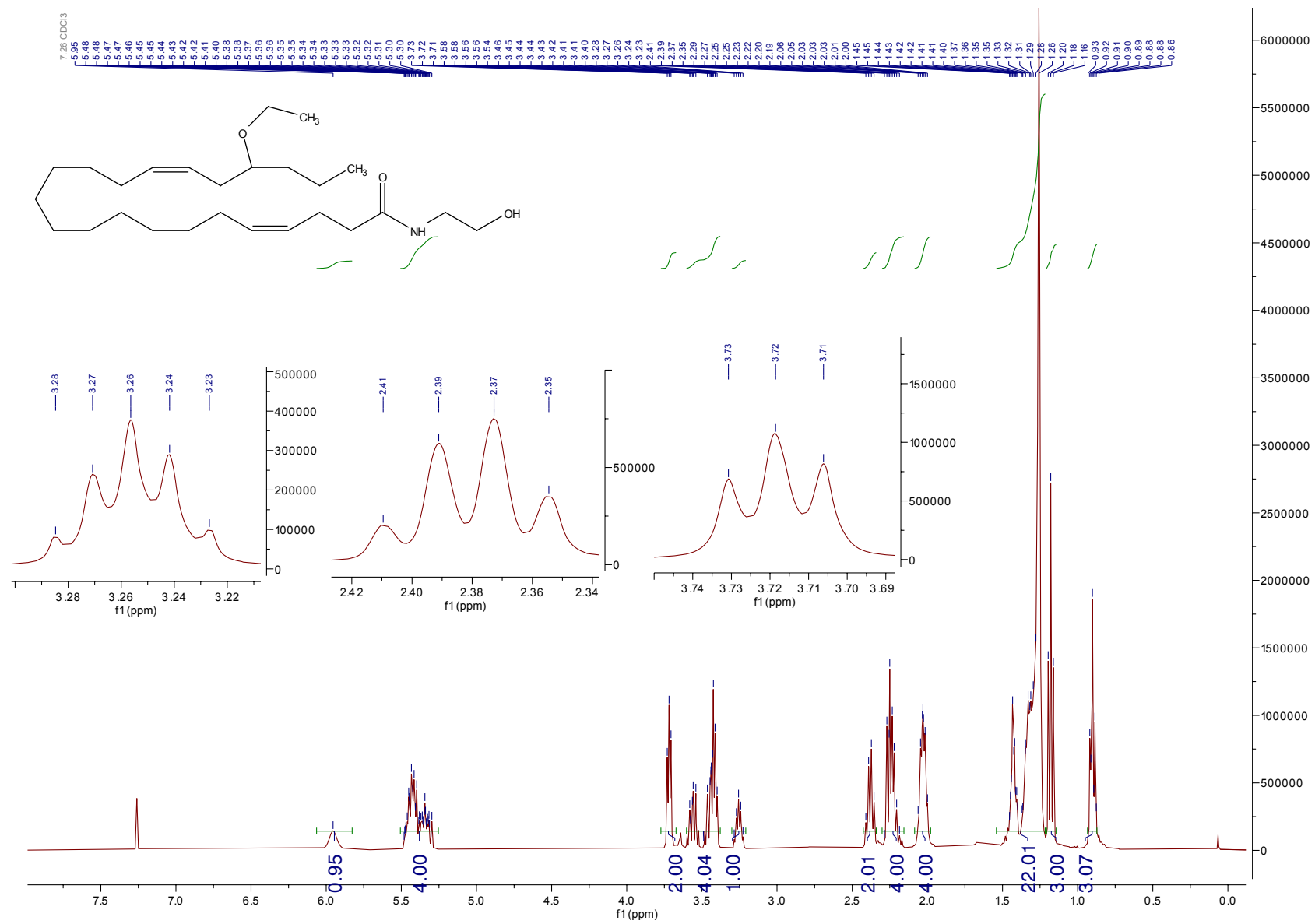


Figure 8.58 ¹H NMR for compound 8.

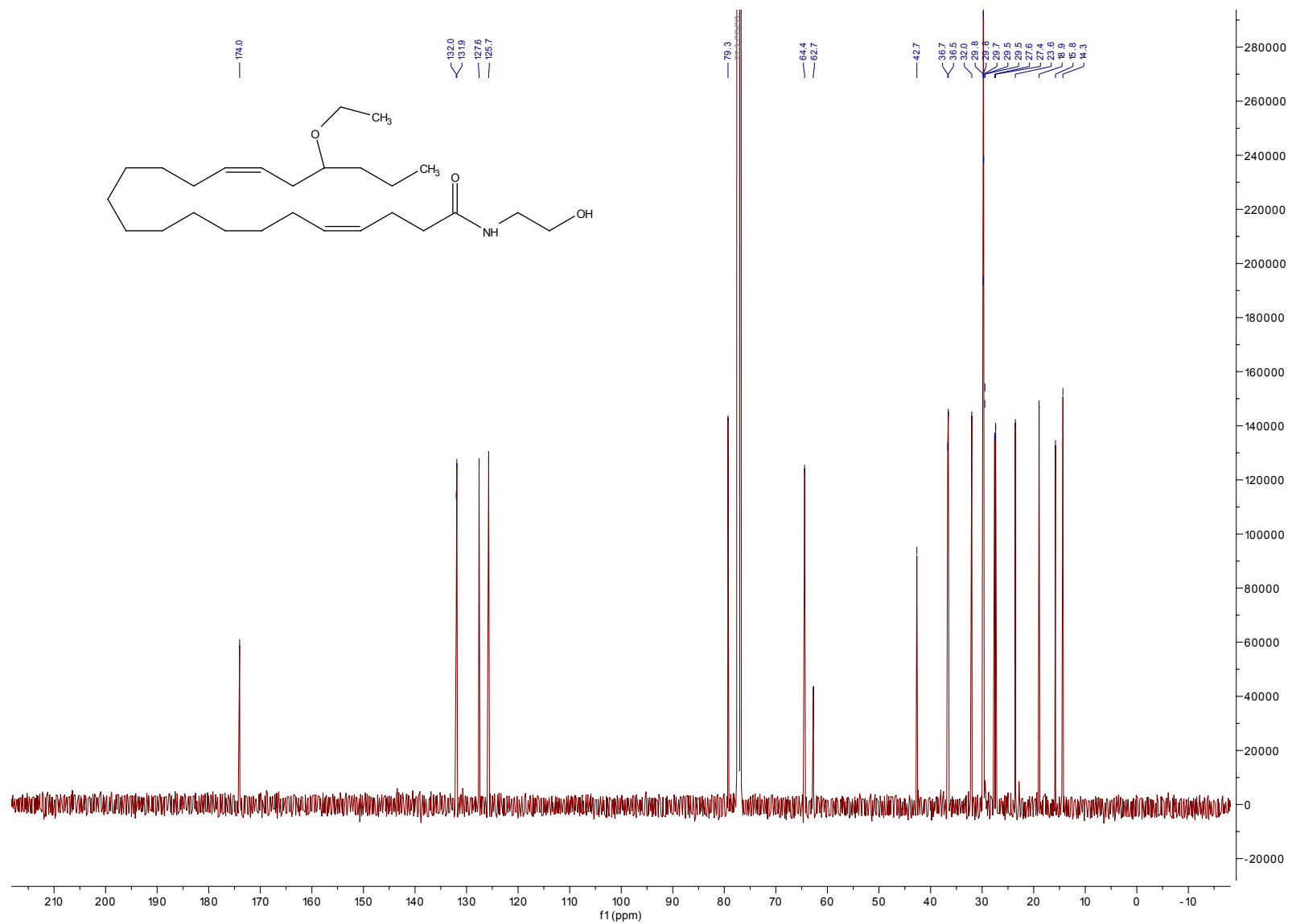


Figure 8.59 ¹³C NMR of compound 8.

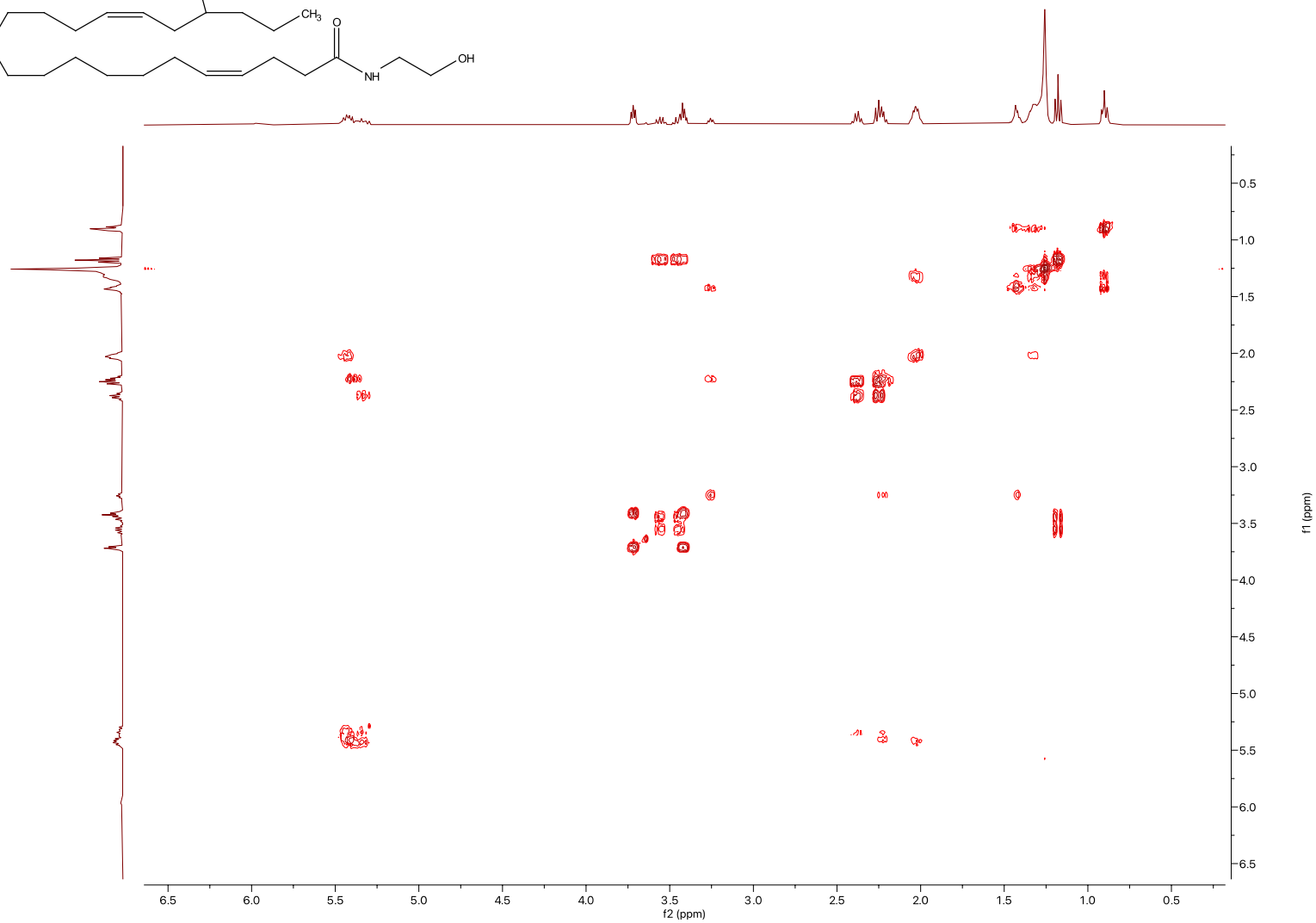
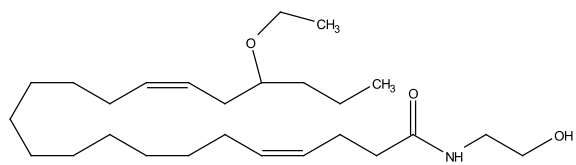


Figure 8.60 COSY of compound 8.

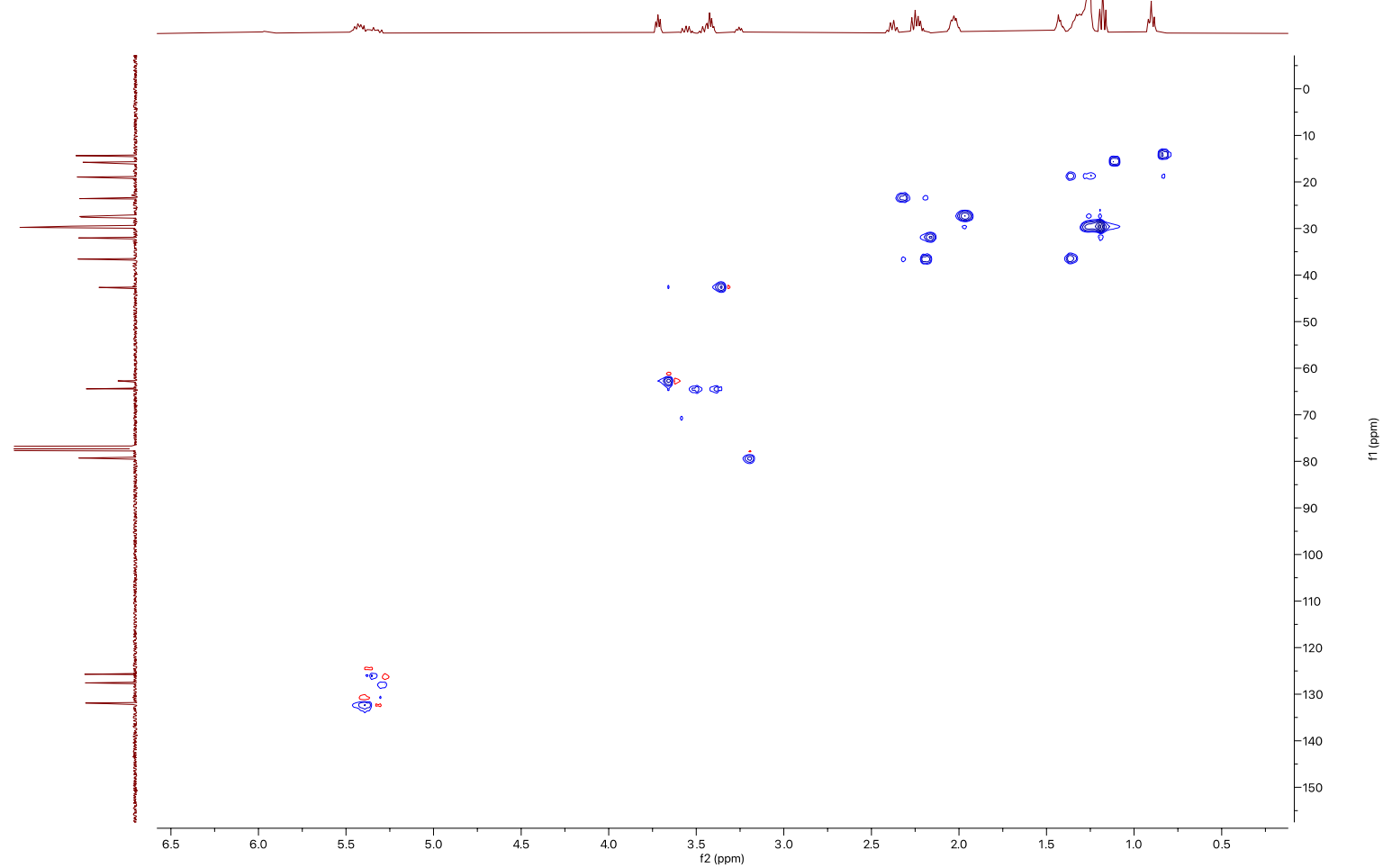
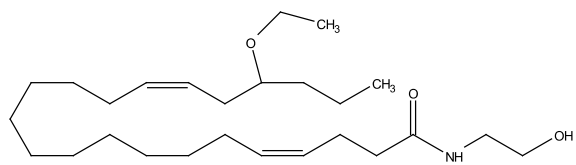
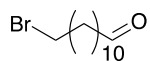


Figure 8.61 HSQC of compound 8.

8.2 HRMS analyses of the synthesized compounds

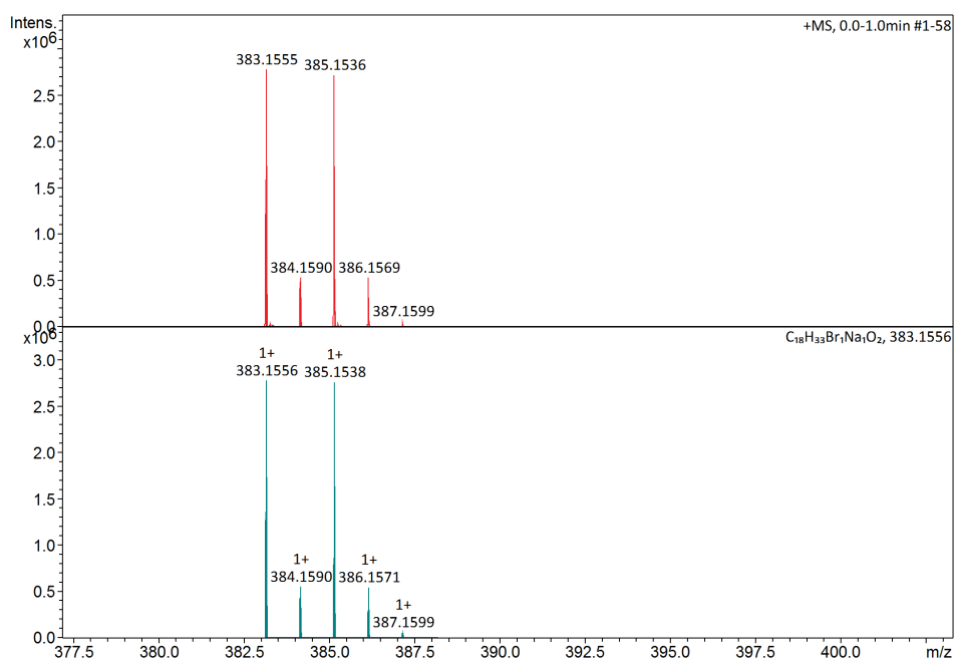


Elemental Analysis Report

Analysis Info	Acquisition Date 05-Oct-22 2:18:24 PM
Sample Name CB009	Analysis Name D:\Data\maxis2022\19098.d
Method ESI_pos_50_1500_os.m	

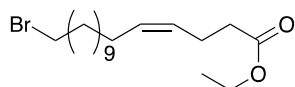
Acquisition Parameter

Source Type	ESI	Set Capillary	3500 V	Set Nebulizer	0.3 Bar
Focus	Not active	Set End Plate Offset	-500 V	Set Dry Heater	200 °C
Scan Begin	50 m/z	Set Charging Voltage	2000 V	Set Dry Gas	4.0 l/min
Scan End	1500 m/z	Set Corona	0 nA	Set Divert Valve	Waste
				Set APCI Heater	0 °C



Meas. m/z	Ion Formula	m/z	err [ppm]
383.1555	C ₁₆ H ₂₈ BrN ₆	383.1553	-0.4
	C ₁₈ H ₃₃ BrNaO ₂	383.1556	0.3

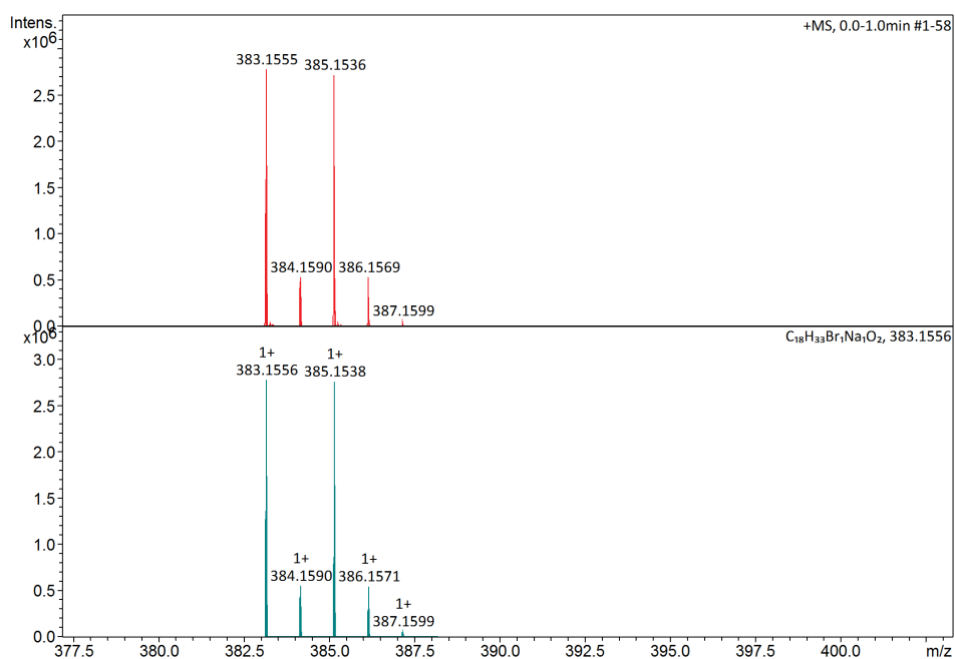
Figure 8.63 HRMS of compound 10



Elemental Analysis Report

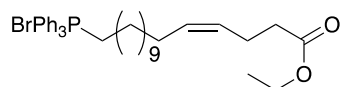
Analysis Info		Acquisition Date	05-Oct-22 2:18:24 PM
Sample Name	CB009	Analysis Name	D:\Data\maxis2022\19098.d
Method	ESI_pos_50_1500_os.m		

Acquisition Parameter					
Source Type	ESI	Set Capillary	3500 V	Set Nebulizer	0.3 Bar
Focus	Not active	Set End Plate Offset	-500 V	Set Dry Heater	200 °C
Scan Begin	50 m/z	Set Charging Voltage	2000 V	Set Dry Gas	4.0 l/min
Scan End	1500 m/z	Set Corona	0 nA	Set Divert Valve	Waste
				Set APCI Heater	0 °C



Meas. m/z	Ion Formula	m/z	err [ppm]
383.1555	C ₁₆ H ₂₈ BrN ₆	383.1553	-0.4
	C ₁₈ H ₃₃ BrNaO ₂	383.1556	0.3

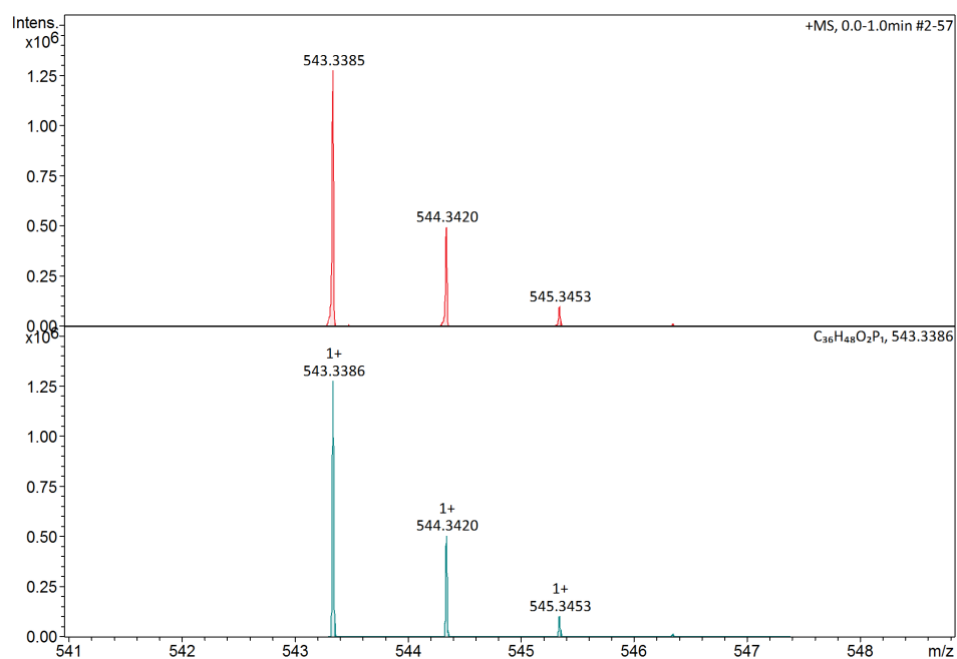
Figure 8.64 HRMS of compound 12.



Elemental Analysis Report

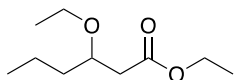
Analysis Info		Acquisition Date	18-Oct-22 1:07:48 PM
Sample Name	CB012	Analysis Name	D:\Data\maxis2022\19108.d
Method	ESI_pos_50_1500_os.m		

Acquisition Parameter					
Source Type	ESI	Set Capillary	3500 V	Set Nebulizer	0.5 Bar
Focus	Not active	Set End Plate Offset	-500 V	Set Dry Heater	200 °C
Scan Begin	50 m/z	Set Charging Voltage	2000 V	Set Dry Gas	4.0 l/min
Scan End	1500 m/z	Set Corona	0 nA	Set Divert Valve	Waste
				Set APCI Heater	0 °C



Meas. m/z	Ion Formula	m/z	err [ppm]
543.3385	C ₃₆ H ₄₈ O ₂ P	543.3386	0.2

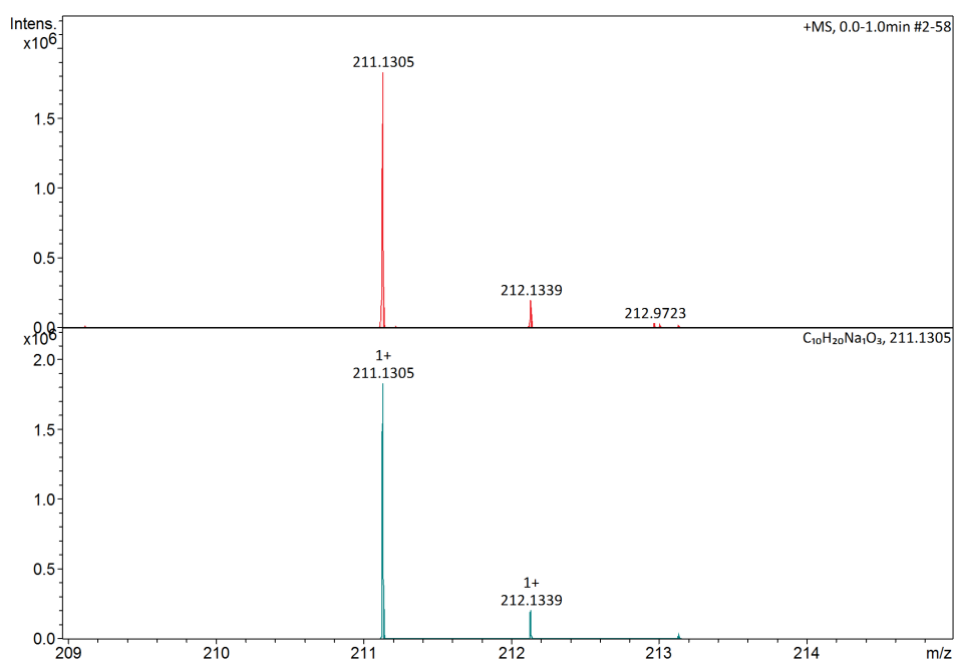
Figure 8. 65 HRMS of compound 2.



Elemental Analysis Report

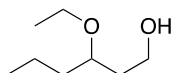
Analysis Info	Acquisition Date 18-Oct-22 1:24:10 PM
Sample Name CB016	Analysis Name D:\Data\maxis2022\19109.d
Method ESI_pos_50_1500_os.m	

Acquisition Parameter					
Source Type	ESI	Set Capillary	3500 V	Set Nebulizer	0.8 Bar
Focus	Not active	Set End Plate Offset	-500 V	Set Dry Heater	200 °C
Scan Begin	50 m/z	Set Charging Voltage	2000 V	Set Dry Gas	4.0 l/min
Scan End	1500 m/z	Set Corona	0 nA	Set Divert Valve	Waste
				Set APCI Heater	0 °C



Meas. m/z	Ion Formula	m/z	err [ppm]
211.1305	C ₁₀ H ₂₀ NaO ₃	211.1305	0.1

Figure 8.66 HRMS of compound 2

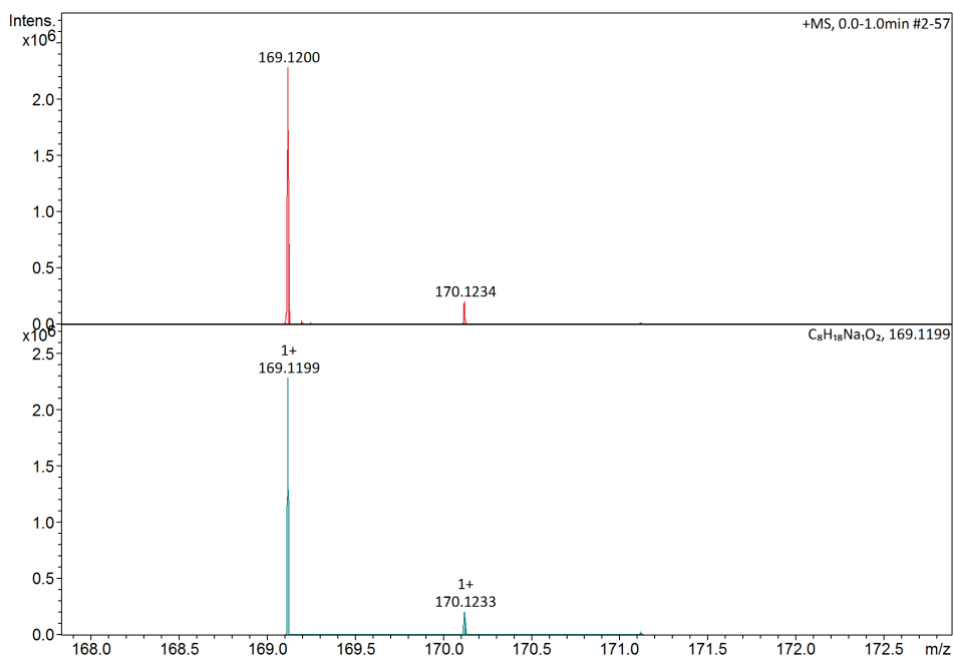


Elemental Analysis Report

Analysis Info		Acquisition Date	09-Nov-22 2:29:28 PM
Sample Name	CB022	Analysis Name	D:\Data\maxis2022\19143.d
Method	ESI_pos_50_1500_os.m		

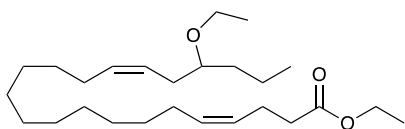
Acquisition Parameter

Source Type	ESI	Set Capillary	3500 V	Set Nebulizer	2.0 Bar
Focus	Not active	Set End Plate Offset	-500 V	Set Dry Heater	200 °C
Scan Begin	50 m/z	Set Charging Voltage	2000 V	Set Dry Gas	4.0 l/min
Scan End	1500 m/z	Set Corona	0 nA	Set Divert Valve	Waste
				Set APCI Heater	0 °C



Meas. m/z	Ion Formula	m/z	err [ppm]
169.1200	C6H13N6	169.1196	-2.4
	C8H18NaO2	169.1199	-0.7

Figure 8.67 HRMS of compound 15.



Elemental Analysis Report

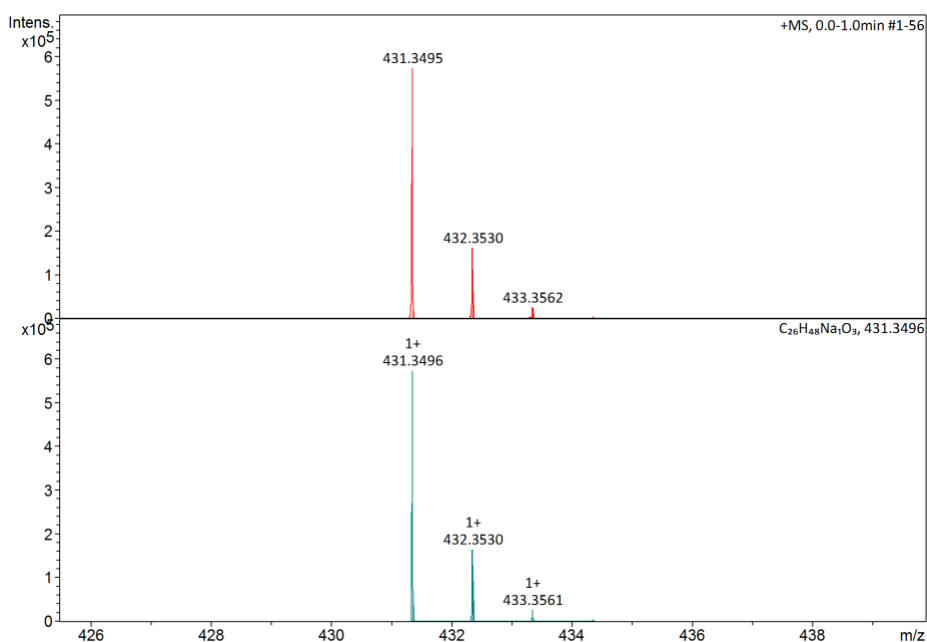
Analysis Info

Sample Name CB024
 Method ESI_pos_50_1500_os.m

Acquisition Date 21-Nov-22 1:20:56 PM
 Analysis Name D:\Data\maxis2022\19151.d

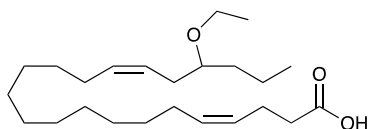
Acquisition Parameter

Source Type	ESI	Set Capillary	3500 V	Set Nebulizer	2.0 Bar
Focus	Not active	Set End Plate Offset	-500 V	Set Dry Heater	200 °C
Scan Begin	50 m/z	Set Charging Voltage	2000 V	Set Dry Gas	4.0 l/min
Scan End	1500 m/z	Set Corona	0 nA	Set Divert Valve	Waste
				Set APCI Heater	0 °C



Meas. m/z	Ion Formula	m/z	err [ppm]
431.3495	C ₂₄ H ₄₃ N ₆ O	431.3493	-0.5
	C ₂₆ H ₄₈ NaO ₃	431.3496	0.2

Figure 8.68 HRMS of compound 4.



Elemental Analysis Report

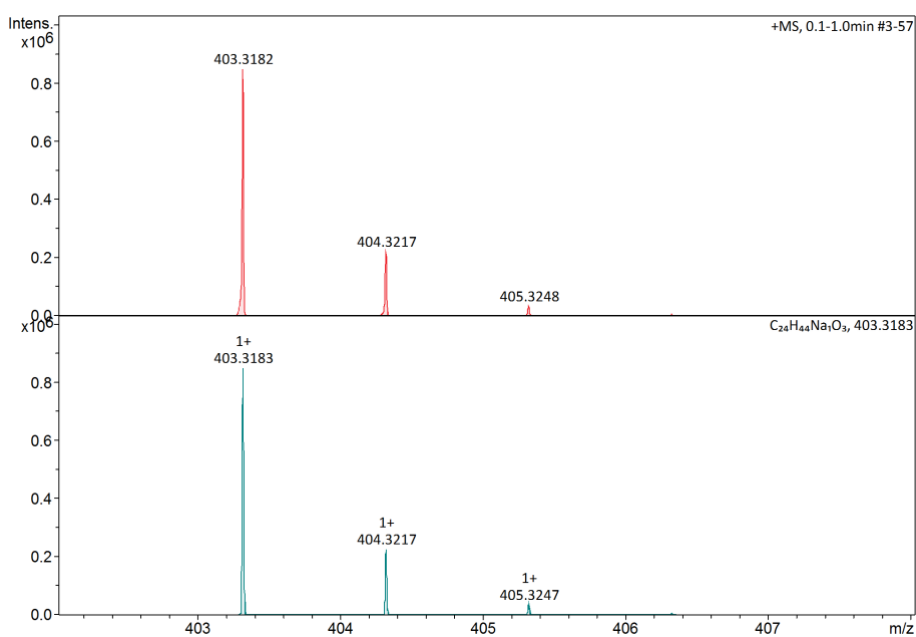
Analysis Info

Sample Name CBO025
Method ESI_pos_50_1500_os.m

Acquisition Date 28-Nov-22 3:38:41 PM
Analysis Name D:\Data\maxis2022\19159.d

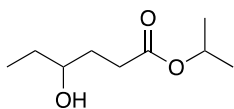
Acquisition Parameter

Source Type	ESI	Set Capillary	3500 V	Set Nebulizer	2.0 Bar
Focus	Not active	Set End Plate Offset	-500 V	Set Dry Heater	200 °C
Scan Begin	50 m/z	Set Charging Voltage	2000 V	Set Dry Gas	4.0 l/min
Scan End	1500 m/z	Set Corona	0 nA	Set Divert Valve	Waste
				Set APCI Heater	0 °C



Meas. m/z	Ion Formula	m/z	err [ppm]
251.1253	C10H15N6O2	251.1251	-1.0
	C12H20NaO4	251.1254	0.1
321.1672	C14H21N6O3	321.1670	-0.7
	C16H26NaO5	321.1672	0.1
403.3182	C22H39N6O	403.3180	-0.5
	C24H44NaO3	403.3183	0.2
425.3001	C21H39N5O4	425.2997	-1.1
	C22H38N6NaO	425.2999	-0.5

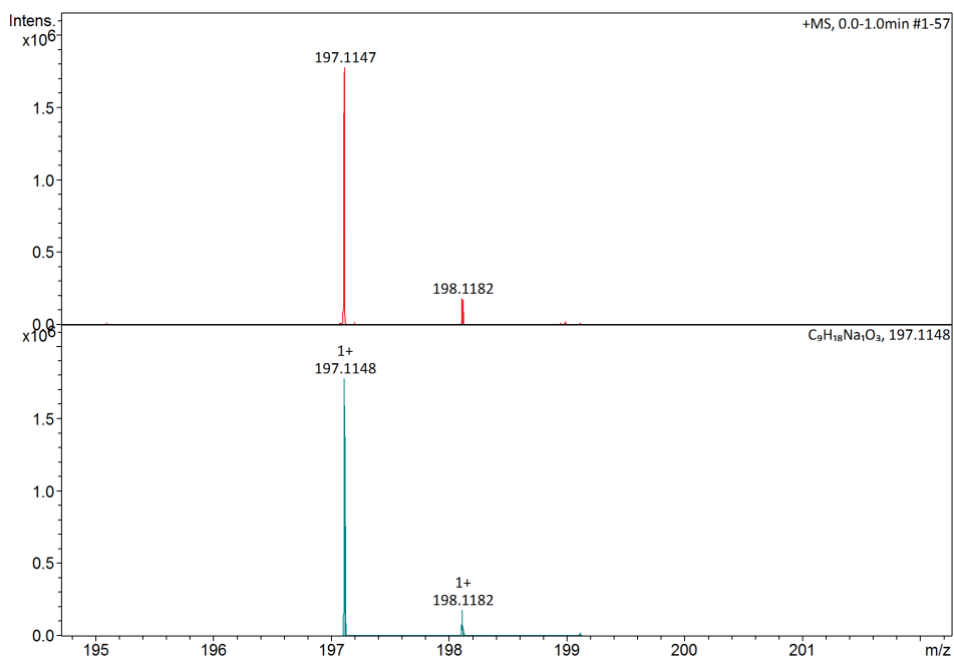
Figure 8.69 HRMS of compound 6.



Elemental Analysis Report

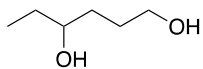
Analysis Info		Acquisition Date	18-Jan-23 10:59:05 AM
Sample Name	CB028	Analysis Name	D:\Data\maxis2023\19221.d
Method	ESI_pos_50_1500_os.m		

Acquisition Parameter					
Source Type	ESI	Set Capillary	3500 V	Set Nebulizer	0.5 Bar
Focus	Not active	Set End Plate Offset	-500 V	Set Dry Heater	200 °C
Scan Begin	50 m/z	Set Charging Voltage	2000 V	Set Dry Gas	4.0 l/min
Scan End	1500 m/z	Set Corona	0 nA	Set Divert Valve	Waste
				Set APCI Heater	0 °C



Meas. m/z	Ion Formula	m/z	err [ppm]
197.1147	C ₇ H ₁₃ N ₆ O	197.1145	-0.8
	C ₉ H ₁₈ NaO ₃	197.1148	0.6

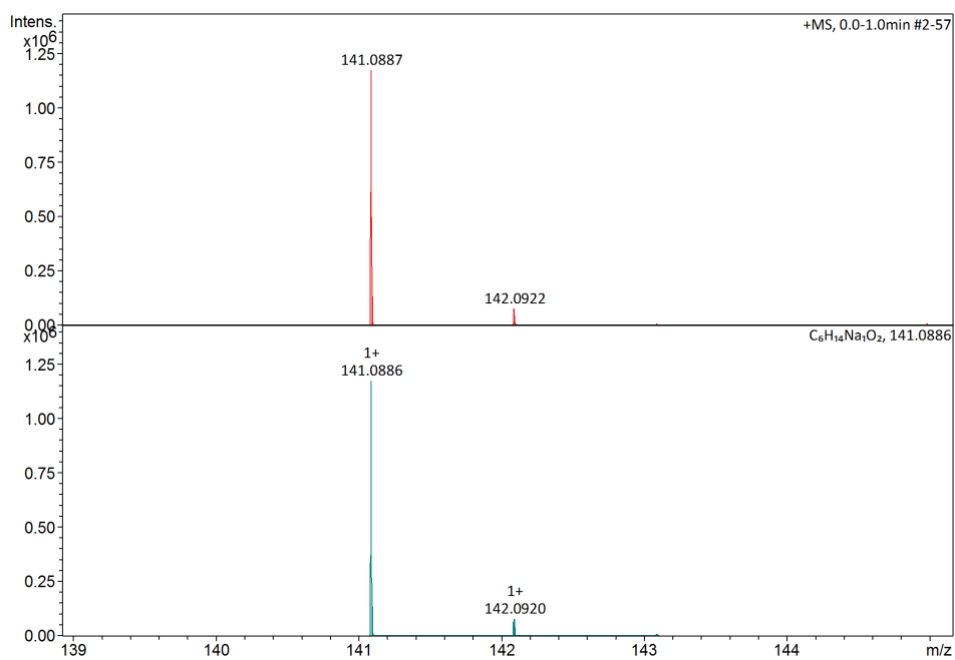
Figure 8.70 HRMS of compound 17.



Elemental Analysis Report

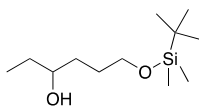
Analysis Info		Acquisition Date	25-Jan-23 1:38:24 PM
Sample Name	CB030	Analysis Name	D:\Data\maxis2023\19243.d
Method	ESI_pos_50_1500_os.m		

Acquisition Parameter					
Source Type	ESI	Set Capillary	3500 V	Set Nebulizer	0.5 Bar
Focus	Not active	Set End Plate Offset	-500 V	Set Dry Heater	200 °C
Scan Begin	50 m/z	Set Charging Voltage	2000 V	Set Dry Gas	4.0 l/min
Scan End	1500 m/z	Set Corona	0 nA	Set Divert Valve	Waste
				Set APCI Heater	0 °C



Meas. m/z	Ion Formula	m/z	err [ppm]
141.0887	C6H14NaO2	141.0886	-0.8

Figure 8.71 HRMS of compound 19.

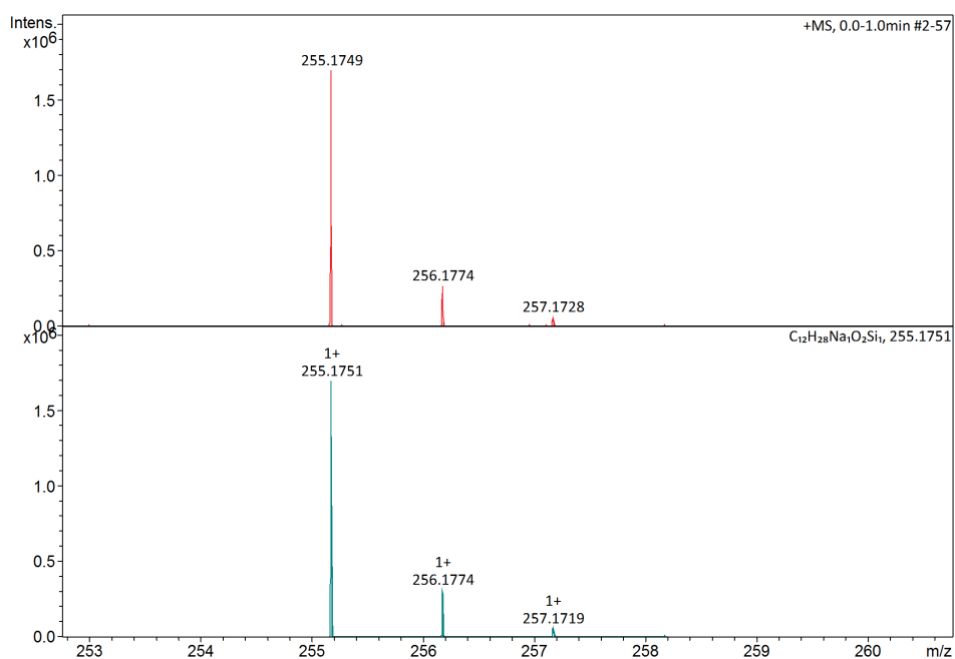


Elemental Analysis Report

Analysis Info		Acquisition Date	27-Jan-23 10:07:51 AM
Sample Name	CB031	Analysis Name	D:\Data\maxis2023\19248.d
Method	ESI_pos_50_1500_os.m		

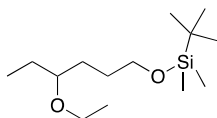
Acquisition Parameter

Source Type	ESI	Set Capillary	3500 V	Set Nebulizer	0.5 Bar
Focus	Not active	Set End Plate Offset	-500 V	Set Dry Heater	200 °C
Scan Begin	50 m/z	Set Charging Voltage	2000 V	Set Dry Gas	4.0 l/min
Scan End	1500 m/z	Set Corona	0 nA	Set Divert Valve	Waste
				Set APCI Heater	0 °C



Meas. m/z	Ion Formula	m/z	err [ppm]
255.1749	C ₁₀ H ₂₃ N ₆ Si	255.1748	-0.5
	C ₁₂ H ₂₈ NaO ₂ Si	255.1751	0.5

Figure 8.72 HRMS of compound 20.



Elemental Analysis Report

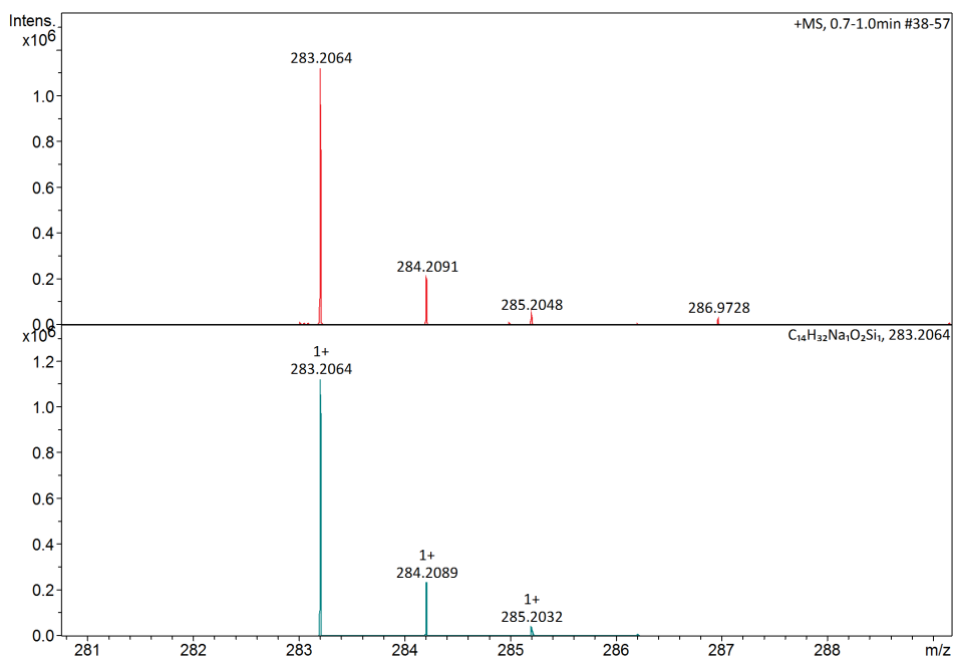
Analysis Info

Sample Name CB033
 Method ESI_pos_50_1500_os.m

Acquisition Date 09-Feb-23 4:23:27 PM
 Analysis Name D:\Data\maxis2023\19290.d

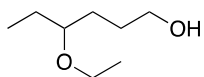
Acquisition Parameter

Source Type	ESI	Set Capillary	3500 V	Set Nebulizer	0.5 Bar
Focus	Not active	Set End Plate Offset	-500 V	Set Dry Heater	200 °C
Scan Begin	50 m/z	Set Charging Voltage	2000 V	Set Dry Gas	4.0 l/min
Scan End	1500 m/z	Set Corona	0 nA	Set Divert Valve	Waste
				Set APCI Heater	0 °C



Meas. m/z	Ion Formula	m/z	err [ppm]
283.2064	C ₁₄ H ₃₂ NaO ₂ Si	283.2064	-0.2

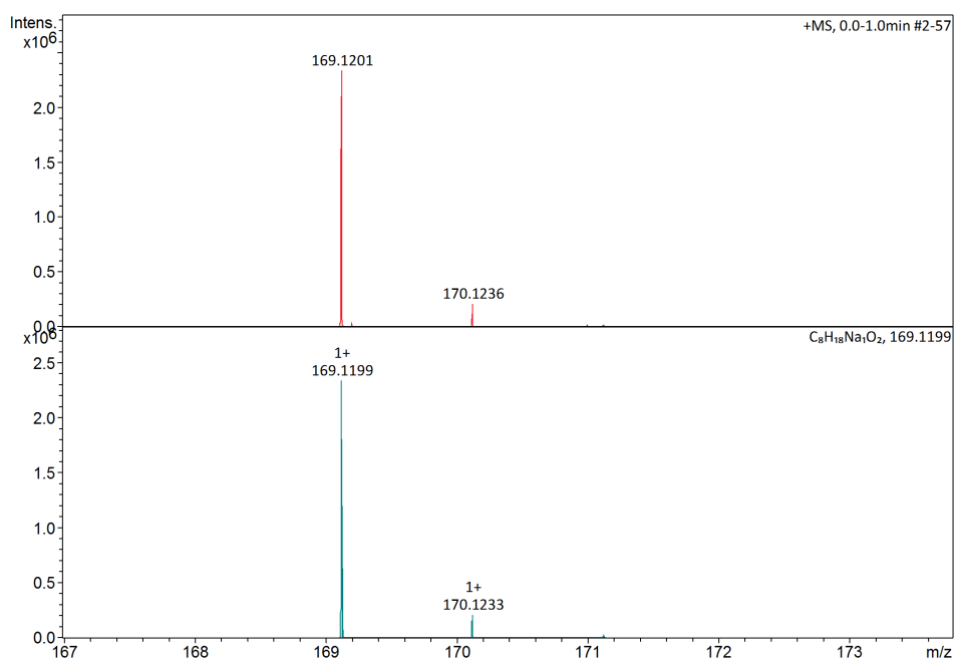
Figure 8.73 HRMS of compound **21a**.



Elemental Analysis Report

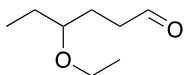
Analysis Info		Acquisition Date	01-Mar-23 4:04:20 PM
Sample Name	CB034	Analysis Name	D:\Data\maxis2023\19344.d
Method	ESI_pos_50_1500_os.m		

Acquisition Parameter					
Source Type	ESI	Set Capillary	3500 V	Set Nebulizer	0.5 Bar
Focus	Not active	Set End Plate Offset	-500 V	Set Dry Heater	200 °C
Scan Begin	50 m/z	Set Charging Voltage	2000 V	Set Dry Gas	4.0 l/min
Scan End	1500 m/z	Set Corona	0 nA	Set Divert Valve	Waste
				Set APCI Heater	0 °C



Meas. m/z	Ion Formula	m/z	err [ppm]
169.1201	C8H18NaO2	169.1199	-1.3

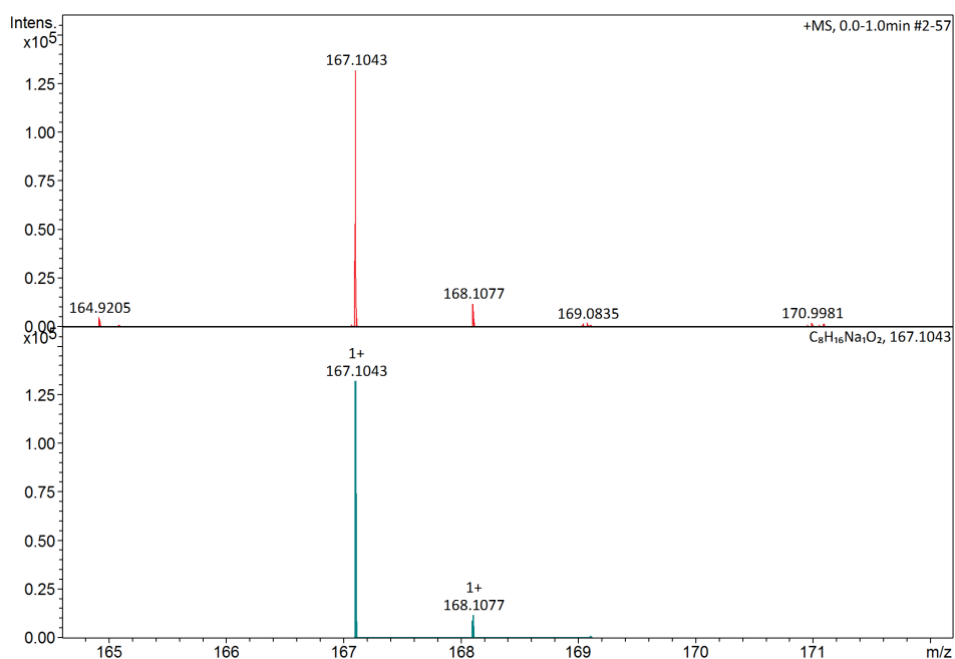
Figure 8.74 Compound **21b**.



Elemental Analysis Report

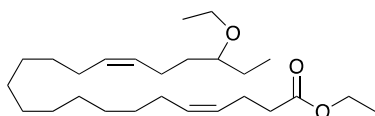
Analysis Info		Acquisition Date	22-Feb-23 3:19:58 PM
Sample Name	CB041	Analysis Name	D:\Data\maxis2023\19327.d
Method	ESI_pos_50_1500_os.m		

Acquisition Parameter					
Source Type	ESI	Set Capillary	3500 V	Set Nebulizer	0.5 Bar
Focus	Not active	Set End Plate Offset	-500 V	Set Dry Heater	200 °C
Scan Begin	50 m/z	Set Charging Voltage	2000 V	Set Dry Gas	4.0 l/min
Scan End	1500 m/z	Set Corona	0 nA	Set Divert Valve	Waste
				Set APCI Heater	0 °C



Meas. m/z	Ion Formula	m/z	err [ppm]
167.1043	C ₈ H ₁₆ NaO ₂	167.1043	-0.1

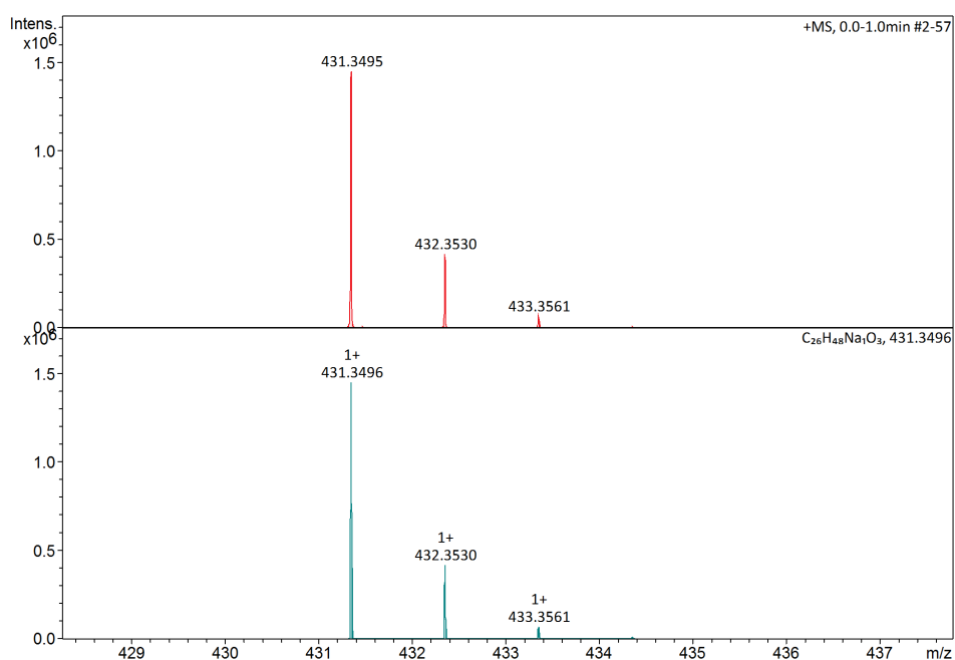
Figure 8.75 HRMS of compound 2.



Elemental Analysis Report

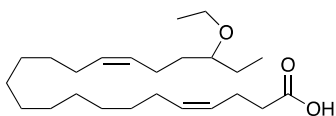
Analysis Info	Acquisition Date 28-Feb-23 2:15:13 PM
Sample Name CB042	Analysis Name D:\Data\maxis2023\19337.d
Method ESI_pos_50_1500_os.m	

Acquisition Parameter					
Source Type	ESI	Set Capillary	3500 V	Set Nebulizer	0.5 Bar
Focus	Not active	Set End Plate Offset	-500 V	Set Dry Heater	200 °C
Scan Begin	50 m/z	Set Charging Voltage	2000 V	Set Dry Gas	4.0 l/min
Scan End	1500 m/z	Set Corona	0 nA	Set Divert Valve	Waste
				Set APCI Heater	0 °C



Meas. m/z	Ion Formula	m/z	err [ppm]
431.3495	C24H43N6O	431.3493	-0.5
	C26H48NaO3	431.3496	0.2

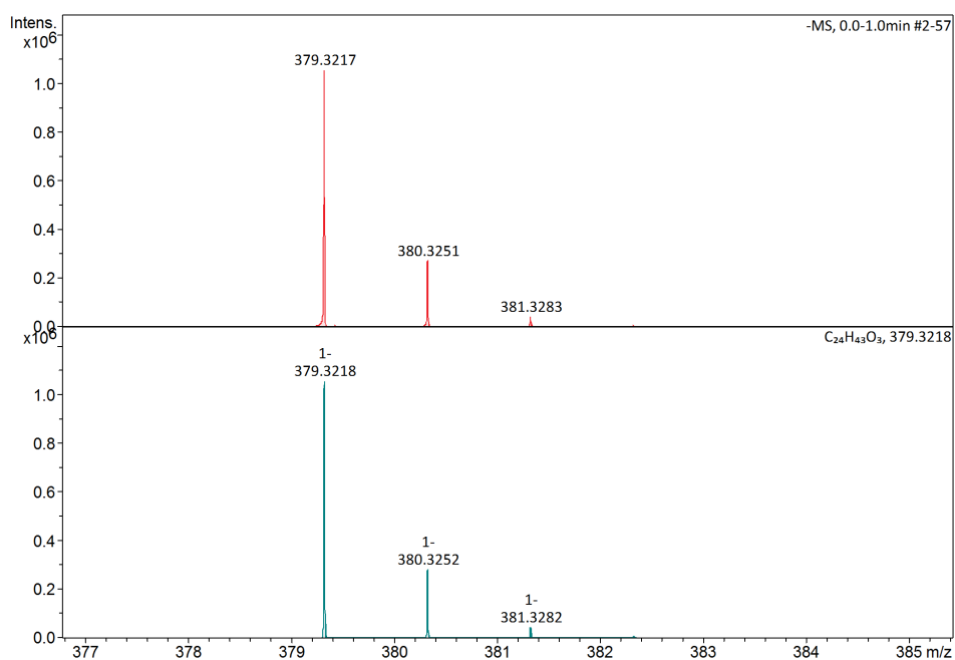
Figure 8.76 HRMS of compound 6.



Elemental Analysis Report

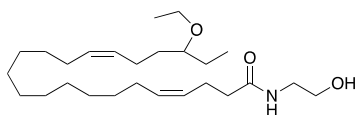
Analysis Info		Acquisition Date	03-Mar-23 2:37:18 PM
Sample Name	CB043	Analysis Name	D:\Data\maxis2023\19359.d
Method	ESI_neg_50_1500_os.m		

Acquisition Parameter					
Source Type	ESI	Set Capillary	3500 V	Set Nebulizer	0.5 Bar
Focus	Not active	Set End Plate Offset	-500 V	Set Dry Heater	200 °C
Scan Begin	50 m/z	Set Charging Voltage	0 V	Set Dry Gas	4.0 l/min
Scan End	1500 m/z	Set Corona	0 nA	Set Divert Valve	Source
				Set APCI Heater	0 °C



Meas. m/z	Ion Formula	m/z	err [ppm]
379.3217	C ₂₄ H ₄₃ O ₃	379.3218	0.1

Figure 8.77 HRMS of compound 6.



Elemental Analysis Report

Analysis Info

Sample Name CB049
 Method ESI_pos_50_1500_os.m

Acquisition Date 19-Apr-23 4:10:48 PM
 Analysis Name D:\Data\maxis2023\19489.d

Acquisition Parameter

Source Type	ESI	Set Capillary	3500 V	Set Nebulizer	0.5 Bar
Focus	Not active	Set End Plate Offset	-500 V	Set Dry Heater	200 °C
Scan Begin	50 m/z	Set Charging Voltage	2000 V	Set Dry Gas	4.0 l/min
Scan End	1500 m/z	Set Corona	0 nA	Set Divert Valve	Waste
				Set APCI Heater	0 °C

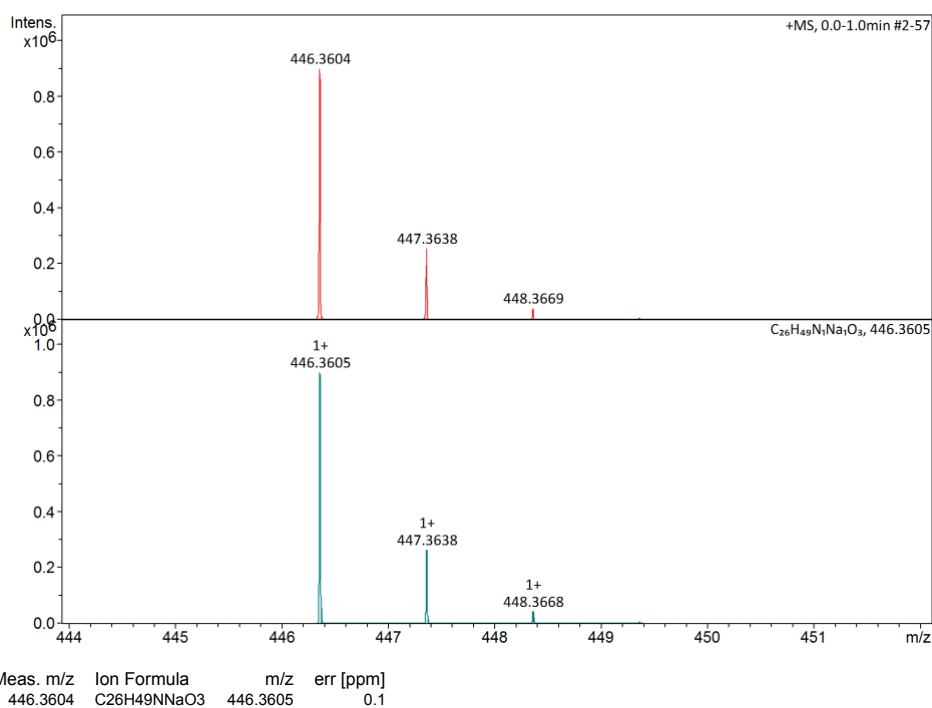
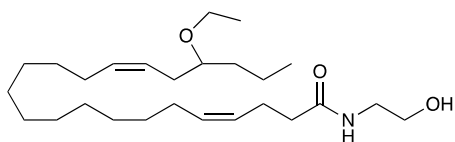
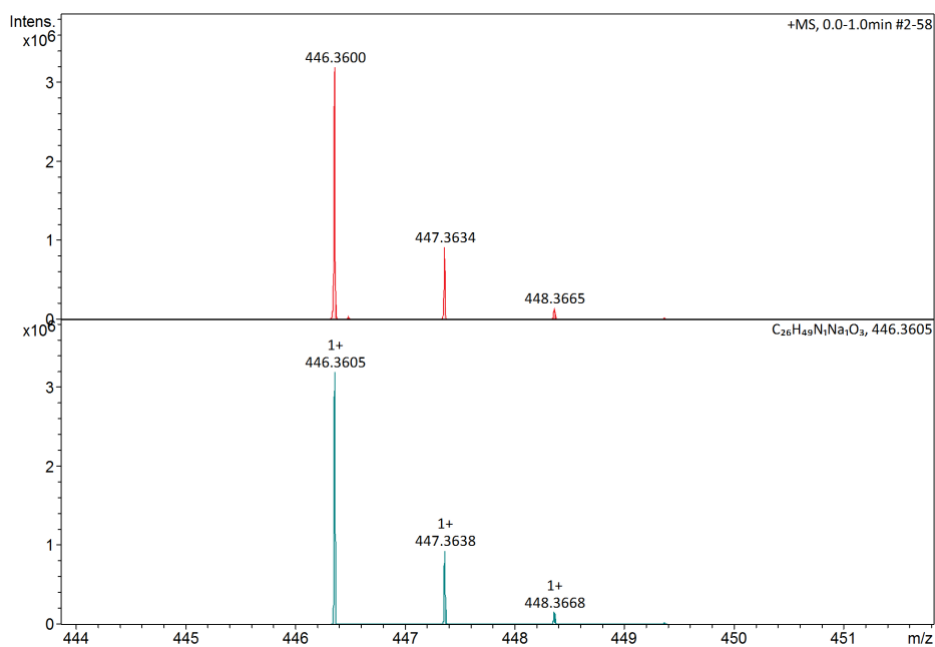


Figure 8.78 HRMS of compound 9.



Elemental Analysis Report

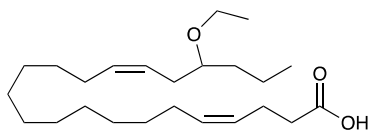
Analysis Info		Acquisition Date	
Sample Name	CB048	11-Apr-23 3:52:30 PM	
Method	ESI_pos_50_1500_os.m	Analysis Name	D:\Data\maxis2023\19465.d
Acquisition Parameter			
Source Type	ESI	Set Capillary	3500 V
Focus	Not active	Set End Plate Offset	-500 V
Scan Begin	50 m/z	Set Charging Voltage	2000 V
Scan End	1500 m/z	Set Corona	0 nA
		Set Nebulizer	0.5 Bar
		Set Dry Heater	200 °C
		Set Dry Gas	4.0 l/min
		Set Divert Valve	Waste
		Set APCI Heater	0 °C



Meas. m/z	Ion Formula	m/z	err [ppm]
446.3600	C24H44N7O	446.3602	0.4
	C26H49NNaO3	446.3605	1.0

Figure 8.79 HRMS of compound 8.

8.3 IR spectra of the synthesized compounds



Sample

Sample Scans:32

Background Scans:8

Resolution:4

System Status:Good

File Location:C:\Users\Public\Documents\Agilent\MicroLab\Results\CB043_2023-04-20T14-11-45.a2r

Method

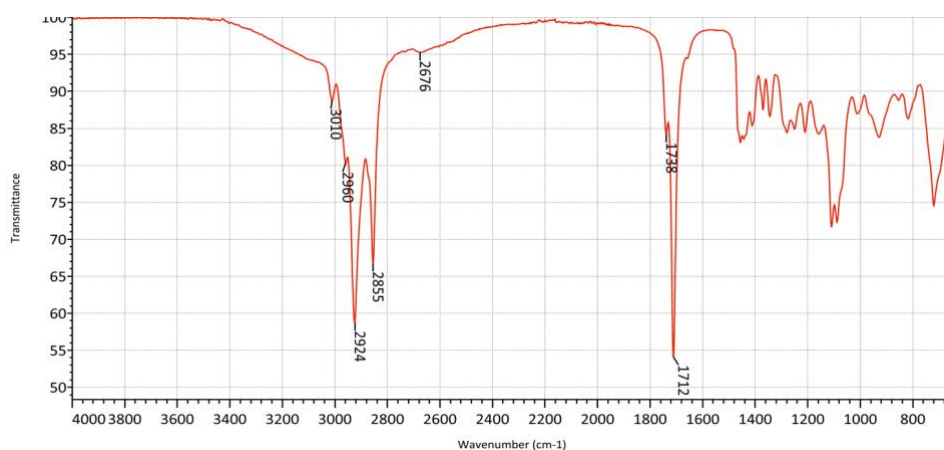
Name:C:\Users\Public\Documents\Agilent\MicroLab\Methods\Test.a2m

User:admin

Date/Time:04.20.2023 2:11:45 p.m.

Range:4000 - 650

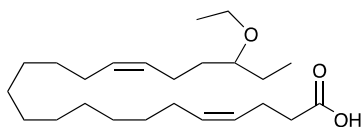
Apodization:Happ-Genzel



Peak Number	Wavenumber (cm ⁻¹)	Intensity
1	1712	54,163
2	1738	84,239
3	2676	95,278
4	2855	66,791
5	2924	58,760
6	2960	80,268
7	3010	88,795

page 1 of 2

Figure 8.80 IR spectrum of compound 6.

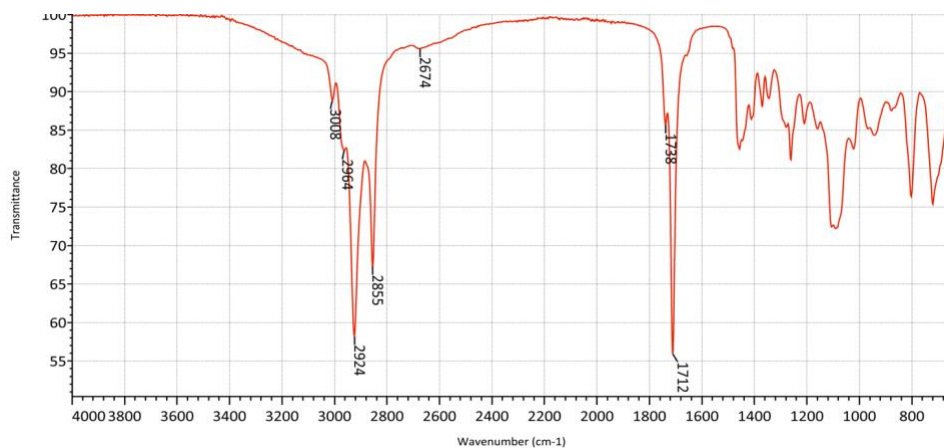


Sample

Sample Scans:32
Background Scans:8
Resolution:4
System Status:Good
File Location:C:\Users\Public\Documents\Agilent\MicroLab\Results\CB025.3.a2r

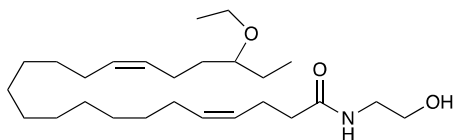
Method

Name:C:\Users\Public\Documents\Agilent\MicroLab\Methods\Test.a2m
User:admin
Date/Time:04.20.2023 1:46:38 p.m.
Range:4000 - 650
Apodization:Happ-Genzel



Peak Number	Wavenumber (cm ⁻¹)	Intensity
1	1712	55,978
2	1738	85,676
3	2674	95,579
4	2855	67,296
5	2924	58,207
6	2964	82,328
7	3008	88,858

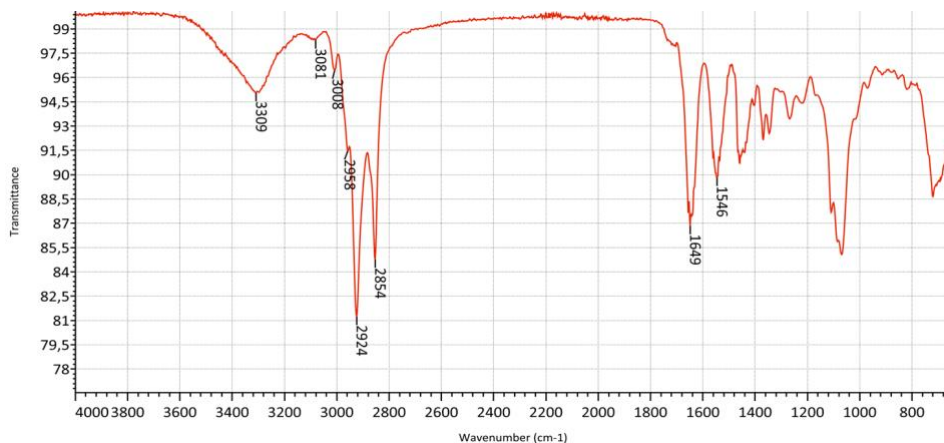
Figure 8.81 IR spectrum of compound 7.



Sample ID:CB049

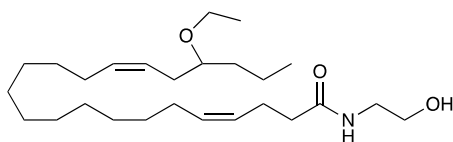
Sample Scans:32
Background Scans:8
Resolution:4
System Status:Good
File Location:C:\Users\Public\Documents\Agilent\MicroLab\Results\CB049_2023-04-20T14-06-28.a2r

Method
Name:C:\Users\Public\Documents\Agilent\MicroLab\Methods\Test.a2m
User:admin
Date/Time:04.20.2023 2:06:28 p.m.
Range:4000 - 650
Apodization:Happ-Genzel



Peak Number	Wavenumber (cm ⁻¹)	Intensity
1	1546	89,814
2	1649	86,843
3	2854	84,772
4	2924	81,231
5	2958	91,467
6	2960	80,268
7	3010	88,795

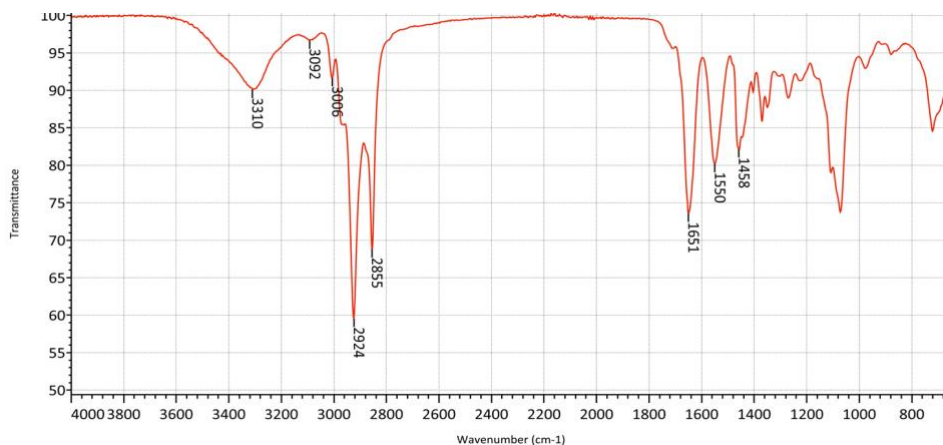
Figure 8.82 IR spectrum of compound 9.



Sample ID:CB048

Sample Scans:32
Background Scans:8
Resolution:4
System Status:Good
File Location:C:\Users\Public\Documents\Agilent\MicroLab\Results\CB048_2023-04-20T14-00-36.a2r

Method
Name:C:\Users\Public\Documents\Agilent\MicroLab\Methods\Test.a2m
User:admin
Date/Time:04.20.2023 2:00:36 p.m.
Range:4000 - 650
Apodization:Happ-Genzel



Peak Number	Wavenumber (cm ⁻¹)	Intensity
1	1458	82,179
2	1550	80,216
3	1651	73,547
4	2855	68,813
5	2924	59,532
6	3006	91,667
7	3092	96,671
8	3310	90,114

Figure 8.82 IR spectrum of compound 8.